SECTION 4

TABLE OF CONTENTS

TABLE OF CONTENTS (CONTINUED)

TABLE OF CONTENTS (CONTINUED)

TABLE OF CONTENTS (CONTINUED)

LIST OF TABLES

LIST OF TABLES (CONTINUED)

LIST OF FIGURES

LIST OF FIGURES (CONTINUED)

LIST OF FIGURES (CONTINUED)

SECTION 4

4.0 REACTOR

4.1 SUMMARY DESCRIPTION

The reactor is designed to meet the performance objectives specified below without exceeding the limits of design and operation specified in Sections 4.2, 4.3, and 4.4. Table 4.4-4 and Appendix 4B list the core mechanical, nuclear, and thermal-hydraulic design parameters.

Beginning in Cycle 16, at the end of a cycle (EOC), the average reactor coolant temperature, T_{AVE}, may be reduced by 12°F (less instrument error). This maneuver may result in reactor coolant inlet temperature of approximately 547°F and will extend the Effective Full Power Life of the core through the negative Moderator Temperature Coefficient. For future cycles, the effects of the T_{AVE} reduction on the core mechanical, nuclear and thermal-hydraulic parameters as well as any potential effects on LOCA and non-LOCA analyses and/or consequences will be addressed by the cycle-specific reload report. (Reference USAR Appendix 4B)

The Davis-Besse reactor was originally designed to operate at a core power level of 2772 MWt, with sufficient design margins to accommodate transient operation and instrument error without damage to the core and without exceeding code pressure limits for the reactor coolant system. License Amendment No. 278 increased rated thermal power to 2817 MWt.

The fuel rod cladding is designed to maintain its integrity for the anticipated operating transients throughout core life. The effects of gas release, fuel dimensional changes, and corrosion- or irradiation-induced changes in the mechanical properties of the cladding are considered in the design of the fuel rod and fuel assembly.

Core reactivity is controlled by Control Rod Assemblies (CRAs) and soluble boron in the coolant. Sufficient CRA worth is available to shut the reactor down with at least a 1% Δk/k subcritical margin in the hot condition at any time during the life cycle with the most reactive CRA stuck in the fully withdrawn position. Equipment is provided to add soluble boron to the reactor coolant to ensure a similar shutdown capability when the reactor is cooled to ambient temperatures.

The reactivity worth of a CRA and the rate at which reactivity can be added are limited to ensure that credible reactivity accidents cannot cause a transient capable of damaging the reactor coolant system or of causing significant fuel failure.

Fuel assemblies are designed for structural adequacy and reliable performance during core operation, handling, and shipping. Design criteria for core operation include steady-state and transient conditions under combined effects of flow-induced vibration, temperature gradients, seismic and LOCA disturbances.

Spacer grids, located along the length of the fuel assembly position fuel rods in a square array and are designed to maintain fuel rod spacing during core operation, handling, and shipping. Spacer grid-to-fuel rod contact loads are established to minimize fretting, but to allow axial relative motion resulting from fuel rod irradiation growth and differential thermal expansion.

The fuel assembly upper and fitting is indexed to the internals plenum assembly by the grid plate immediately above the fuel assemblies to ensure proper alignment of the fuel assembly guide tubes to the control rod guide tube. The guidance of the control rod assembly and axial

power shaping rod assembly is designed so that these assemblies will never be disengaged from the fuel assembly guide tubes during operation.

4.2 MECHANICAL DESIGN

4.2.1 Fuel

4.2.1.1 Mechanical Limits

4.2.1.1.1 Fuel Rods

The fuel design data for the most current cycle is described in the applicable reload report and associated approved B&W Fuel Company topical reports. Commencing with Cycle 13, Reference 58's approval by the NRC allowed use of M5 alloy for use in cladding and structural components (i.e. end caps, spacer grids and guide tubes). The following is a description of the original design.

The Zircaloy-4 cladding is designed to withstand strain resulting from the combined effects of reactor pressure, fission gas pressure, and both fuel thermal expansion and irradiation growth. Cladding strain resulting from normal and upset operating conditions is limited as follows:

a. The Davis-Besse 1 stress parameters were developed by a conservative fuel rod stress analysis. For design evaluation the primary membrane stress must be less than two-thirds of the minimum specified unirradiated yield strength and all stresses must be less than the maximum specified unirradiated yield strength. In all cases, the margin is in excess of 30%. The following conservatisms with respect to Davis-Besse 1 fuel were used in the analysis:

    1. A lower post-densification internal pressure.

    2. A lower initial pellet density.

    3. A higher system pressure.

    4. A higher thermal gradient across the cladding.

b. Primary stresses which are not relieved by small material deformation, are limited so as not to exceed either the yield strength of the material or 75% of the stress rupture life of the material. An example of such a stress is the circumferential membrane stress in the cladding due to internal or external pressure.

c. Secondary stresses, which are relieved by small material deformation, are permitted to exceed the yield strength. Strain limits for this stress condition are based on low-cycle-fatigue techniques, not to exceed 90% of material fatigue life. Evaluation of cyclic loading is based on conservative estimates of the number of cycles to be expected. An example of this type of stress is the thermal stress resulting from thermal gradients across the cladding thickness.

d. Combinations of these two types of stresses, in addition to the individual treatment outlined above, are evaluated for low-cycle fatigue. The fuel design criteria specify a limit of 1.0% on cladding tensile circumferential plastic strain. The pellet design is so that the tensile plastic cladding strain is less than 1% at 55,000 MWd/mtU. The following cladding strain conservatisms are applicable with respect to the Davis-Besse 1 fuel:

1. The maximum specification value for the fuel pellet diameter was used.

2. The maximum specification value for the fuel density was used.

3. The cladding inside diameter used was the lowest permitted specification tolerance.

4. The maximum expected 3-cycle local pellet burnup is less than 55,000 MWd/mtU.

Minimum margins for cladding collapse pressure are as follows:

a. 10% margin over system design pressure on short-time collapse at fuel rod end voids. End voids must not collapse (must be either freestanding or have adequate support) on a long-time basis.

b. 10% margin over system operating pressure on short-time collapse at hot spot average temperature of the cladding wall. Cladding must be freestanding at system design pressure on a short-time basis at the hot spot average temperature through the cladding wall.

4.2.1.1.2 Fuel Assembly Components

The fuel design data for the most current cycle is described in the applicable reload report and associated approved B&W Fuel Company topical reports. Commencing with Cycle 13, Reference 58's approval by the NRC allowed the use of M5 alloy for use in cladding and structural components (i.e. end caps, spacer grids and guide tubes). The following is a description of the original design.

Primary stresses in fuel supporting components, such as end fittings, spacer grids, guide tubes, and holddown components are limited to 85% of the material yield strength for normal and upset operating conditions. These limits are determined by mathematical analysis and testing of the individual components.

4.2.1.1.3 Shock and Seismic Loadings

The fuel design data for the most current cycle is described in the applicable reload report and associated approved B&W Fuel Company topical reports. Commencing with Cycle 13, Reference 58's approval by the NRC allowed the use of M5 alloy for use in cladding and structural components (i.e. end caps, spacer grids and guide tubes). The following is a description of the original design.

The following limits are not exceeded for the Maximum Probable Earthquake (smaller):

a. Loads on the fuel assembly spacer grid do not exceed the elastic load-carrying capacity of the spacer grid as determined by production grid testing.

b. Loads on all other fuel assembly components are limited to 85% of yield as determined by testing and analysis.

The following limits are not exceeded for the Maximum Possible Earthquake (larger): Loss-of-Coolant Accident (LOCA), and combined Maximum Possible Earthquake and LOCA.

a. Loads on the fuel assembly spacer grid do not exceed the load that would permanently distort the guide tubes and prevent control rod insertion as determined by production spacer grid testing.

b. Loads on the control rod guide tubes and end spacer grid assembly do not exceed 85% of the Euler critical buckling load.

c. Loads on the end spacer grid skirt and end fitting are limited to 85% of the load that produces failure (as determined by production component analysis and testing).

Detailed criteria and the method of analysis for seismic and LOCA conditions are provided in B&W topical report BAW-10041, Analysis of Fuel Assembly Stress Due to Seismic Excitation and Loss-of-Coolant Accident for B&W's Nozzle-Supported Vessel.

4.2.1.2 Explanation and Justification of Design Bases

The mechanical design bases have been established to ensure that the fuel assembly and constituent components remain structurally sound and thus prevent the release of fuel and/or fission products to the reactor coolant throughout the design lifetime at the design conditions. The conservatism of the design of the fuel assembly and control components allow the safe shutdown of the reactor under even the most severe postulated accident conditions.

4.2.1.2.1 Properties

The fuel design data for the most current cycle is described in the applicable reload report and associated approved B&W Fuel Company topical reports. Commencing with Cycle 13, Reference 58's approval by the NRC allowed the use of M5 alloy for use in cladding and structural components (i.e. end caps, spacer grids and guide tubes). The following is a description of the original design.

The basis for the design of the fuel rod is discussed in Subsection 4.2.1.1.1. Materials testing and actual in-reactor operation of Zircaloy cladding within the industry have demonstrated that Zircaloy-4 and M5 material has sufficient corrosion resistance and mechanical properties to maintain the integrity and serviceability required for design burnup.

Additional supporting information on the cladding properties is provided under Experimental Results (Subsection 4.2.1.2.6).

4.2.1.2.2 Stress Strain Limits

The fuel design data for the most current cycle is described in the applicable reload report and associated approved B&W Fuel Company topical reports. Commencing with Cycle 13, Reference 58's approval by the NRC allowed the use of M5 alloy for use in cladding and structural components (i.e. end caps, spacer grids and guide tubes). The following is a description of the original design.

The stress limits have been set to keep the resulting cladding strain from exceeding 1.0%. The results of tests (Subsection 4.2.1.2.6) and the operation of Zircaloy-clad UO_2 fuel rods indicate that the rods can be safely operated to the point where total permanent strain is 1.5% or higher

in the temperature range applicable to PWR cladding. The design allowable permanent strain is 1%.

4.2.1.2.3 Fuel Swelling

The fuel design data for the most current cycle is described in the applicable reload report and associated approved B&W Fuel Company topical reports. Commencing with Cycle 13, Reference 58's approval by the NRC allowed the use of M5 alloy for use in cladding and structural components (i.e. end caps, spacer grids and guide tubes). The following is a description of the original design.

Based on the Bettis Atomic Power Laboratory experimental data, swelling of the fuel rods is estimated as outlined below.

The fuel is assumed to swell uniformly in all directions, conservatively neglecting axial plastic flow into the end dishes. Thermal expansions are calculated as described below. When the fuel cracks, the crack voids are assumed to be available to absorb fuel growth.

The external effect of fuel swelling is assumed to occur at 0.16% $\Delta V/10^{20}$ f/cc until the as-fabricated void in the pellets is filled. From that time on, swelling is assumed to take place at 0.7% $\Delta V/10^{20}$ f/cc until the maximum burnup of 13.6 x 10^{20} f/cc (55,000 MWd/mtU) is reached.

Studies of cladding strain at various gaps indicate that the rod with the minimum gap experiences the greatest cladding strain in spite of its improved gap conductivity. Cladding permanent strain reaches a maximum at the end of life. Cladding strain for fuel rods with maximum density and the minimum gap allowed by the specification will also meet the design maximum allowable permanent strain. The fuel in rods with nominal gaps, nominal density, and average burnup will not grow enough to cause either tensile hoop stress or strain in the cladding.

Fuel rod operating conditions pertinent to fuel swelling considerations are listed in Table 4.2-2, and additional supporting information is provided under Experimental Results (Subsection 4.2.1.2.6).

4.2.1.2.4 Effects of Burnup on Fuel Conductivity and Melting

The fuel design data for the most current cycle is described in the applicable reload report and associated approved B&W Fuel company topical reports. Commencing with Cycle 13, Reference 58's approval by the NRC allowed the use of M5 alloy for use in cladding and structural components (i.e. end caps, spacer grids and guide tubes). The following is a description of the original design.

The variations in the conductivity and the melting point of fuel with burnup have been adequately considered in the design and analysis of the fuel. The conservative manner in which the variations are handled is discussed in Subsection 4.4.2.8.4, Fuel Temperature.

4.2.1.2.5 Surveillance and Testing

The fuel design data for the most current cycle is described in the applicable reload report and associated approved B&W Fuel Company topical reports. Commencing with Cycle 13, Reference 58's approval by the NRC allowed the use of M5 alloy for use in cladding and

structural components (i.e. end caps, spacer grids and guide tubes). The following is a description of the original design.

Information obtained from post-irradiation examinations (PIE) of fuel assemblies and constituent components from various B&W-designed plants was incorporated into the evaluation of the design bases as the information became available.

4.2.1.2.6 Experimental Results

The fuel design data for the most current cycle is described in the applicable reload report and associated approved B&W Fuel Company topical reports. Commencing with Cycle 13, Reference 58's approval by the NRC allowed the use of M5 alloy for use in cladding and structural components (i.e. end caps, spacer grids and guide tubes). The following is a description of the original design.

As outlined below, existing experimental information supports the various individual design parameters and operating conditions for the maximum design burnup, 55,000 MWd/mtU.

a. Application of Experimental Data to Design Adequacy of Cladding-Fuel Initial Gap to Accommodate Differential Thermal Expansion:

   Six rabbit capsules, each containing three Zircaloy-2 clad rods of 5-inch fuel length, were irradiated in the Westinghouse Test Reactor (ref. 1) at power levels up to 24 kW/ft. The 94% theoretical density (TD) UO_2 pellets (0.430 OD) had initial cladding-fuel diametral gaps of 6, 12, and 25 mils. No dimensional changes were observed. Central melting occurred at 24 kW/ft only in rods that had the 25-mil initial gap.

   Two additional capsules were tested (ref. 2). The specimens were similar to those described above except for length and initial gap.

   Initial gaps of 2, 6, and 12 mils were used in each capsule. In the A-2 capsule, three 38-inch-long rods were irradiated to 3450 MWd/mtU at 19 kW/ft maximum. In the A-4 capsule, four 6-inch-long rods were irradiated to 6250 MWd/mtU at 22.2 kW/ft maximum. No central melting occurred in any rod, but diameter increases up to 3 mils in the A-2 capsule and up to 1.5 mils in the A-4 capsule were found in the rods with the 2-mil initial gap.

   In addition to demonstrating the adequacy of Zircaloy-clad UO_2 pellet rods to operate successfully at the power levels of interest (and without central melting), these experiments demonstrate that the design initial cladding-fuel minimum gap of 4.5 mils is adequate to prevent unacceptable cladding diametral increase due to differential thermal expansion between the clad and the fuel at beginning of life. A maximum local diametral increase of less than 0.001 inch is indicated for fuel rods having the minimum initial gap, operating at the maximum overpower condition.

b. Adequacy of Available Voids to Accommodate Cladding-Fuel Differential Expansion, Including Effects of Fuel Swelling:

   Zircaloy-clad, UO_2 pellet-type rods have performed successfully in the Shippingport reactor up to approximately 40,000 MWd/mtU. Bettis Atomic Power Laboratory (ref. 2) has irradiated plate-type $U0_2$ fuel (96 to 98% TD) up to 127,000 MWd/mtU and at

fuel center temperatures between 1300 and 3800°F. This work indicates fuel swelling rates of 0.16% $\Delta V/10^{20}$ f/cc until fuel internal voids are filled, then 0.7% $\Delta V/10^{20}$ f/cc after internal voids are filled.

This "breakaway" point appears to be independent of temperature over the range studied and dependent on cladding restraint and the void volume available for collection of fission products. The additional cladding restraint and greater fuel plasticity (from higher fuel temperature) of rod-type elements tend to reduce these swelling effects by providing greater resistance to radial swelling and lower resistance to longitudinal swelling than was present in the plate-type test specimens. This confirmed in part by the work of Frost, Bradbury, and Griffiths of Harwell (ref. 3), in which 0.25-inch-diameter UO_2 pellets clad in 0.020-inch stainless steel with a 2-mil diametral gap were irradiated to 53,300 MWd/mtU at a fuel center temperature of 3180°F without significant dimensional change.

In other testing (ref. 4), 0.150-inch OD, 82 to 96% TD oxide pellets (20% Pu, 80% U) clad with 0.016-inch stainless steel with 6- to 8-mil diametral gaps have been irradiated to 77,000 MWd/mtU at fuel temperatures high enough to approach central melting without apparent detrimental results. Comparable results were obtained on rods swaged to 75% TD and irradiated to 100,000 MWd/mtU.

c. Post-Irradiation Fuel Assemblies Test:

A two-phase experiment was conducted by B&W, sponsored by the Department of Energy as part of its program to improve uranium utilization by extending the burnup of light water reactor fuel. The results of the tests tend to support the adequacy of B&W's design.

For phase one, standard B&W Mark-B (15x15) pressurized water reactor fuel rods were destructively examined after one cycle of irradiation in the Oconee 1 reactor. Fuel rod average burnup ranged from 10,603 to 11,270 MWd/mtU for the rods examined. Data obtained included fuel rod extraction loads, rod dimensional changes, cladding tensile properties, fuel pellet gap length, fission product distribution, fission gas and crud composition, fuel densification, chemical burnup analysis, and fuel and cladding microstructure. As expected, parametric changes were well within the design envelope. Superficial corrosion and wear were found at spacer grid contact points. However, the 19 rods examined were structurally sound and exhibited no indications of cladding defects associated with pellet-cladding interactions. Both plate- and pin-like (or spherical) forms of hydride precipitation were observed. The cladding exhibited a 37% increase in yield strength while retaining 69% of its original ductility.

For phase two standard B&W Mark B (15x15) pressurized water reactor fuel assemblies were nondestructively examined after three cycles of irradiation prior to reinsertion in the Oconee 1 reactor for a fourth cycle of operation. Burnups of the five assemblies examined averaged 30,600 MWd/mtU and are expected to average approximately 40,000 MWd/mtU on completion of the fourth (extended) cycle of operation. Data obtained included fuel assembly and fuel rod dimensions, water channel spacings, holddown spring forces, and fuel column axial gap and stack lengths. The results reported indicated that the assemblies performed well through three cycles of operation. All of the data were within design limits and agreed well with values of predicted performance.

4.2.1.2.7 Fuel Irradiation Studies at B&W

The fuel design data for the most current cycle is described in the applicable reload report and associated approved B&W Fuel Company topical reports. Commencing with Cycle 13, Reference 58's approval by the NRC allowed the use of M5 alloy for use in cladding and structural components (i.e. end caps, spacer grids and guide tubes). The following is a description of the original design.

The performance of B&W test fuel rods irradiated in the Babcock & Wilcox Test Reactor (BAWTR) support the B&W design criteria for fuel rods. The pellet-type rods have been irradiated to burnups of 75,000 MWd/mtU in a systematic study that included test variables of heat rate, burnup, cladding thickness, and fuel-cladding gap.

4.2.1.3 Design Description and Drawings

The complete core has 177 fuel assemblies arranged in a square lattice to approximate a cylinder. All fuel assemblies are identical in mechanical construction and mechanically interchangeable in any core location. Each fuel assembly will accept any control assembly.

The fuel is sintered, cylindrical pellets of low-enriched uranium dioxide. The pellets are clad in Zircaloy-4 or M5 tubing and sealed by Zircaloy-4 or M5 end caps, welded at each end. The cladding, fuel pellets, end caps, and fuel support components form a fuel rod. The basic fuel assembly (Figure 4.2-2) is normally composed of two hundred and eight fuel rods, sixteen control rod guide tubes, one instrument tube assembly, eight spacer grids and two end fittings. Fuel rods with defective cladding may be removed or replaced with dummy fuel rods. The guide tubes, spacer grids, and end fittings form a structural cage to arrange the rods and tubes in a 15x15 array. The center position in the assembly is reserved for instrumentation. Control rod guide tubes are located in 16 locations of the array. Fuel assembly components, materials, and dimensions are listed in Table 4.2-1 and in Appendix 4B, Reload Report, for nuclear, thermal-hydraulic, and mechanical design data corresponding to the current fuel cycle.

4.2.1.3.1 Fuel Rod

The fuel design data for the most current cycle is described in the applicable reload report and associated approved B&W Fuel Company topical reports. Commencing with Cycle 13, Reference 58's approval by the NRC allowed the use of M5 alloy for use in cladding and structural components (i.e. end caps, spacer grids and guide tubes). The following is a description of the original design.

All fuel rods are internally pressurized with helium. The fuel is in the form of sintered and ground pellets of low-enriched uranium dioxide. Pellet ends are dished to minimize differential thermal expansion between the fuel and the cladding and chamfered to minimize cladding ridging at fuel pellet interfaces. Radial growth of the fuel during burnup is accommodated by pellet porosity, radial clearance between the pellets and the cladding, and by a small amount of permanent strain in the cladding. Fuel growth is calculated by the method given in Reference 5.

Above the fuel column is a spring spacer that separates the fuel from the fuel rod upper end cap. This spacer keeps the fuel column in place during shipping and handling. In operation, the spacer permits axial differential growth and thermal expansion between the fuel and the cladding; it also provides radial support for the cladding.

Below each fuel column is a spring spacer which axially locates the bottom of the fuel column and separates the fuel from the lower fuel rod end cap. This spring is designed to deflect under high column loads to reduce axial strain in the cladding.

Fission gas release from the fuel is vented to voids within the pellets, to the radial gap between the pellets and the cladding, and to the void spaces at the top and bottom ends of the fuel rods.

The fuel rod end voids are designed to be freestanding. However, should cladding creep exceed expected limits, radial support is provided by the spring spacers.

To ensure against spring spacer binding, adequate clearance between the cladding and spring is provided. The spring radial expansion during compression is accounted for in calculating this clearance. The upper spacer spring is fabricated from 302 stainless steel. The lower spacer spring material is A-286 alloy. A pressurized fuel rod is shown in Figure 4.2-1.

4.2.1.3.2 Fuel Assembly

The fuel assembly design data for the most current cycle is described in the applicable reload report and associated approved B&W Fuel Company topical reports. Commencing with Cycle 13, Reference 58's approval by the NRC allowed the use of M5 alloy for use in cladding and structural components (i.e. end caps, spacer grids and guide tubes).

General - The fuel assembly shown in Figure 4.2-2 is of the canless type, wherein the eight spacer grids, the end fittings, and the guide tubes form the basic structure. Fuel rods are supported at each spacer grid by contact points or lines integral with the walls of the cell boundary. The guide tubes are attached to the upper and lower end fittings with guide tube nuts or screws. The use of similar material in the guide tubes and fuel rods results in minimal differential thermal expansion.

Spacer Grids - Spacer grids are constructed from slotted strips which are fitted together in "egg-crate" fashion. Each grid has 32 strips, 16 perpendicular to 16, which form the 15x15 lattice. The square walls formed by the interlaced strips provide support for the fuel rods in two perpendicular directions. Contact points or lines on the walls of each square opening are integrally punched in the strips.

Lower End Fitting - The lower end fitting positions the assembly in the lower core grid plate. The lower ends of the fuel rods rest on the grid of the lower end fitting. Starting with Cycle 13, new fuel lower end fittings contain a fine mesh debris filter. Penetrations are provided in the lower end fitting for attaching the control rod guide tubes for access to the instrumentation tube and to permit coolant flow directly into the bottom of the fuel assembly. Starting with batch 17 the fuel rods do not rest on the lower end fitting and the debris filter consist of curved blades.

Upper End Fitting - The upper end fitting positions the upper end of the fuel assembly in the upper core grid plate structure and provides means for coupling the handling equipment. A number on each upper end fitting provides positive identification.

Integral with each upper end fitting are a holddown spring and spider to provide a positive holddown margin to oppose hydraulic forces.

Penetrations are provided in the upper end fitting grid for the guide tubes and to permit coolant flow directly out of the upper end of the fuel assembly.

Guide Tubes - The Zircaloy or M5 guide tubes provide continuous guidance for the control rods when the rods are inserted in the fuel assembly during operation and provide the structural continuity for the fuel assembly. Welded to each end of a guide tube are threaded sleeves which secure the guide tubes to each end fitting by lock-welded nuts. The spacer grids provide transverse location for the guide tubes. Starting with batch 17 the guide tubes are secured to the lower end fitting using screws.

Instrumentation Tube - This Zircaloy or M5 tube serves as a channel to guide, position, and contain the incore instrumentation within the fuel assembly. The instrumentation probe is guided up through the lower end fitting to the desired core elevation. It is retained axially at the lower end fitting by a retainer sleeve.

Spacer Sleeves - The spacer tube sleeves fit around the instrument tube between spacer grids and prevent axial movement of the spacer grids during primary coolant flow through the fuel assembly. Starting with batch 17 spacer sleeves are no longer used, the spacer grids are welded to the guide tubes.

Dummy Fuel Rod - Stainless steel filler rods may be inserted in place of defective fuel rods. The dummy fuel rods are designed to minimize thermal, mechanical, and metallurgical effects on the spacer grid cell.

4.2.1.4 Design Evaluation

The fuel design data for the most current cycle is described in the applicable reload report and associated approved B&W Fuel Company topical reports. Commencing with Cycle 13, Reference 58's approval by the NRC allowed the use of M5 alloy for use in cladding and structural components (i.e. end caps, spacer grids and guide tubes). The following is a description of the original design.

Fuel rod cladding is subjected to external hydrostatic pressure, to gradually increasing internal pressure, to thermal stresses, to vibration, and to the effects of differential expansion of the fuel and cladding caused by thermal expansion and by fuel growth due to irradiation effects. In addition, the properties of the cladding are influenced by thermal and irradiation effects. The analysis of these effects is discussed below.

Stress analysis for cladding is based on several conservative assumptions that make the actual margins of safety greater than those calculated. Fission gas release rates, initial gas fuel backpressures, fuel growth, and changes in mechanical properties with irradiation and temperature (ref. 6, 7) are based on a conservative evaluation of currently available data.

Shown in Figure 4.2-3 are the internal fuel rod pressure history for the worst rod and the nominal rod in the Davis-Besse Nuclear Power Station core. The worst rod was determined from analytical peaking versus burnup histories for the Davis-Besse Nuclear Power Station core. This fuel rod was conservatively assumed to have a 10% uncertainty factor applied to both burnup and peaking. The nominal rod was assumed to have the same burnup as the worst rod but to have a radial x local peaking factor of 1.0 and nominal tolerances. The comparison of these two cases is intended to show the range in fuel rod pressure versus burnup existing between the worst case rod and the nominal rod. It should be noted that there are fuel rods which fall below the nominal case but none which fall above the worst case rod.

4.2.1.4.1 Material Adequacy

The fuel design data for the most current cycle is described in the applicable reload report and associated approved B&W Fuel Company topical reports. Commencing with Cycle 13, Reference 58's approval by the NRC allowed the use of M5 alloy for use in cladding and structural components (i.e. end caps, spacer grids and guide tubes). The following is a description of the original design.

The capability of Zircaloy-clad UO_2 fuel in solid form to perform satisfactorily in service has been demonstrated by the operation of the SA-1 assembly in the Vallecitos and Dresden (ref. 8) loadings, in Shippingport cores, and through the results of their supplementary development programs, up to approximately 45,000 MWd/mtU.

4.2.1.4.2 Vibration Analysis

The fuel design data for the most current cycle is described in the applicable reload report and associated approved B&W Fuel Company topical reports. Commencing with Cycle 13, Reference 58's approval by the NRC allowed the use of M5 alloy for use in cladding and structural components (i.e. end caps, spacer grids and guide tubes). The following is a description of the original design.

The semi-empirical expression developed by Burgreen (ref. 9) was used to calculate the flow-induced vibratory amplitudes for the fuel assembly and fuel rod. The calculated amplitude is less than 0.010 inch for the fuel assembly and less than 0.005 inch for the rod. Experimental results in support of this analysis are described in Subsection 4.2.1.4.9.

4.2.1.4.3 Pressure Effects

The fuel design data for the most current cycle is described in the applicable reload report and associated approved B&W Fuel Company topical reports. Commencing with Cycle 13, Reference 58's approval by the NRC allowed the use of M5 alloy for use in cladding and structural components (i.e. end caps, spacer grids and guide tubes). The following is a description of the original design.

Normal Operation - Cladding stresses due to external and internal pressure at the beginning of life are considerably below the yield strength. Circumferential stresses due to external pressure (calculated using those combinations of cladding dimensions, ovality, and eccentricity that produce the highest stress) are shown in Table 4.2-2. The maximum compressive stress in the expansion void at the system design pressure is the sum of compressive membrane stress plus compressive bending stress due to ovality at the cladding OD. Stress conditions are listed for the Beginning of Life (BOL).

End-of-Life Power Conditions - At the End of Life (EOL) fission gas pressure does not exceed the 3300 psi selected as the design basis. At this pressure, the differential would result in a circumferential tensile stress at normal operating pressure. This stress value, shown in Table 4.2-2, is about 1/4 of the short-time burst. The possibility of stress rupture has been investigated using finite-difference methods to estimate the long-time effects of the increasing pressure on the cladding. The predicted pressure-time relationship produces stresses that are less than 1/3 of the stress levels that would produce stress rupture at EOL. Outpile stress rupture data were used, but the margin on stress (greater than 3:1) is more than enough to account for decreased stress rupture strength due to irradiation.

End-of-Life Shutdown Conditions - The primary coolant system can be cooled down at a maximum rate of 100°F/hr. During this cooldown period it is desirable to maintain a compressive load on the fuel cladding until it has cooled to at least 425°F, where all significant hydrides have had a chance to precipitate under a favorable stress field. The pressurizer and primary system will be cooled down at rates producing a net compressive load on the cladding until the cladding has reached 425°F. Table 4.2-2 shows coolant conditions, and stress levels are shown for two stages of the normal cooldown cycle to the desired temperature level.

The total production of fission gas and maximum internal cladding pressure is based on the analysis of fuel rod power and burnup histories resulting from fuel depletion and fuel cycling. The fission gas release is based on temperature versus release fraction, as shown in Figure 4.4-8. Fuel temperatures are calculated for small radial and axial increments. The total fission gas release is calculated by integrating the incremental releases.

Fuel burnup, temperature and gas release conditions are determined by evaluating the following factors for the most conservative conditions:

1. Gas conductivity at the end-of-life with fission gas present.

2. Influence of the pellet-to-cladding radial gap and the contact heat-transfer coefficient on fuel temperature and release rate.

3. Unrestrained radial and axial thermal growth of the fuel pellets relative to the cladding.

4. Hot rod local peaking factors.

5. Radial distribution of fission gas production in the fuel pellets.

6. The fuel temperatures used to determine fission gas release and internal gas pressure have been calculated at the reactor rated power and maximum design overpower condition. Fuel temperature, total free gas volume, fission gas release, and internal gas pressure have been evaluated for a range of initial diametral clearances. This evaluation shows that the highest internal pressure results when the maximum design diametral gap is assumed because of the resulting high average fuel temperature. The release rate increases rapidly with an increase in fuel temperature, and unrestrained axial growth reduces the relatively cold gas end plenum volumes. A conservative thermal expansion model is used to calculate fuel temperatures as a function of initial cold diametral clearance as outlined in Subsection 4.4.2.8.4.

7. Power burnup histories and nuclear calculations of power peaks are considered in evaluating fuel and cladding performance.

Temperature Transients/Depressurization Accidents - Depressurization accidents and their effect on fuel rod cladding integrity are discussed in Section 6.3. Fuel rod pressures and cladding stresses are calculated for the design basis LOCA. The results of these calculations, the consideration of refined calculated techniques and other factors, e.g., the results documented in NUREG-0630, are further translated into the establishment of operational and protection system limits which ensure the integrity of the fuel cladding.

4.2.1.4.4 Potential for Waterlogging Rupture

The fuel design data for the most current cycle is described in the applicable reload report and associated approved B&W Fuel Company topical reports. Commencing with Cycle 13, Reference 58's approval by the NRC allowed use of the M5 alloy for use in cladding and structural components (i.e. end caps, spacer grids and guide tubes). The following is a description of the original design.

The B&W fuel assembly and fuel rod have been conservatively designed to avoid failure of the cladding which would allow water to enter the fuel rod. However in the event of a cladding penetration the indicated (ref. 10) critical parameters of fuel density the reactor power increase rate the coolant temperature and the fuel rod heat flux are such that a waterlogging rupture would not occur quickly. This would allow time for corrective action of defective fuel replacement before adjacent fuel would be affected.

4.2.1.4.5 Potential for Chemical Reactions, Including Effects of Hydriding

The fuel design data for the most current cycle is described in the applicable reload report and associated approved B&W Fuel Company topical reports. Commencing with Cycle 13, Reference 58's approval by the NRC allowed use of the M5 alloy for use in cladding and structural components (i.e. end caps, spacer grids and guide tubes). The following is a description of the original design.

B&W exercises controls to ensure that unwanted impurities are not uniformly dispersed throughout the cladding prior to irradiation, and unwanted impurities are not allowed to react with the cladding during irradiation. Examples of these two precautionary measures can be illustrated by using hydrogen and iron as impurity atoms. In the case of hydrogen, the allowable concentration of hydrides that are uniformly dispersed is limited to the lowest level that can be obtained commercially. In this way the cladding will not be embrittled by ZrH_2 inclusions, which act as stress risers in the event that they appear as a second phase after solid solubility limits are exceeded. Further, the moisture content of the uranium fuel pellets is limited so that the hydride from the water vapor will not react locally with the zirconium after the oxygen has been reacted. Sources other than water vapor are limited to control the hydride reaction of the cladding. These controls limit the amount of free hydrogen and hydrocarbons from oils, greases, and plastics. Likewise, the cladding is not autoclaved or "prefilmed."

Iron, in the form of either mild steel or stainless steel, can react with zirconium and form a low-melting-point solid solution, i.e., the eutectic reaction. To prevent the eutectic reaction, these steels are excluded from contacting the cladding insertions of the fuel rod where temperatures are high enough to produce a reaction.

Other technical bases indicate that fluorine and chlorine can both impair the corrosion performance of the cladding. B&W restricts the fluorine and chlorine content of the fuel pellets to very low values. Also, the cladding is not allowed to be pickled and thus introduce fluorine subsequent to the final anneal.

Finally, B&W recognizes that zirconium hydride inclusions will precipitate in the direction of compressive stresses and normal to the direction of tensile stresses. Accordingly, B&W specified that the cladding be in compression down to 425°F during reactor shutdown. This precludes the precipitation of radially oriented hydrides that otherwise act as stress risers. As noted, B&W is most concerned about the chemical reaction of hydrides and zirconium, and

precautions are taken to minimize hydriding in the cladding and the effects on the cladding integrity.

4.2.1.4.6 Fretting Corrosion

The fuel design data for the most current cycle is described in the applicable reload report and associated approved B&W Fuel Company topical reports. Commencing with Cycle 13, Reference 58's approval by the NRC allowed use of the M5 alloy for use in cladding and structural components (i.e. end caps, spacer grids and guide tubes). The following is a description of the original design.

An extensive experimental and test program has been performed at B&W's Research Center at Alliance, Ohio, on fretting and wear in the B&W fuel assembly (Subsection 4.2.1.4.9). Production fuel assembly components have been tested in air and water at cold and PWR temperature, pressure, and flow conditions to simulate long-term contact conditions. Long-term testing of production fuel assemblies was also conducted at PWR conditions in the Control Rod Drive Line (CRDL) facility. Both new and relaxed assemblies were monitored and tested for fretting and wear due to the fuel rod and fuel assembly flow-induced vibrations. The results of the experiments and tests have shown that the B&W fuel assembly will be free from detrimental fretting corrosion for its design life.

4.2.1.4.7 Cycling and Fatigue

The fuel design data for the most current cycle is described in the applicable reload report and associated approved B&W Fuel Company topical reports. Commencing with Cycle 13, Reference 58's approval by the NRC allowed use of the M5 alloy for use in cladding and structural components (i.e. end caps, spacer grids and guide tubes). The following is a description of the original design.

In the heat-producing zone, the stress and temperature are such that the cladding material may creep enough to allow an increase in cladding ovality until further creep is restrained by support from the fuel. If fuel-cladding contact occurs, the cladding is subject to cyclic stresses and strains caused by power and pressure transients. To minimize cladding fatigue damage, all fuel rods will be internally pressurized with helium. Fatigue analyses, based on conservative assumptions, show that the previously specified design limits (Subsection 4.2.1.1) are met for pressurized fuel rods.

4.2.1.4.8 Dimensional Stability

The fuel design data for the most current cycle is described in the applicable reload report and associated approved B&W Fuel Company topical reports. Commencing with Cycle 13, Reference 58's approval by the NRC allowed use of the M5 alloy for use in cladding and structural components (i.e. end caps, spacer grids and guide tubes). The following is a description of the original design.

Fuel Rod Cladding - Short-time collapse tests have demonstrated a cladding collapse pressure in excess of 4000 psi at the expansion void maximum temperature. The collapse pressure margin is a minimum of approximately 2.2. Extrapolation to hot spot average cladding temperature indicates a collapse pressure of 3500 psi and a minimum margin of approximately 1.9, which also greatly exceeds the requirement.

Fuel rod cladding dimensional stability against creep collapse has been analytically verified to ensure that the design bases of Subsection 4.2.1.1 have been satisfied. The analysis employs the methods and procedures described in B&W Topical Report BAW-10084P, Rev. 1, "Program to Determine In-Reactor Performance of B&W Fuels Cladding Creep Collapse (October 1976)."

Guide Tube - The 0.058-inch diametral clearance between the control rod guide tube and the control rod is provided to cool the control rod and to ensure adequate freedom to insert the control rod. As indicated below, studies have shown that fuel rods will not bow sufficiently to touch the guide tube. Thus, the guide tube will not undergo deformation due to fuel rod bowing effects. Initial lack of straightness of the fuel rod and guide tube, plus other adverse tolerance conditions, could conceivably reduce the 0.088-inch nominal gap between the fuel rod and guide tube to a minimum of about 0.038 inch, including amplification of bowing due to axial friction loads from the spacer grid. The maximum expected flux gradient of 1.176 across a fuel rod will produce a temperature difference of about 12°F, which will result in a thermal bow of less than 0.002 inch. Under these conditions, the thermal gradient across the fuel rod diameter would have to be on the order of 300°F for the fuel rod to touch the guide tube.

A DNB occurring on the side of a fuel rod adjacent to a guide tube would result in a large temperature difference. In this case, however, investigation has shown that the cladding temperature would be so high that insufficient strength would be available to generate a force great enough to cause a significant deflection of the guide tube. In addition, the guide tube would experience an opposing gradient that would resist fuel rod bowing, and its internal cooling would maintain temperatures much lower than those in the fuel rod cladding, thus retaining the guide tube strength.

4.2.1.4.9 Experimental Programs

The fuel assembly design data for the most current cycle is described in the applicable reload report and associated approved B&W Fuel Company topical reports. Commencing with Cycle 13, Reference 58's approval by the NRC allowed use of the M5 alloy for use in cladding and structural components (i.e. end caps, spacer grids and guide tubes). The following is a description of the original design.

Fuel Assembly - The structural characteristics of the fuel assembly that are pertinent to loadings resulting from normal operation, handling, earthquake, and accident conditions have been experimentally investigated in the CRDL and other test facilities at B&W's Alliance Research Center. The facilities simulate PWR temperature, pressure, and coolant flow conditions and allow for variations of those conditions.

A production prototype full-sized fuel assembly has been tested for 3700 hours at PWR temperature, pressure, and flow conditions in the CRDL test facility. The principal objective of these tests was to evaluate fuel assembly and fuel rod vibration and/or fretting wear resulting from flow-induced vibration. Vibratory amplitudes have been found to be very small, and, except for a few isolated instances, no unacceptable wear has been observed. The few isolated instances of wear have been attributed to pretest spacer grid damage. The damage mechanism for the spacer grids used in the investigation was a deliberate mechanical relaxation of the grid cells. The resulting wear was due to impact fretting. This will not happen in the Davis-Besse core as there will be no pre-loading of the production grids and impact fretting cannot occur. The fuel assembly's average mid-span amplitude was found to be less than 1.0 mil. The average fuel rod amplitude was less than 0.1 mil. Peak amplitudes were found to be less than 6.0 mils and 0.25 mil for the fuel assembly and the fuel rod, respectively.

The spacer grid-to-fuel rod contact area was made 10 times reactor size and tested in a loop simulating the coolant flow Reynolds number of interest. Thus, visually, the shape of the fuel rod support areas was optimized with respect to minimizing the severity of flow vortices and pressure drop.

New production and simulated relaxed full-sized fuel assemblies have been tested in the CRDL and other test facilities to determine structural characteristics, such as natural frequency and damping, for use in seismic and LOCA analyses. Natural frequencies and amplitudes resulting from flow-induced vibration were measured at various temperatures and flow velocities, up to reactor operating conditions. Additional tests have been conducted to determine the effect of number, type, and location of spacer grids on fuel assembly structural characteristics such as natural frequency, damping, and stiffness.

Fuel Rod - Extensive short-time collapse tests were conducted on Zircaloy-4 tube specimens as part of B&W's overall creep-collapse testing program. Initial test specimens had an OD of 0.436 inch with wall thicknesses of 0.020, and 0.028 inch. Ten 8-inch-long specimens of each thickness were individually tested at 680°F at slowly increasing net external pressure until collapse occurred. Collapse pressures for the 0.020-inch wall specimens ranged from 1800 to 2200 psig, for the 0.024-inch specimens from 2800 to 3200 psig, and for the 0.028-inch specimens from 4500 to 4900 psig. The material yield strength of these specimens ranged from 65,000 to 72,000 psi at room temperature and was 35,900 psi at 680°F.

Additional Zircaloy-4 short-time collapse specimens were prepared from material with a yield strength of 78,000 psi at room temperature and 48,500 psi at 615°F. Fifteen specimens with an OD of 0.410 inch and an ID of 0.365 inch (0.0225-inch nominal wall thickness) were tested at 615°F at increasing pressure until collapse occurred. Collapse pressures ranged from 4470 to 4960 psig.

Creep-collapse testing was conducted on the 0.436-inch-OD specimens. Twelve specimens of 0.024-inch wall thickness and thirty specimens of 0.028-inch wall thickness were tested in a single autoclave at 680°F and 2050 psig. During this test, two 0.024-inch-wall specimens collapsed during the first 30 days, and two collapsed between 30 and 60 days. Creep-collapse testing was then performed on thirty 0.410-inch OD by 0.365-inch ID (0.0225-inch normal wall) specimens for 60 days at 615°F and 2140 psig. None of these specimens collapsed, and there were no significant increases in ovality after 60 days.

The results of the 60-day creep-collapse tests on the 0.410-inch-OD specimens showed no indication of incipient collapse. The 60-day period for creep-collapse testing was used since it exceeds the point of primary creep of the material, yet is long enough to enter the stage when fuel rod pressure begins to build up during reactor operation, i.e., past the point of maximum differential pressure that the cladding would be subjected to in the reactor.

These tests were followed by additional creep-collapse tests in which 60 specimens of variable wall thickness were subjected to a net external pressure of 2085 psi at 685°F until collapse occurred. The cladding wall thicknesses were 0.0285, 0.0263, 0.0251, and 0.0240 inch. The cladding thickness included the range of tolerances for production cladding, and the pressure represented the fuel rod maximum pressure differential (without prepressurization) at operating conditions. The temperature was selected to conservatively approximate inpile creep rates. It was found that the 0.024-inch specimens collapsed in less than a month, and several 0.0263-inch-wall specimens collapsed in less than three months. Subsequent to these tests, prepressurization of fuel rods has been initiated to reduce the rate of collapse. Prepressurization has caused the rates of collapse to decrease significantly. The rate of

collapse of fuel rod cladding varies directly with the differential pressure across the cladding wall. The fuel rods in the Davis-Besse core are prepressurized to a significant degree. This lowers the differential pressure across the cladding throughout rod life and thus reduces the possibility of collapse.

However, in the event that inpile creep rates exceed those expected, backup support is provided in the upper void region, where cladding temperatures of approximately 650°F occur in the hot channels. A spring spacer has been designed as a backup spacer. The spacer provides radial support to the cladding without causing excessive axial restraint on the fuel expansion. Analytical results have indicated that the spacer can withstand the shipping acceleration of the fuel pellets without permanent deformation. Tests have been performed to demonstrate that the spring spacer will provide backup support to the cladding. The spacers were enclosed in production Zircaloy cladding and subjected to 2500 psi at 750°F. This represents the design system external pressure for the cladding and the nominal operating temperature of the spacer. Post-autoclave examinations revealed that the cladding was adequately supported.

4.2.1.5 Testing and Inspection

B&W-NPGD equipment specifications require that core components be fabricated under an approved quality control program. This includes shop quality control provisions and special process procedures.

The B&W Commercial Nuclear Fuel Plant manufactures core components under a controlled manufacturing system which includes complimentary written process procedures and inspection provisions. These fabrication activities are supported by quality control provisions, e.g., document control, control of special processes, in process and final inspection, gauge control, corrective action, etc.

For the original design, the tests and inspections described below are those specified for the various components and assemblies. Additional testing and inspection are performed routinely to ensure that the test and inspection program is adequate and to further ensure the quality of the final product. B&W has concluded that a change from 6X to 3X is equal to or better than a 6X magnification inspection. The basis for this conclusion is as follows:

(1) The type of defects of concern are detectable with 3X magnification.

(2) The use of 3X would allow an equipment change which would facilitate the inspection. Available 6X magnifiers have a small field of view, whereas a 3X magnifier has a large field and an integral fluorescent light. The superior lighting and large field combine to produce at least as thorough an inspection as with the 6X magnifier.

(3) To assure the above, B&W performed inspection on all types of welds containing typical defects. The result was that the 3X inspection detected all defects found by the 6X inspection.

This change is applicable to Subsection 4.2.1.5.1, 4.2.1.5.3, 4.2.1.5.4, and 4.2.1.5.5

4.2.1.5.1 Fuel Rods

The fuel design data for the most current cycle is described in the applicable reload report and associated approved B&W Fuel Company topical reports. Commencing with Cycle 13, Reference 58's approval by the NRC allowed use of the M5 alloy for use in cladding and structural components (i.e. end caps, spacer grids and guide tubes). The18 following is a description of the original design.

A program of tests and inspection is performed throughout the manufacturing of fuel rods to ensure the integrity of the cladding in the as-fabricated fuel rods. Each tube is 100% nondestructively tested for defects using ultrasonic inspection. The inside and outside diameters and the wall thickness of the tubing are inspected for actual dimensions on a 100% basis. Also, the finished fuel rods are 100% visually inspected for surface defects. The fuel rod end cap seal welds are 100% inspected for surface irregularities using an optical magnification of 3X. The surfaces of all fuel rod components and all completed fuel rods are 100% inspected to ensure that the criteria for cleanliness are satisfied. As a final inspection, all rods are helium leak- checked in a vacuum.

Destructive testing of production components is conducted statistically to further ensure the integrity of the cladding. Specimens from each lot of tubing are subjected to a 14-day corrosion test, after which the hydrogen content of each sample is determined. Samples of end cap-to-cladding welds are also subjected to a corrosion test. Additional tests on end cap weld samples are conducted to determine the presence of cracks, voids, inclusions, porosity, lack of penetration, or other weld imperfections when metallurgically examined.

4.2.1.5.2 Fuel Pellets

The fuel design data for the most current cycle is described in the applicable reload report and associated approved B&W Fuel Company topical reports. The following is a description of the original design.

The characteristics of fuel pellets are determined statistically through a program of tests and inspections described below. Random samples from each lot of pellets are chemically analyzed. Certified reports are recorded for each lot with the following information:

1. Analytical test results, including weight percent uranium, wt % 235U, O/U ratio, moisture, absorbed gas, impurities, and total equivalent boron content.

2. Data on variables from the sampling plans for the pellet average diameter, weight, density, and surface finish.

3. Weight and length of each stack.

4. Pellet symbol and stack identification records.

5. Uranium accountability documentation as required by applicable government regulations.

6. Identification of lots of isotopically blended uranium along with the measured enrichments, the enrichment tolerances, and the quantity of material involved.

In addition, B&W overchecks incoming material to ensure that all specification requirements are met.

4.2.1.5.3 Spacer Grids

The fuel assembly design data for the most current cycle is described in the applicable reload report and associated approved B&W Fuel Company topical reports. Commencing with Cycle 13, Reference 58's approval by the NRC allowed use of the M5 alloy for use in cladding and structural components (i.e. end caps, spacer grids and guide tubes). The following is a description of the original design.

Fuel assembly spacer grids are tested and inspected under a statistical program to ensure that the dimensions of the grids and the fuel assembly are acceptable.

Welds are inspected at 3X magnification, which provides a 95% confidence that the specifications for dimensional size and location and for the absence of cracks and lack of penetrations or other imperfections are met 95% of the time (95/95 confidence level). The spacer grids are also 100% inspected for outside dimensions and flatness.

4.2.1.5.4 Fuel Assembly

The fuel assembly design data for the most current cycle is described in the applicable reload report and associated approved B&W Fuel Company topical reports. Commencing with Cycle 13, Reference 58's approval by the NRC allowed use of the M5 alloy for use in cladding and structural components (i.e. end caps, spacer grids and guide tubes). The following is a description of the original design.

The completed fuel assemblies are inspected statistically to ensure a 95/95 confidence level that the assemblies are dimensionally correct. In addition, the fuel assemblies are subjected to an envelope inspection on a 100% basis. The assemblies are also 100% inspected to ensure that the critical specified end fitting dimensions (surfaces mating with the reactor internals) are correct. The guide tube assemblies of each completed fuel assembly are inspected full length by an inspection fixture that simulates the control rod assembly.

Fuel assemblies are dimensionally inspected on a statistical basis for fuel rod, guide tube, and instrumentation tube pitch to ensure acceptable water channel dimensions in the final assembly. Welds in the final assembly are inspected for imperfections using a 3X magnification. In addition, metallographic examination of welds is performed on a statistical basis. Completed fuel assemblies are inspected to ensure a 95/95 confidence level that the cleanliness specifications are met.

4.2.1.5.5 Control and Axial Power Shaping Assemblies

The design data for the most current cycle is described in the applicable reload report and associated approved B&W Fuel Company topical reports. The following is a description of the original design.

Control and axial power shaping assemblies and their constituent components are tested and inspected throughout manufacture to ensure the integrity of the assembly and the absorber rods.

The tubing used for Control Rod (CR) and Axial Power Shaping Rod (APSR) cladding is inspected for inside and outside diameters and for minimum wall thickness, nondestructively tested for defects using ultrasonic inspection, and inspected for compliance with the cleanliness specifications - all on a 100% basis.

The finished CR and APSR closure welds are 100% vacuum-leak tested and visually inspected at 3X magnification, and the CRs and APSRs are also 100% inspected for surface defects.

The completed CR and APSR assemblies are dimensionally inspected on a statistical basis to ensure that dimensional specifications are met. The CR and APSR spiders are tested on a 100% basis to ensure proper alignment and engagement with the respective drive couplings. Each completed CR and APSR assembly is inspected (full length) in a specially designed fixture that simulates the fuel assembly guide tubes.

4.2.1.5.6 Post-Shipment Inspection Program

New control rods, fuel assemblies, internals, and their shipping containers are visually inspected at the reactor site by the station personnel.

A reactor engineer is notified of the arrival of a fuel shipment at the station before it may be received. An inspection report is then filled out in accordance with the directions given in a station procedure. This procedure provides for verification of container serial numbers with shipping notice, accelerometer trip check, field integrity verification, execution of NRC-741 form which is a Nuclear Material Transfer Report, and proper documentation verification.

After the fuel shipment has been properly received, the container is checked for internal cleanliness, loose parts, and condition of the polyethylene bag. The ID numbers of the fuel assemblies are then checked against the shipping notice. If all documentation is proper, the fuel assemblies are then removed from the container and inspected individually for dents, scratches, cracks and misalignment.

Assemblies which do not pass inspection are marked with a status tag and are stored dry. The inspection report is placed in the receipt inspection file, and management is notified of the inspection results.

Assemblies which pass inspection are stored in dry or wet storage as determined by the reactor engineer.

4.2.2 Reactor Vessel Internals

Reactor internal components include the plenum assembly and the core support assembly. The core support assembly comprises the core support shield, core barrel, lower grid, flow distributor, incore instrument guide tubes, thermal shield, and surveillance specimen holder tubes. Figure 4.2-4 shows the reactor vessel, the internals arrangement, and the reactor coolant flow path. Figure 4.2-5 shows the core flooding nozzle arrangement.

Reactor internal components do not include fuel assemblies, Control Rod Assemblies (CRAs), or incore instrumentation. Fuel assemblies and CRAs are described in Subsection 4.2.1 and Subsection 3.9.3, control rod drives in Subsection 4.2.3, and incore instrumentation in Subsection 4.3.5.

The reactor internals are designed to support the core, to maintain fuel assembly alignment, to limit fuel assembly movement, and to maintain CRA guide tube alignment between fuel assemblies and control rod drives. They also direct the flow of reactor coolant, provide gamma and neutron shielding, provide guides for incore instrumentation between the reactor vessel lower head and the fuel assemblies, support the surveillance specimen assemblies in the annulus between the thermal shield and the reactor vessel wall, and support the internal vent valves. These vent valves provide an emergency steam release path from the upper plenum region above the core to the upper downcomer region in the event of a cold leg break. All reactor internal components can be removed from the reactor vessel to allow inspection of the internals and the reactor vessel internal surface.

A shop fitup and checkout of the internal components in an as-built reactor vessel mockup ensured proper alignment of mating parts before shipment. Dummy fuel assemblies and CRAs were used to check fuel assembly clearances and CRA free movement.

To minimize lateral deflection of the lower end of the core support assembly as a result of horizontal seismic loading, integral weld-attached, deflection-limiting guide lugs have been welded to the reactor vessel inside wall. The lugs will also limit the rotation of the lower end of the core support assembly that could result from flow-induced torsional loadings. The lugs allow free vertical movement of the lower end of the internals for thermal expansion throughout all ranges of reactor operating conditions. In the unlikely event that a flange, circumferential weld, or bolted joint might fail, the lugs will limit the possible core drop to 1/2 inch or less. A 1/2-inch core drop will not allow the lower end of the CRAs to disengage from their respective fuel assembly guide tubes, even if the CRAs are in the full-out position. In this position, approximately 6-1/2 inches of rod length remains in the fuel assembly guide tubes. A core drop of 1/2 inch will not result in a significant reactivity change. The core cannot rotate and bind the drive lines because rotation of the core support assembly is prevented by the guide lugs.

The core support components are designed to meet the stress requirements of the ASME Code, Section III, in effect on date of order during normal operation and transients. Topical Report BAW-10008, Part 1, Rev. 1 is supplemented by Appendix 4A, Faulted Condition Analysis of Toledo, Davis-Besse Reactor Internals. A detailed stress analysis of the internals under accident conditions has been completed using the methods reported in topical report Appendix 4A Reactor Internals Stress and Deflection Due to Loss-of-Coolant Accident and Maximum Hypothetical Earthquake. The results of this analysis are shown in Table 4.2-5. It is shown that although there is some internals deflection, the internals will not fail because the stresses are within established limits. These deflections would not prevent CRA insertion because the control rods are guided throughout their travel, and the guide-to-fuel assembly alignment cannot change because positive alignment features are provided between them, and the deflections do not exceed allowable values. Additional criteria and analyses are given in B&W topical report BAW-10051, Rev. 1, Design of Reactor Internals and Incore Instrument Nozzles for Flow-Induced Vibrations. All core support circumferential weld joints in the internals shells are inspected to the requirements of the ASME Code, Section III.

An integrated head assembly (IHA) was installed during outage 17M. Qualification of the core support components for seismic and LOCA loadings with the IHA installed is discussed in section 3.9.1.5.

4.2.2.1 Plenum Assembly

The plenum assembly, located directly above the reactor core, is removed as a single component before refueling. It consists of a plenum cover, upper grid, CRA guide tube

assemblies, and a flanged plenum cylinder with openings for reactor coolant outlet flow. The plenum cover is constructed of a series of parallel flat plates intersecting to form square lattices; it has a perforated top plate and an integral flange at its periphery. The cover assembly is attached to the plenum cylinder top flange. The perforated top plate has matching holes to position the upper end of the CRA tubes. Lifting lugs are provided for remote handling of the plenum assembly. These lifting lugs are welded to the cover grid. The CRA guide tubes are welded to the plenum cover top plate and bolted to the upper grid. The CRA guide assemblies provide CRA guidance, protect the CRA from the effects of coolant cross-flow, and provide structural attachment of the grid assembly to the plenum cover.

Each CRA guide assembly consists of an outer tube housing, a mounting flange, 12 perforated slotted tubes, and four sets of tube segments which are oriented and attached to a series of castings so as to provide continuous guidance for the CRA full stroke travel. The outer tube housing is welded to a mounting flange, which is bolted to the upper grid. Design clearances in the guide tube accommodate misalignment between the CRA guide tubes and the fuel assemblies. Final design clearances were established by tolerance studies and CRDL prototype test results. The test results are described in BAW-10029, Rev. 3, Control Rod Drive System Tests.

The plenum cylinder consists of a large cylindrical section with flanges on both ends to connect the cylinder to the plenum cover and the upper grid. Holes in the plenum cylinder provide a flow path for the coolant water. The upper grid consists of a perforated plate which locates the lower end of the individual CRA guide tube assembly relative to the upper end of a corresponding fuel assembly. The grid is bolted to the plenum cylinder lower flange. Locating keyways in the plenum assembly cover flange engage the reactor vessel flange locating keys to align the plenum assembly with the reactor vessel, the reactor closure head CRD penetrations, and the core support assembly. The bottom of the plenum assembly is guided by the inside surface of the lower flange of the core support shield.

4.2.2.2 Core Support Assembly

The core support assembly consists of the core support shield, core barrel, lower grid assembly, flow distributor, thermal shield, incore instrument guide tubes, surveillance specimen holder tubes, and internals vent valves. Static loads from the assembled components and fuel assemblies and dynamic loads from CRA trip, hydraulic flow, thermal expansion, seismic disturbances, and LOCA loads are all carried by the core support assembly.

The core support assembly components are described as follows:

1. Core Support Shield:

   The core support shield is a flanged cylinder which mates with the reactor vessel opening. The forged top flange rests on a circumferential ledge in the reactor vessel closure flange. The core support shield lower flange is bolted to the core barrel. The inside surface of the lower flange guides and aligns the plenum assembly relative to the core support shield. The cylinder wall has two nozzle openings, which seal to the reactor vessel outlet nozzles by the differential thermal expansion between the stainless steel core support shield and the carbon steel reactor vessel. The nozzle seal surfaces are finished and fitted to a predetermined cold gap providing clearance for core support assembly installation and removal. At reactor operating temperature, the mating metal surfaces are in contact to make a seal without exceeding allowable stresses in

either the reactor vessel or internals. Four vent valve mounting rings are welded in the support shield wall. Four internals vent valves are installed in these mounting rings to provide a steam flow path between the upper plenum region above the core and the upper downcomer region in the event of a postulated cold leg (reactor coolant inlet) pipe rupture.

2. Core Barrel:

The core barrel supports the fuel assemblies, lower grid, flow distributor, and incore instrument guide tubes. The core barrel consists of a flanged cylinder, a series of internal horizontal former plates bolted to the cylinder, and a series of vertical baffle plates bolted to the inner surfaces of the horizontal formers to produce an inner wall enclosing the fuel assemblies. The core barrel cylinder is flanged on both ends; the upper flange is bolted to the mating lower flange of the core support shield, and the lower one is bolted to the lower grid assembly. The Upper Core Barrel bolts are locked in place with locking cups after final assembly. Sixty of the 108 Lower Core Barrel bolts are locked in place with locking cups while the remaining 48 Lower Core Barrel bolts are lock-welded after final assembly. Coolant flow is downward along the outside of the core barrel cylinder and upward through the fuel assemblies contained in the core barrel. A small portion of the coolant flows upward through the space between the core barrel outer cylinder and the inner baffle plate wall. Coolant pressure in this space is maintained lower than the core coolant pressure to avoid tension loads on the bolts attaching the plates to the horizontal formers.

3. Lower Grid Assembly:

The lower grid assembly aligns and supports the fuel assemblies, supports the thermal shield and flow distributor, and aligns the incore instrument guide tubes with the fuel assembly instrument tubes. The lower grid consists of two grid structures separated by short tubular columns and surrounded by a forged flanged cylinder. The upper structure is a perforated plate, and the lower one is a machined forging. The top flange of the forged cylinder is bolted to the lower flange of the core barrel. A perforated flat plate placed midway between the two grid structures aids in distributing coolant flow before it enters the core. Alignment of fuel assemblies and incore instruments is provided by pads bolted to the upper perforated plate.

4. Flow Distributor:

The flow distributor is a perforated dished head with an external flange which is bolted to the bottom flange of the lower grid. The flow distributor supports the incore instrument guide tubes and distributes the inlet coolant entering the bottom of the core.

5. Thermal Shield:

A cylindrical stainless steel thermal shield is installed in the annulus between the core barrel cylinder and the reactor vessel inner wall. The thermal shield reduces the incident gamma absorption internal heat generation in the reactor vessel wall and thereby reduces the resulting thermal stresses. The thermal shield upper end is restrained against inward and outward vibratory motion by

restraints bolted to the core barrel cylinder. The lower end is shrunk-fit on the lower grid flange and secured by 96 high-strength bolts.

6. Surveillance Specimen Holder Tubes:

Surveillance Specimen Holder Tubes (SSHT) are installed on the thermal shield outer wall, as shown in Figure 4.2-5, to contain the surveillance specimen capsules. A total of six tubes, each capable of containing two surveillance specimen capsules, have been installed in the locations shown in Figure 4.2-5. This provides the capability of irradiation of additional surveillance capsules over those required for Davis-Besse 1. The design of the SSHT is described in detail in B&W Topical Report BAW-10051, Supp. 1. Vibration measurement assessment program for the surveillance specimen holder tube assembly is described in B&W Owners Group Report, BAW-10038A, Supplement 1. BAW-10039, Supplement 1, describes the predicted responses and the results of the interpretation from the measurements that verify structural integrity. The surveillance program is described in Subsection 5.4.7.

7. Incore Instrument Guide Tube Assembly:

The incore instrument guide tube assemblies guide the incore instrument assemblies from the instrument penetrations in the reactor vessel bottom head to the instrument tubes in the fuel assemblies. Horizontal clearances are provided between the reactor vessel instrument penetrations and the instrument guide tubes in the flow distributor to accommodate misalignment. The 52 incore instrument guide tubes are designed so they will not be affected by the core drop described in Subsection 4.2.2.

8. Internals Vent Valves:

Internals vent valves are installed in the core support shield to prevent a pressure unbalance which might interfere with core cooling following a postulated inlet pipe rupture. Under all normal operating conditions, the vent valve will be closed. In the unlikely event of a pipe rupture in the cold leg of the reactor loop, the valves will open to permit steam generated in the core to flow directly to the leak, and will permit the core to be rapidly re-covered and adequately cooled after emergency core coolant has been supplied to the reactor vessel. For small breaks, especially the double-ended break of a core flooding line, the vent valves allow the system to maintain core integrity without any modification to the Emergency Core Cooling System (ECCS) design. For large breaks, the vent valves allow higher flooding rates by preventing excessive pressure increase in the upper plenum. The vent valves improve the performance of the ECCS during the course of a Loss of Coolant Accident (LOCA). The number and size of the vent valves have been shown, through analysis of large and small breaks, (Subsection 6.3.3) to produce acceptable results. The design of the internals vent valve is shown in Figures 4.2-6 and 4.2-7.

Each valve assembly consists of a hinged disc, valve body with sealing surfaces, split-retaining ring, and fasteners. Each valve assembly is installed into a machined mounting ring integrally welded in the core support shield wall. The mounting ring contains the necessary features to retain and seal the perimeter of the valve assembly. Also, the mounting ring includes an alignment device to

maintain the correct orientation of the valve assembly for hinged-disc operation. Each valve assembly will be remotely handled as a unit for removal or installation. Valve component parts, including the disc, are of captured-design to minimize the possibility of loss of parts to the coolant system, and all operating fasteners include a positive locking device. The hinged-disc includes a device for remote inspection of disc function. Vent valve materials are listed in Table 4.2-4.

The vent valve materials were selected on the basis of their corrosion resistance, surface hardness, anti-galling characteristics, and compatibility with mating materials in the reactor coolant environment.

The arrangement consists of four 14-in. inside diameter vent valve assemblies installed in the cylindrical wall of the internals core support shield (refer to Figure 4.2-6). The vent valves are identical to those of the Oconee class reactors with a frictional k-factor of 3.9. The valve centers are coplanar and are 42 in. above the plane of the reactor vessel coolant nozzle centers. In cross section, the valves are spaced around the circumference of the core support shield wall.

The hinge assembly consists of a shaft, two valve body journal receptacles, two valve disc journal receptacles, and four flanged shaft journals (bushings). Loose clearances are used between the shaft and journal inside diameters and between the journal outside diameters and their receptacles. The hinge assembly is shown and the clearance gaps are identified in Figure 4.2-7. The bushing clearances are listed in Table 4.2-3. By observation and comparison of the tabulated clearances and change in clearance, it is apparent that the thermal change is minimal (10% or less) and will not affect the disc venting function. Moreover the results given are very conservative because they are based on a temperature differential of 510°F, and the actual temperature differential would be closer to a 10°F to 60°F range.

The valve disc hinge journal contains integral exercise lugs for remote operation of the disc with the valve installed in the core support shield.

The hinge assembly provides eight loose rotational clearances and two end clearances to minimize any possibility of impairment of disc-free motion in service. In the event that one rotational clearance should bind in service, seven loose rotational clearances would remain to allow unhampered disc-free motion. In the worst case, at least three clearances of a particular combination must bind or seize solidly to adversely affect the valve disc-free motion.

In addition, the valve disc hinge loose clearances permit disc self-alignment so that the external differential pressure adjusts the disc seal face to the valve body seal face. This feature minimized the possibility of increased leakage and pressure-induced deflection loadings on the hinge parts in service.

The external side of the disc is contoured to absorb the impact load of the disc on the reactor vessel inside wall without transmitting excessive impact loads to the hinge parts as a result of a loss-of-coolant accident.

4.2.2.3 Evaluation of Internals Vent Valve

In the event of a postulated reactor cold leg break, a vapor lock problem could arise if water is trapped in the steam generator blocking the flow of steam from the top of the reactor vessel to the break. Under this condition, the steam pressure at the top of the reactor would rise and force the steam bubbles through the water leg in the bottom of the steam generator. This same differential pressure that develops a water leg in the steam generator will develop a water leg in the reactor vessel which could lead to uncovering of the core.

The most direct solution to this problem is to equalize the pressure across the core support shield, thus eliminating the depression of the water level in the core. This was accomplished by installing vent valves in the core support shield to provide direct communication between the top of the core and the coolant inlet annulus. These vent valves open on a very low-pressure differential to allow steam generated in the core to flow directly to the leak from the reactor vessel. Although the flow path in the steam generator is blocked, this is of no consequence since there is an adequate flow path to remove the steam being generated in the core.

During the vent valve conceptual design phase, criteria were established for valves for this service. The design criteria were (1) functional integrity, (2) structural integrity, (3) remote handling capability, (4) individual part-capture capability, (5) functional reliability, (6) structural reliability, and (7) leak integrity through the design life. The design criteria resulted in the selection of the hinged-disc (swing-disc) check valve, which was considered suitable for further development.

Because of the unique purpose and application of this valve, B&W recognized the need for a complete detailed design and development program to determine valve performance under nuclear service conditions. This program included both analytical and experimental methods of developing data. It was performed primarily by B&W and the selected valve vendor or his subcontractors.

Vent valve preliminary design drawings were prepared and analyzed both by B&W and the vendor/subcontractor. Specifications and drawings were prepared, and orders were placed with the vendor for the design, development, fabrication, and test of a full-size prototype vent valve. The prototype valve was completed and subjected to the tests described in Subsection 4.2.2.4. All testing was successfully completed, and minor problems encountered during valve assembly handling or use were corrected to arrive at the final design for the production valve.

The only significant problem encountered during test was seizing of one jackscrew. This was attributable to an excessive thickness of “Electrolyze” which spalled off the screw threads. This problem was corrected by reducing the specified “Electrolyze” thickness from 0.0015” to 0.0004” max., and no further galling was encountered. To further enhance resistance to galling, the final design jackscrew has a 1-1/8”-8 Acme thread form instead of a 1”-12 UNF and the material is an age hardened corrosion resistant alloy instead of 410 S.S. No further jackscrew problems have occurred or are anticipated on the basis that the surfaces are separated by the low friction “Electrolyze,” different materials of different hardnesses are used, loose fits are employed, and thread contact stresses are low (3775 psi).

The final design of this valve is shown in Figure 4.2-6. The valve disc hangs closed in its natural position to seal against a flat, stainless steel seat inclined five degrees from vertical to prevent flow from the inlet coolant annulus to the plenum assembly above the core. In the event of a LOCA, the reverse pressure differential will open the valves. At all times during normal reactor operation, the pressure in the coolant annulus on the outside of the core support shield

is greater than the pressure in the plenum assembly on the inside of the core support shield. Accordingly, the vent valves will be held closed during normal operation. With four reactor coolant pumps operating, the normal pressure differential is 42 psi, resulting in approximately 6000 pounds closing force on the vent valve. Similarly, for three pump operation and for one pump operation in each coolant loop the approximate vent valve closing force is 3375 pounds and 1500 pounds, respectively.

Under accident conditions, the valve will begin to open when a pressure differential of 0.15 psi develops in a direction opposite to the normal pressure differential. At this point, the opening force on the valve counteracts the natural closing force. With this pressure differential, the water level in the core would be above the top of the core. In order for the core to be half uncovered, assuming solid water in the bottom half of the core, a pressure differential of 3.7 psi would have to be developed. This would provide an opening force greater than 10 times that required to open the valve completely. This is a conservative limit since it assumes equal density in the core and the annulus surrounding the core. The hot, steam-water mixture in the core will have a density much less than that of the cold water in the annulus, and somewhat greater pressure differentials could be tolerated before the core is more than half uncovered.

An analytical evaluation was made of the performance of the vent valves in the core support shield. This analysis demonstrated that adequate steam relief exists so that core cooling will be accomplished and is described in detail in Subsection 6.3.3.1.

The behavior of the valve disc during LOCA conditions was investigated, and the rather complex dynamic behavior of the disc during LOCA was analyzed as a series of simpler models which provide conservative predictions of peak stresses and deflections.

The valve disc remains closed initially for the LOCA hot leg (36” pipe) case, and the disc opening on subsequent differential pulses is less than one-half of the initial disc to vessel wall impact velocity for the LOCA cold leg (28” pipe) case. Therefore, the disc motion and initial impact with the vessel inside wall was chosen as the worst case and the only one requiring consideration. The cold-leg LOCA pressure time history acting on the disc was approximated by a piecewise linear time function. The moment due to pressure was equated to the rotary inertia of the disc to determine the velocity of impact with the vessel inside wall.

The model chosen for the initial impact consisted of three effective springs and two masses to represent the disc with its lug, the compliance of the disc, and the vessel inside wall.

Loads generated on impact were based on the conservation of energy. The stresses obtained for these loads indicated that the elastic model assuming conservation of energy was not valid and that the impact must assume plastic deformation.

A plastic analysis provided the following information:

a. Crush deformation of lug after disc corner contacts the vessel wall is predicted to be 0.165 inches.

b. The total deformation of lug from contact with the vessel wall until disc assembly motion is arrested is predicted to be 0.483 inches.

c. The total angular deformation at the plastic hinge is predicted to be 0.016 radians.

d. An analysis was performed on the reactor vessel wall for disc assembly impact, and the results indicate that while the stainless steel cladding is deformed locally the reactor maintains its structural and pressure boundary integrity.

Because of conservative assumptions used in the above plastic analysis, actual deformations will be considerably less than the above predicted values. Although plastic deformation may occur as predicted above on impact, the disc will retain its structural integrity. Plastic deformation of the disc dissipates the stored kinetic energy stored in the disc effectively; thus, the energy available for rebound is less than 1 percent of the initial impact energy and is too low to overcome the pressure differential and cause impact on the valve body. Disc and body hinge components were analyzed for worst case disc impact loadings and the resulting stresses were found to be less than the allowable limits. A comparison of the results showed the initial cold leg LOCA disc-wall impact to result in the only significant loading to produce a plastic deformation, which absorbs most of the kinetic energy of the disc, resulting in a very low rebound velocity. As a consequence, the initial impact is the most violent and the only one requiring consideration. Therefore, the valve disc free-motion (venting) function will be unaffected.

From the above, it is concluded that vent valve performance will not be impaired during the course of an accident because disc-free motion part stresses remain within allowable limits, disc structural integrity is maintained, vessel pressure boundary integrity is maintained, and plastic deformation of the disc seating surface improves the venting function.

With reference to Figure 4.2-6, each jackscrew assembly consists of a jackscrew, internally splined mating nut ring, nut ring spring, and capture cover and cover attachment fasteners (socket head cap screws). In the figure, the splined nut ring and its spring are hidden from view by the capture cover. The potential for loss of jackscrew assembly parts during the plant lifetime is considered remote on the basis that the jackscrews and capture parts are accessible for visual inspection during scheduled refueling outages. A jackscrew loss is considered remote because a failure in service is highly improbable with the low compressive load (1000) psi involved, and the jackscrew is retained in the valve body by a central shoulder and the ends are threaded into the retaining rings. An in-service failure of the splined nut ring and its spring is remote because these parts are subjected to little or no load, and even if they did fail all parts would be retained within the capture cover. Capture cover failure and loss is highly improbable on the same basis that it is not loaded in service. The capture cover is attached to the upper retaining ring by socket head cap screws which are lock welded to the cover at installation. By design, these screws are retention rather than structural devices and are not loaded in service. These screws do not require a pre-load to hold the formed cover in place; therefore, a loss of pre-load by lock welding would not jeopardize the cover or screw installation or structural integrity. Two fillet welds 180° apart are used to lock weld each screw head to the capture cover, and in the absence of loads on both the cover and screws the likelihood of lock weld failure and loss of screw heads is considered remote. With the capability to inventory these cap screw heads visually at scheduled refuelings, any problem related to the loss of these screws would be apparent early in the plant life and the valve assemblies could be removed for corrective action.

The internals vent valves are described, including materials and hinge part loose clearances, in Subsection 4.2.2.2.

The internals vent valves have been tested for ability to withstand the effects of vibratory excitations and for other functional characteristics as described in Subsection 4.2.2.4.

4.2.2.4 Internals Tests and Inspection

The internals upper and lower plenum hydraulic design is evaluated and guided by the results from the 1/6 scale model flow test which is described in Subsection 4.4.2.6. These test results have guided the design to obtain minimum flow maldistribution, and test data allowed verification of vessel flow and pressure drops.

The effects of internals misalignment was evaluated on the basis of the test results from the CRDL tests described in Subsection 4.4.2.6. These test results, correlated with the internals guide tube design, ensure that the CRA can be inserted at specified rates under conditions of maximum misalignment.

Internals shop fabrication quality control tests, inspection, procedures, and methods are similar to those for the pressure vessel described in Subsection 17.1.3 of the FSAR. The internals surveillance specimen holder tubes and the material irradiation program are described in Subsection 5.4.7.

A listing is included herewith for all internals nondestructive examinations and inspections with applicable codes or standards applicable to all core structural support material of various forms. In addition, one or more of these examinations is performed on materials or processes which are used for functions other than structural support (i.e. alignment dowels, etc.) so that virtually 100 percent of the completed internals and parts are included in the listing. Internals raw materials are purchased to ASME Code Section II or ASTM material specifications. Certified material test reports are obtained and retained to substantiate the material chemical and physical properties. All internals materials are purchased and obtained to a low cobalt limitation. The ASME Code Section III, as applicable for Class A vessels, is generally specified as the requirement for reference level non-destructive examination and acceptance. In isolated instances when ASME III cannot be applied, the appropriate ASTM Specifications for nondestructive testing are imposed. All welders performing weld operations on internals are qualified in accordance with ASME Code Section IX applicable Edition and Addenda. The primary purpose of the following list of nondestructive tests is to locate, define, and determine the size of material defects to allow an evaluation of defect, acceptance, rejection, or repair. Repaired defects are similarly inspected as required by applicable codes.

a. Ultrasonic Examination

    1. Wrought or forged raw material forms are 100 percent inspected throughout the entire material volume to ASME III, Class A.

    2. Personnel conducting these examinations are trained and qualified.

b. Radiographic Examination (includes X-ray or radioactive sources)

    1. Cast raw material forms are 100 percent inspected to ASME III Class A or ASTM.

    2. All circumferential full penetration structural weld joints which support the core are 100 percent inspected to ASME III Class A.

    3. All radioqraphs are reviewed by qualified personnel who are trained in their interpretation.

c. Liquid Penetrant Examination

1. Cast form raw material surfaces are 100 percent inspected to ASME III Class A or ASTM.

2. Full penetration non-radiographic or partial penetration structural welds are inspected by examination of root and cover passes to ASME III Class A.

3. All circumferential full penetration structural weld joints which support the core have cover passes inspected to ASME III Class A.

4. Personnel conducting these examinations are trained and qualified.

d. Visual (5X Magnification) Examination

This examination is performed in accordance with and results accepted on the basis of a B&W Quality Control Specification which complies with NAV-SHIPS 250-1500-1. Each entire weld pass and adjacent base metal are inspected prior to the next pass from the root to and including the cover passes.

1. Partial penetration non-radiographically or non-ultrasonically feasible structural weld joints are 100 percent inspected to the above specification.

2. Partial or full penetration attachment weld joints for non-structural materials or parts are 100 percent inspected to the above specification.

3. Partial or full penetration weld joints for attachment of mechanical devices which lock and retain structural fasteners.

4. Personnel conducting these examinations are trained and qualified.

After completion of shop fabrication, the internals components are shopfitted and assembled to final design requirements. The assembled internals components undergo a final shop fitting and alignment of the internals with the “as built” dimensions of the reactor vessel. Dummy fuel and CRA’s are used to ensure that ample clearances exist between the fuel and internals structures guide tubes to allow free movement of the CRA throughout its full stroke length in various core locations. Fuel assembly mating fit is checked at all core locations. The dummy fuel and CRA’s are identical to the production components except that they are manufactured to the most adverse tolerance space envelope, and they contain no fissionable or absorber materials.

All internal components can be removed from the reactor vessel to allow inspection of all vessel interior surfaces. Internals components’ surfaces can be inspected when the internals are removed to the canal underwater storage location.

The internals vent valves were designed to relieve the pressure generated by steaming in the core following a LOCA so that the core remains sufficiently cooled. The valves were designed to withstand the forces resulting from rupture of either a reactor coolant inlet or outlet pipe. To verify the structural adequacy of the valves to withstand the pressure forces and perform the venting function, the following tests were performed:

a. A full-size prototype valve assembly (valve disc retaining mechanism and valve body) was hydrostatically tested to the maximum pressure expected to result during the blowdown.

b. Sufficient tests were conducted at zero pressure to determine the frictional loads in the hinge assembly, the inertia of the valve disc, and the disc rebound resulting from impact of the disc on the seat so that the valve response to cyclic blowdown forces may be determined analytically.

c. A prototype valve assembly was pressurized to determine the pressure differential required to cause the valve disc to begin to open. A determination of the pressure differential required to open the valve disc to its maximum open position was simulated by mechanical means.

d. A prototype valve assembly was successfully installed and removed remotely in a test stand to confirm the adequacy of the vent valve handling tool.

e. A 1/6 scale model valve disc closing force (excluding gravity) test is described in Subsection 4.4.2.6.

f. The full-size prototype valve's response to vibration was determined experimentally to verify prior analytical results which indicated that the valve disc would not move relative to the body seal face as a result of vibration caused by transmission of core support shield vibrations. The prototype valve was mounted in a test fixture which duplicated the method of valve mounting in the core support shield. The test fixture with valve installed was attached to a vibration test machine and excited sinusoidally through a range of frequencies which encompassed those which may reasonably be anticipated for the core support shield during reactor operation. The relative motion between the valve disc and seat was monitored and recorded during test. The test results indicated that there was no relative motion of the valve to its seat for conditions simulating operating conditions. After no relative motion was observed or recorded during test, the valve disc was manually forced open during test to observe its response. The disc closed with impact on its seat, rebounded open, and reseated without any adverse effects to valve seal surfaces, characteristics, or performances. From this oscillograph record, the natural frequency of the valve disc was conservatively calculated as approximately 1500 cps; whereas, the range of frequencies for the Davis-Besse system (including internals components) has been established as 15 to 160 cps. These frequencies are separated by an ample margin to conclude that no relative motion between the valve disc and its seat will occur during normal reactor operation.

Each production valve was subjected to tests (b) and (c) above except that no additional analysis were performed in conjunction with test (b).

The valve disc, hinge shaft, shaft journals (bushings), disc journal receptacles, and valve body journal receptacles have been designed to withstand without failure the internal and external differential pressure loadings resulting from a loss-of-coolant accident. These valve materials are non-destructively tested and accepted in accordance with the ASME Code III requirements for Class A vessels as a reference quality level.

During scheduled refueling outages after the reactor vessel head and the internals plenum assembly have been removed, the vent valves are accessible for visual and mechanical

inspection. A hook tool will be provided to engage with the valve disc exercise lug described in Subsection 4.2.2.2. With the aid of this tool, the valve disc will be manually exercised to evaluate the disc freedom. The hinge design incorporates special features, as described in Subsection 4.2.2.2 to minimize the possibility of valve disc motion impairment during its service life. The valve disc can be raised with the aid of the hook tool providing the capability to perform remote visual inspection of the vent valves for evaluation of seating surfaces should it become necessary.

Remote installation and removal of the vent valve assemblies if required is performed with the aid of the vent valve handling tool which includes unlocking and operating features for the retaining ring jackscrews.

An inspection of hinge parts is not planned until such time as a valve assembly is removed because its free-disc motion has been impaired. In the unlikely event that a hinge part should fail during normal operation, the most significant indication of such a failure would be a change in the free-disc motion as a result of altered rotational clearances.

4.2.3 Reactivity Control Systems

There are two reactivity control systems, the control rod drive control system and the boron "feed-and-bleed" control system.

4.2.3.1 Description

4.2.3.1.1 Control Rod Drive Control System (CRDCS)

The discussion of the Control Rod Drive (CRD) Control System in this section is limited to a mechanical description of the control rod assemblies, axial power shaping rod assemblies, and the CRD mechanism. Further discussion of CRD control system design and operation is given in Chapter 7.

4.2.3.1.1.1 Control Rod Assembly (CRA) and Extended Life Control Rod Assembly (ELCRA)

Each control rod assembly type (Figure 4.2-8) has 16 control rods, a stainless steel spider, and a female coupling. The 16 control rods are attached to the spider by means of a nut threaded to the upper shank of each rod. After assembly, all nuts are lock welded. The control rod drive is coupled to the CRA by a bayonet type connection. Full length guidance for the CRA is provided by the control rod guide tube of the upper plenum assembly and by the fuel assembly guide tubes. The CRA's and guide tubes are designed with adequate flexibility and clearances to permit freedom of motion within the fuel assembly guide tubes throughout the stroke.

Each control rod has a section of neutron absorber material. The absorber material is an alloy of silver-indium-cadmium. The CRA rod is clad in cold-worked type 304 stainless steel tubing. The ELCRA rod is clad in inconel tubing. End pieces are welded to the tubing to form a water- and pressure-tight container for the absorber material. The tubing provides the structural strength of the control rods and prevents corrosion of the absorber material. A spring spacer similar to that in the fuel assembly is used to prevent absorber motion within the cladding during shipping and handling, and to permit differential expansion in service.

Principal data pertaining to the CRA and ELCRA are presented in Table 4.2-6.

4.2.3.1.1.2 Axial Power Shaping Rod Assembly (APSRA) Black and Gray Type

Both types of APSRAs have the same mechanical design features. Commencing with cycle 6, the original design or "black" APSRAs are no longer in use, since they were replaced with the "gray" APSRAs.

Each axial power shaping rod assembly (Figure 4.2-9) has 16 axial power shaping rods, a stainless steel spider, and a female coupling. The 16 rods are attached to the spider by means of a nut threaded to the upper shank of each rod. After assembly all nuts are lock welded. The axial power shaping rod drive is coupled to the APSRA by a bayonet connection. The female couplings of the APSRA and CRA have slight dimensional differences to ensure that each type of rod can only be coupled to the correct type of drive mechanism.

When the APSRA is inserted into the fuel assembly it is guided by the guide tubes of the fuel assembly. Full length guidance of the APSRA is provided by the control rod guide tube of the upper assembly. As the full out position of the control rod drive stroke, the lower end of the APSRA remains within the fuel assembly guide tube to maintain the continuity of guidance throughout the rod travel length. The APSRA's are designed to permit maximum conformity with the fuel assembly guide tube throughout travel.

Each axial power shaping rod has a section of neutron absorber material which is clad in cold-worked, type 304 stainless steel tubing. This tubing provides the structural strength for the axial power shaping rods and prevents corrosion of the absorber material. The absorber section is sealed by both an internal plug and an end plug shown in Figure 4.2-9. The original or "black" APSRAs contained an absorber which is an alloy of silver-indium-cadmium. The "gray" APSRAs design contains an absorber which is an Inconel alloy. The section of tubing above the absorber is vented so it is always filled with borated water, and consequently the pressure differential across the tube wall is negligible. Pertinent data for both types of design of APSRAs are shown in Table 4.2-7.

4.2.3.1.1.3 Control Rod Drive (CRD) Mechanism

The shim safety CRD mechanism (B&W type "C" CRDM), is an electro-mechanical device consisting of an electrically driven, rotating nut assembly (rotor) within a pressure vessel; a four-pole, six-winding stator; and a leadscrew that converts rotary motion of the nut to linear travel of the leadscrew and CRA.

During normal operation, the drive is used to raise, lower, or maintain control rod position within the reactor in response to electrical signals from a CRD motor control system (control system). The control system provides a DC sequentially programmed input to the four-pole, reluctance-type drive motor to produce a rotating magnetic field for the rotor assembly. The rotor assembly is split so that when power is applied to the stator, the rotor assembly segment arms pivot to mechanically engage the roller nuts with the leadscrew threads. As the stator coils are sequenced, the rotor rotates (steps) to a new position. There are 12 mechanical steps for each electrical revolution, and two electrical revolutions result in one mechanical revolution of the rotor. One rotor revolution results in 3/4-inch leadscrew and control rod translation. The power supply provides pulse rates for run and jog. Run speed is 30 inches per minute of leadscrew and control rod motion, and jog speed is 3 inches per minute. The switching sequence from the power supply establishes the direction of rotation.

The drive is designed to "trip" whenever power to the stator is interrupted. During such a power loss, the rotor assembly segment arms pivot, releasing the mechanical contact between the

roller nut and the leadscrew. The leadscrew and control rod are then pulled into the reactor core to the full-in position by gravity. A trip may be manually initiated at the control board, by the reactor protective system, or in general, through a loss of power to the stator.

Unique design features of the drive include:

1. A fast trip response whenever power is interrupted to the stator.

2. Exclusive use of static-type seals; no rotary or dynamic seals are used.

3. A leadscrew coupling design that provides easy attachment of the leadscrew to the reactor control rod from a position external to the reactor vessel.

4. Electrical components and connections that are mounted external to the reactor vessel environment and can easily be removed for maintenance.

The Axial Power Shaping Rod (APSR) drive has essentially the same features as the shim safety CRD except for the trip function. The APSR drive is modified so that the roller nut assembly cannot disengage from the leadscrew on a loss of power to the stator. A brake is designed into the APSR drive that prevents motion of the leadscrew-CRA when power is interrupted to the stator.

Additional information concerning the type “C” CRDM is provided in B&W Topical Report BAW-10029A, Rev. 3.

4.2.3.1.1.4 Burnable Poison Rod Assembly (BPRA)

The initial design of the Davis-Besse core included the utilization of 68 Burnable Poison Rod Assemblies (BPRA’s). The BPRA’s, in conjunction with the CRA’s and the Boron Reactivity Control System, provided a supplemental method for core reactivity control.

As a result of operational problems encountered with the BPRA’s at a similar B&W operating reactor, Crystal River, all 68 BPRA’s were removed from the Davis-Besse core. Necessary changes to operating conditions and fuel loading patterns were implemented. A safety evaluation was performed by B&W of the changes necessitated by removal of the 68 BPRA’s and is documented in B&W topical report BAW-1489, Rev. 1 Attachment 1 to Application to Amend Operating License for Removal of Burnable Poison Rod and Orifice Rod Assemblies – Davis-Besse Nuclear Generating Station Unit 1 (May 1978).

Commencing with Cycle 5, due to increased reactor operating cycle lengths, BPRA’s were again used to control core reactivity. The upper end fitting design of those fuel assemblies containing BPRA’s was changed such that the BPRA retention mechanism is built into each fuel assembly and retainer assemblies are no longer required. Design details for the BPRAs are in the Cycle 5 Reload Report, BAW-1827. The number of BPRAs for subsequent cycles is indicated in the corresponding Reload Reports. Commencing with Cycle 12, a transition from the use of BPRAs to the inclusion of an Integral Absorber, gadolinia, within the fuel rods began. No BPRAs have been used since Cycle 12, however, their use in future cycles remains a core design option.

4.2.3.1.2 Boron Reactivity Control

Boron in solution is used to control the following relatively slow-moving reactivity changes:

a. The moderator reactivity in going from ambient to operating temperatures.

b. Equilibrium xenon and samarium.

c. The excess reactivity required for fuel burnup and fission product buildup throughout cycle life.

In the feed and bleed operation, boric acid from the chemical addition system is pumped to the makeup tank where it is then injected into the reactor coolant system by the makeup system. During emergency shutdown operations boric acid from the BWST would be injected into the core by the HPI pumps.

The description of the systems used to supply and control boric acid is found in Subsection 9.3.6.

4.2.3.2 Design Bases

a. Mechanical Insertion Requirements

The Control Rod Drive (CRD) provides for controlled insertion of the CRAs into the reactor core. The drives are also capable of trip for emergency reactor conditions. When the drive mechanisms are required to respond to a trip signal, the action of the control rod drive system and the drive mechanism shall result in a positive, nonreversible initiation of the trip function. The trip command shall have priority over all other commands.

b. Materials Selection

The materials from which the drive mechanisms are fabricated are selected based on the function of the individual part, the environment in which it will operate, and the requirements of applicable Codes. The factors of wear, galling, corrosion and/or radiation resistance, and susceptibility to stress-corrosion cracking are of special importance for parts exposed to the reactor coolant. Quality standards for material selection, fabrication, and inspection are specified to ensure the safety functions of the housing essential to accident prevention. Materials conform to ASME Section II, Material Specifications. All welding is performed by personnel qualified under the ASME Code, Section IX, Welding Qualifications.

The control rod drive mechanism pressure boundary components are designed, fabricated and tested in accordance with ASME Section III which renders possibility of functional failure to a minimal. Wherever possible in the design of the internal working parts of the drive mechanism, acceptable stress levels at appropriate temperatures for materials used were taken from the ASME Boiler & Pressure Vessel Code, Section 3. When appropriate properties were not available from the code, they were obtained from other reputable sources including AMS specifications, ASTM standards and vendors' data. This practice lends itself to the minimization of the possibility of functional failure.

c. Positioning Requirements

The CRD control system provides for controlled withdrawal, insertion, and holding of the CRAs to establish and maintain the power level required for a given reactor coolant boron concentration. Continuous rod position indication as well as full-in and full-out position indication, are provided for each CRD.

For the design basis of the boron reactivity control system see Subsection 9.3.6.

4.2.3.3 Evaluation

a. Material Adequacy Throughout Design Life

The prototype CRD mechanism underwent a test program at Diamond Power Specialty Corporation. The test was conducted under simulated reactor operating conditions of pressure, temperature, and water chemistry. A dummy-weight assembly was used to simulate the weight of the drive line components in an operating reactor installation. The life testing of the mechanism was designed to duplicate the stroke, travel, and reactor trips expected in a 20-year operational life in regulating rod service.

After the life test, the drive mechanism was disassembled and examined for wear. For all components except the roller nuts the measured wear was increased by a factor of four. The functional and structural adequacy of the component was then re-examined, using the resultant wear in the stress analysis. A factor of two was applied for the roller nuts, and in all cases, the wear did not adversely affect the functional or structural integrity of the mechanism.

In addition to the wear analysis of the mechanism, the internal components of the drive were carefully examined for indications of corrosion, failure, cracking, etc. All pressure boundary components were liquid-penetrant inspected to detect signs of failure.

The overall inspection of the materials produced the following results:

1. No evidence of corrosion.

2. No evidence of cracking or failure.

3. Wear values showing good compatibility between the materials of wearing surfaces.

4. Generally good overall appearance of the components.

b. Results of Dimensional and Tolerance Analysis

The life test at Diamond Power was conducted under 100% misalignment conditions. The actual magnitude of the 100% misalignment was determined by a study of the design tolerances of the reactor vessel, reactor internals, and fuel assembly, as explained in B&W Topical Report BAW-10029A, Rev. 3.

Throughout the entire life test program, trip times remained well below the specified requirements. Wear of critical components was examined. No adverse wear was experienced.

c. Analysis of Pressure Forces That Could Eject Rods

As a result of an accident, the control rods could theoretically be ejected, which would suddenly vent reactor pressure to the containment vessel. The resultant pressure differential could possibly act to withdraw the CRA.

Release of reactor pressure could conceivably occur in one of the following ways:

a. A complete shear in one of the two threaded areas of the closure insert assembly--this part is designed, fabricated, and inspected according to Section III of the ASME Code for Nuclear Power Plant Components. This ensures a high margin for safety and makes this shear phenomenon highly unlikely.

b. A failure of one of the circumferential welds--this occurrence is also highly improbable. All welds in the control rod drive mechanism are controlled by Sections III and IX of the ASME Code. All welds are qualified, inspected, and appropriately documented.

c. A shear of the holddown bolts that attach the drive mechanism to the reactor flange--the possibility of this event is minimal. The bolts are also a Code item conforming to ASME Section III, designed to preclude failure.

A detailed evaluation of the consequences of a CRA ejection event is provided in Subsection 15.4.3.

4.2.3.4 Test and Inspections

Control Rod Drive Mechanism:

Surveillance requirements and functional tests of the eight control rod groups are described in the Technical Specifications.

Control and Axial Power Shaping Assemblies:

Control and axial power shaping assemblies and their constituent components are tested and inspected throughout manufacture to ensure the integrity of the assembly and the absorber rods.

The tubing used for Control Rod (CR) and Axial Power Shaping Rod (APSR) cladding is inspected for inside and outside diameters and for minimum wall thickness, nondestructively tested for defects using ultrasonic inspection, and inspected for compliance with the cleanliness specifications--all on a 100% basis.

The finished CR and APSR closure welds are 100% vacuum-leak tested and visually inspected at 6X magnification, and the CRs and APSRs are also 100% inspected for surface defects.

The completed CR and APSR assemblies are dimensionally inspected on a statistical basis to ensure that dimensional specifications are met. The CR and APSR spiders are tested on a

100% basis to ensure proper alignment and engagement with the respective drive couplings. Each completed CR and APSR assembly is inspected (full length) in a specially designed fixture that simulates the fuel assembly guide tubes.

4.2.3.5 Instrumentation

a. Position Indication - The CRD mechanism position indication system is described in Chapter 7.

b. Stator Temperature - Stator temperature is monitored by a thermocouple. An alarm is actuated if the temperature reaches a predetermined setpoint, and a mandatory shutdown is encountered at 180°F. Each CRD stator is equipped with two thermocouples although only one is monitored at a time.

4.2.3.5.1 Mechanical Reactivity Control System

The Control Rod Drive Mechanism Control System (CRDMCS) maneuvers each Control Rod (CR) via a Control Rod Drive Mechanism (CRDM) to control reactivity. Each CRDM provides position signals indicating its CR's position to the CRDMCS. These position signals are used for indication and control functions by the CRDMCS (See Subsection 7.7.1.3 for details). Each CRDM provides a stator temperature signal to the computer system. This temperature signal is monitored to detect abnormal increases in a CRDM's stator temperature to prevent damage to its stator.

4.2.3.5.2 Reactivity Monitoring

There are three reactivity monitoring systems. They are the Incore Monitoring System (IMS), the out-of-core Nuclear Instrumentation (NI) and the Ex-Core Neutron Flux Detectors. The NI is part of the NI & RPS.

The NI provides three overlapping ranges of out-of-core monitored neutron flux level indication. The first two (source and intermediate ranges) are used for startup and shutdown indication. The last (power range) is used for operating indication. See Section 7.8 for details.

The IMS provides incore monitored neutron flux level indication. This indicates core performance. See Section 7.9 for details.

The Ex-Core Neutron Flux Detectors provide source range and wide range flux level indication at the post accident racks located in the main control room. See Section 7.13.3.11 for details.

4.2.3.5.3 Chemical Reactivity Control

The instrumentation provided for the chemical reactivity control system as described for the makeup system, is essentially the makeup flow integrator (batch controller). The batch controller serves as the element of control for changing boron concentration in the primary coolant. The operation of the batch controller is described in Subsection 9.3.4.2.2.

TABLE 4.2-1

Fuel Assembly Dimensions and Materials

Item	Material	Dimensions, in.
Fuel Rod		
Fuel	See Appendix 4B	See Appendix 4B
Cladding	See Appendix 4B	See Appendix 4B
Fuel rod pitch	--	See Appendix 4B
Active fuel length	See Appendix 4B	See Appendix 4B
Nom. fuel-cladding gap (BOL)	--	Note (1)
Fuel Assembly		
FA pitch	--	See Appendix 4B
Overall length	--	
CR guide tube	See Appendix 4B	See Appendix 4B
Instr tube	See Appendix 4B	See Appendix 4B
End fittings	See Appendix 4B	--
Spacer grid strips	See Appendix 4B	See Appendix 4B
Spacer sleeve	See Appendix 4B	See Appendix 4B
Dummy Fuel Rod	See Appendix 4B	See Appendix 4B

Note: (1) (Cladding ID - Fuel OD)/2
(2) Deleted

TABLE 4.2-2

Cladding Circumferential Stresses

Case	P(external) psia	P(internal) psia	T(clad) °F	σ(bending)+ σ(membrane)	σ(total), psi	Yield strength,[5] psi	Ultimate strength[5] psi
1. BOL-preoperational	2200([1])	705	532	-19,000	-19,000	48,000	57,000
hot standby-0% power	2500[2]	705	532	-23,800	-23,800	48,000	57,000
2. BOL-void section of	2200	1295	650	-10,800	-10,800	45,000	50,000
cladding-100% power	2500	1295	650	-14,800	-14,800	45,000	50,000
3. BOL-void section of	2200	1320	650	-10,500	-10,500	45,000	50,000
cladding-114% power	2500	1320	650	-14,400	-14,400	45,000	50,000
4. BOL-fueled section of	2200	1295	722	-10,800	-14,400	42,000	44,500
cladding-100% power	2500	1295	722	-14,800	-18,400	42,000	44,500
5. BOL-fueled section of	2200	1320	731	-10,500	-14,500	42,000	42,000
cladding-114%power	2500	1320	731	-14,500	-18,500	42,000	44,000
6. EOL-hot standby-0%	2200	760	532	-18,000	-18,000	48,000	57,000
power	2500	760	532	-22,500	-22,500	48,000	57,000
7. EOL-fueled section of	2200	3300[3]	697	+9,900[4]	+14,100	43,000	46,000
cladding-100% power,	2500	3300[3]	697	+7,200[4]	+11,000	43,000	46,000
design int. pressure							
8. EOL-fueled section of	2200	3300[3]	705	+9,900[4]	+14,400	43,000	46,000
cladding-114% power,	2500	3300[3]	705	+7,200[4]	+11,300	43,000	46,000
design int. pressure							
9. EOL-fueled section of	2200	1908	697	-3,350	-5,700	43,000	46,000
cladding-100% power	2500	1908	697	-6,900	-9,300	43,000	46,000
10. EOL-fueled section	2200	2013	705	-2,100	-4,800	43,000	46,000
of cladding-114% power	2500	2013	705	-5,600	-8,300	43,000	46,000

TABLE 4.2-2 (Continued)

Cladding Circumferential Stresses

Case	P(external) psia	P(internal) psia	T(clad) °F	σ(bending)+ σ(membrane)	σ(total), psi	Yield strength,(5) psi	Ultimate strength(5) psi
11. EOL-immediately	2200	1430	535	- 9,100	- 9,150	48,000	57,000
after shutdown	2500	1430	535	-12,900	-13,000	48,000	57,000
12. EOL at 425F cladding temp	1725	1255	425	- 5,450	- 5,450	50,000	62,500

(1) System operating pressure.

(2) System design pressure.

(3) Fuel rod cladding internal design pressure.

(4) Pressure stress only.

(5) Cladding is specified with 45,000 psi minimum yield strength at 650°F. Minimum room temperature strengths are approximately 75,000 psi yield strength (0.2% offset) and 85,000 psi ultimate tensile strength.

TABLE 4.2-3

Vent Valve Shaft and Bushing Clearances (Inches)

Clearance Gaps are illustrated in Figure 4.2-7

A. Cold Clearance Dimensions at 70°F

Bushing ID	1.500 to 1.505	
Shaft OD	1.490 to 1.485	
	0.010 to 0.020	Clearance (Gaps 1, 2, 7, and 8)
Body ID	2.000 to 2.005	
Bushing OD	1.997 to 1.995	
	0.003 0.010	Clearance (Gaps 3, 4, 5, and 6)

Bushing End Clearance (Gaps 9 and 10)

Body Lugs	5.765 to 5.780	
Disc Hub	4.750 to 4.740	
	1.015 to 1.040	
	0.992 to 0.980	
	0.013 to 0.060	End Clearance (Gaps 9 and 10)
Bushing Flange	0.245 x 4 = 0.980	
	0.248 x 4 = 0.992	

B. Hot Clearance Differential Change From 70 to 580°F

Linear coefficient of thermal expansion of the materials for a temperature change of 70 to 600°F.

Shaft:	A276-Type 431	6.7×10^{-6} in./in./°F
Bushing:	Stellite #6	8.1×10^{-6}
Bodies:	CF8 Stainless	9.82×10^{-6}

$$\Delta T = 580 - 70 = 510°F$$

Shaft	$\Delta D = D \alpha \Delta T = 1.5 (6.7 \times 10^{-6})$	510 = 0.0051
Bushing ID	$= 1.5 (8.1 \times 10^{-6})$	510 = 0.0062
		-0.0011 Increase
Bushing OD	$= 2 (8.1 \times 10^{-6})$	510 = 0.0083
Body ID	$= 2 (9.82 \times 10^{-6})$	510 = 0.0100
		+0.0017 Increase
Bushing Endplay Hot		
CF8 Body	$\Delta L = 1 (9.82 \times 10^{-6})$	510 = 0.0050
Stellite #6 Bushing Flange	$= 1 (8.1 \times 10^{-6})$	510 = 0.0041
		-0.0009 Increase

TABLE 4.2-4

Internals Vent Valve Materials

Valve Part Name	Material and Form	Material Specification No.
Valve Body	304 SS Casting (1)	ASTM A351-CF8
Valve Disc	304 SS Casting (1)	ASTM A351-CF8
Disc Shaft	431 SS Bar (2)	ASTM A276 Type 431 Cond. T
Shaft Bushings	Stellite No. 6	
Retaining Rings (Top and Bottom)	15-5 pH (H 1100) SS Forgings	AMS 5658
Ring Jackscrews	”A-286 Superalloy” SS (3)	AMS 5737 C
Jackscrew Bushings	431 SS Bar	ASTM A276 Type 431 Cond. A
Misc. Fastners, Covers, Locking Devices, etc.	304 SS Plate Bar etc.	ASTM A240, ASTM A276

[1] Carbide solution annealed, C_{max} 0.08%, Co_{max} 0.2%.

[2] Heat treated and tempered to Brinell Hardness Number (BHN) range of 290-320.

[3] Heat treated to produce a BHN of 248 minimum.

TABLE 4.2-5

Stress Summary for Davis-Besse Internals

Comments	Stress type	Case I: Normal Stress intensity, psi	Case I: Normal Allowable stress, psi	Case II: Upset Stress intensity, psi	Case II: Upset Allowable stress, psi	Case III: Faulted Stress intensity, psi	Case III: Faulted Allowable stress, psi
Lower grid plate							
Outlet pipe rupture	P_L+P_b	300	24,000	450	28,800	24,200	37,500
Inlet pipe rupture	P_L+P_b	300	24,000	450	28,800	15,650	37,500
Plenus cover	P_L+P_b	1,300	24,500	2,800	28,000	36,550	37,500
Plenus cylinder reinforcing plate	P_L+P_b	900	23,400	1,000	28,000	14,400	37,500
Upper guide tubes	P_m	125	15,600	250	18,700	6,750	37,500
	P_L+P_b	405	23,400	810	28,000	11,910	37,500
Upper guide tube sectors	P_L+P_b	50	23,400	100	28,000	4,700	37,500
Core support shield top flange							
Subcooled part of LOCA	P_m	700	15,600	1,380	18,700	19,250	37,500
	P_L+P_b	950	23,400	1,400	28,000	30,650	37,500
Saturated part	P_m	700	15,600	1,380	18,700	12,050	37,500
	P_L+P_b	950	23,400	1,400	28,000	33,200	37,500
Core support shield lower flange							
Subcooled part of LOCA	P_m	1,010	15,600	2,125	18,700	16,000	37,500
	P_L+P_b	1,150	23,400	2,650	28,000	18,200	37,500
Saturated part	P_m	1,010	15,600	2,125	18,700	10,800	37,500
	P_L+P_b	1,150	23,400	2,650	28,000	18,650	37,500
Core barrel top flange							
Subcooled part of LOCA	P_m	800	15,600	1,700	18,700	16,000	37,500
	P_L+P_b	850	23,400	1,750	28,000	17,000	37,500
Saturated part	P_m	800	15,600	1,700	18,700	10,600	37,500
	P_L+P_b	850	23,400	1,750	28,000	23,000	37,500
Baffle plates	P_L+P_b	14,800	23,400	14,800	28,000	27,450	37,500
Internal bolts							
Core barrel-core	P_m	40,300	54,000	40,700	82,000	55,000	82,000
Support shield joint	P_L+P_b	46,100	81,000	46,500	82,000	77,900	82,000

NOTE: Qualification of the reactor vessel internal components with the integrated head assembly (IHA) installed is discussed in section 3.9.1.5.

TABLE 4.2-6

Control Rod Assembly and Extended Life Control Rod Assembly Data

Item	Data
Total Number of CRAs and ELCRAs	53
Number of control rods per assembly	16
Outside diameter of control rod	0.440 in.
Cladding thickness (CRA/ELCRA)	0.021 in./0.0225 in.
Cladding material (CRA/ELCRA)	Type 304 SS, cold-worked/Inconel
End plug material (CRA/ELCRA)	Type 304 SS, annealed/Inconel
Spider material	SS Grade CF3M
Poison material	80% Ag, 15% In, 5% Cd
Female coupling material	Type 304 SS, annealed
Length of poison section (CRA/ELCRA)	134 in./139 in.
Stroke of control rod	139 in.

TABLE 4.2-7

Axial Power Shaping Rod Assembly Data

Item	Data
	(Gray/Black[1])
Number of axial power shaping rod assemblies	8
Number of axial power shaping rods per assembly	16
Outside diameter of axial power rod	0.440 in.
Cladding thickness	0.027 in./0.021 in.
Cladding material	Type 304 SS, cold-worked
Plug material	Type 304 SS, annealed
Poison material	Inconel 600/80% Ag, 15%In, 5% Cd
Spider material	SS, Grade CF3M
Female coupling material	Type 304 SS, annealed
Length of poison section	63 in./36 in.
Stroke of APSR	139 in.
Poison Diameter	0.375 in.

[1] The original or “black” APSRAs are no longer in use.

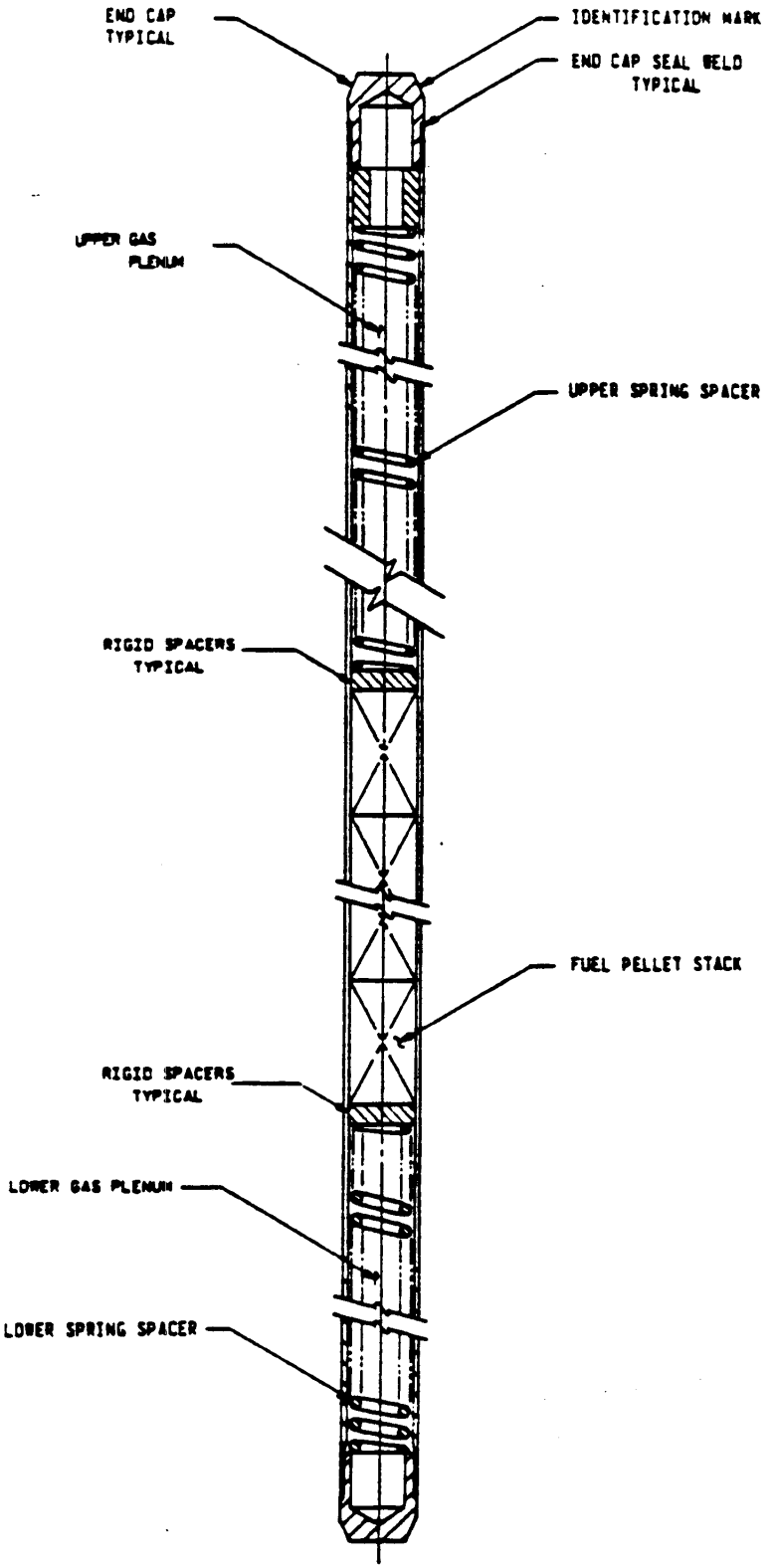

DAVIS-BESSE NUCLEAR POWER STATION
PRESSURIZED FUEL ROD ASSEMBLY
FIGURE 4.2-1

REVISION 0
JULY 1982

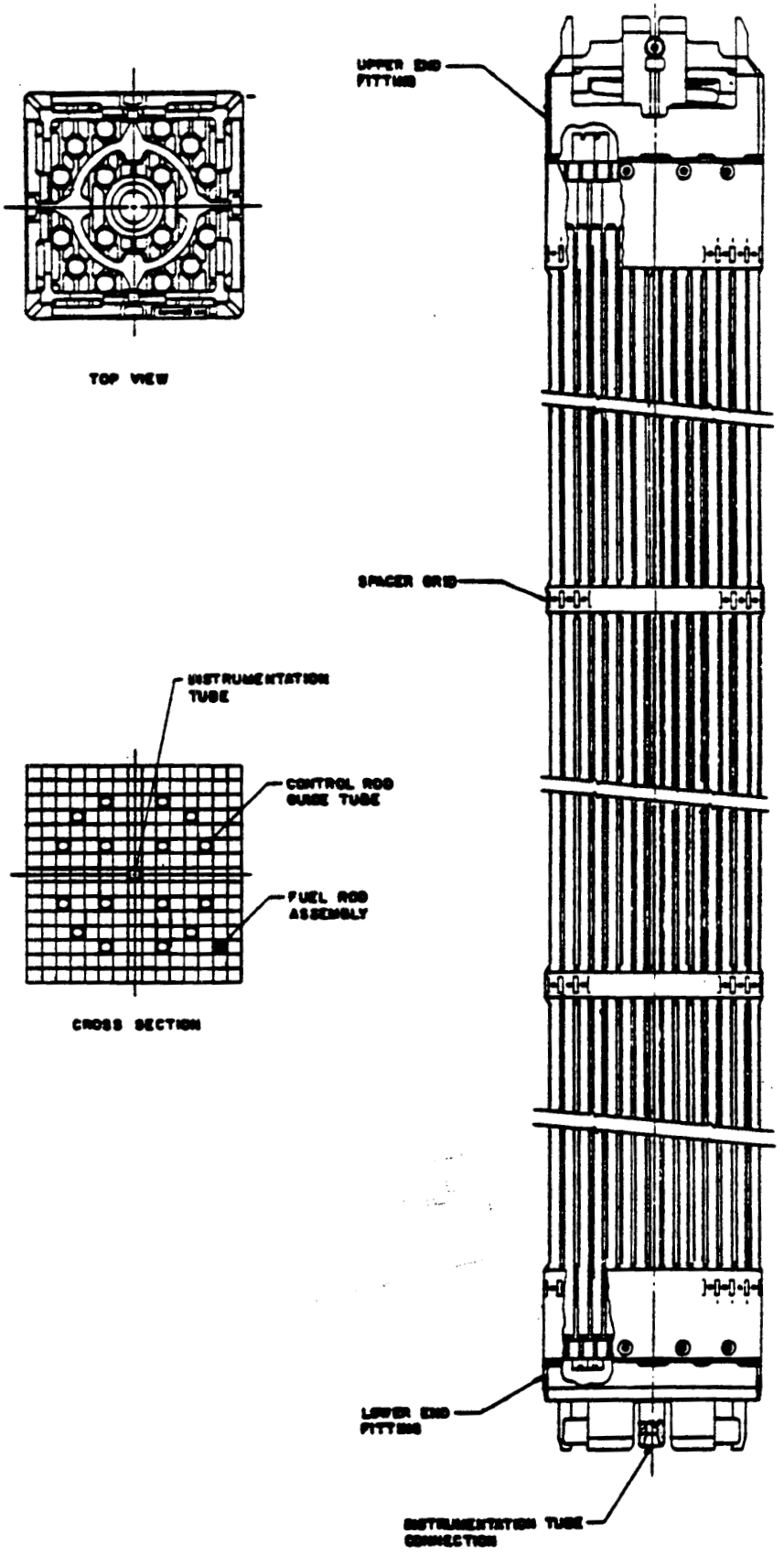

DAVIS-BESSE NUCLEAR POWER STATION
FUEL ASSEMBLY
FIGURE 4.2-2

REVISION 0
JULY 1982

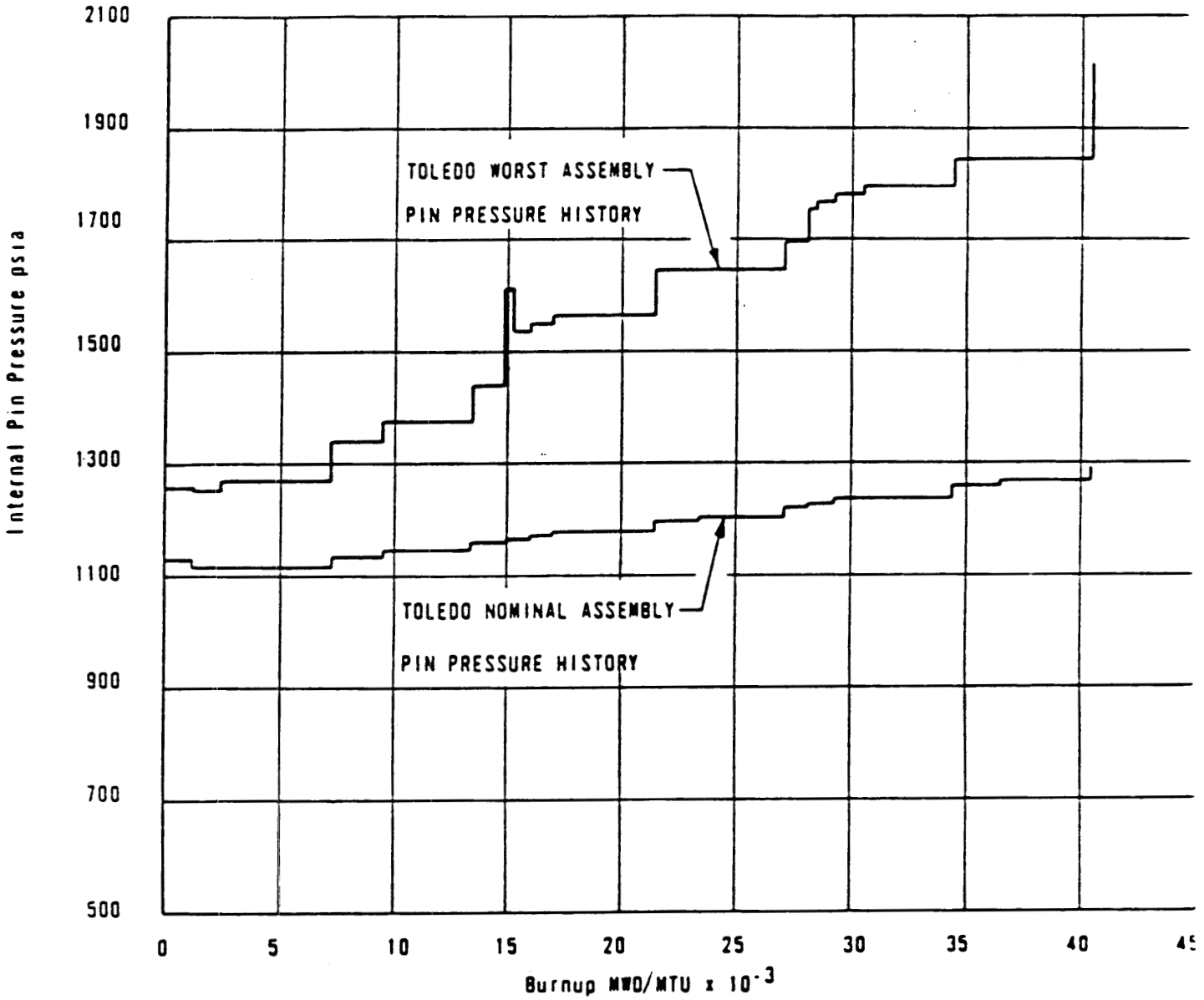

DAVIS-BESSE NUCLEAR POWER STATION
INTERNAL PIN PRESSURE VERSUS BURNUP
FIGURE 4.2-3

REVISION 0
JULY 1982

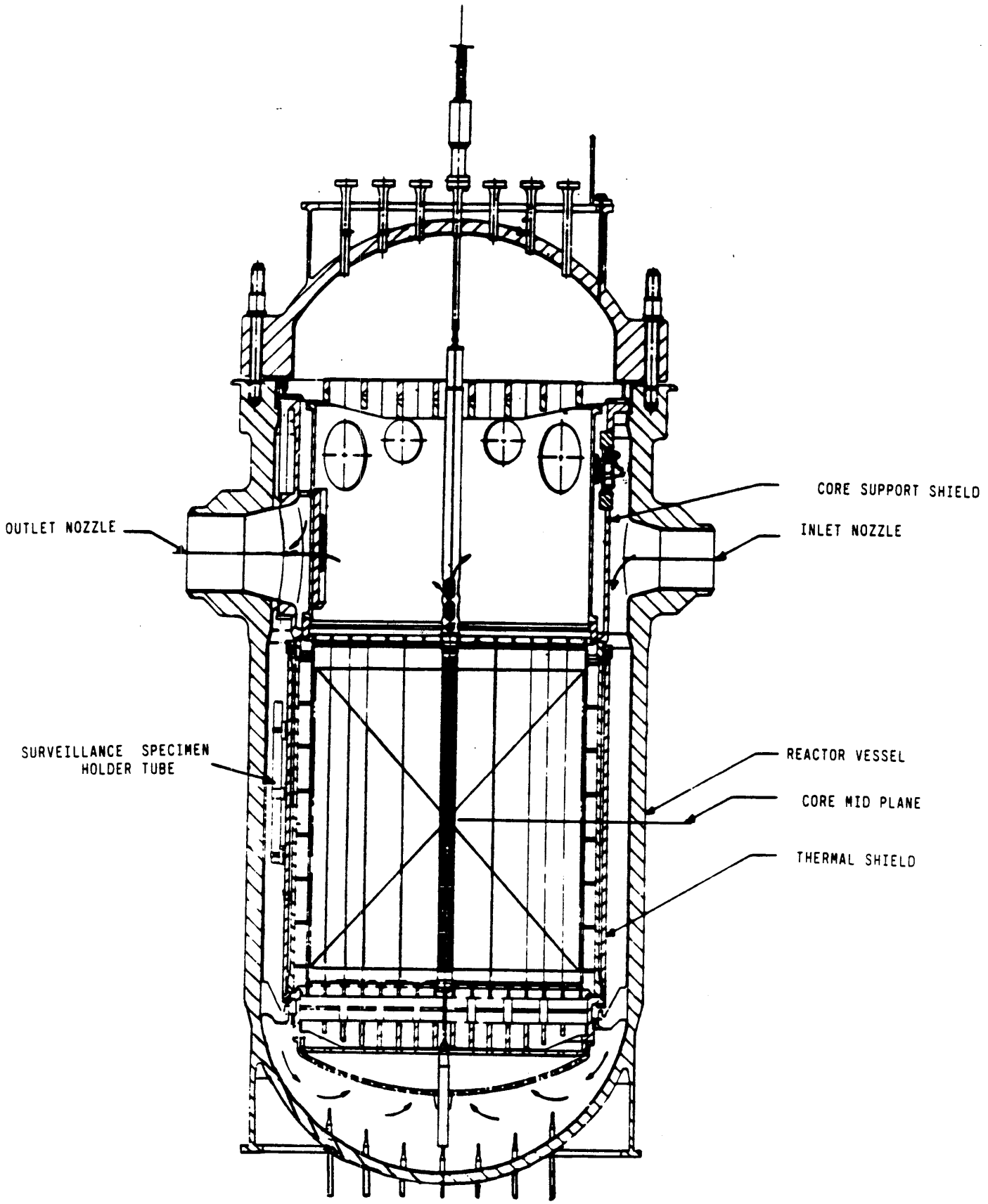

DAVIS-BESSE NUCLEAR POWER STATION
REACTOR VESSEL AND INTERNALS
GENERAL ARRANGEMENT
FIGURE 4.2-4

REVISION 0
JULY 1982

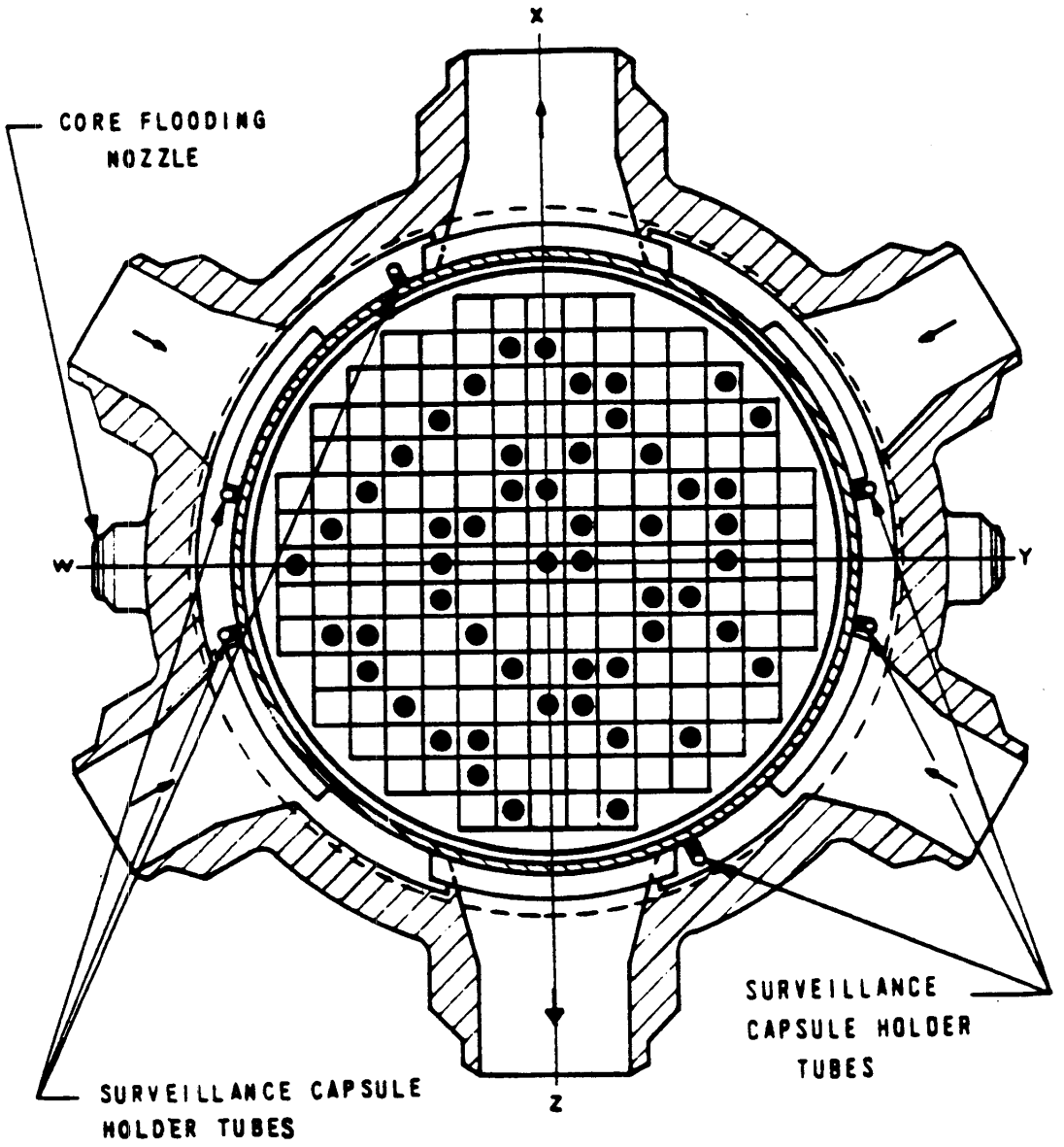

DAVIS-BESSE NUCLEAR POWER STATION
REACTOR VESSEL CROSS SECTION
FIGURE 4.2-5

REVISION 0
JULY 1982

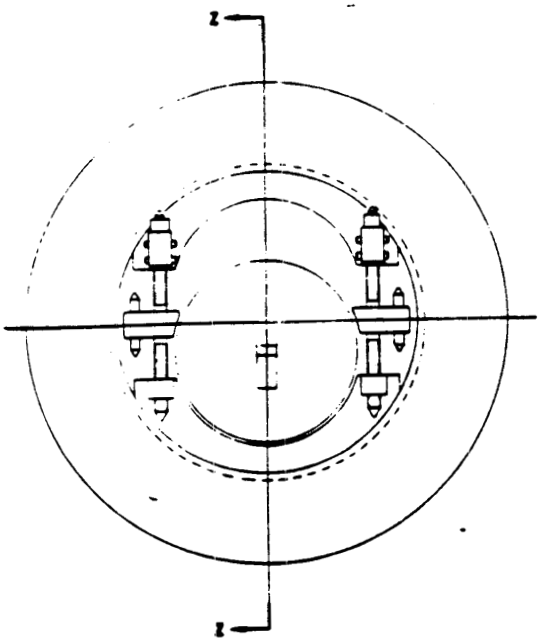

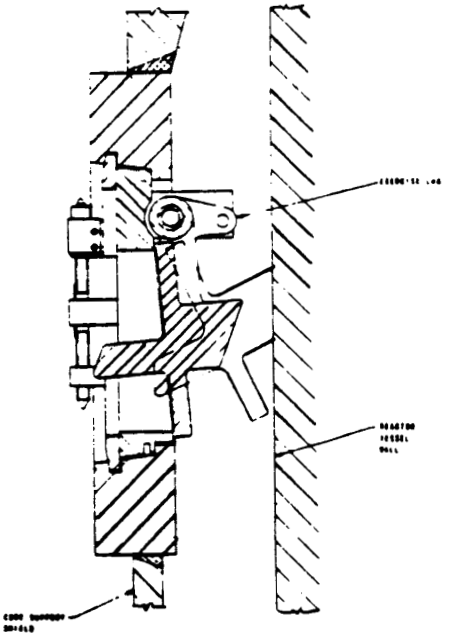

SECTION Z-Z

DAVIS-BESSE NUCLEAR POWER STATION
INTERNALS VENT VALVE

FIGURE 4.2-6

REVISION 0
JULY 1982

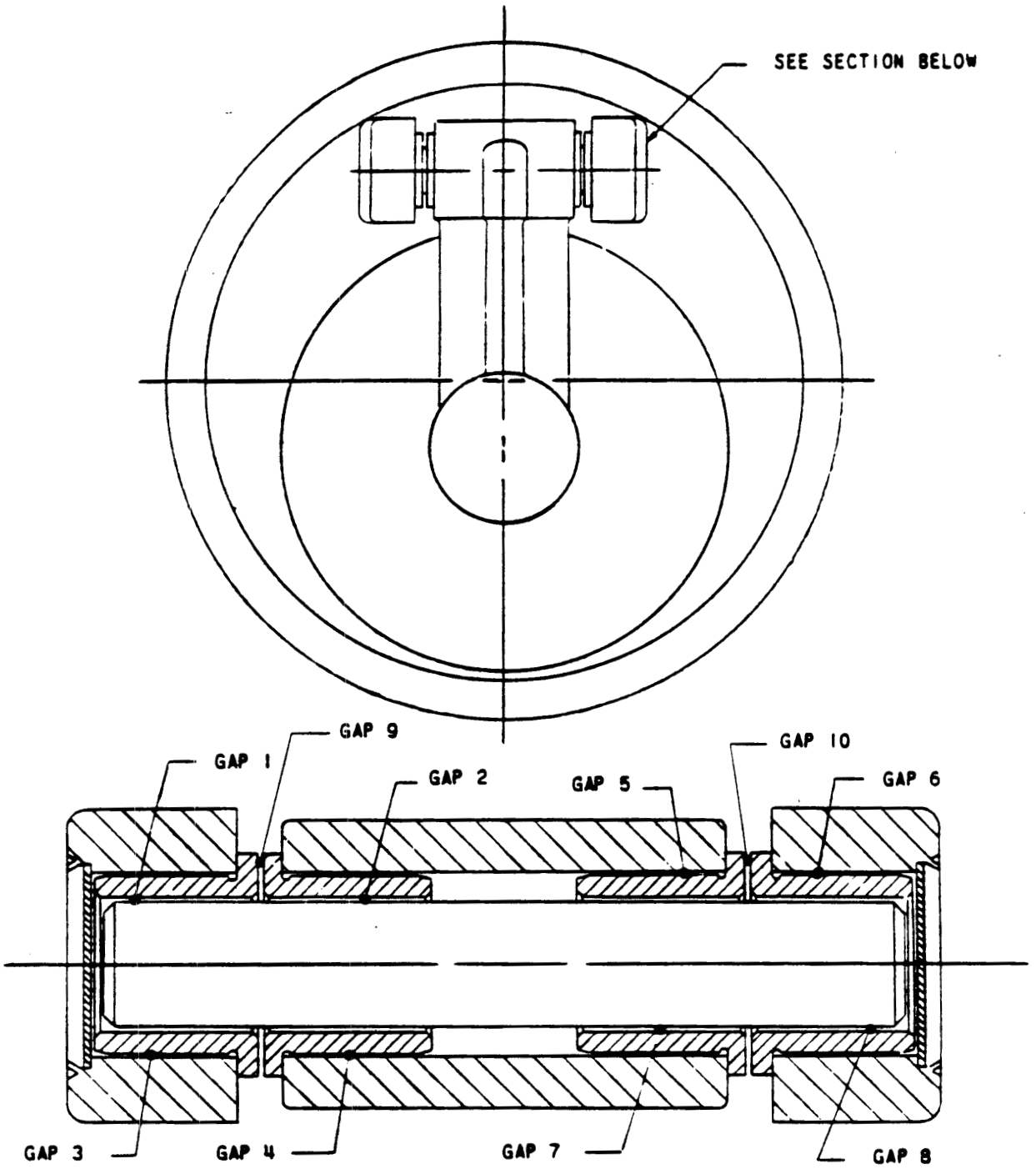

INTERNALS VENT VALVE
CLEARANCE GAPS
FIGURE 4.2-7

REVISION 0
JULY 1982

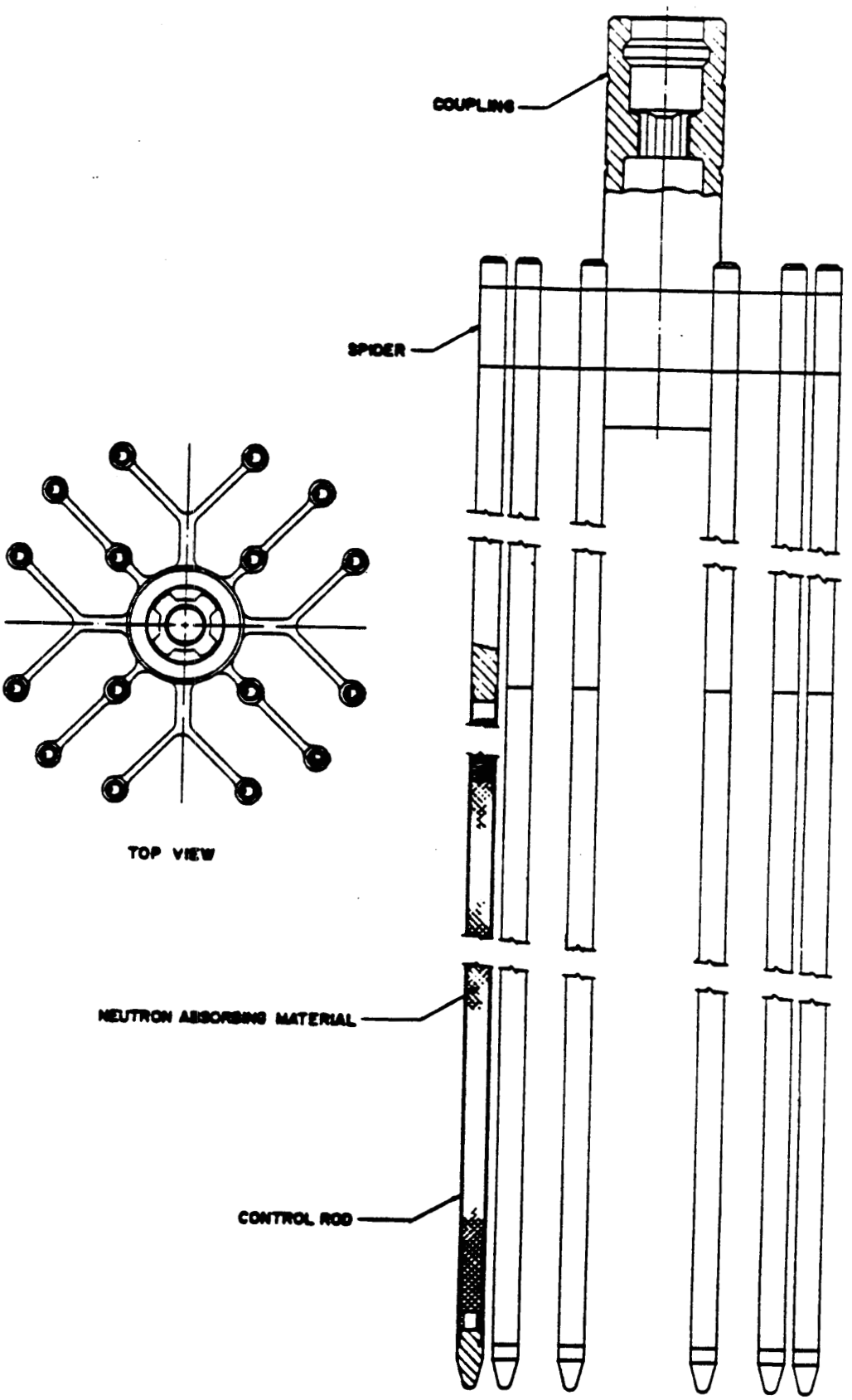

DAVIS-BESSE NUCLEAR POWER STATION
CONTROL ROD ASSEMBLY
FIGURE 4.2-8

REVISION 0
JULY 1982

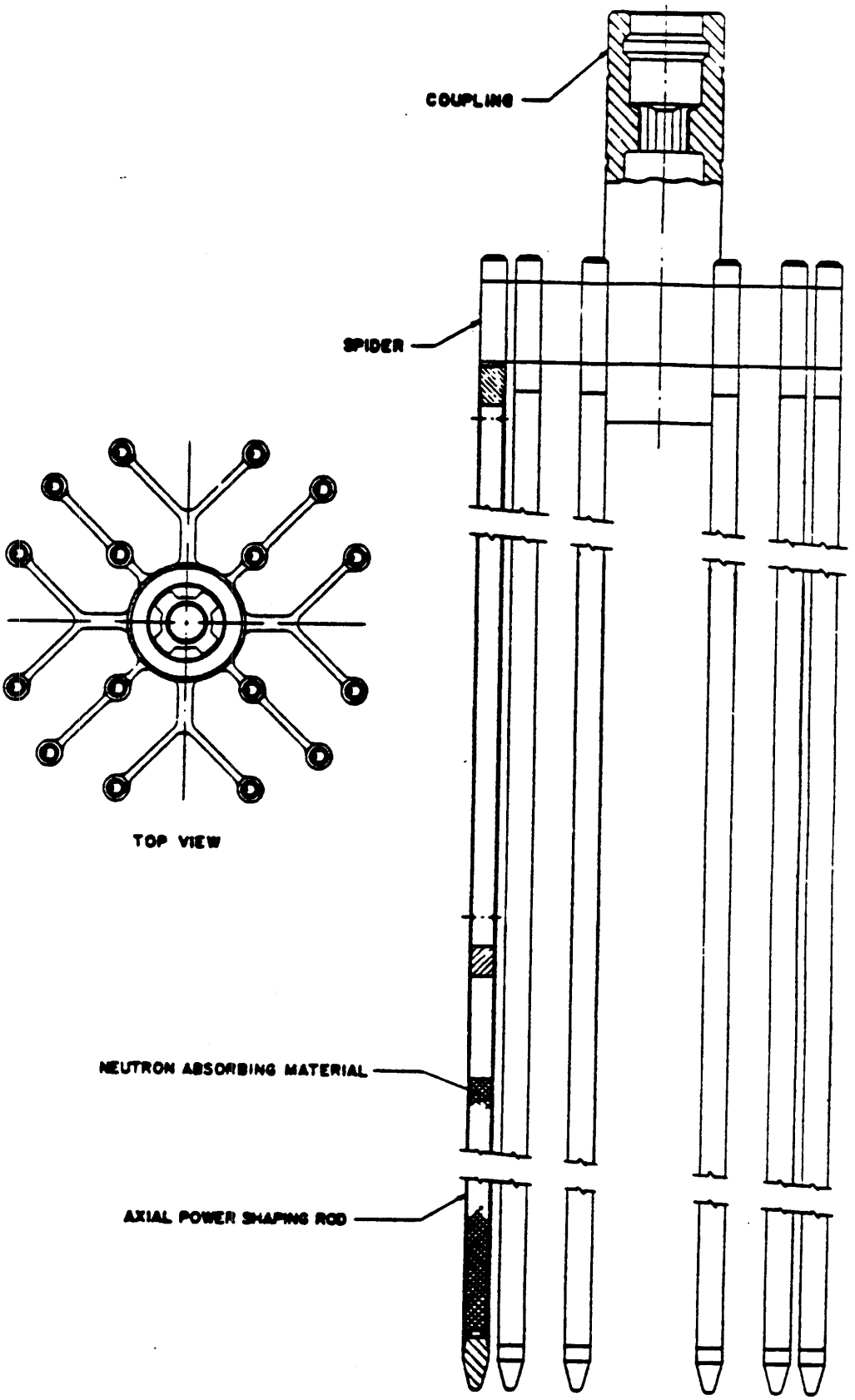

DAVIS-BESSE NUCLEAR POWER STATION
AXIAL POWER SHAPING
ROD ASSEMBLY REVISION 0
FIGURE 4.2-9 JULY 1982

4.3 NUCLEAR DESIGN

4.3.1 Design Bases

The nuclear design data for the most current cycle is described in the applicable reload report and associated approved B&W Fuel Company topical reports. Commencing with Cycle 13, Reference 58's approval by the NRC allowed use of the M5 alloy for use in cladding and structural components (i.e. end caps, spacer grids and guide tubes). The following is a description of the original design.

The Davis-Besse reactor is designed to operate at 2772 MWt with sufficient nuclear design margins to accommodate transient operation without damage to the core.

Core reactivity is controlled by Control Rod Assemblies (CRAs) and soluble boron in the coolant. Sufficient CRA worth is available to shut the reactor down with at least a 1% Δk/k sub-critical margin in the hot condition at any time during the life cycle with the most reactive CRA stuck in the fully withdrawn position. Equipment is provided to add soluble boron to the reactor coolant to ensure a similar shutdown capability when the reactor is cooled to ambient temperatures.

The reactivity worth of a CRA and the rate at which reactivity can be added are limited to ensure that credible reactivity accidents cannot cause a transient capable of damaging the reactor coolant system or causing significant fuel failure.

1. Fuel is designed for a maximum local burnup of 55,000 MWd/mtU.

2. The power Doppler coefficient is negative. However, the control system is capable of compensating for reactivity changes resulting from either positive or negative nuclear coefficients.

3. The core has sufficient excess reactivity to produce the design power level and life time without exceeding the control capacity or shutdown margin.

4. Control reactivity insertion rates are limited to a maximum value of 2.3×10^{-4} (Δk/k) / sec for a single regulating CRA group withdrawal and 4.4×10^{-6} (Δk/k) / sec for soluble boron removal.

5. Reactor control and maneuvering procedures do not produce power distributions that violate the thermal criteria. The low reactivity worth of CRA groups inserted during power operation limits power peaks to acceptable values.

6. Sufficient control is available to produce an adequate shutdown margin.

7. The shutdown margin can be maintained throughout core life with the CRA of highest worth stuck out of the core.

8. The shim safety rod drives provide CRA insertion and withdrawal rates consistent with the required reactivity changes for reactor operational load changes. This rate is based on the worths of the various rod groups, which have been established to limit power- peaking flux patterns to design values. The maximum reactivity addition rate is specified to limit the magnitude of a possible nuclear excursion resulting from a control system or operator malfunction. The normal

insertion and withdrawal velocity has been established as 30 inches per minute. The drive provides a trip of the CRA, which results in a rapid shutdown of the reactor for conditions that cannot be handled otherwise by the reactor control system. The trip setpoint is based on the results of various reactor emergency analyses, including instrument and control delay times, and on the amount of reactivity that must be inserted before the CRA decelerates. The maximum travel time for a 2/3-insertion on a CRA trip has been established as 1.40 seconds.

9. The control of excess reactivity is provided by soluble boron and CRAs. Soluble boron is used to control the moderator temperature deficit (70 to 532°F), equilibrium xenon and samarium, fuel burnup and fission product buildup. Reactivity components due to Doppler deficit, moderator temperature deficit (532 to 582°F), dilution control, shutdown margin, and xenon undershoot are controlled by movable CRAs.

10. Approximately one third of the fuel is removed from the core and replaced with fresh fuel at the end of each fuel cycle. The fresh fuel is enriched enough so that the core has enough excess reactivity to produce the design power level and lifetime without exceeding the control capacity or shutdown margin. In general, fresh fuel is located in the core interior and contains Burnable Poison Rod Assemblies (BPRA's) so that power-peaking limits are not exceeded.

11. Reactivity control is distributed among the control components so that the power reactivity coefficient is always negative in the operating range (50 to 112% power).

12. The core is stable against azimuthal xenon oscillations. For a given combination of events axial instability could exist. Therefore, eight partial-length APSRs are used to maintain an acceptable axial distribution of power.

13. Backup and emergency shutdown provisions information regarding emergency shutdowns is provided in response to General Design Criteria 27, 28, 29, 30, 31, 32, 43, and 44 (Appendix 3D).

4.3.2 Description

4.3.2.1 Excess Reactivity and Shutdown Margins

The nuclear design data for the most current cycle is described in the applicable reload report and associated approved B&W Fuel Company topical reports. Commencing with Cycle 13, Reference 58's approval by the NRC allowed use of the M5 alloy for use in cladding and structural components (i.e. end caps, spacer grids and guide tubes). The following is a description of the original design.

The excess reactivity associated with various core conditions is tabulated in Table 4.3-3. Reactivity control using soluble boron and movable CRAs is explained as follows:

a. Control by Soluble Boron

Boron in solution is used to control the following relatively slow-moving reactivity changes:

1. The moderator deficit in going from ambient to operating temperatures.

2. Equilibrium xenon and samarium.

3. The excess reactivity required for fuel burnup and fission product buildup throughout cycle life.

4. Transient xenon resulting from daily load changes.

b. Control by Movable CRAs

1. Power level changes (Doppler) and regulation.

2. Between 0 and 25% of rated power, reactivity compensation by CRA is required as a result of the linear increase of the reactor coolant temperature from 532°F to the normal operating temperature.

3. Additional reactivity is held by a group of partially inserted CRAs (25% insertion maximum) to allow periodic rather than continuous soluble boron dilution. Automatic withdrawal of these CRAs during operation is allowable to a 5% insertion limit, where the dilution procedure is initiated and this group of CRAs is reinserted.

4. A shutdown margin of 1% Δk/k below the hot critical condition also contributes to the reactivity controlled by CRAs.

4.3.2.1.1 Reactivity Shutdown Analysis

The nuclear design data for the most current cycle is described in the applicable reload report and associated approved B&W Fuel Company topical reports. The following is a description of the original design.

Each cycle is evaluated at BOC and EOC for shutdown capability. An examination of the shutdown margin calculation shows that the shutdown can be accomplished during the current cycle with the most reactive control rod assembly stuck in the full-out position.

Under conditions where a cooldown to containment vessel ambient temperature is required, concentrated soluble boron will be added to the reactor coolant to produce a shutdown margin of at least 1% Δk/k.

4.3.2.2 Reactivity Coefficients

The nuclear design data for the most current cycle is described in the applicable reload report and associated approved B&W Fuel Company topical reports. The following is a description of the original design.

Reactivity coefficients form the basis for studies involving normal and abnormal reactor operating conditions. These coefficients have been investigated as part of the analysis of this core and are described below as to function and overall range of values:

1. Doppler Coefficient - The Doppler coefficient reflects the change in reactivity as a function of fuel temperature. A rise in fuel temperature results in an increase in the

effective absorption cross section of the fuel (the Doppler broadening of the resonance peaks) and a corresponding reduction in neutron production.

The Doppler coefficient is due primarily to Doppler broadening of the Uranium-238 resonances with increasing fuel temperature. Temperature-dependent resonance integrals, which include Doppler broadening, are calculated by the B&W proprietary RIP program and are based on the experimental work of Hellstrand, Blomberg, and Horner (ref. 11). Calculated and experimental resonance integrals for UO_2 rods of different radii are compared in Figure 4.3-2. The curves for r = 0.5 are representative of this core.

Uncertainties in the calculated values of the Doppler coefficient may be attributed in part to the slight mismatch between the RIP and Hellstrand calculations, but primarily to uncertainties involved in predicting fuel temperatures. Since the Doppler coefficient is a function of fuel temperature, a value calculated at a certain power level is dependent on the accuracy of predicting the fuel temperature at that power level.

In the nuclear calculations, this uncertainty due to fuel temperature is applied conservatively. That is, the highest expected fuel temperature is used to determine Doppler deficit for shutdown reactivity analysis and a lower fuel temperature is used for conservatism in the xenon stability analysis.

2. Moderator Pressure Coefficient - The moderator pressure coefficient relates the change in moderator density resulting from a reactor coolant pressure change to the corresponding effect on neutron production. This coefficient is opposite in sign and considerably smaller when compared to the moderator temperature coefficient. A typical range of pressure coefficients over a life cycle would be - $3x10^{-7}$ to $+3x10^{-6}$ $(\Delta k/k)$/psi.

3. Moderator Temperature Coefficient - The moderator temperature coefficient relates a change in neutron multiplication to the change in reactor coolant temperature. Reactors using soluble boron as a reactivity control have a less negative moderator temperature coefficient than do cores controlled solely by movable or fixed CRAs. The major temperature effect on the coolant is a change in density: an increasing coolant temperature produces a decrease in water density and a proportional reduction in boron concentration. The concentration change results in a positive reactivity component by reducing the absorption in the coolant. The magnitude of this component is proportional to the total reactivity held by soluble boron. Distributed poisons (BPRs or inserted control rods) have a negative effect on the moderator coefficient for a specified boron concentration. That is, the moderator coefficient for a system with 1200 ppm boron in the coolant and 1% rod worth inserted will be more negative than for a system with 1200 ppm boron and no rods inserted.

4. pH Coefficient - Currently, there is no definite correlation that will permit the prediction of pH reactivity effects. Some of the parameters needing correlation are the effects relating pH reactivity change for various operating reactors, pH effects versus reactor operating time at power, and changes in effects with varying cladding, temperature, and water chemistry. Yankee, Saxton, and Indian Point Station No. 1 have experienced reactivity changes at the time of pH changes, but there is no clear cut evidence that pH is the direct reactivity-influencing variable

without considering other items such as cladding materials, fuel assembly crud deposition, system average temperature, and previous system water chemistry.

The pH characteristic of this design is shown in Table 4.3-9 where the cold values are measured and the hot values are calculated. Saxton experiments (ref. 12) indicate a pH reactivity effect of 0.0016 Δk/k/ΔpH unit change with and without local boiling in the core. Considering the system makeup rate of 35,000 lb/hr and the core in the hot condition with 1200 ppm boron in the coolant, the corresponding changes in pH unit per hour for Lithium-7 dilution (starting with 0.5 ppm Lithium-7). Applying the pH worth value quoted above from Saxton, the total reactivity insertion rate for the hot condition is 3.1×10^{-8} Δk/k/sec. This reactivity insertion rate can be easily compensated by the operator or the automatic control system.

5. Power Coefficient - The power coefficient, α_p, is the fractional change in neutron multiplication per unit change in core power level. A number of factors contributed to α_p, but only the moderator temperature coefficient and the Doppler coefficient contributions are significant. The power coefficient can be written as:

$$\alpha_p = \alpha_m \frac{\partial T_m}{\partial p} + \alpha_f \frac{\partial T_f}{\partial p}$$

where α_m = moderator temperature coefficient,

α_f = fuel Doppler coefficient,

$\frac{\partial T_m}{\partial p}, \frac{\partial T_f}{\partial p}$ = change in moderator and fuel temperature per unit change in core power.

The power Doppler reactivity coefficient, which is identical to the power coefficient for constant average moderator temperature, was calculated for the current fuel cycle.

6. Fuel Thermal Expansion Coefficient - The fuel thermal expansion coefficient relates a change in reactivity to a change in fuel dimensions and density caused by thermal expansion. The effect of thermal expansion of the cladding is taken into account in this coefficient. This coefficient is always negative and is small when compared with the Doppler coefficient. The value for this coefficient is -0.02×10^{-4} Δk/k/°F.

7. Moderator Void Coefficient - The moderator void coefficient relates a change in neutron multiplication to the presence of voids in the moderator. Moderator void coefficients are listed in Table 4.3-10 for hot, cold, and intermediate temperature conditions. A graph of the percentage change in Δk/k for percentage voids is shown in Figure 4.3-3. Table 4.3-10 and Figure 4.3-3 are calculated values in corresponding to a moderator soluble boron content of 1100 ppm.

4.3.2.3 Control Rod Assembly Reactivity Worth

The nuclear design data for the most current cycle is described in the applicable reload report and associated approved B&W Fuel Company topical reports. The following is a description of the original design.

Rod worth calculations were performed with the PDQ07 (ref. 13) - HARMONY (ref. 14) computer program in x-y geometry. Rod group No. 8 (APSRs) was assumed to be 37.5% withdrawn.

4.3.2.4 Reactivity Worth of Fuel Assemblies and Shim Material

The nuclear design data for the most current cycle is described in the applicable reload report and associated approved B&W Fuel Company topical reports. The following is a description of the original design.

The hot and cold reactivity worth of a fuel assembly is given in Table 4.3-3. These values are based on an assembly with 3.5 wt% Uranium-235 enrichment in unborated water. These are the conditions that result in the highest neutron multiplication factor.

4.3.2.5 Reactivity of Miscellaneous Materials

The nuclear design data for the most current cycle is described in the applicable reload report and associated approved B&W Fuel Company topical reports. The following is a description of the original design.

The only materials in the core that can experience movement or change in composition under normal conditions are the CRAs and changes in moderator density. The reactivity worths of these materials are specified in Subsections 4.3.2.1 and 4.3.2.2.

4.3.2.6 Reactivity Insertion Rates

The nuclear design data for the most current cycle is described in the applicable reload report and associated approved B&W Fuel Company topical reports. The following is a description of the original design.

Figure 4.3-4 displays a typical figure of the integrated rod worth of three overlapping rod banks as a function of distance withdrawn. The indicated groups are those used in the core during power operation. Using approximately 3.2% Δk/k CRA groups and a 30-inch per minute drive speed in conjunction with the reactivity response given in Figure 4.3-4 yields a maximum reactivity insertion of 2.3×10^{-4} (Δk/k)/sec. The maximum reactivity insertion rate for soluble boron removal is 4.4×10^{-6} (Δk/k)/sec.

4.3.2.7 Power Distribution

The nuclear design data for the most current cycle is described in the applicable reload report and associated approved B&W Fuel Company topical reports. The following is a description of the original design.

The power is distributed in the core in a manner consistent with thermal and hydraulic design limits. The proper distribution is obtained by analyzing core power throughout the cycle lifetime to determine the appropriate enrichment gradients, control rod pattern, and BPRA loading

scheme. Table 4.3-12 gives the highest local power peaks for the steady-state case, the case with the control rod banks at extreme positions, and the case with the control rod banks at normal positions during a design transient (100-30-100% full power). Values for radial, axial, and total peaking factors are provided for beginning of life and end of life conditions.

4.3.2.8 Power Decay Curves

The nuclear design data for the most current cycle is described in the applicable reload report and associated approved B&W Fuel Company topical reports. The following is a description of the original design.

Figure 4.3-7 displays the BOL power decay curves with and without a stuck rod for CRA worths corresponding to a minimum 1% hot shutdown margin. The power decay is initiated by the trip of the CRA with a 300-ms delay from initiation to start of CRA motion. The time required for insertion of a CRA 2/3 of the distance into the core is 1.4 seconds.

4.3.2.9 Minimum Critical Mass

The minimum critical mass, with and without xenon and samarium poisoning, may be specified as a single assembly or as multiple assemblies in various geometric arrays. The unit fuel assembly has been investigated for comparison. A single, cold, clean fuel assembly enriched to 5.0 wt% is subcritical in water. Two assemblies side-by side are supercritical under these conditions.

4.3.2.10 Neutron Flux Distribution

The nuclear design data for the most current cycle is described in the applicable reload report and associated approved B&W Fuel Company topical reports. The following is a description of the original design.

Energy dependent neutron fluxes were determined by a discrete ordinate solution of the Boltzmann transport equation. Specifically, ANISN, a one-dimensional code, and DOT, a two-dimensional code, were used. In both codes, the system is modeled radially from the core out to the air gap outside the pressure vessel. The model includes the core with a time averaged radial power distribution core liner, barrel, thermal shield, pressure vessel, and water regions. Inclusion of the internal components is necessary to account for the distortions of the required energy spectrum by attenuation in these components. The ANISN code uses the CASK 22-group neutron cross section set with an S_6 order of angular quadrature and a P_3 expansion of the scattering matrix. The problem is run along a radius across the core flats. Azimuthal variations are obtained with a DOT r-theta calculation that models one-eighth of a plan-view of the core (at the core midplane) and includes a pin by pin, plant specific time averaged power distribution. The DOT calculation uses S_6 quadrature and a P_1 cross section set derived from CASK.

Fluxes calculated with this DOT model must be adjusted to account for lack of P_3 cross section detail in calculations of anistotropic scattering, a perturbation caused by the presence of the capsule (where applicable) and the axial power distribution. The first two items are both energy and radial-location dependent, whereas the latter is axial location dependent. A P_3/P_1 correction factor is obtained by comparing two ANISN 1-D model calculations in which only the order to scattering was varied. The capsule perturbation factor is obtained from a comparison of two DOT x-y model calculations, one with a capsule explicitly modeled-SS304 cladding, A1 filler region, and carbon steel specimens–and the other with water in those regions. The effect of

axial power distribution has been determined from a typical 177 FA plant burnup calculation as a function of axial location for the outer rows of fuel assemblies. The net result from these parameter studies is a flux adjustment factor K which is applicable to calculate data from the DOT model.

Plant specific analytical results based on the calculation technique described above were converted to activities and then compared with dosimeter measurements from surveillance capsules from 5 similar reactors. All these comparisons are within 15% of the dosimeter measurement. The fluence predictions used for the Davis-Besse Unit 1 reactor vessel surveillance program are discussed in USAR Section 5.4.7.

4.3.2.11 Core Lifetime, Fuel Burnup, and Fuel Replacement Program

Design power level, average fuel assembly and local, maximum fuel rod burnups, and refueling patterns are given in Appendix 4B, Reload Report.

4.3.2.12 Xenon Stability Analysis and Control

The nuclear design data for the most current cycle is described in the applicable reload report and associated approved B&W Fuel Company topical reports. The following is a description of the original design.

The Davis-Besse core has been analyzed to determine the character of power oscillations that are induced by xenon oscillations.

The regional power can be expressed as an exponential-sinusoidal function of the form:

$$P(t) = P_0 e^{bt} \sin\left[\frac{2\pi}{T}\right] t + \tau_0 + A_0 ,$$

where P(t) = power at time t,

P_0 = amplitude relative to A_0 at t = 0,

b = stability index, hr^{-1},

T = period, hr.

τ_0 = phase shift,

A_0 = average power.

The stability index b and the period T describe the behavior of power oscillations in a region of the core after some perturbation has disrupted the normal power level. A positive index denotes a diverging oscillation; a negative stability index denotes a converging oscillation.

Stability indexes and periods of oscillation were calculated for three cases: a nominal BOL case performed at 4 FPD, a nominal EOL case, and a compounded error (CE) case performed at 4 FPD. The nominal EOL and BOL cases were performed using nominal input values of fission rate, macroscopic fission cross section, neutron flux, xenon concentration, and xenon decay constant. The CE case was performed using input parameters that differ from nominal values

by the uncertainty in calculation of the nominal value. The input parameters used in this CE case are the ones that produce the most unstable condition.

The results for these three cases are tabulated in Table 4.3-13. The analysis shows that the azimuthal stability index is always negative. However, the axial stability index is positive under certain conditions. The system is provided with a group of eight partial-length movable CRAs. This group of control rods has sufficient reactivity holddown capability to suppress axial power oscillations caused by a redistribution of xenon. Therefore, the core is protected against xenon oscillations.

4.3.3 Nuclear Evaluation

The nuclear design data for the most current cycle is described in the applicable reload report and associated approved B&W Fuel Company topical reports. Commencing with Cycle 13, Reference 58's approval by the NRC allowed use of the M5 alloy for use in cladding and structural components (i.e. end caps, spacer grids and guide tubes). The following is a description of the original design.

This section discusses analytical models and their application and describes core instabilities associated with xenon oscillation. A large number of computer codes are used in making reactor design calculations, and the choice the code set or sets used is discussed below by design area:

1. Nuclear Calculation Model - The reactivity of a pressurized water reactor core is calculated in one, two, or three dimensions. The geometry chosen depends on the type of calculations to be made. In a "clean" type of calculation where there are no strong, localized absorbers of a type differing from the rest of the lattice, one-dimensional analysis is satisfactory. This type of problem is solved by the one-dimensional B&W proprietary depletion package code LIFET, which utilizes the MUFT (ref. 21) and WANDA (ref. 22) codes and the B&W proprietary RIP, TAME, and AMOP computer programs. A brief description of LIFET follows.

    a. Calculation of Epithermal Cross Sections: The epithermal neutron energy spectrum for each composition region is calculated using the B_1 (or P_1) transport approximation with the Fermi age slowing-down treatment for heavy nuclides and the Grueling-Goertzel (ref. 23) treatment for the light nuclides. For nuclides exhibiting resonances in the epithermal energy range, the effective resonance integral, corrected for shielding effects and Doppler broadening, is calculated by either the narrow resonance or narrow resonance-infinite absorber model for each epithermal multigroup. For tightly packed heterogeneous lattices, the Dancoff factor is calculated by the method of Sauer (refs. 24 and 25). In computing the epithermal spectrum, both inelastic scattering and (n, 2n) reactions are taken into account. After calculating the neutron spectrum, macrogroup (three groups or less) diffusion constants are obtained by averaging over the spectrum. The resonance integral calculation in LIFET is adapted from the RIP program. This program is based on the work of Dresner (ref. 26) and that of Adler, Hinman and Nordheim (ref. 27). Effective resonance integrals are calculated at each resolved and unresolved peak for each resonance nuclide. The effective resonance integral for each energy interval in the multigroup structure is then the sum of the integrals over all peaks in the multigroup. These multigroup

resonance integrals are subsequently used in the epithermal spectrum calculation.

b. Calculation of Thermal Cross Sections: A thermal spectrum calculation is performed for each composition region of a reactor. Since these regions are not strictly homogeneous, a space-energy calculation should be performed to account for the heterogeneous configuration. For the case of uniformly distributed fuel rods in a moderating medium, the space-energy flux may be described in terms of separate space-and-energy-dependent terms. The AMOP routine in the proprietary LIFET program describes the heterogeneous effects by calculating effective microscopic cross sections for each nuclide. These cross sections reflect the geometric configuration of the fuel rods, claddings and moderator. The TAME routine then calculates the energy dependence of the flux for an equivalent homogeneous region. Finally, the cross sections are averaged over the energy spectrum to obtain a single thermal cross section set for use in the multigroup diffusion calculation.

2. Reactivity Analysis of Critical Experiments – Thirty-one UO_2 and PuO_2-UO_2 critical assemblies were analyzed to verify the methods described above. This verification program was undertaken for two purposes. The first objective was to determine the validity of these methods for predicting the k_{eff} of critical assemblies using a one-dimensional model. The second objective was to investigate the applicability of the present thermal and epithermal spectrum calculations for determining the effective cross sections to be used in the analysis of large power reactors. The criticality portion of the LIFET program was used to determine k_{eff} for the critical assemblies. This one-dimensional (cylindrical) analysis was performed with four-group cross sections - one thermal group and three epithermal groups. The group structure used for the group collapse is given below.

Group	Energy Range
1	9.12 keV to 10 MeV
2	61.4 eV to 9.12 keV
3	1.85 eV to 61.4 eV
4 (thermal)	0.0 eV to 1.85 eV

The 17 UO_2 criticals selected for analysis are described in references 28 through 32. The k_{eff} was calculated for each assembly assuming the “resonance” treatment for resonance absorption and using the four-group structure. These values are referred to as the reference values. Statistically, $k^r_{eff} = 0.9983 \pm 0.0047$, where 0.9983 is the arithmetic mean and the error corresponds to one standard deviation of a sample about the mean. All values of k^r_{eff} are between 0.9912 and 1.0068.

A comparison was also made between k^r_{eff} and k_{eff} calculated using a two-group structure. Statistically, $k_{eff}^{(2\text{-group})} = 1.0032 \pm 0.0080$ for the UO_2 criticals.

For all UO_2 criticals, the difference in k_{eff} between the two-group and four-group analyses was +0.0049 ± 0.0040 with the two-group being higher. The important feature is that the difference decreases rapidly as the assembly radius increases. Hence, for a PWR with a radius of about 150 cm, the difference between the two- and four-group treatments would diminish to less than 0.05%. This fact justifies the use of a two-group structure for large power reactors. The increased accuracy of the four-group treatment appears in the calculation of the leakage, which is important only in small assemblies.

Eleven PuO_2-UO_2 and three UO_2 critical assemblies were studied. These UO_2 assemblies were considered because their lattice parameters were similar to those of the PuO_2-UO_2 assemblies and their Uranium-235 content was greater than that of the other UO_2 criticals. These criticals are described in detail in References 33 and 34. A criticality calculation was performed on each PuO_2-UO_2 assembly using the "resonance" treatment for resonance absorption in the epithermal energy range and a four-group structure for the calculation of k_{eff}. These are referred to as the reference values. Statistically, k^r_{eff} = 1.001 ± 0.0048. All values of k^r_{eff} are between 0.9889 and 1.0073. A second comparison was made between k^r_{eff} and $k_{eff}^{(2\text{-group})}$ corresponding to a two-group structure. $k_{eff}^{(2\text{-group})}$ 1.0135 ± 0.0070 for the PuO_2-UO_2 critical assemblies. For the fourteen criticals, the mean difference between the two-group and four-group k_{eff} was 0.0134 ± 0.0061.

It is apparent that the difference between the two- and four-group structures is essentially the same for the PuO_2-UO_2 and UO_2 criticals. The very small assemblies (e.g., 12.94 cm radius) show errors between the two-group structures in excess of 2%.

For all UO_2 and PuO_2-UO_2 critical assemblies, k^r_{eff} = 0.991 ± 0.0047. This indicates that the present methods, employing the "resonance" treatment for resonance absorption and the four-group structure, predict k_{eff} for uniform lattices quite accurately. The one-dimensional model is adequate for assemblies that are nearly cylindrical. However, for square assemblies, k^r_{eff} may differ from the mean value by as much as 1%. A two-dimensional criticality calculation is used for these assemblies.

The two-group treatment yields $k_{eff}^{(2\text{-group})}$ = 1.0079 ± 0.0074 and $\Delta k_{eff}^{(2\text{-group})}$ = 0.0088 ± 0.0050 for all UO_2 and PuO_2-UO_2 critical assemblies.

For small assemblies, $\Delta k_{eff}^{(2\text{-group})}$ is greater than 2% indicating the importance of the group structure on the leakage calculation. For large assemblies, such as a PWR, the difference is less than 0.05%. For uniform lattices of fuel pins in a large reactor, the two-group cross sections calculated according to the methods described in this section are adequate for design calculations.

3. Power Distribution Analysis of Critical Experiments - A series of detailed three-dimensional power distribution measurements have been performed at the B&W Critical Experiments Laboratory. These experiments were designed to provide detailed power distribution measurements, with both partial- and full-length control rods, against which analytical methods and results can be checked. A detailed description of the tests and results can be found in Reference 35.

The PDQ07 program was used to calculate the power distributions corresponding to the measured values. Since PDQ07 is a three-dimensional program, the core geometry can be described more exactly where necessary. The composition overlay accurately describes both fuel and poison pins in the control rod regions. Solution points are placed along the boundary and in the center of the cells in the fuel rod regions. The thermal feedback option in PDQ07 is not exercised because the temperature variations are small. As in the actual measurements, the power densities are normalized to the value at mid-height of the 20th pin (standard rod) on the west radius (shown in Figure 4.3-9).

The two-group coefficients input to PDQ07 for fuel pins, borated water, and aluminum-water reflector are generated by the LIFET program. Homogenized poison pins are used to obtain absorption coefficients. Figure 4.3-10 shows graphs of the normalized relative power distributions at 35 cm, mid-plane, and 105 cm from the core bottom for the east traverse from core center. These radial distributions correspond to the case where the control rod clusters are withdrawn 72.5, 92.1, and 72.5 cm for the north, central, and south positions, respectively. The axial normalized power distributions at positions A, B, and C (Figure 4.3-9) are shown in Figure 4.3-11.

The radial and axial normalized power distributions calculated with the PDQ07 program agree quite well with the measured distributions. There are, however, deviations near control rod locations.

4. Application of Computer Codes to Nuclear Design – PDQ05 (ref. 36) and PDQ07, in conjunction with HARMONY, have been used in quarter core x-y geometry to deplete the core through several cycles. This model was instrumental in choosing core enrichments, core loading schemes, and shuffle patterns. EOL mass balance and megawatt days per tonne (MWd/t) produced by each assembly were obtained from these cases. The same model was used to calculate rod bank worths, critical boron concentration, and total available rod worth, as well as isothermal moderator coefficients and other undistributed reactivity coefficients. Hot and cold ejected and stuck rod worths were calculated with two-dimensional PDQ, showing the full core.

   In a depletion calculation, the time steps used are primarily 50 days in length except for the beginning and end of the fuel cycle. Boron reactivity worth is calculated by observing the k_{eff} associated with two boron concentrations. Since everything else is held constant, the change in reactivity divided by the change in boron concentraton gives the boron worth. These worths are computed as a functon of burnup and boron concentration.

   The three-dimensional PDQ07 code is also an integral part of core design work. B&W has modified this program to include thermal feedback effects. This option is used in almost all three-dimensional calculations. Extensive analyses have been made of the following:

   a. Control rod maneuvering.

   b. Xenon stability analysis control.

   c. Reactivity coefficients.

A three-dimensional analysis with feedback must be utilized for these problems primarily to obtain an accurate description of the radial and axial power distributions. These distributions are necessary in the evaluation of thermal margin.

5. Fuel Cycle Analysis - The x-y PDQ model with HARMONY was used to calculate fuel cycles for this reactor. The fuel assembly arrangement in the core is shown in Figure 4.3-12.

6. Control Rod Analysis - B&W has developed a procedure for the analysis of the reactivity worth of small cylindrical Ag-In-Cd control rods. The procedure has been verified against a set of 14 critical experiments in which the variables included: number of rods per cluster, arrangement of rods within the cluster, number of clusters in the core, and soluble boron concentration. Approximately half the experiments included water holes to simulate withdrawn rods. Table 4.3-14 compares calculated and experimental reactivity worths.

   The experiments were performed at the B&W Critical Experiments Laboratory with lattices of aluminum-clad uranium oxide fuel rods. Enrichment of the fuel was 2.46 wt% Uranium-235. The Ag-In-Cd rods used in the experiments had an absorber diameter of 0.400 inch. Geometric arrangements of the control rods were chosen to encompass the reference design for the power cores. Experimental rod worths were determined by calibration against soluble boron concentration. The critical soluble poison concentration was determined for each configuration with rods in and again with rods out. (Soluble poison concentrations quoted in the table are for the rods in situation.) Soluble poison concentrations were measured with an absolute accuracy of ±5ppm and a precision of ±3ppm. References 37 and 38 describe the experiments in detail.

   The analytical method used in this analysis is based on the PDQ code with coefficients generated by B&W's LIFET program. Key features include the allowance for interference and overlap effects between resonances and isotopes in the Ag-In-Cd rod, and calculation of the relative fluxes in the control rod and surrounding fuel in an 80-group thermal model.

4.3.4 Nuclear Tests and Inspection

4.3.4.1 Critical Experiments

The nuclear design data for the most current cycle is described in the applicable reload report and associated approved B&W Fuel Company topical reports. Commencing with Cycle 13, Reference 58's approval by the NRC allowed use of the M5 alloy for use in cladding and structural components (i.e. end caps, spacer grids and guide tubes). The following is a description of the original design.

An experimental program to verify the relative reactivity worth of the CRA has been completed. Detailed testing has established the worth of the CRA under various conditions similar to those for the reference core. These parameters include control rod arrangement in a CRA, fuel enrichments, fuel element geometry, CRA materials, and soluble boron concentration in the moderator.

Gross and local power-peaking were also studied, and three-dimensional power- peaking data were taken as a function of CRA insertion. Detailed peaking data were also taken between fuel assemblies and around the water holes left by withdrawn CRAs. The experimental data have been analyzed and were used to benchmark the analytical models used in the design.

4.3.4.2 Zero Power, Approach to Power, and Power Testing

The nuclear design data for the most current cycle is described in the applicable reload report and associated approved B&W Fuel Company topical reports. The following is a description of the original design.

Boron worth and CRA worth (including stuck-CRA worth) will be determined by physics tests at the beginning of each core cycle. The boron worth and CRA worth at a given time in core life will be based on CRA position indication and calculated data as adjusted by operating data.

The reactor coolant will be analyzed in the laboratory periodically to determine the boron concentration, and the reactivity held in the boron then is calculated from the concentration and the reactivity worth of boron.

The method of maintaining the hot shutdown margin (hence, the stuck-CRA margin) is related to operational characteristics (load patterns) and to the power-peaking restrictions on CRA patterns at power. The CRA pattern restrictions ensure that sufficient reactivity is always fully withdrawn to provide adequate shutdown with the stuck-CRA margin.

Operation under power conditions normally is monitored by in-core instrumentation, and the resulting data analyzed.

4.3.4.3 Power Maldistributions

The core is protected against a maldistribution of power by quality control procedures and by constant monitoring of the movable CRA position. Four conditions that could produce power maldistribution are misaligned control rods, azimuthal xenon oscillations, fuel misloading, and improper use of the APSR bank. These conditions are discussed below.

1. Misaligned Control Rods - The reactor has a control function to protect against a rod out of step with its group. The position of each rod is compared with the average of the group. If a fault is detected at power levels above 60% of rated power, a rod withdrawal inhibit is activated, if the Control Rod Drive System is in automatic. Technical Specifications and the associated implementing procedures, specify the maximum misalignments, misalignment times, and reactor power limits.

   Radial power tilts may be detected with the incore or out-of-core instrumentation. The operator can monitor the upper or lower set of out-of-core detectors or the incore detectors using the computer to determine the radial power symmetry condition.

   The APSR drives are also equipped with position monitors and the alarm function for a rod out of step with the group average. These drives, however, do not permit rod drops. With the power removed from the rod drive windings of the APSR, the roller nut does not disengage and the rod remains in its position. Since the maneuvering range for these rods is only 3 to 4 feet, it is not likely that thermal

limits would be exceeded if one of the rods were stuck and the rest of the group were moved.

2. Azimuthal Xenon Oscillations - This reactor is predicted to have a substantial margin to threshold for azimuthal xenon oscillations. Therefore, this mode is not considered a power-peaking problem.

3. Fuel Misloading the fuel pins in an assembly is prevented by loading controls and procedures. Each fuel rod is identified by an enrichment code. The manufacturing process relies on administrative procedures and quality control checks. Fuel pellet and pin enrichment loading errors are prevented by extensive loading controls and procedures. One such manufacturing process, to assure that fuel pellets have been properly loaded, is by in-process gamma-scanning.

   Gross fuel assembly misplacement in the core is prevented by administrative core loading procedures and the prominent display of identification markings on the upper end fitting of each assembly. The fuel handling bridges and grapple mechanisms are designed for accurate indexing and positioning. To ensure seating of assemblies on the fuel grid, hoist tape readings are verified. In addition to this, visual verifications are utilized.

   (a) Prior to the commencement of loading operations, a check is made to ensure that fuel assemblies have been stored in their proper storage locations in the spent fuel pool and that control components are inserted in the proper fuel assemblies.

   (b) During loading or unloading of each assembly into or out of the reactor core the following visual verifications are made:

      i. When picking up the assembly, two persons independently visually verify that it has been picked up from the proper location in the spent fuel pool or the reactor core.

      ii. When the assembly is placed in the final location, two persons independently visually verify that it has been placed in the proper location in the core or spent fuel pool.

   (c) Prior to installing the reactor upper internals, the core loading is independently verified by two persons visually surveying the core and recording the fuel assembly numbers versus core location. This record is then compared to the core loading plan. This type of misplacement would be detected with the incore detectors during startup tests. During this phase, the response of the incore detectors is compared with calculations. Even if an assembly were out of position, the operator could monitor the incore detectors to determine whether a trend was developing toward a radial power tilt. Upon return to power operation after refueling, and to an even greater extent upon initial increase to power, the operator carefully monitors both incore and out-of-core detectors to ensure that core symmetry exists within Technical Specification limits.

4. Precluding Axial Imbalances - During steady-state operation, the axial power shape is very nearly symmetrical about the midplane since the operator is

periodically adjusting the partial-length control rod bank to minimize imbalance. However, during power maneuvering it is possible that the power could be tilted toward the outlet or the inlet.

The resulting effects on DNB and/or fuel melt design limits have been analyzed for a similar B&W PWR design to establish the allowable limits on axial imbalance consistent with the thermal design case. Imbalance trip setpoints have been established (Appendix 4B) for a reactor protection system function (overpower trip based on flow and imbalance) that ensure DNB and fuel temperature limits are not exceeded. Additionally, operating imbalance limits have been established and are evaluated for each fuel cycle. These operating imbalance limits, in addition to the trip setpoints, take into consideration refined calculational techniques and other considerations, e.g., NUREG-630, in establishing operating limits on imbalance. The results of these evaluations for each fuel cycle are documented in the Reload Report, Appendix 4B.

Trip setpoints are verified prior to a cycle's startup and provide core protection, including preclusion of excessive axial power imbalance, up to and including the design overpower level.

During startup testing, incore instrumentation is available to confirm that the out-of-core axial imbalance is as expected. That is, incore instrumentation is used to establish that the out-of-core trip setpoints are consistent with the actual incore imbalance data.

In addition to the trip setpoints and comparison of ex-core to in-core instrumentation outputs, alarm setpoints are provided to alert the operator to core conditions which, if not corrected, could potentially allow a non-conservative condition with respect to the Technical Specifications. Annunciator alarms are initiated if any one of the following conditions exist: (1) APSR's out of limits, (2) regulatory control rods out of limits, (3) core tilt out of limits, and (4) imbalance outside of API envelopes.

4.3.5 Instrumentation Application

Instrumentation and control systems include the Reactor Protection System (RPS), the Safety Features Actuation System (SFAS), the Control Rod Drive Control System (CRDCS), the Integrated Control System (ICS), the Nuclear Instrumentation System (NI), the Non-Nuclear Instrumentation System (NNI), and the Incore Monitoring System (IMS).

The protection systems, which consist of the RPS and the SFAS, perform safety functions. This section discusses instrumentation functional requirements for monitoring and measuring important parameters.

4.3.5.1 Reactor Protection System Instrumentation (RPS)

The basic function of the RPS instrumentation related to the nuclear design is to provide trip signals to protect the reactor core against fuel rod cladding damage. These signals ensure that reactor power level and distribution are within the design limits for existing conditions. The parameters measured include reactor core power, core imbalance, core power-to-flow ratio, and pressure/temperature. Design limits used within the RPS for the aforementioned parameters are described in Section 7.2 of this USAR and in Appendix 4B, the current cycle Reload Report.

4.3.5.2 Safety Features Actuation System Instrumentation (SFAS)

The SFAS monitors variables to detect loss of reactor coolant system boundary integrity. Upon detection of “out-of-limit” conditions of these variables, it initiates emergency core cooling and/or containment isolation.

4.3.5.3 Control Rod Drive Control System Instrumentation (CRDCS)

The functions for the control rod drive instrumentation are: (1) positioning the CRA, (2) indication of CRA position, (3) monitoring of conditions that are important to safety and reliability, and (4) indicating full insertion of CRA after receipt of RPS trip signal.

For position indications between -10% and 0% withdrawn, the rod is to be considered 0% withdrawn. For position indications between 100% and 105%, the rod is to be considered 100% withdrawn. For a position indication less than -10%, or greater than 105%, the signal is to be considered bad.

4.3.5.4 Integrated Control System (ICS)

The ICS provides the proper coordination of the reactor, steam generator feedwater control, and turbine under all operating conditions. The functional criteria related to the nuclear design are maintenance of constant average reactor coolant temperature over the load range from the low level limit to 100% of rated power and maintenance of constant turbine header pressure at all loads.

4.3.5.5 Nuclear Instrumentation (NI)

The Nuclear Instrumentation System is designed to supply the reactor operator with neutron information over the full operating range of the reactor and to supply reactor power information to the RPS, ICS and ARTS. The nuclear instrumentation gives a continuous measurement of reactor power from source level to approximately 125% of rated power. Measurements representing power in the top and bottom halves of the core are used to determine axial core power imbalance.

4.3.5.6 Non-Nuclear Process Instrumentation (NNI)

The non-nuclear process instrumentation provides the required input signals of process variables for the RPS and the regulating and auxiliary systems. It performs the required process control functions in response to those systems and provides instrumentation for startup, operation, and shutdown of the reactor system under normal and emergency conditions. With respect to nuclear design, an important function of this instrumentation is to provide control and interlocks to permit continuous letdown of reactor coolant and makeup to the system to adjust the reactor coolant boron concentration.

4.3.5.7 Incore Monitoring System (IMS)

The Incore Monitoring System provides neutron flux detectors to monitor core performance. Incore, self-powered neutron detectors measure the neutron flux in the core to provide a history of power distribution during power operation. The data obtained provide power distribution information and fuel burnup information to assist in fuel management. The station computer provides normal system readout. Each individual detector measures the neutron flux in its

vicinity and is used to determine the local power density. The individual power densities are then averaged and a peak-to-average power ratio is calculated. This information can be used to ensure core design limits are not violated, detect power oscillations, and detect misloaded fuel assemblies. Incore thermocouples are also installed and utilized to measure core outlet temperatures. All of the thermocouples have an extended range of 0-2300°F to enable the capability to monitor core exit temperatures under postulated accident conditions.

4.3.5.8 Anticipatory Reactor Trip System (ARTS)

The ARTS is a system which initiates a reactor trip if the reactor power is at or greater than 45% of rated thermal power (See ARTS System Description in subsection 7.4.1.4.1.) and a turbine trip occurs, or if a trip of both main feedwater pump turbines occurs. The initiation of the ARTS reactor trip is designed to preclude challenging the High RCS Pressure Trip of the RPS and other devices designed to accomodate and protect against the high RCS temperature and pressure conditions which would follow a turbine trip or loss of feedwater condition, e.g., the relieving of the pilot operated relief valves.

4.3.5.9 Ex-Core Neutron Flux Detectors

The Ex-Core Neutron Flux Detectors consist of two (2) safety grade, Class 1E, electrically independent, physically separated fission chamber radiation level instrument strings, with the capability of a calibrated range of 10^{-2} - 10^{10} n/cm^2 sec. This signal is processed for source range (10^{-1} - 10^5 cps) and wide range indication (10^{-8} - 2 x 10^2 power). Continuous indicators have been provided in the post accident racks located in the main control room. The signal processor also provides audible indication in the main control room and in containment.

TABLE 4.3-3

Excess Reactivity Conditions

Excess Reactivity, CRG 8 at Nominal HFP Position, No Xenon for 70°F, 300°F, and HZP Cases, Equilibrium Xenon for HFP Case, HFP Equilibrium Samarium for all Cases

Temperature, °F	Core Excess Reactivity, % Δk/k	Cycle Lifetime, EFPD
68	16.76	0
68	9.57	390
300	15.58	0
300	8.40	390
HZP	12.98	0
HZP	5.49	390
HFP	7.90	4
HFP	-0.85(3)	390

	k_{eff}
Single fuel assembly (1)	0.80
Cold (2)	0.90

(1) Based on enrichment of 3.5 wt%.

(2) A center-to-center assembly pitch of 31 inches is required for this keff in cold, unborated water with no xenon or samarium.

(3) Negative value is due to power coastdown.

TABLE 4.3-9

pH Characteristics

Lithium-7, ppm	Temp, °F	Boron concentration, ppm	pH units
0.5	70	1800	5.0
2.0	70	1800	5.6
0.5	580	1200	7.0
2.0	580	1200	7.5
0.5	580	17	7.2
2.0	580	17	7.8
0.5	70	17	7.9
2.0	70	17	8.5

TABLE 4.3-10

Uniform Void Coefficients with 1100 ppm Soluble Boron

Moderator temp, °F	Pressure, psia	%(Δk/k)/ % void
70	15	-0.0685
300	800	0.0774
530	2200	-0.0059
580	2200	-0.0136

TABLE 4.3-12

Calculated Three Dimensional Power Peaks

	Normal (Design Transient)	Steady-State
BOL		
Radial	1.51	1.50
Axial	1.61	1.46
Total	2.43	2.19
Near EOL		
Radial	1.34	1.32
Axial	1.76	1.19
Total	2.36	1.57
EOL		
Radial	---	1.30
Axial	---	1.20
Total	---	1.56

TABLE 4.3-13

Core Stability Against Xenon-Induced Power Oscillations

Case	Moderator coeff, $(\Delta k/k)°F$	Stability index, h^{-1} Axial	Azimuthal
Nominal BOL	0.1426×10^{-6}	+0.009	-0.075
Nominal EOL	0.1855×10^{-4}	-0.004	-0.068
Compounded errors, BOL	$+1.0 \times 10^{-4}$	+0.056	-0.035

TABLE 4.3-14

Calculated and Experimental Rod and Rod Assembly Comparison

Core No.	Clusters per core	Ag-In-Cd rods per cluster	H_2O holes, fraction of core	Soluble boron, ppm	CR worth, %Δk/k	
					Experimental	Calculated
5-B	4	4	0.051	1,232	2.02 ± 0.09	2.13 ± 0.02
4-F	4	9	0.0	1,219	3.36 ± 0.09	3.43 ± 0.02
5-C	2	12	0.056	1,167	2.36 ± 0.09	2.44 ± 0.02
4-D	1	16	0.0	1,139	1.45 ± 0.09	1.35 ± 0.02
5-D	2	16	0.058	1,118	2.86 ± 0.09	2.78 ± 0.02
4-E	1	20	0.0	1,365	1.52 ± 0.09	1.48 ± 0.02
5-E	2	20	0.059	1,082	3.06 ± 0.09	3.02 ± 0.02

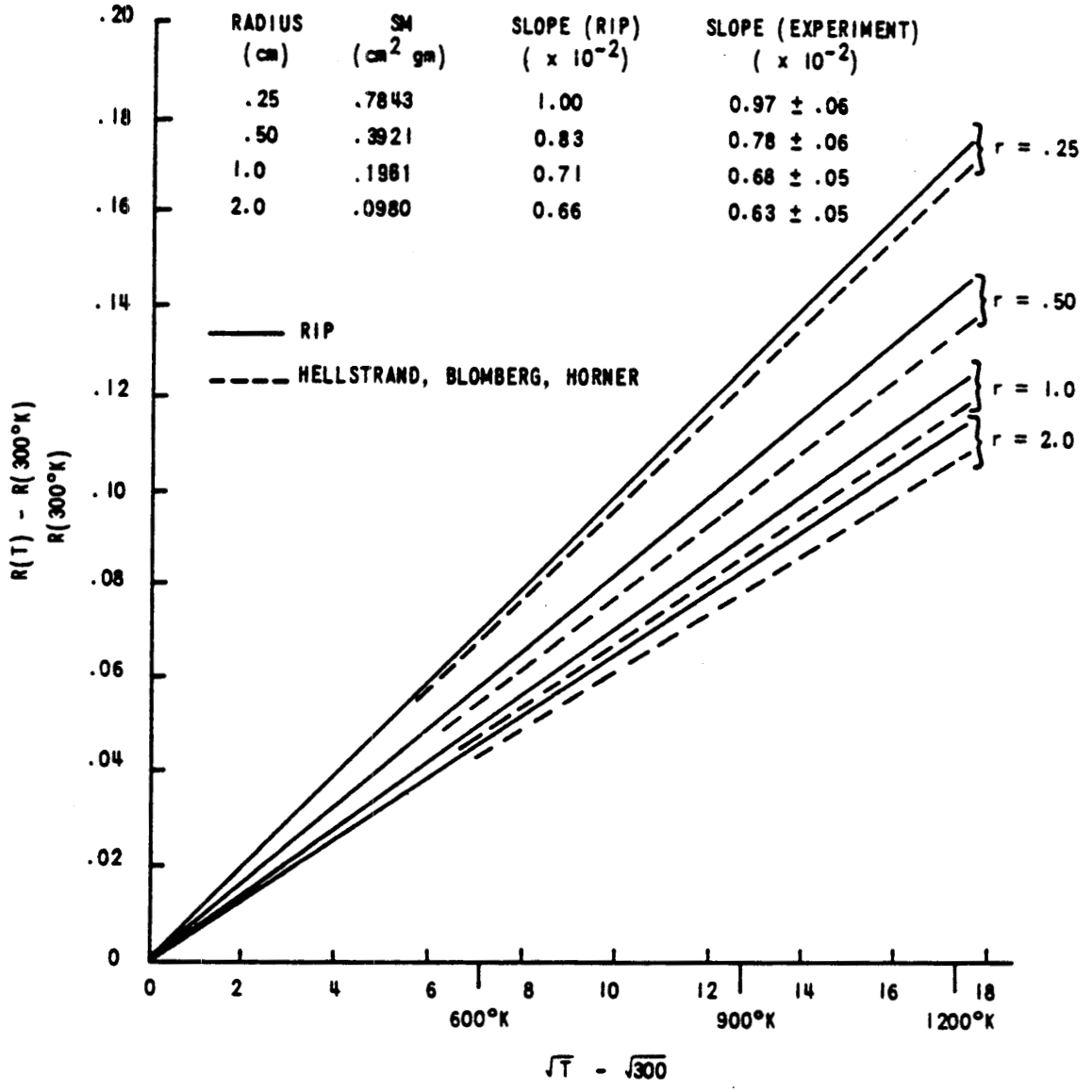

DAVIS-BESSE NUCLEAR POWER STATION
FRACTIONAL CHANGE IN THE RESONANCE INTEGRAL AS A FUNCTION OF $\sqrt{T} - \sqrt{300}$ FOR UO_2 RODS
(T IN DEGREES K)
FIGURE 4.3-2

REVISION 0
JULY 1982

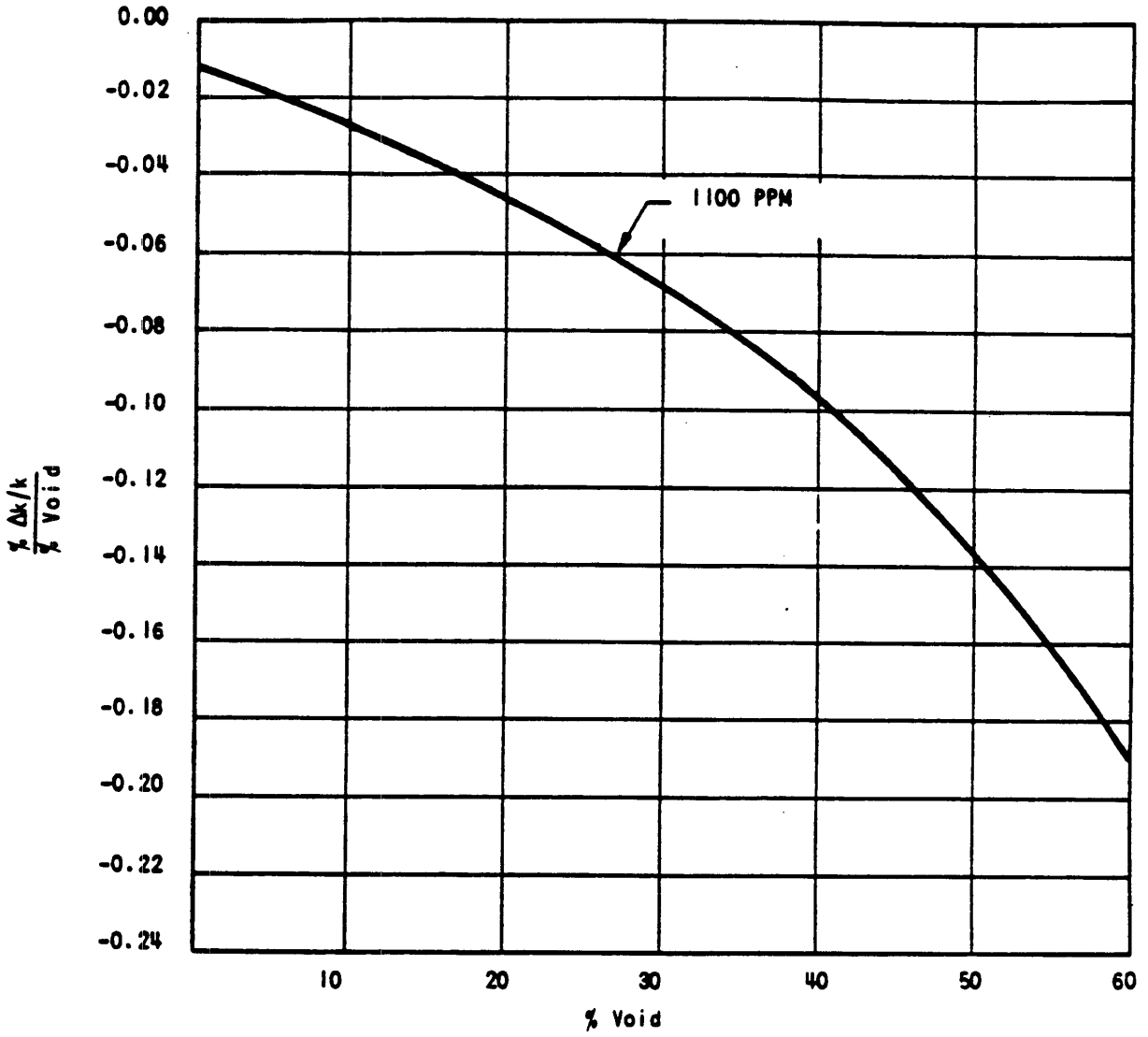

DAVIS-BESSE NUCLEAR POWER STATION
UNIFORM VOID COEFFICIENT FOR
THE DAVIS BESSE CORE
FIGURE 4.3-3

REVISION 0
JULY 1982

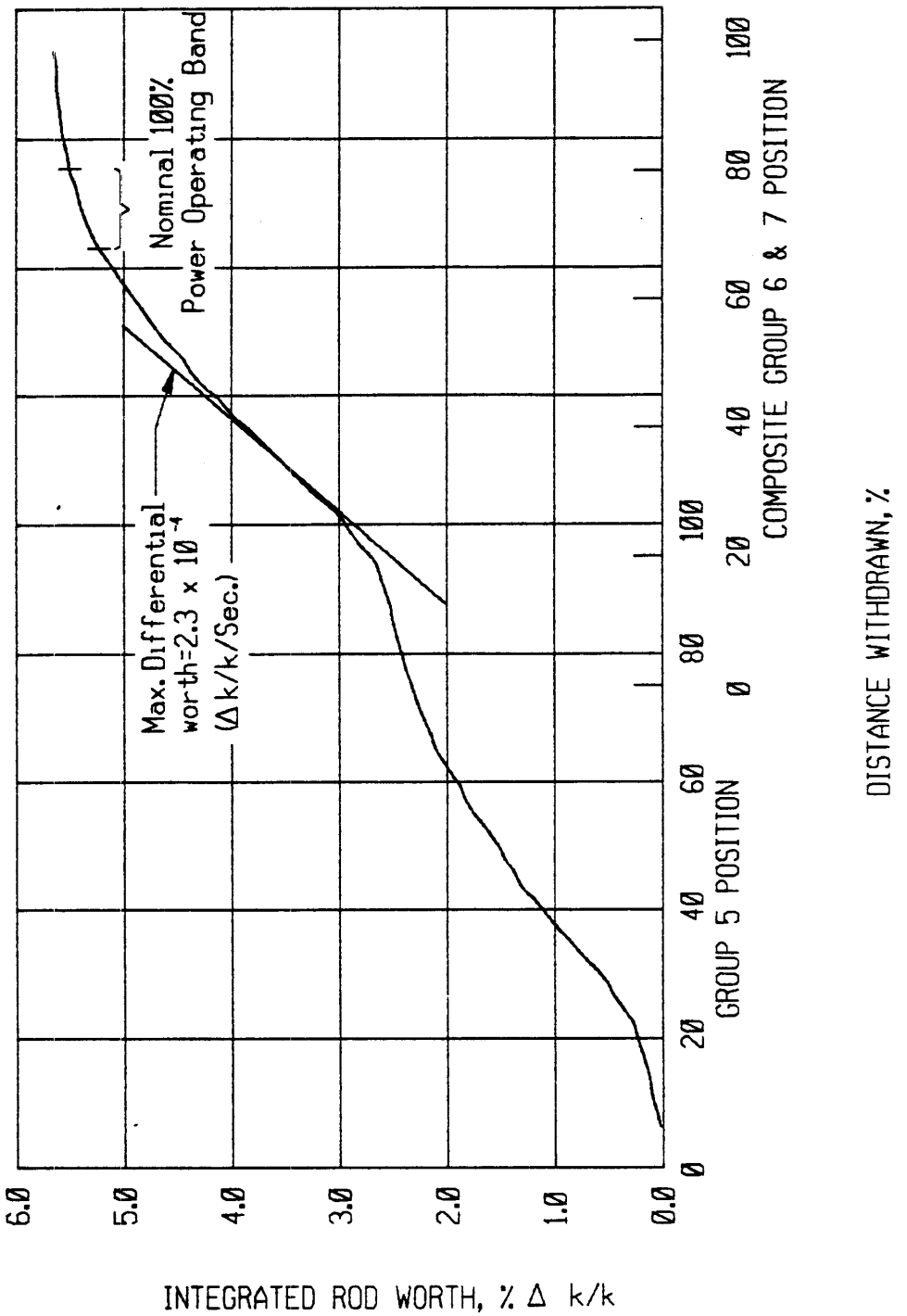

DAVIS-BESSE NUCLEAR POWER STATION
AUTOMATIC CONTROL ROD GROUPS-TYPICAL WORTH CURVE
VS DISTANCE WITHDRAWN
FIGURE 4.3-4

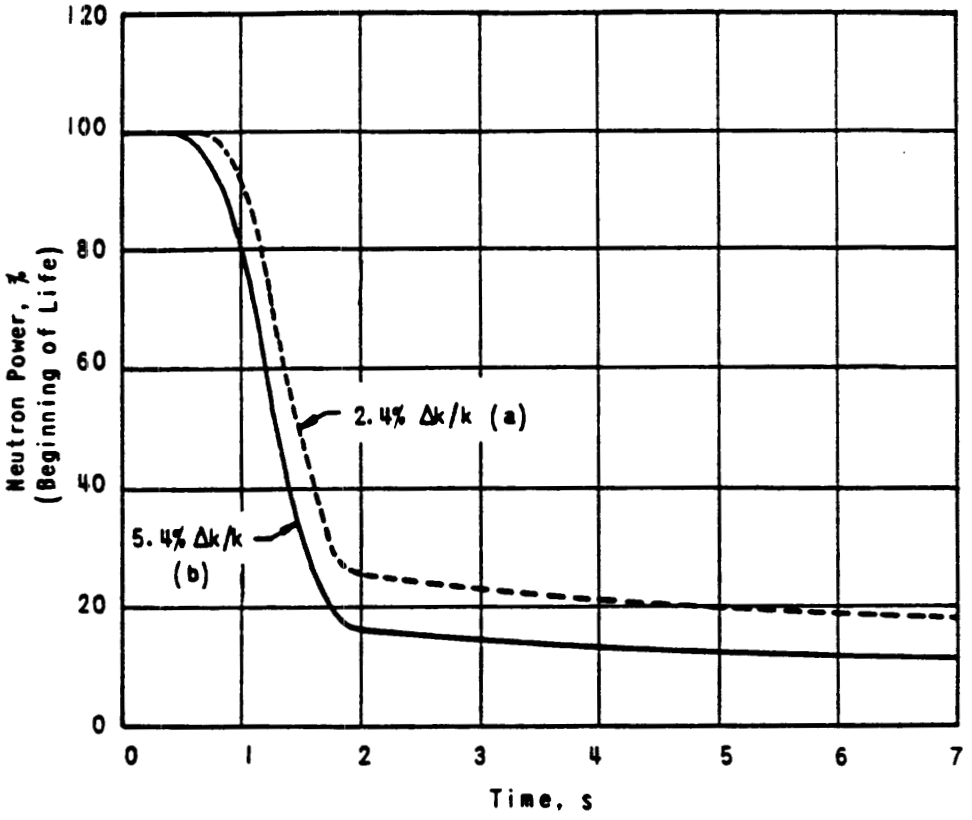

(a) Rod worth required for a 1% shutdown margin

(b) Rod worth required for a 1% shutdown margin + stuck rod worth

DAVIS-BESSE NUCLEAR POWER STATION
PER CENT NEUTRON POWER VERSUS TIME FOLLOWING TRIP
FIGURE 4.3-7

REVISION 0
JULY 1982

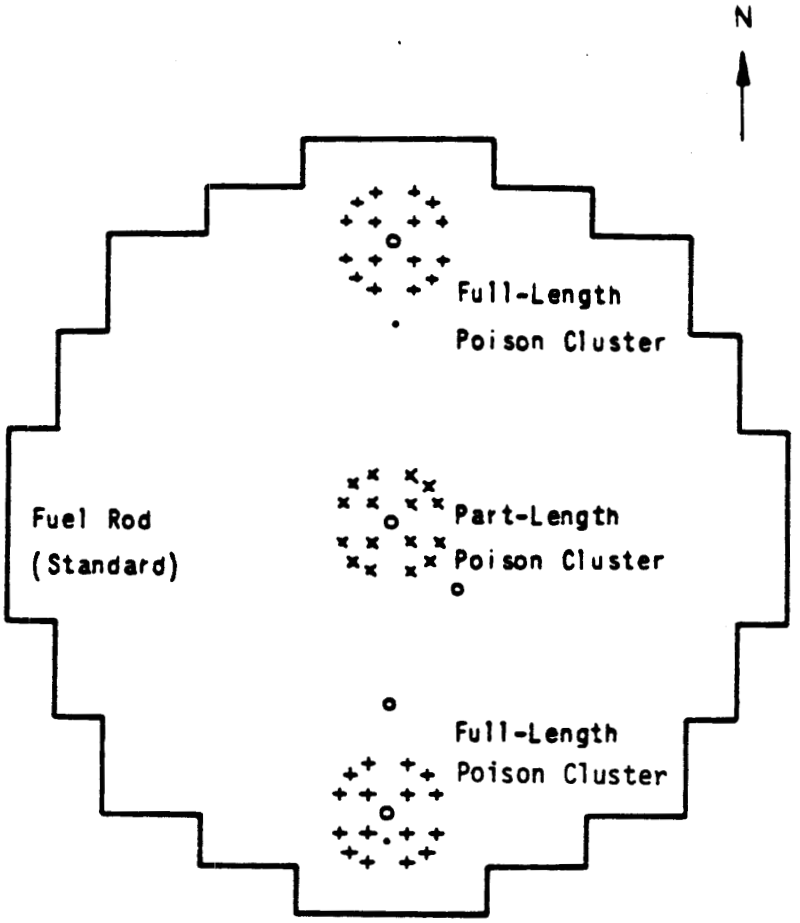

DAVIS-BESSE NUCLEAR POWER STATION
LOADING DIAGRAM FOR CORE IV-H
FIGURE 4.3-9

REVISION 0
JULY 1982

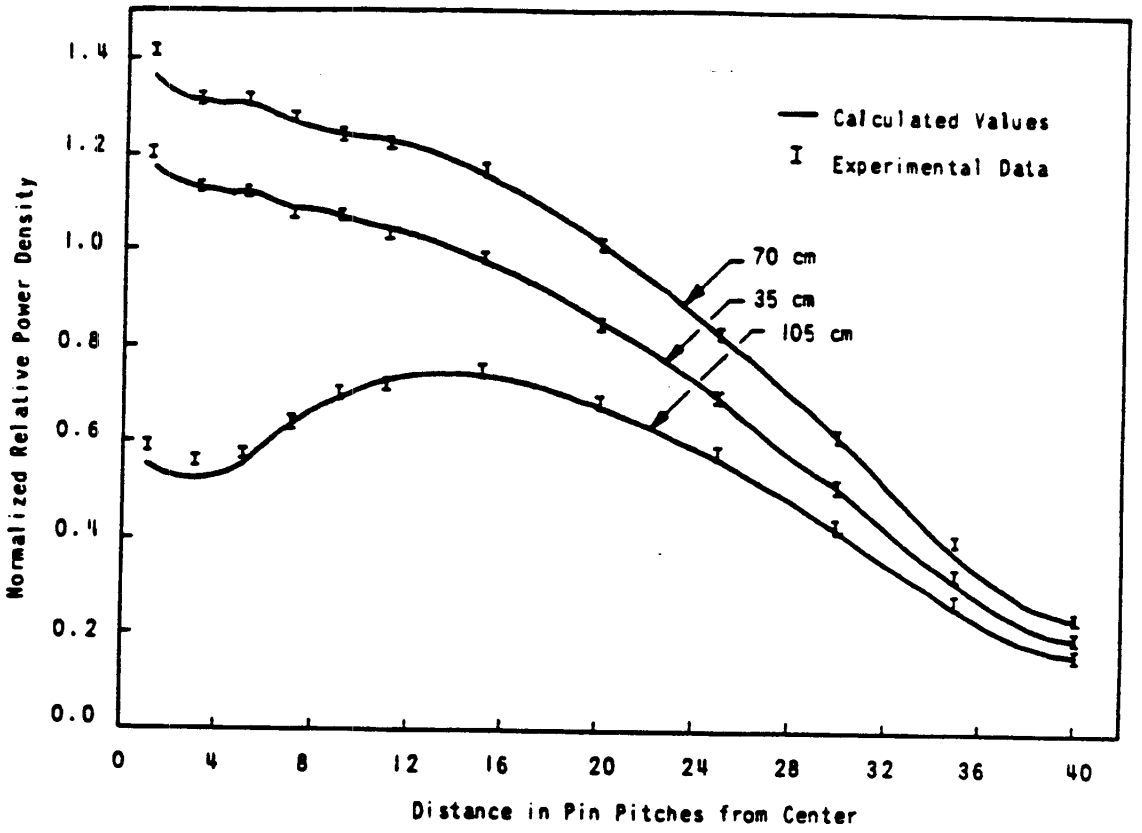

DAVIS-BESSE NUCLEAR POWER STATION
RADIAL POWER DISTRIBUTION AT THREE LEVELS FROM BOTTOM OF CORE
FIGURE 4.3-10

REVISION 0
JULY 1982

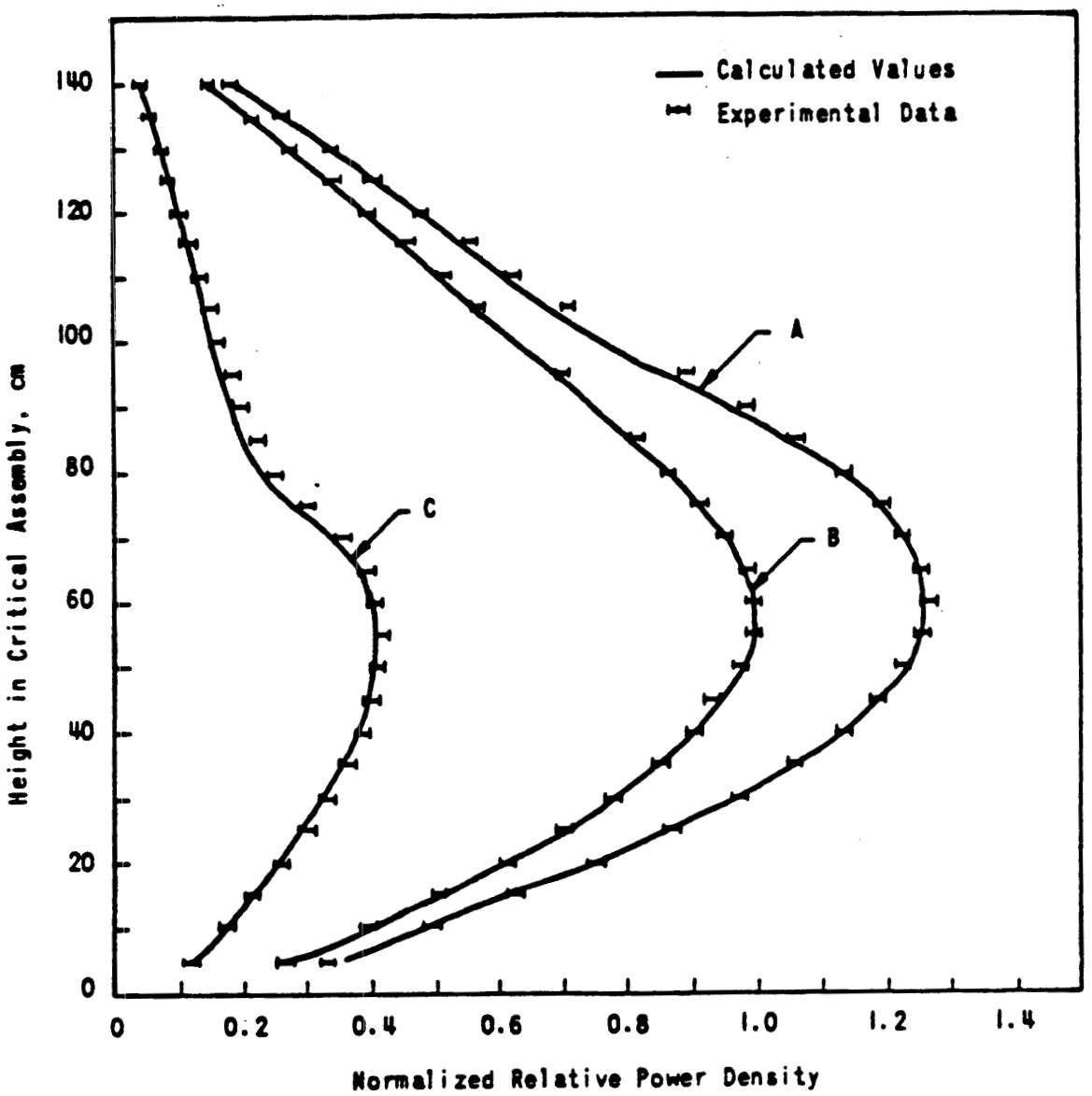

DAVIS-BESSE NUCLEAR POWER STATION
AXIAL POWER DISTRIBUTION AT THREE SELECTED POSITIONS IN THE CORE
FIGURE 4.3-11

REVISION 0
JULY 1982

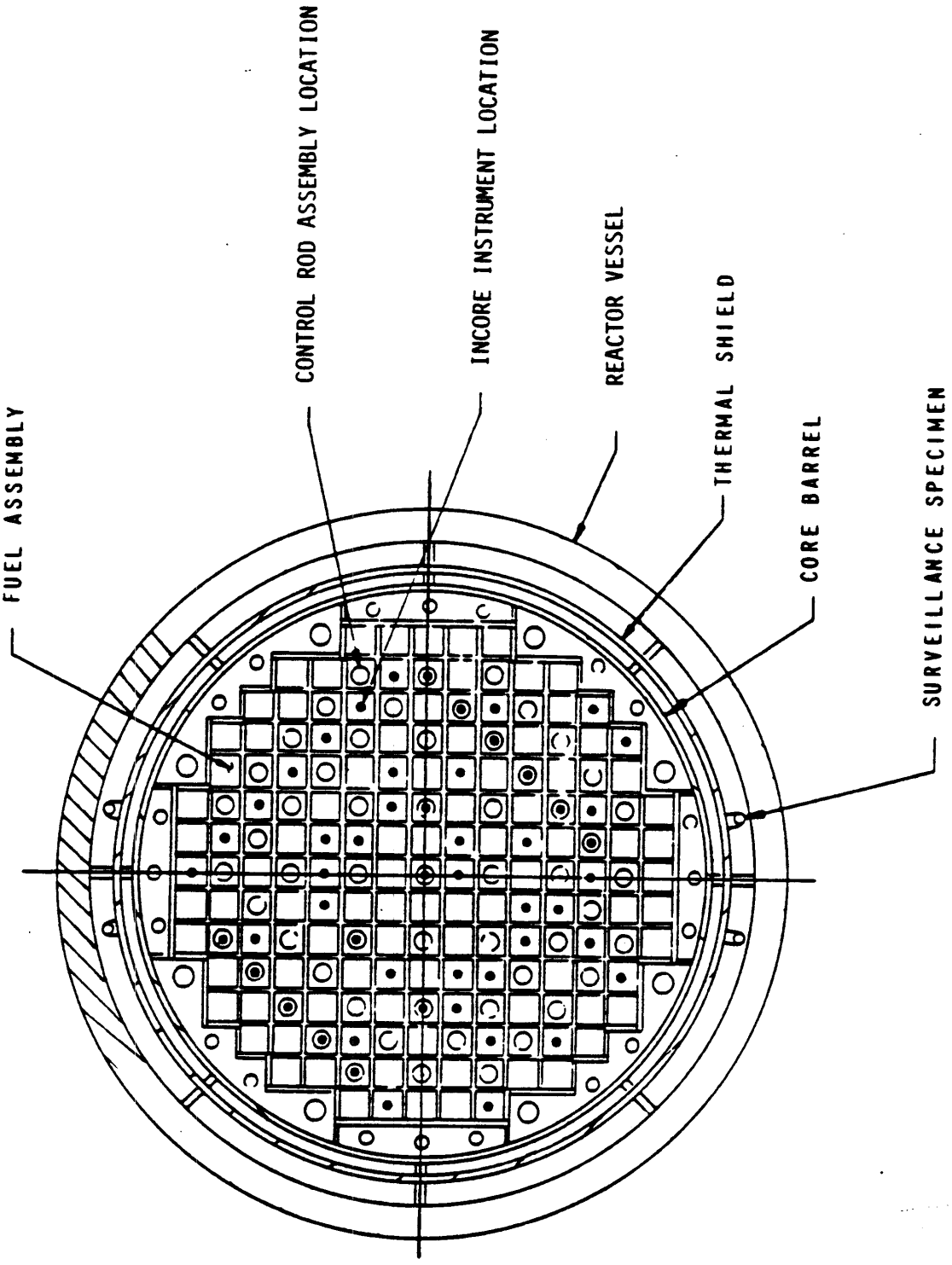

DAVIS-BESSE NUCLEAR POWER STATION
REACTOR VESSEL AND INTERNALS CROSS SECTION
FIGURE 4.3-12

REVISION 0
JULY 1982

4.4 THERMAL AND HYDRAULIC DESIGN

4.4.1 Design Bases

The thermal and hydraulic design data for the current cycle is described in the applicable reload report and associated approved topical reports. Commencing with Cycle 13, Reference 58's approval by the NRC allowed use of the M5 alloy for use in cladding and structural components (i.e. end caps, spacer grids and guide tubes). The following is a description of the original design.

The bases for the thermal and hydraulic design are established to enable the reactor to operate at 2772 MWt rated power with sufficient design margins to accommodate both steady-state and transient operation without damage to the core and without exceeding the code pressure limits for the Reactor Coolant System. The thermal-hydraulic design bases also help ensure that the fuel rod cladding will maintain its integrity during both steady-state operation and anticipated operational transients occurring throughout core life.

Fuel cladding integrity is ensured by subjecting the core to the following thermal-hydraulic limitations:

a. No central melting in the fuel at the design overpower (112% of rated power).

b. The minimum allowable DNBR during normal operation and anticipated transients is 1.30 with the W-3 correlation for the first fuel cycle and with the BAW-2 correlation for subsequent fuel cycles.

c. Although the generation of net steam is allowed in the hottest core channels, flow stability is ensured during all steady-state and operational transient conditions.

By preventing a departure from nucleate boiling, the cladding and fuel are not subjected to excessively high temperatures.

The core flow distribution and coolant velocities are established to provide adequate cooling capability to the hottest core channels and to maintain minimum DNB ratios greater than the design limit.

4.4.2 Description

4.4.2.1 Thermal Hydraulic Design Parameters

Table 4.4-1 compares the reactor thermal-hydraulic initial design parameters for Davis-Besse, Rancho Seco, and Oconee Unit 1.

4.4.2.2 Cladding Thermal Conditions

The thermal and hydraulic design data for the current cycle is described in the applicable reload report and associated approved topical reports. Commencing with Cycle 13, Reference 58's approval by the NRC allowed use of the M5 alloy for use in cladding and structural components (i.e. end caps, spacer grids and guide tubes). The following is a description of the original design.

A digital computer code is used to calculate cladding temperature along with other thermal-hydraulic conditions. The program uses external coolant conditions and heat transfer coefficients determined from thermal-hydraulic solutions. The cladding conductivity is varied with temperature using the correlation given in References 39, 40, and 41.

The assumptions of maximum design conditions (Subsection 4.4.3.4) at the design overpower were applied in the calculation of the outer and inner diameter cladding surface temperatures (shown in Figure 4.4-1) for the hottest unit cell. The nuclear peaking factors associated with this condition are the maximum design radial-local of 1.71 and the 1.5 cosine reference design axial flux shape.

Nucleate boiling conditions prevail at the hot spot, and the Jens and Lottes relationship (Subsection 4.4.2.8) for the coolant-to-cladding ΔT for boiling is used to determine the cladding surface temperature. The resulting greatest average cladding temperature is 716°F at a core operating pressure of 2120 psig.

For comparison, the cladding temperatures associated with the most probable design condition are shown in Figure 4.4-2. The radial-local peaking factor in this situation, 1.70, was used in conjunction with the 1.5 cosine axial flux shape. The resulting maximum average cladding temperature was 712°F. No bulk boiling exists in the channel for this condition.

4.4.2.3 Critical Heat Flux

The thermal and hydraulic design data for the current cycle is described in the applicable reload report and associated approved topical reports. The following is a description of the original design.

One specific criterion for the thermal-hydraulic design of the core is to be safely below the Departure from Nucleate Boiling (DNB) heat flux at the design overpower and/or during anticipated transients. The Critical Heat Flux (CHF) correlation through which the design criterion was evaluated for the first fuel cycle is the W-3 correlation. Subsequent fuel cycle design criteria were derived from utilizing the BAW-2 CHF correlation. The W-3 correlation, in addition to the W-3S[1] (W-35 is modified W-3 for spacer grid factor) and BAW-2 correlations, is explained in detail in Subsection 4.4.2.8. The analytical techniques, including methods of application and associated peaking factors, are provided in Subsection 4.4.3.4.

The minimum DNB ratios for the various channel types located in the highest-powered fuel assembly in the core are presented in Table 4.4-2. The values are given for the design overpower at maximum design conditions (Subsection 4.4.3.4) and also for the rated power at the most probable condition (Subsection 4.4.3.4) for all channel types. Also included in Table 4.4-2 is a comparison of the W-3 correlation with the W-3S and BAW-2 correlations with the associated channel mass velocities.

The limiting channel for all conditions is the hot unit cell. Shown in Figures 4.4-3 and 4.4-4 are the distributed allowable heat flux as predicted by the W-3 correlation and the calculated surface heat flux for the maximum design conditions and most probable design conditions, respectively. Shown in Figure 4.4-5 are the resultant DNB ratios along the channel for the previously mentioned design conditions.

4.4.2.4 Flux Tilt Margin

The thermal and hydraulic design data for the current cycle is described in the applicable reload report and associated approved topical reports. The following is a description of the original design.

In general, it should be noted that no significant radial flux tilts are expected to occur since rod sequencing patterns are symmetrical with respect to the azimuthal direction. If the criterion on rod symmetry is violated, then the reactor is brought to a safe operating power level until the malfunction has been rectified. In addition, quadrant power tilt limits have been established for the incore and out-of-core detector systems as stipulated in Technical Specification 3.2.4. These limits protect the core so that it operates within the thermal design criteria at all times.

4.4.2.5 Void Fraction and Quality Results

The thermal and hydraulic design data for the current cycle is described in the applicable reload report and associated approved topical reports. The following is a description of the original design.

The various void fraction and quality results are presented in Table 4.4-3 for two reactor operating conditions: 1) maximum design at 112% of rated power and 2) the most probable design conditions at 100% rated power. In addition, results of the analysis show exit values pertaining to the core itself, the worst bundle, and the limiting subchannel within the worst bundle as indicated in Table 4.4-3.

The most conservative condition, 112% power for the maximum design case, results in an acceptable void volume in the core. The void volume distribution over the active length for the maximum design limiting unit cell is shown in Figure 4.4-6.

4.4.2.6 Coolant Flow Distribution

The thermal and hydraulic design data for the current cycle is described in the applicable reload report and associated approved topical reports. The following is a description of the original design.

The physical arrangement of the reactor vessel internals and nozzles results in a favorable distribution of coolant flow to the various fuel assemblies. Reactor internal structures above and below the active core are designed to minimize unfavorable flow distribution. A one-sixth scale model of the reactor and internals has been tested to demonstrate the adequacy of the internals arrangements. The tests have verified the conservatism of the design inlet flow distribution and have been reported in B&W Topical Report BAW-10037, Rev. 2, Reactor Vessel Model Flow Tests.

The flow distribution factor, which indicates the amount of flow the bundle is receiving, has been normalized to 1.0; it is a function of the fuel assembly location and the quantity of heat being produced in the assembly. The ratio of flow to power is compared for all of the fuel assemblies based on the reference design radial peaking distribution as shown in Figure 5.3-1. For the maximum design condition, it is assumed that the flow in the hot bundle position is 5% less than the average bundle flow under isothermal conditions corresponding to the model flow test conditions. The results of the model flow test indicate that the assumed 5% flow maldistribution is conservative.

4.4.2.7 Pressure Drop Loads

The thermal and hydraulic design data for the current cycle is described in the applicable reload report and associated approved topical reports. The following is a description of the original design.

The total steady-state, unrecoverable pressure drop from below the flat plate distributor to the upper grid assembly, including the core at 100% power, is listed in Table 4.4-4. The core pressure drops and hydraulic loads occurring during accident conditions are discussed in Subsection 4.2.2 and B&W Topical Report BAW-10041.

The hydraulic force on the fuel assembly receiving the most flow is shown as a function of system flow in Figure 4.4-7. Additional forces acting on the fuel assembly are the assembly weight and a holddown spring force, which result in a net downward force at all times during normal station operation.

4.4.2.8 Thermal Hydraulic Correlations

The following historical design discussion treats the correlations and physical data employed in thermal-hydraulic calculations for pressure drop, critical heat flux, heat-transfer coefficients, and fuel temperatures.

4.4.2.8.1 Pressure Drop

The thermal and hydraulic design data for the current cycle is described in the applicable reload report and associated approved topical reports. The following is a description of the original design.

The procedure for calculating core pressure can be derived by considering the energy equation for an incompressible fluid in steady flow with no shaft work and a constant flow area as follows:

$$\frac{G^2 dv}{g_c} + \frac{1}{v}\frac{g}{g_c}\cos\theta dz + dp\,\frac{1}{v}\delta F = 0$$

where: G = mass velocity, lbm/ft^2 -sec,

v = specific volume, ft^2/lbm,

g_c = constant in Newton's second law = 32.17 lbm-ft/lbf-sec^2,

g = local acceleration of gravity, ft/sec^2,

θ = angle that channel makes with the vertical,

z = space dimension, ft,

p = pressure, lbf/ft^2,

F = unrecoverable pressure losses, lbf-ft/lbm.

Integrating over a small increment so that the coolant properties may be taken as average values results in

$$p_2 - p_1 = -\frac{1}{v}(z_2 - z_1)\frac{g}{g_c}\cos\theta - \frac{G}{g_c}(v_2 - v_1) - \Delta p_f - \Delta p_{Sg}$$

where: Δp_f = pressure drop due to friction,

Δp_{Sg} = pressure drop due to spacer grids.

The subscript 2 denotes the position downstream which makes the pressure loss negative as written. It should be noted that all of the thermodynamic properties are computed from curve fits to the 1967 ASME Steam Tables.

1. Heating Region:

   The frictional pressure drop is obtained from

$$\Delta p_f = \frac{fL\bar{v}}{D_e}\frac{G^2}{2g_c}$$

where f is the Moody friction factor as given by

$$f = f_{iso}\left[1 - 0.001914\ \overline{\Delta T_f}\right]$$

and

$$f_{iso} = \left[2\log_{10}\left[\frac{\varepsilon_r/D_e}{3.715} - \frac{5.028}{Re}\log_{10}\left(\frac{\varepsilon_r/D_e}{3.715} + \frac{16.76}{Re}\right)\right]\right]^{-2}$$

$$\Delta T_f = \frac{q''}{0.023(k_B/D_e)Re^{0.8}Pr^{1/3}}$$

where D_e = equivalent hydraulic diameter, ft,

ε_r = relative roughness, ft,

$Re = GD_e/\mu$, Reynolds number,

$Pr = C_p\,\mu/k$, Prandtl number,

μ = viscosity, lbm/hr-ft,

q" = heat flux, Btu/hr-ft^2.

The pressure drop due to the spacer grids is obtained from

$$\Delta P_{Sg} = K_c v \frac{G^2}{2g_c}$$

where:

$$K_c = C_K \quad (1.4 - 2.4\sigma + \sigma^2),$$

σ = ratio of flow area in spacer grid to unobstructed flow in tube region; the term $(1.4 - 2.4\sigma + \sigma^2)$ is a good fit to the Kays and London form-loss curves at high Reynolds number comparable to those that exist in PWR cores,

C_K = empirical adjustment factor to Kays and London losses; this factor is determined experimentally since spacer grids do not act as expansions and contractions.

2. Local Boiling Region:

The initiation of local boiling for the following pressure drop calculations is defined by solving the nonboiling Colburn convection equation and the Jens and Lottes equation for wall temperature. Local boiling is considered to start when the Jens and Lottes wall temperature is equal to the wall temperature predicted by the Colburn equation. The Moody friction factor is given by

$$f = f_{iso}\left(1 - 0.0025\,\Delta T^*\right)\left[1 + 0.76\left(10^6 / G\right)^{2/3}\overline{\varphi}\right]$$

where

$$\overline{\varphi} = 1 - \frac{\Delta T^*}{\Delta T_f},$$

$$\Delta T^* = \frac{60\,(q'' / 10^6)^{1/4}}{e^{P/900}}.$$

For the calculation of pressure drops due to acceleration, contractions, and expansions, the specific volume is given by

$$v = \frac{(1 - x^*)^2}{1 - \alpha} v_f + \frac{x^{*2}}{\alpha} v_g.$$

For the calculation of pressure drop due to friction and fluid head, the specific volume is given by

$$\frac{1}{v} = \frac{1 - \alpha}{v_f} + \frac{\alpha}{v_g},$$

where α, the coolant void fraction, and x*, the nonequilibrium quality, are dependent on the amount of local boiling, as noted in items a, b, and c below.

The void program uses a combination of Bowring's (ref. 42) model with Zuber's (ref. 43) correlation between void fraction and quality. The Bowring model considers three different regions of forced convection boiling:

a. Highly Subcooled Boiling - In this region, the bubbles adhere to the wall while moving upward through the channel. This region is terminated when the subcooling decreases to a point where the bubbles break through the laminar sublayer and depart from the surface. The highly subcooled region starts when the surface temperature of the cladding reaches the surface temperature predicted by the Jens and Lottes equation. The highly subcooled region ends when

$$T_{sat} - T_{bulk} = \frac{\eta\phi}{V} \qquad (1)$$

where

ϕ = local heat flux, Btu/hr-ft^2,

$\eta = 1.863 \times 10^{-5} (14 + 0.0068p)$, ft^3-hr- °F/Btu-sec,

V = velocity of coolant, fps,

p = pressure, psia.

The void fraction in this region is computed in the manner of Maurer (ref. 44), except that the end of the region is determined by equation 1 rather than by a vapor layer thickness. The nonequilibrium quality at the end of the region is compared from the void fraction as follows:

$$x^*_d = \frac{1}{1 + \frac{\rho_f}{\rho_g}\left(\frac{1}{\alpha_d} - 1\right)} \qquad (2)$$

where

x^*_d = nonequilibrium quality at end of region 1,

α_d = void fraction at $T_{sat} - T_{bulk} = \eta / V$,

ρ_f = liquid component density, lb/ft^3,

ρ_g = vapor component density, lb/ft^3.

b. Slightly Subcooled Boiling - In this region, the bubbles depart from the wall and are transported along the channel (condensation of the bubbles is neglected). This region extends to a point where the thermodynamic quality is equal to the apparent quality. In general, this is the region of major concern in the design of pressurized water reactors.

The nonequilibrium quality in this region is computed from the formula

$$x^* = x^*_d + \frac{P_h}{\dot{m} h_{fg}(1+\varepsilon)} \int_{z_d}^{z} (\phi - \phi_{SP})dz \qquad (3)$$

where

x^* = nonequilibrium quality in region 2,

h_{fg} = latent heat of vaporization, Btu/lb,

$\frac{1}{1+\varepsilon}$ = fraction of heat flux above the single-phase heat flux that actually goes to producing voids,

ϕ_{SP} = single-phase heat flux, Btu/hr-ft^2,

$\dot{m}$ = mass flow rate, lb/hr.

P_h = heated perimeter, ft,

z = channel distance, ft.

The void fraction in this region is computed from

$$\alpha = \frac{x^*}{C_O\left[x^* + \frac{\rho_g}{\rho_f}(1-x^*)\right] + \frac{38.3 A_f \rho_g}{\dot{m}}\left[\frac{\sigma g g_c(\rho_f - \rho_g)}{\rho_f^2}\right]^{1/4}} \qquad (4)$$

where

g = acceleration due to gravity, ft/sec^2

g_c = constant in Newton's 2nd law,
= 32.17 lbm-ft/lbf-sec^2,

C_O = Zuber's distribution parameter,

A_f = flow area, in.^{2},

σ = surface tension,

α = void fraction.

Equation 4 results from rearranging the equations (ref. 43) and assuming bubbly turbulent flow in determining the relative velocity between the vapor and the fluid. Zuber has shown that equation 4 produces a better prediction of the void fraction than do earlier models based on empirical slip ratios.

c. Bulk Boiling - In this region, the bulk temperature is equal to the saturation temperature, and all the energy transferred to the fluid results in net vapor generation. Bulk boiling begins when the thermodynamic (heat balance) quality, x, is greater than the nonequilibrium quality, x*. The void fraction in this region is computed using equation 4 with the thermodynamic quality x replacing x*.

3. Two-Phase Flow Region:

The two-phase friction pressure drop equation follows the same form as the heating pressure drop with the friction factor, f, calculated by

$$\left[(f_{iso})sat\right]\left[\frac{f_{TPF}}{f_{iso}}\right]\frac{\phi_{LO}{}^{2}}{\left[\phi_{LO}\right]^{2} Q_{M.N.}}$$

where

$(f_{iso})sat = f_{iso}$ evaluated at GD_e / μ_{sat}

f_{TPF}/f_{iso} = Martinelli-Nelson local multiplier tabular values as a function of pressure and quality for a fixed portion of the program.

$\frac{\phi_{LO}{}^{2}}{\left[\phi_{LO}\right]^{2} Q_{M.N.}}$ = mass velocity correction multiplier for the Martinelli-Nelson friction multiplier. This is also built into the program in table form as a function of quality and mass velocity.

The specific volume of saturated liquid is used in the calculation of the frictional pressure drop, and the specific volumes for calculating the other components of the pressure drop are computed in the same manner as in the local boiling region.

4.4.2.8.2 Critical Heat Flux Correlations

The thermal and hydraulic design data for the current cycle is described in the applicable reload report and associated approved topical reports. The following is a description of the original design.

The heat-transfer relationship, used to predict limiting heat transfer conditions and to satisfy the thermal design criteria for the initial design and first cycle of Davis-Besse core operation, is the W-3 critical heat flux correlation. Subsequent fuel cycles utilize the BAW-2 correlation which is also described in this subsection. The W-3 correlation equations are as follows:

1. W-3 Uniform Flux DNB Correlation for Single Channel

$$\frac{Q''_{DNB,eu}}{10^6} = (2.022 - 0.00043302\,P)$$

$$+ (0.1722 - 0.0000984\,P)\exp[(18.177 - 0.004129\,P)X]$$

$$[(0.1484 - 1.596X + 0.1729X\,|X|)\,G/10^6 + 1.037]$$

$$[1.157 - 0.869X][0.2664 + 0.8357\exp(-3.151\,D_e)]$$

$$[0.8258 + 0.000894\,(H_{sat} - H_{in})]$$

where

Q" = flux, Btu/hr-ft^2,
P = pressure, psia,
G = mass velocity, lb/hr-ft^2,
X = quality, expressed as fraction,
D_e = equivalent diameter, in.,
H = enthalpy, Btu/lb.

The calculation of $Q''_{DNB,eu}$ for the W-3 correlation is based on data taken over the following ranges of hydraulic conditions:

1000 psia	≤	P	≤ 2300 psia
-0.15	≤	X	≤ +0.15
0.2 in.	≤	D	≤ 0.7 in.
1 x 10^6 lb/hr-ft^2	≤	G	≤ 5 x 10^6 lb/hr-ft^2
10 in.	≤	heated length of channel	≤ 144 in.
0.88	≤	heated perimeter / wettedperimeter	≤ 1.0
		H_{IN}	≥ 400 Btu/lb

2. W-3 Nonuniform Flux DNB Correlation for Single Channel and Axially Nonuniform Beat Flux

$$Q''_{DNB,N} = \frac{Q''_{DNB,eu}}{F}$$

where

$Q''_{DNB,N}$ = DNB heat flux for the nonuniformly heated Channel,

$Q''_{DNB,eu}$ = equivalent uniform DNB flux,

$$F = \left[\frac{C}{Q'' \ell_{DNB} [1 - \exp(-C\ell_{DNB})]} \right]$$

$$x \left[\int_{O}^{\ell_{DNB}} Q''(Z) \exp[-C(\ell_{DNB} - Z)] dZ \right]$$

$$C = \frac{0.15(1 - X_{DNB})^{4.31}}{(G/10^6)^{0.478}} \text{ in.}^{-1}$$

ℓ_{DNB} = distance from inception of local boiling to point of DNB,

Z = distance from inception of local boiling measured in direction of flow.

After the critical heat flux (CHF = $Q_{DNB,eu}$ or $Q_{DNB,N}$) has been evaluated, the DNB ratio is calculated as

$$DNBR = \frac{CHF}{Q''_S x F_{w3}}$$

where

Q''_S = actual heat flux

$$= \frac{\overline{Q} x P_{axial} x P_{rad} x P_{loc} x F_{op} x F''_q}{A_{ht}}$$

$\overline{Q}$ = avg heat rate, Btu/hr,

P_{axial} = axial heat flux factor as function of distance along the channel,

P_{rad} = radial peaking factor,

P_{loc} = local pin peaking factor,

F_{op} = ratio of reactor power to 100% power,

F''_q = hot channel factor on local heat flux

A_{ht} = area of heat ans, ft^2,

F_{w3} = burnout factor.

It should be noted that, depending on the situation being analyzed, the hot channel factors on pin power and local surface heat flux may change; however, at no time will they be less than 1.0. This is explained in Subsection 4.4.3.4.

Comparisons have been given in Subsection 4.4.2.3 for various CHF correlations. The first of these is the W-35. This routine evaluates a DNB ratio which is equal to the DNB ratio given by the W-3 routine, but it is multiplied by a factor, FS, as shown below:

$$FS = 1.0 + 0.03\frac{W}{A_f x 10^6}\left[\frac{\alpha}{0.019}\right]^{0.35}$$

where W = channel flow, lb/hr

A_f = flow area in the tube region, ft^2,

α = intensity of turbulence.

The same data ranges apply to the W-35 as those imposed on the W-3.

The second correlation used for comparison is the BAW-2. The equations are as follows:

1. BAW-2 Critical Beat Flux Correlation for Uniform Axial Flux Profiles

$$q''_u = \frac{(a-b)D_e\left[A_1(A_2G)^{[A_3+A_4(P-2000)]} - (A_9 G x H_{fg})\right]}{A_5(A_6G)^{[A_7+A_8(P-2000)]}}$$

where q''_u = uniform critical heat flux, Btu/hr-ft^2,

P = pressure, psia,

G = mass velocity, lb/hr-ft^2,

x = quality,

D_e = equivalent diameter, in.,

H_{fg} = latent heat of vaporization, Btu/lb

a = 1.15509,

b = 0.40703,

$A_1 = 0.37020 \times 10^8$,

$A_2 = 0.59137 \times 10^{-6}$,

$A_3 = 0.83040$,

$A_4 = 0.68479 \times 10^{-3}$,

$A_5 = 12.710$,

$A_6 = 0.30545 \times 10^{-5}$,

A_7 = 0.71186,

A_8 = 0.20729 x 10^{-3},

A_9 = 0.15208.

2. BAW-2 Critical Heat Flux Correlation for Nonuniform Axial Flux Profiles

$$q''_C = q''_u / F_D$$

Where q''_C = nonuniform critical heat flux, Btu/hr-ft^2,

q''_u = uniform critical heat flux, Btu/hr-ft^2,

$$F_D = K_D \frac{C}{q''[1 - \exp(-CL_{CHF})]} \int_0^{L_{CHF}} [q''(z)] \exp [-C(L_{CHF} - z)]dz$$

$$C = A_{21} \frac{(1-x)^{A_{22}}}{(G/10^6)^{A_{23}}}$$

L_{CHF} = critical heat flux location, in.,

z = distance along channel, in.,

q" = local heat , Btu/hr-ft^2,

K_D = 1.02508,

A_{21} = 0.24867,

A_{22} = 7.82293,

A_{23} = 0.45758.

Again the DNB ratio is calculated in the same manner as for the W-3 with all appropriate terms as shown above.

4.4.2.8.3 Heat Transfer Film Coefficients

The thermal and hydraulic design data for the current cycle is described in the applicable reload report and associated approved topical reports. The following is a description of the original design.

The forced convection film coefficient used to predict the surface temperature of the cladding prior to inception of local boiling is the Colburn equation:

$$h = (C)(0.023)(k_B / De)(Re_B)^{0.8}(Pr_B)^{1/3}$$

where

h = convective film coefficient, Btu/hr-ft^2-°F,

C = Colburn factor on geometry,

k_B = bulk coolant conductivity, Btu/hr-ft^2-°F,

De = equivalent diameter of channel, ft

Re_B = bulk coolant Reynolds number,

Pr_B = bulk coolant Prandtl number.

In general, it is very difficult to predict a forced convection film coefficient for water coolant in local boiling. The best method to date is that given by Jens and Lottes. Thus, the initiation of local boiling is defined as the point at which the surface temperature predicted by the Colburn equation equals that predicted by the Jens and Lottes equation. The surface temperature predicted by the Colburn equation is as follows:

$$T_S = (q''_S/h) - T_B$$

where

T_S = surface temperature predicted by Colburn equation, °F,

q''_S = surface heat flux as defined in Subsection 4.4.2.8.2, Btu/hr-ft^2

T_B = bulk coolant temperature, °F.

The surface temperature predicted by the Jens and Lottes correlation is as follows:

$$T_S = \Delta T_{JL} + T_{sat'}$$

$$\Delta T_{JL} = 60\,[\exp - (P/900)]\,(q''_S/10^6)^{1/4}$$

where

T_S = surface temperature predicted by Jens and Lottes, °F,

T_{sat} = bulk coolant saturation temperature, °F,

ΔT_{JL} =Jens and Lottes wall superheat, °F,

P = coolant pressure, psia

q''_S = surface heat flux as defined in Subsection 4.4.2.8.2, Btu/hr-ft^2.

In the two-phase flow region, the surface temperature is equal to the Jens and Lottes surface temperatures.

In the superheat region, the surface temperature is calculated using the modified Colburn equation as previously described since it is assumed to be accurate for both single-phase liquid and vapor environments.

4.4.2.8.4 Fuel Temperatures

The thermal and hydraulic design data for the current cycle is described in the applicable reload report and associated approved topical reports.

The correlations and physical data employed in determining important characteristics for fuel temperature and internal gas pressure calculations are described in BAW-10141P-A, Rev. 1 TACO Fuel Pin Performance Analysis (Reference 54).

4.4.2.9 Core Operational Transients

The thermal and hydraulic design data for the current cycle is described in the applicable reload report and associated approved topical reports. The following is a description of the original design.

Four operational transients were analyzed to determine minimum core DNB ratio. The analyses included core response to (1) a conservative 10% per minute power loading requirement (20% up to 100% MWe, normal loading requires 5%/min from 90% to 100% MWe), (2) a 10% per minute power unloading requirement (100% down to 20% MWe), (3) a step load requirement of 10% (90% up to 100% MWe), and (4) a step unloading of 100 to 90% MWe. Core temperature, pressure, and power conditions for all of the above were such that the minimum DNB ratio was never below the ratio predicted at 100% steady-state power conditions. The results are shown in Figures 4.4-9 and 4.4-10. The normal operating controls are set so that, should an overpower transient occur, they would preserve a DNBR of 1.30 at 112 percent power. The design overpower condition of 112 percent power assumes design RC flow is available. Should the measured RC flow decrease below design RC flow, Technical Specification 3.2.5 specifies the required actions to be taken. Core responses to other anticipated transients are discussed in Chapter 15.

4.4.2.10 Thermal Hydraulic Analysis Uncertainties

Following is a historical design discussion of the methods employed to estimate and account for the peak or limiting conditions for thermal-hydraulic analysis.

4.4.2.10.1 Pressure Drop

The thermal and hydraulic design data for the current cycle is described in the applicable reload report and associated approved topical reports. The following is a description of the original design.

The total core pressure drop consists of summing the individual pressure drops due to acceleration, contraction and expansion, friction, and elevation. Pressure drop calculations require the estimation of friction factors, material surface roughness, abrupt and gradual expansions, turn losses, etc.

Acceleration ΔP is caused by density changes and is calculated using values tabulated in the 1967 ASME Steam Tables. The determination of pressure drop across a spacer grid or end

fitting is an approximate calculational procedure based on and verified by hydraulic testing of individual grids, end fittings, complete bundles, etc. Kays and London form loss coefficients are used to predict abrupt expansions and contractions and Moody friction factors are used to calculate friction pressure drop. In the two-phase flow region, the Martinelli-Nelson local multiplier is applied to the friction factor.

The elevation ΔP is calculated by multiplying the incremental axial distance by the local density.

Any uncertainties associated with orificing effects have been noted in Subsection 4.4.2.6. To reiterate, the Vessel Model Flow Test (VMFT) results indicate that the 5% flow maldistribution factor applied to the limiting fuel assembly is conservative. Thus, the minimum flow factor as determined statistically from the VMFT data for the center flow region of the core is a factor of 2 less than the 5% factor in determining the core performance.

4.4.2.10.2 Fuel Temperatures

The fuel design data for the current cycle is described in the applicable reload report and associated approved topical reports.

The design criterion for fuel temperature is that no melting occur at any time in life up to the design overpower condition (112%). The linear heat rate at which fuel melting occurs, fuel rod internal pressures, and fuel temperatures are predicted by the thermal code TACO2.

The uncertainties and conservatisms associated with this prediction are discussed in Reference 54.

4.4.2.10.3 Cladding Temperature

The thermal and hydraulic design data for the current cycle is described in the applicable reload report and associated approved topical reports. The following is a description of the original design.

In general, cladding surface temperatures at normal operating conditions never rise more than several degrees above the coolant saturation temperature and thus present no problems in terms of maintaining cladding integrity. The uncertainties associated with predicting cladding temperatures can be traced to the methods and correlations used in the analysis and the accuracy associated with instrumentation used to determine the values of the thermodynamic properties.

To ensure that the predicted cladding surface temperature is a maximum rather than a minimum value, several adjustments are made in the analysis. These adjustments follow closely the definition of the maximum design condition as outlined in Subsection 4.4.3.4. The reduced flow and increased inlet temperature both contribute to a higher cladding surface temperature. The application of hot channel factors results in a higher cladding surface temperature since F_q and F_a indirectly produce an increase in the average bulk coolant temperature.

4.4.2.11 Thermal Hydraulic Design Parameter

Table 4.4-4 lists the historical design thermal-hydraulic parameters. Thermal-hydraulic design conditions for the current fuel cycle are provided in Section 6 of Appendix 4B, Reload Report.

4.4.3 Evaluation

4.4.3.1 Hydraulics Evaluation

The design data for the current cycle is described in the applicable reload report and associated approved topical reports. Commencing with Cycle 13, Reference 58's approval by the NRC allowed use of the M5 alloy for use in cladding and structural components (i.e. end caps, spacer grids and guide tubes).

a. The results of vessel model flow tests are contained in B&W Topical Report BAW-10037, Rev. 2.

b. The empirical correlations selected for use in analyses for both single-phase and two-phase flow conditions are discussed in Subsection 4.4.2.8.

c. The reactor coolant pump characteristics are shown in Figure 4.4-12, which is a typical head capacity curve for the Davis-Besse pumps. The design operating points for four-pump, three-pump, and two-pump operation are marked on the figure and tabulated below.

Pump Characteristics

Pump combination loop 1/loop 2	Flow, gpm/pump	Required NPSH, psi	Available NPSH, psi
2/2	88,000	35	960
2/1	92,100/118,000	39/77	960
1/1	120,400/120,400	82/82	960

As shown in the tabulation above and in Figure 4.4-12, the maximum NPSH requirement occurs when one pump is operating in each loop. The NPSH margin ($NPSH_{available} - NPSH_{required}$) is 878 psi at operating temperature and pressure.

4.4.3.2 Power Distribution Influence

The thermal and hydraulic design data for the current cycle is described in the applicable reload report and associated approved topical reports. The following is a description of the original design.

The core has been designed to allow power maneuvering with control rods. During steady-state operation the axial power shape is very nearly symmetrical about the midplane, since the operator is periodically adjusting the partial-length control rod bank to minimize imbalance. However during power maneuvering, it is possible that the power could be tilted toward the outlet or the inlet.

The resulting effects of axial imbalance and the associated radial peaking distributions on DNB and/or fuel design limits have been analyzed to establish the allowable limits on axial imbalance consistent with the maximum thermal design case as described in Subsection 4.4.3.4. The imbalance trip setpoints have been established for a reactor protection system function that ensures that the thermal design criteria on DNB and fuel temperature limits are not exceeded. In addition to the trip setpoints, alarms are provided to alert the operator to core conditions which, if not corrected, could potentially allow a non-conservative condition with respect to the Technical Specifications. The annunciator alarm is initiated if any one of the following conditions exist: (1) APSR's out of limits, (2) regulating control rods out of limits, (3) core tilt out of limits, and (4) imbalance outside of API envelopes. The imbalance limit envelope and the appropriate design conditions are given in Technical Specification 2.1.

The imbalance envelope is the result of analyses of power shapes that may exist in the core. Power distributions can have an arbitrary axial shape provided the associated combined radial peak yields an acceptable result in terms of the design thermal limits. Figure 4.4-13 shows the position versus allowable peak for DNBR conditions equivalent to a symmetrical cosine distribution. The maximum design radial-local power factor of 1.71 has been used in Figure 4.4-13. Figure 4.4-14 presents the allowable conditions when the radial-local power factor is 1.60 instead of 1.71. A comparison of Figures 4.4-13 and 4.4-14 shows the additional allowable outlet peak for less than the maximum design radial-local.

4.4.3.3 Core Thermal Response

The thermal and hydraulic design data for the current cycle is described in the applicable reload report and associated approved topical reports. The following is a description of the original design.

Table 4.4-4 shows core and hot channel steady-state design conditions. During transient operation, the core response is determined for variations of system power, flow, and pressure and core inlet temperature. For power loading and unloading transients, the hot channel DNB ratio is shown in Subsection 4.4.2.9. Core conditions during other anticipated operational transients are discussed and shown in Chapter 15.

4.4.3.4 Analytical Techniques

The analytical techniques discussed below were used for the original core thermal-hydraulic design calculation.

4.4.3.4.1 Design Conditions

The thermal and hydraulic design data for the current cycle is described in the applicable reload report and associated approved topical reports. The following is a description of the original design.

The core performance is analyzed for two basic conditions: maximum design conditions and the most probable conditions. The former situation is the most severe, and the latter provides a convenient comparison for the expected conditions in the core.

Maximum Design Conditions - The maximum design condition is analyzed at the overpower limit of 112%, which will not be exceeded under any circumstances. This condition also assumes that the worst nuclear, thermal, and mechanical conditions exist simultaneously in a particular subchannel. If this particular channel meets all the thermal design criteria, then it can be safely assumed that all other channels in the core will be no worse thermally than this limiting channel.

The maximum design conditions are then represented by the following assumptions:

a. The limiting fuel assembly possesses the fuel pin with the maximum value of FΔh (1.71) as determined from examination of the reference design radial peaking distribution and from examination of the maximum, nominal, and minimum fuel assembly spacing to find the effects on the local peaking distribution.

b. The maximum value of F_z nuclear (max/avg axial fuel rod heat input) is determined for the limiting transient or steady-state conditions.

c. Every channel in the core is assumed to have the nominal pressure drop associated with the core flow conditions.

d. The limiting fuel assembly is assumed to receive only 95% of the flow associated with an average core bundle at 100% of system flow (four-pump operation).

e. The limiting fuel assembly is assumed to have a reduced peripheral flow area due to adjacent fuel assembly proximity.

f. On the subchannel types with maximum values of FΔh, three different hot channel factors are applied.

    1. The channel is assumed to have a reduced flow area, represented by the hot channel factor F_A, of less than 1.0.

    2. The fuel pin will have the greatest heat output by virtue of F''_g, which increases the local surface heat flux, and F_g, which increases the overall fuel pin power rating; both values are greater than 1.0 (see Table 4.4-4).

Most Probable Design Conditions - In general, the most probable design condition is defined as that which occurs at the nominal power rating (100%) of the core. In addition, this analysis assumes that nominal specified conditions prevail in the core for the reference design peaking condtions. Thus, the most probable design conditions are assumed to be the same as the maximum conditions with the following exceptions:

a. The limiting fuel assembly is assumed to have a nominal value of FΔh nuclear (1.70).

b. The limiting fuel assembly is assumed to have no flow maldistribution, nor is there a flow area penalty for the peripheral flow channels due to bundle spacing.

c. Hot channel factors are not applied to the subchannels; thus, they have a nominal flow area and the maximum calculated value of heat input. F_q and F''_q are assigned a value of 1.0.

4.4.3.4.2 Pressure Drop

The thermal and hydraulic design data for the current cycle is described in the applicable reload report and associated approved topical reports. The following is a description of the original design.

An accurate pressure drop model is required for the TEMP code because the individual channel flow rate is determined by dividing the total bundle flow in such a manner that the plenum to plenum pressure drop of each channel is equal. Three different flow regimes are considered in the calculation of pressure drop: heat addition without boiling, with local boiling, and with bulk boiling. The calculational techniques used to determine the pressure drop in these regions are discussed in Subsection 4.4.2.8. In general, the methods used in TEMP are extensions of the recommendations made in Reference 45. The uncertainties associated with pressure drop calculations are discussed in Subsection 4.4.2.10. For a detailed discussion of the TEMP program, see B&W topical report BAW-10021.

4.4.3.4.3 Hot Channel Factors

The thermal and hydraulic design data for the current cycle is described in the applicable reload report and associated approved topical reports. The following is a description of the original design.

The calculation of DNB heat flux involves the coolant enthalpy rise and the coolant flow rate. Therefore, the uncertainties on DNB heat flux must include the uncertainties on coolant enthalpy rise and coolant flow rate. The coolant enthalpy rise is a function of both the heat input and the flow rate. It is possible to separate these two effects; the statistical hot channel factors required are a heat input factor, F_Q, and a flow area factor, F_A. In addition, a statistical heat flux factor, F''_Q is required; the heat flux factor statistically describes the variation in surface heat flux. The DNBR is most limiting when the DNB heat flux is based on minimum flow area (small F_A) and maximum heat input (large F_Q) and when the surface heat flux is large (large F''_Q). The DNB correlation is provided in a best-fit form, i.e., a form that best fits all the data on which the correlation is based. To afford protection against DNB, the DNB heat flux computed by the best-fit correlation is divided by a DNB factor (BF) greater than 1.0 to yield the design DNB surface heat flux. The basic relationship,

$$\mathrm{DNBR} = \frac{q''_{\mathrm{DNB}}}{\mathrm{BF}} \times f(F_A, F_Q) \times \frac{1}{q''_{\mathrm{surface}} \times F''_Q},$$

involves as parameters statistical hot channel and DNB factors. The DNB factor above is assigned a value of unity when reporting DNB ratios, so that the margin at a given condition is shown directly by a DNBR greater than 1.0, i.e., 1.30 in the hot channel.

Selected heat-transfer data are analyzed to obtain a correlation. Since thermal and hydraulic data are generally well represented with a Gaussian (normal) distribution, mathematical parameters that quantitatively rate the correlation can be easily obtained for the histogram.

In analyzing a reactor core, the statistical information required to describe the hot channel subfactors may be obtained from data on the as-built core, from data on similar cores that have been constructed, or from the specified tolerances for the proposed core. The design factors

are shown graphically in Figures 4.4-15 and 4.4-16. All the plots have the same characteristic shape whether they are subfactors, hot channel factors, or DNB factors. The factor increases with either increasing population or confidence. The value used for the statistical hot channel and DNB factor is a function of the percentage of confidence desired in the result, and the portion of all possibilities desired, as well as the amount of data used in determining the statistical factor. An assumption used frequently in statistical analyses is that the data available represent an infinite sample of those data. The implications of this assumption should be noted. For instance, if limited data are available, such an assumption leads to a somewhat optimistic result. The assumption also implies that more information exists for a given sample than is indicated by the data; it implies 100% confidence in the end result. The B&W calculational procedure does not make this assumption; rather it uses the specified sample size to yield a result that is much more meaningful and statistically rigorous.

The local surface heat flux factor (F''_Q) is a function of variations in the fuel pellet size, density, enrichment, and cladding diameter. The hot channel factor on average pin power is a function of variations in stack weight, length, and enrichment. These variations have been obtained from specified tolerances and/or measured data and have been combined statistically to obtain the appropriate hot channel factor.

The hot channel factors on local surface heat flux and average pin power can be written as follows:

$$F''_Q = 1 + k\,Cv\,(F''_Q)$$

$$F_Q = 1 + k\,Cv\,(F_Q)$$

where:

F''_Q = statistical hot channel factor on local surface heat flux,

F_Q = statistical hot channel factor on average pin power,

k = statistical tolerance factor based on sample size, confidence level, and population protected,

Cv = coefficient of variation.

The values of F_Q and F''_Q used in designing the core are given in Table 4.4-4, and they are also shown graphically in Figure 4.4-16.

Associated with the hot channel factors F_Q and F''_Q is a statistical tolerance factor that implies that there is a 99% confidence that 95% of the population is protected.

The hot channel factor on the flow area reduction factor is determined for the as-built fuel assembly by taking channel flow area measurements and statistically determining an equivalent hot channel flow area reduction factor. Interior channel measurements and measurements of the channels formed by the outermost fuel rods with adjacent assemblies have been analyzed. Coefficients of variation for each type of channel have been determined. In the analytical solution for a channel flow, each channel flow area is reduced over its entire length by the F_A

factors shown in Figure 4.4-16 for the desired population protected at a 99% confidence. The hot channels have been analyzed using values for 95% population protected, or an F_A of 0.98 in the interior cells and an F_A of 0.97 in the wall cells, as reported in Table 4.4-4.

A penalty factor for rod bowing was calculated for each fuel batch in a fuel cycle's core load. The magnitude of the rod bow penalty applied to each fuel cycle was equal to or greater than the necessary burnup-dependent DNBR rod bow penalty for the applicable cycle minus a credit of one percent for the flow area reduction factor as described above. The rod bow penalty factor is applied to all plant operating limits which are based on DNBR criteria. A rod bow topical report, Reference 53, which addresses the mechanisms and resulting local conditions of rod bow, has been submitted and approved by the NRC. The topical report concludes that rod bow penalty is insignificant and offset by the reduction in power production capability of a fuel assembly with irradiation. As such, no reduction in DNBR (and affected plant operating limits) is now required to accomodate postulated fuel rod bow conditions.

In addition, there is a fuel melting hot channel factor, F_{fm}, used in calculating the maximum linear heat rate. The value used for F_{fm} is 1.03, which represents a 99% confidence and a 99% population protected.

In general, these factors are used in direct solution for channel enthalpies and are not expressed as factors on enthalpy rise, as is often done.

4.4.3.4.4 Fuel Temperatures

The fuel design data for the current cycle is described in the applicable reload report and associated approved topical reports.

a. Beginning-of-Life Fuel Temperature

TACO2 (Reference 54), a fuel temperature and gas pressure computer code is run for a predetermined set of parameters corresponding to BOL conditions. These parameters consist of gas composition in the prepressurized fuel rod, the maximum BOL nuclear radial power peak, and an axial power shape of 1.5 max/avg. Plots showing BOL maximum and average fuel temperatures versus linear heat rate kW/ft) are shown in Figures 4.4 17 and 4.4 18. Both nominal and maximum design diametral gap conditions (7.0 and 8.5 mils, respectively) are shown.

b. End-of-Life Fuel Temperature

Fuel rod properties change as a result of irradiation. TACO2 incorporates appropriate modeling to account for the effects of these changes and is used to predict the variation of fuel temperatures with power and burnup. Figures 4.4-19 and 4.4-20 show the affects of irradiation on volumetric average and center-line temperatures, respectively, for a condition where the local linear heat generation rate has been assumed to be 18 kW/ft. These temperatures were calculated using the methods described in Reference 54 at BOL because of the production and release of fission gas products with fuel burnup. EOL centerline and average fuel temperatures versus linear heat rate (kW/ft) are shown in Figures 4.4-19 and 4.4-20.

c. Fuel Pin Internal Pressure

The maximum prepressurized fuel rod internal pressure is determined using TACO2. The input required for this analysis is the worst nuclear radial peaking power history. This worst-power history is associated with the worst peaking over the assembly's lifetime and the worst burnup combination.

4.4.3.5 Hydraulic Stability

The thermal and hydraulic design data for the current cycle is described in the applicable reload report and associated approved topical reports. The following is a description of the original design.

An analysis was conducted to investigate the possibility of hydraulic oscillations occurring in a reactor flow channel. The single channel studied is the hot channel in the reactor core, which is parallel to the other channels and is assumed to share a constant pressure drop across its length with the other channels. Since the channel of highest thermal state is studied, provisions have been made for the boiling and two-phase flow that can cause prohibitive flow instability. The program establishes a steady-state condition, then imposes a heat disturbance; the flow transient is then calculated as a function of time.

The two curves showing the resulting flow transients (Figure 4.4-21) were run at 100 and 170% power. The inlet conditions to the channel in each case were the nominal conditions for the hot channel at 100% power. Both cases were subjected to a perturbation of 5% of the initial power level at time equal to zero. From these curves it is easy to see that both cases are stable because the oscillations damp out; in an unstable case, each oscillation would become larger.

4.4.3.6 Temperature Effects on Waterlogged Elements

The design data for the current cycle is described in the applicable reload report and associated approved topical reports. The following is a description of the original design.

The potential for a waterlogged fuel rod is discussed in Subsection 4.2.1.4.4. If a cold fuel rod were to become waterlogged and experience a temperature transient, it is possible that the internal pressure of the rod could exceed system pressure. The internal pressure is dependent on the temperature transient, the amount of water in the fuel rod, and the size of the assumed defect that permitted waterlogging in the first place.

If the temperature transient and water content of the fuel rod are maximized, then the internal pressure of the fuel rod may be calculated as a function of defect size. If the size of the defect has a flow area equivalent to a hole approximately 3 mils in diameter or larger, the internal pressure of the fuel rod remains below the allowable pressure of 3300 psi.

The effects of oxidation and hydriding make it improbable that a defect would have a uniform area through the cladding sufficiently small to cause excessive pressure in the fuel rod. The ΔT across the cladding, oxidation, and hydriding will all tend to flare the defect, leaving a thin portion of the cladding controlling the defect size. Therefore, if the pressure were to increase, the thin portion of the cladding surrounding the defect that was controlling the flow of steam would enlarge and relieve the pressure.

4.4.3.7 Temperature Effects During Operational Transients

The thermal and hydraulic design data for the current cycle is described in the applicable reload report and associated approved topical reports. The following is a description of the original design.

To investigate the possibility of rod bowing and fuel damage, a pressurized water reactor fuel rod has been analyzed during an assumed DNB condition. The cladding temperature distribution was obtained from the analysis discussed in Subsection 4.4.3.10. The analyzed condition yields a maximum cladding temperature of 1025°F (Figure 4.4-22). The ultimate strength of Zircaloy-4 cladding at 1100°F is approximately 15,000 psi (refs. 46 and 47). Therefore, on a short-term basis, the rod would be capable of withstanding an internal rod pressure of 4200 psi. The maximum internal fuel rod pressure obtained under the postulated conditions is 2060 psia. This indicated that the cladding would collapse on the fuel rather than burst. Therefore, neither internal nor external pressure would cause sudden failure of the fuel rods. The fuel center temperature distribution is shown in Figure 4.4-23. The maximum fuel temperature experienced in this analysis is 3585°F. This is well below the melting temperature (4800°F) for UO_2 fuel at approximately 43,000 MWd/mtU burnup (ref. 48), as shown in Figure 4.4-23.

Bowing of the fuel rod at the cladding hot spot (1025°F) was calculated to be 0.049 inch.

4.4.3.8 Energy Release and Potential for Chemical Reaction

The thermal and hydraulic design data for the current cycle is described in the applicable reload report and associated approved topical reports. The following is a description of the original design.

Assuming that a DNB condition occurs, the cladding temperature increases as a result of the transition and film boiling regions. The Baker-Just equation (ref. 49) can be used to determine the energy produced and the thickness of metal reacted as a function of temperature.

The energy release and the potential for a chemical reaction are evaluated assuming that a DNB condition has created an abnormal cladding temperature. A parametric study was conducted with cladding temperatures of 1000, 1200, and 1400°F, which more than cover the expected DNB cladding temperatures. The cladding temperatures are assumed to remain constant with time.

The energy produced per unit length of cladding by the zirconium-water reaction is small compared to the energy produced by the fuel element. Figure 4.4-24 shows a parametric study of the energy released due to the chemical reaction with time. The cladding thickness reacted is quite small; Figure 4.4-25 shows a parametric study of the cladding thickness reacted with time.

4.4.3.9 Rupture of Waterlogged Element

The thermal and hydraulic design data for the current cycle is described in the applicable reload report and associated approved topical reports. The following is a description of the original design.

The pressure pulse that results from the rupture of an assumed waterlogged fuel rod causes no significant damage to the rest of the core. Several tests have been run in test reactors under conditions more severe than are experienced in PWR reactors with no significant damage.

The tests run for the U.S. Atomic Energy Commission in Idaho Nuclear (refs. 50-52) have all shown that less than 3% of the nuclear energy is converted to mechanical energy in terms of a pressure pulse. In these tests, the most significant damage caused by the failed rods was bowing of adjacent rods.

4.4.3.10 Effects of Coolant Flow Blockage

The thermal and hydraulic design data for the current cycle is described in the applicable reload report and associated approved topical reports. The following is a description of the original design.

A PWR fuel rod has been analyzed during an assumed DNB condition. The analysis was performed at 100% power with an assumed abnormal flow condition (inlet flow blockage) that would cause a DNB. The minimum DNB ratios (W-3) occurring in the blocked channel are shown as a function of inlet area blockage in Figure 4.4-26. A DNB ratio of 1.00 occurs if approximately 69% of the channel inlet flow area is blocked.

Operation at the postulated conditions would result in a maximum fuel rod surface temperature of 1025°F and a maximum fuel temperature below the melting point for UO_2, as discussed in Subsection 4.4.3.7. The energy release and the potential for a chemical reaction under these conditions are discussed in Subsection 4.4.3.8.

4.4.4 Testing and Verification

The thermal and hydraulic design data for the current cycle is described in the applicable reload report and associated approved topical reports. Commencing with Cycle 13, Reference 58's approval by the NRC allowed use of the M5 alloy for use in cladding and structural components (i.e. end caps, spacer grids and guide tubes). The following is a description of the original design.

B&W has gone to considerable lengths to initially test their design and then to verify the results through as-fabricated dimensional measurements.

The physical arrangement of the reactor vessel internals and nozzles results in a nonuniform distribution of coolant flow to the various fuel assemblies. Reactor internal structures above and below the active core are designed to minimize unfavorable flow distribution. The B&W 177 fuel assembly plant, with Mark B fuel, has several inherent design features to minimize or eliminate the potential of baffle gap flow problems. These design features are as follows:

1) The B&W design is significantly different from the other vendor's design in that in the B&W design, there is a small differential pressure between the bypass region and the core.

2) The B&W design utilizes edge bolts in the baffle plates to assure that unwanted gaps do not form in the baffle plates.

3) A series of 1 3/8-inch holes are drilled in the baffle plates at several elevations to relieve the pressure differential between the bypass region and the core in the

event of a LOCA. During normal operation, these holes help eliminate any pressure differential between the core and bypass region. Also, a series of narrow slots are machined into the baffle plates in the center of the baffle plates. Some crossflow through these openings may exist; however, the velocities are low and are not considered a problem.

4) No flow related fuel rod failures on B&W 177 fuel assembly plants have been identified.

A 1/6-scale model test of the reactor and internals was conducted to demonstrate the adequacy of the design values used. The test results are given in B&W Topical Report BAW-10037, Rev. 2 Reactor Vessel Model Flow Tests.

In order to verify and ensure that the hot channel factor on flow area reduction (FA), is not being exceeded, a continuing program of as-built dimensional measurements on fuel assembly pitch spacings is being conducted. In addition, the statistical gap used in the fuel rod design has been verified through as-built dimensional data on the fuel cladding and pellets. The results show that the maximum gap of 8.5 mils has a 99% confidence that 95% of the population will be below this upper design limit.

4.4.5 Incore Instrumentation Application

Incore, self-powered neutron detectors measure the neutron flux in the core to provide a history of power distribution during power operation. The data obtained provide power distribution and fuel burnup information to assist in fuel management. The station computer provides normal system readout. Thermocouples in the incore detector strings provide radial temperature distribution data at the core exit. Additionally, eight (8) incore thermocouples are selectable as input for each of two (2) instrumentation channels used to indicate the saturation conditions and margin between actual temperature and the saturation temperature corresponding to the RCS pressure. Other temperature measurements selectable as inputs are provided by hot leg temperatures used by the RPS.

TABLE 4.4-1

Thermal-Hydraulic Core Design Summary Comparison

Reactor	Davis-Besse	Rancho Seco	Oconee Unit 1
Design core heat output, MWt	2772	2772	2568
Design core heat output, 10^6 Btu/hr	9461	9461	8765
Nominal system pressure, psia	2170	2200	2200
Vessel coolant inlet temp, °F	557.7	557	554
Vessel coolant outlet temp, °F	606.3	607.7	603.8
Core coolant outlet temp, °F	611.7	610.6	606.2
Heat Transfer and Fluid Flow at Design Power			
Total heat transfer surface area in core, ft^2	49,734	49,734	49,734
Avg heat flux, Btu/hr-ft^2	189,000	185,090	171,470
Max heat flux, Btu/hr-ft^2	483,000	576,885	534,440
Avg power density in core, kW/ℓ	90.0	90.0	83.38
Avg thermal output, kW/ft	6.105	6.105	5.656
Max thermal output, kW/ft	18.28	19.03	17.63
Max cladding surface temp, °F	654	654	654
Avg core fuel temp, °F	1200	1200	1150
Max fuel temp at hot spot, °F	4060	4170	3970
Total reactor coolant flow, 10^6 lb/hr	143.39	137.8	131.32
Core avg coolant velocity, fps	15.74	16.52	15.73
Core flow area (eff for heat transfer), ft^2	49.17	49.17	49.17
Power Distribution			
Max/Avg power ratio (FΔh nuc)	1.71	1.78	1.78
Max/Avg power ratio (F_z nuc)	1.70	1.70	1.70
Overall power ratio (F_a nuc)	2.91	3.03	3.03
Power generated in fuel and cladding, %	97.3	97.3	97.3
Hot Channel Factors			
Power peaking factor, F_s	1.011	1.011	1.011
Local heat flux factor, F''_Q	1.014	1.014	1.014
Flow area reduction factor (F_A)			
Interior bundle cells	0.98	0.98	0.98
Peripheral bundle cells	0.97	0.97	0.97
Hot spot max/avg heat flux ratio (F_Q nuc. and mech.)	2.99	3.12	3.12
DNB Ratio			
Design overpower, % design power	112	112	114
DNB ratio at design overpower (W-3)	1.41	1.39	1.55
DNB ratio at design power (W-3)	1.79	1.75	2.0

TABLE 4.4-2

DNB Ratios in Fuel Assembly Channels (W-3)

Cell type	G lb/hr-ft^2 x 10^{-6}	Minimum DNBR		
		W-3	W-3S	BAW-2
Maximum Design Conditions, 112% Power				
Unit	2.23	1.41	1.51	1.79
Corner	1.99	1.43	1.54	1.87
Wall (periph.)	2.09	1.51	1.62	1.95
Control Rod	2.01	1.45	1.56	1.85
Most Probable Design Conditions, 100% Power				
Unit	2.51	2.16	2.35	2.54
Corner	2.21	2.29	2.48	2.65
Wall (periph.)	2.56	2.23	2.43	2.72
Control Rod	2.25	2.28	2.47	2.59

TABLE 4.4-3

Coolant Exit Void Fraction and Quality

Condition	Max design, 112% power	Most probable, 100% power
Average core exit condition		
Void fraction, %	1.93	0.04
Quality, %	0.03	0.0
Hottest FA exit condition		
Void fraction, %	26.70	0.2
Quality, %	5.61	0.0
Hottest unit cell exit condition		
Void fraction, %	33.4	0.8
Quality, %	7.6	0.0

TABLE 4.4-4

Thermal Hydraulic Core Design Summary

Reactor

Design core heat output, MWt	2772
Design core heat output, 10^6 Btu/hr	9461
Nominal system pressure, psia	2170
Total reactor coolant flow, 10^6 lb/hr	143.39
Vessel coolant inlet temp, °F	557.7(1)
Vessel coolant outlet temp, °F	606.3

Heat Transfer and Fluid Flow at Design Power

Total core heat transfer surface area, ft^2	49,734
Core flow area effective for heat transfer, ft^2	49.17
Core avg coolant velocity, fps	15.74
Avg thermal output, kW/ft	6.105
Max thermal output, kW/ft	18.28
Avg core fuel temp, °F	1200
Max fuel temp at hot spot, °F	4060
Avg core heat flux, Btu/hr-ft^2	1.89×10^5
Max core heat flux, Btu/hr-ft^2	4.83×10^5
Max cladding surface temp, °F	654
Total unrecoverable core pressure drop, psi	17.2
Max fuel rod internal pressure	
At design power, psi	*
At design overpower, psi	*

Power Distribution

Max/avg power ratio (FΔh nuc.)	1.71
Max/avg power ratio (F_z nuc.)	1.70
Power generated in fuel and cladding, %	97.3
Overall power ratio (F_q nuc)	2.91

Hot Channel Factors

Pin power factor, F_Q	1.011
Local heat flux factor, F''_Q	1.014
Flow area reduction factor (F_A)	
Interior bundle cells	0.98
Peripheral bundle cells	0.97
Hot spot max/avg heat flux ratio (F_Q nuc and mech)	2.99

DNB Data

Design overpower, % design power	112
DNB ratio at design overpower (W-3)	1.41
DNB ratio at design power (W-3)	1.79

TABLE 4.4-4 (Continued)

Thermal Hydraulic Core Design Summary

*Maximum fuel rod internal pressures are provided in Appendix 4B.

(1) Beginning in Cycle 16, at the end of a cycle (EOC), the average reactor coolant temperature, T_{AVE}, may be reduced by 12°F (less instrument error). This maneuver may result in reactor coolant inlet temperature of approximately 547°F and will extend the Effective Full Power Life of the core through the negative Moderator Temperature Coefficient. For future cycles, the effects of the T_{AVE} reduction on the core mechanical, nuclear and thermal-hydraulic parameters as well as any potential effects on LOCA and non-LOCA analyses and/or consequences will be addressed by the cycle- specific reload report. (Reference USAR Appendix 4B)

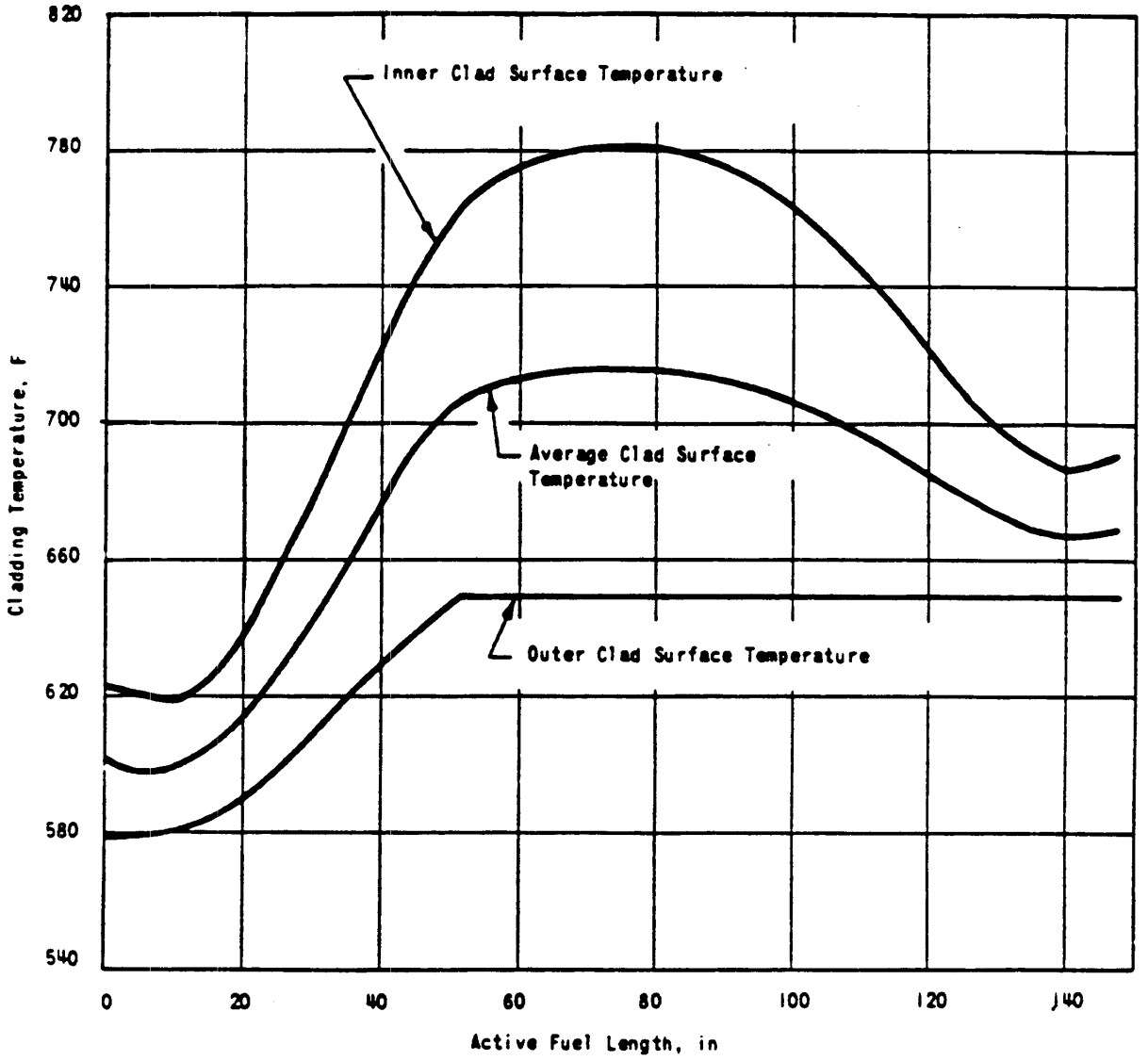

DAVIS-BESSE NUCLEAR POWER STATION
CLAD TEMPERATURES VERSUS AXIAL LENGTH FOR MAXIMUM DESIGN CONDITIONS AT 112 PERCENT POWER
FIGURE 4.4-1

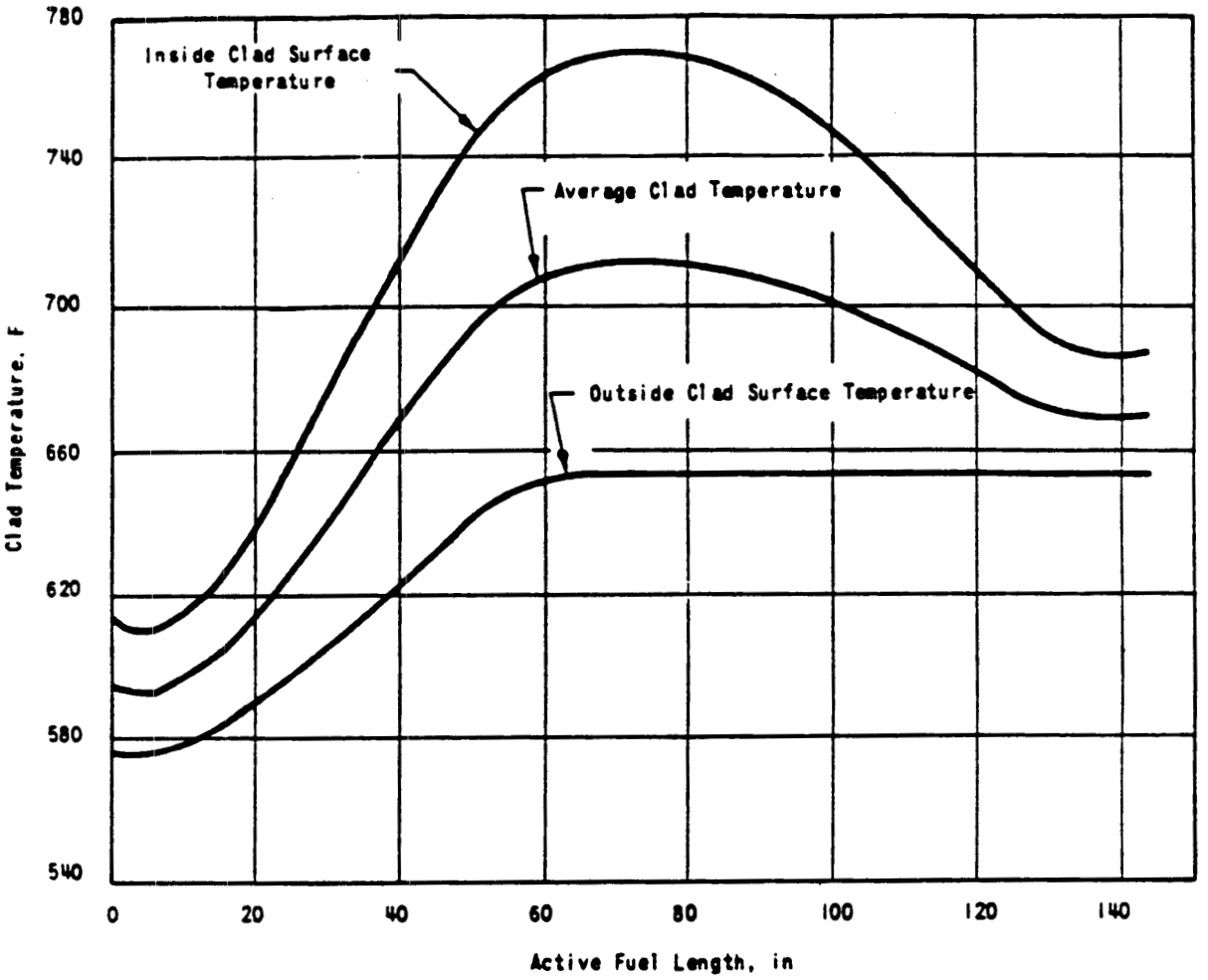

DAVIS-BESSE NUCLEAR POWER STATION
CLADDING TEMPERATURE VERSUS AXIAL LENGTH FOR MOST PROBABLE CONDITIONS AT RATED POWER
FIGURE 4.4-2

REVISION 0
JULY 1982

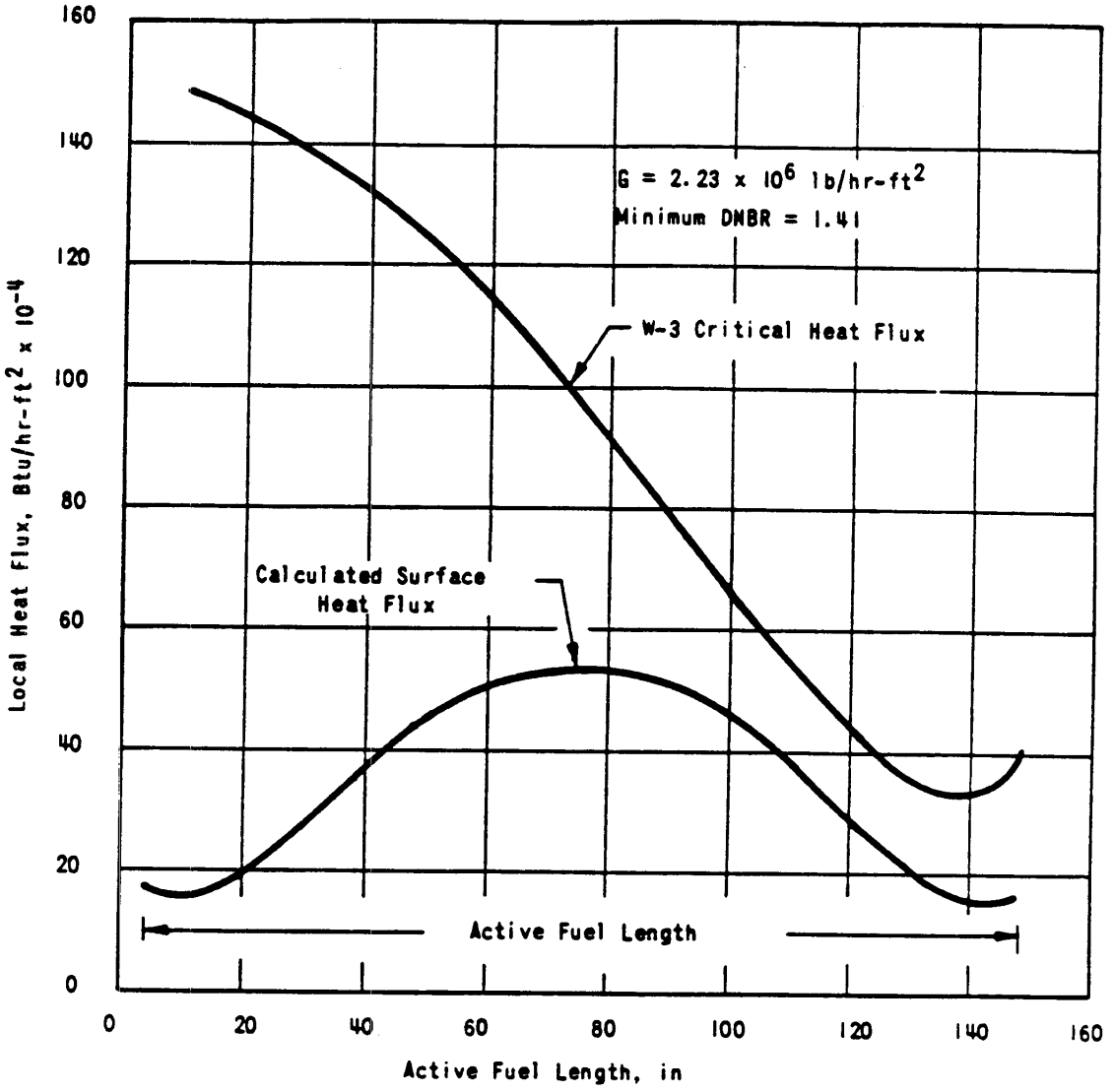

DAVIS-BESSE NUCLEAR POWER STATION
CALCULATED AND DESIGN LIMIT LOCAL HEAT FLUX VERSUS AXIAL LOCATION IN THE HOT UNIT CELL FOR MAXIMUM DESIGN CONDITIONS AT THE DESIGN OVERPOWER
FIGURE 4.4-3

REVISION 0
JULY 1982

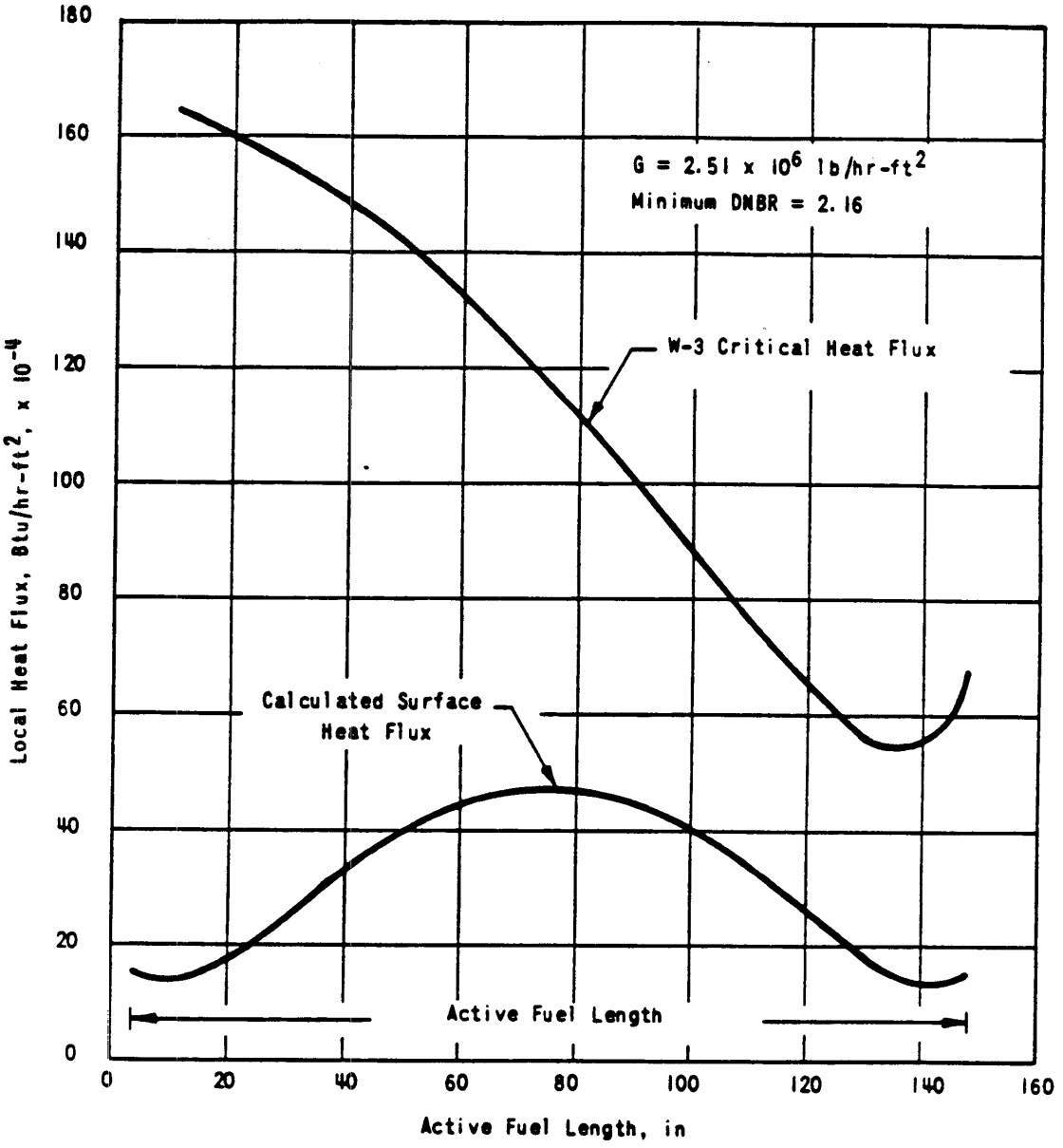

DAVIS-BESSE NUCLEAR POWER STATION
CALCULATED AND DESIGN LIMIT LOCAL HEAT FLUX VERSUS AXIAL LOCATION IN THE HOT UNIT CELL FOR MOST PROBABLE CONDITIONS AT RATED POWER
FIGURE 4.4-4

REVISION 0
JULY 1982

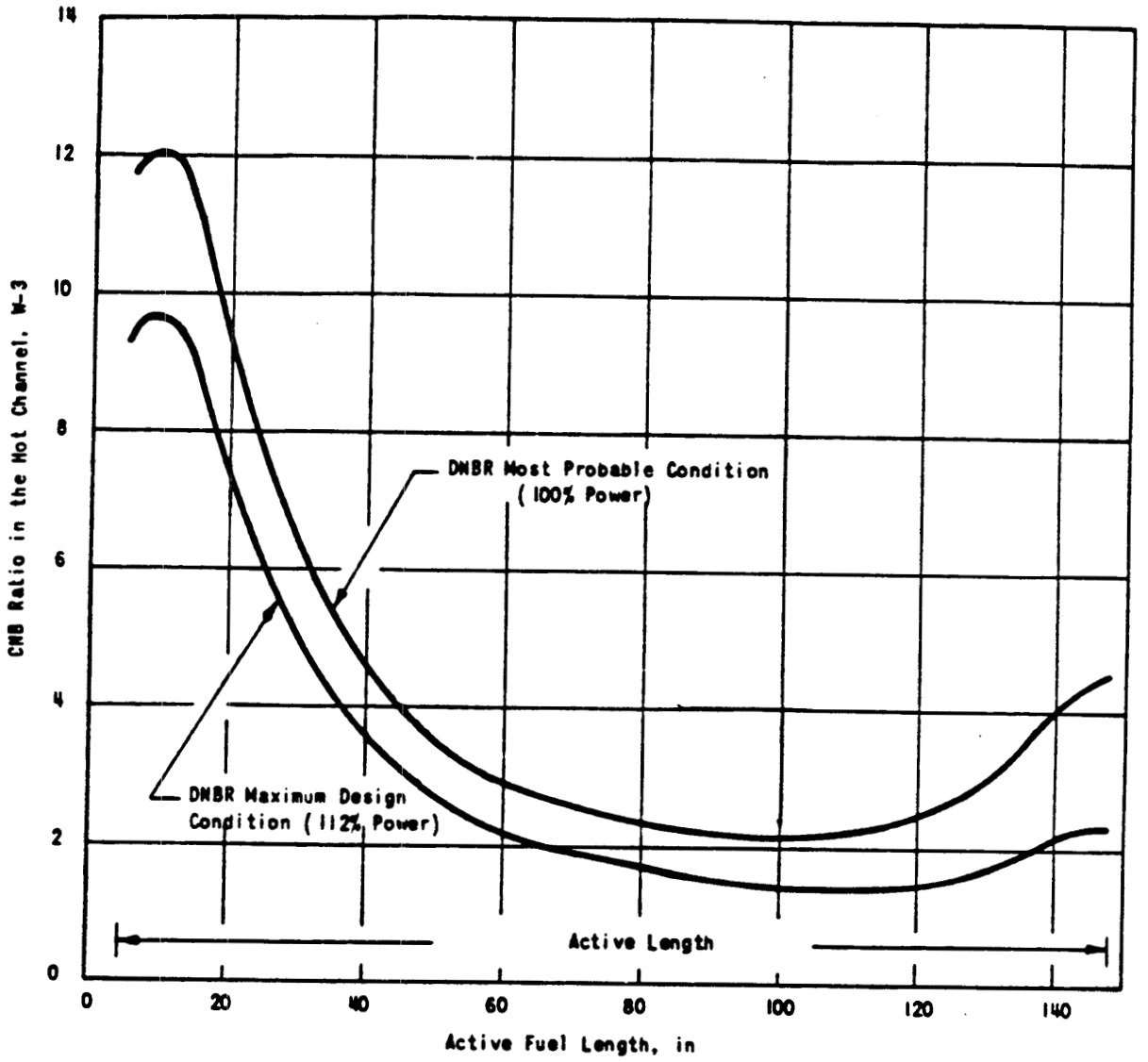

DAVIS-BESSE NUCLEAR POWER STATION
HOT CHANNEL DNB RATIO VERSUS ACTIVE FUEL LENGTH
FIGURE 4.4-5

REVISION 0
JULY 1982

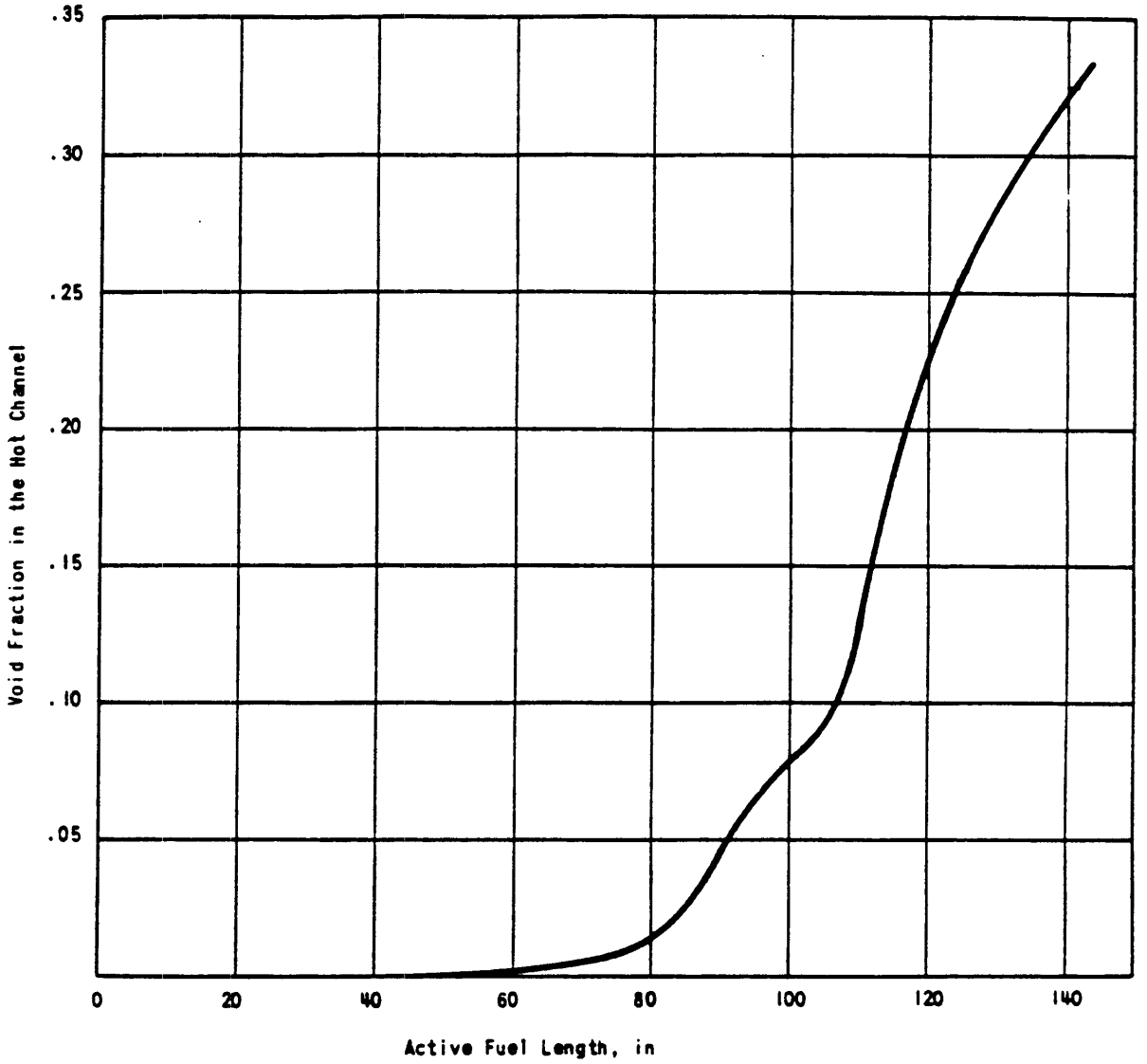

DAVIS-BESSE NUCLEAR POWER STATION
VOID FRACTION IN HOT UNIT CELL VERSUS AXIAL LOCATION FOR MAXIMUM DESIGN CONDITIONS AT 112% POWER

FIGURE 4.4-6 REVISION 0
JULY 1982

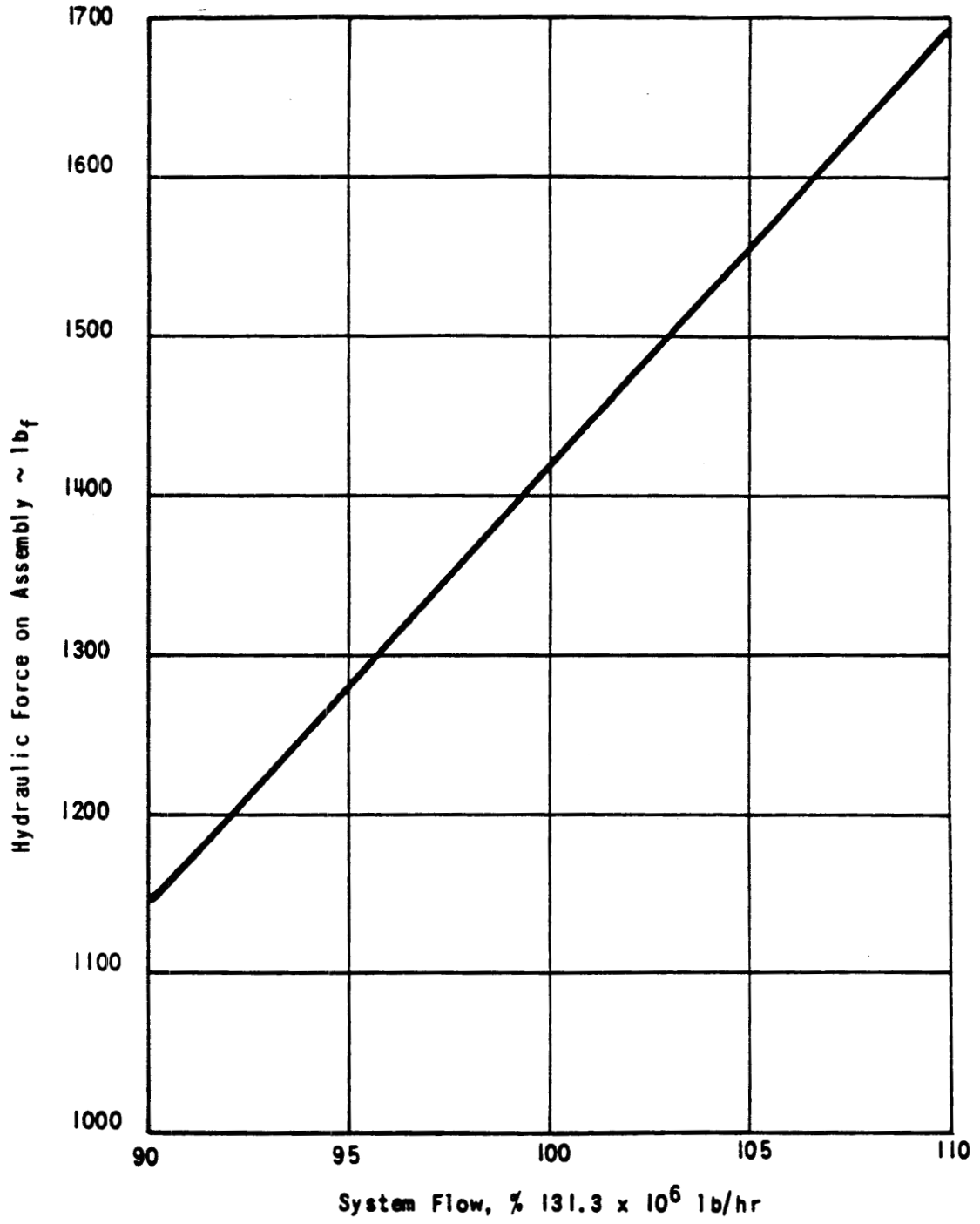

DAVIS-BESSE NUCLEAR POWER STATION
HYDRAULIC FORCE VERSUS PERCENT SYSTEM FLOW, 112% POWER

FIGURE 4.4-7

REVISION 0
JULY 1982

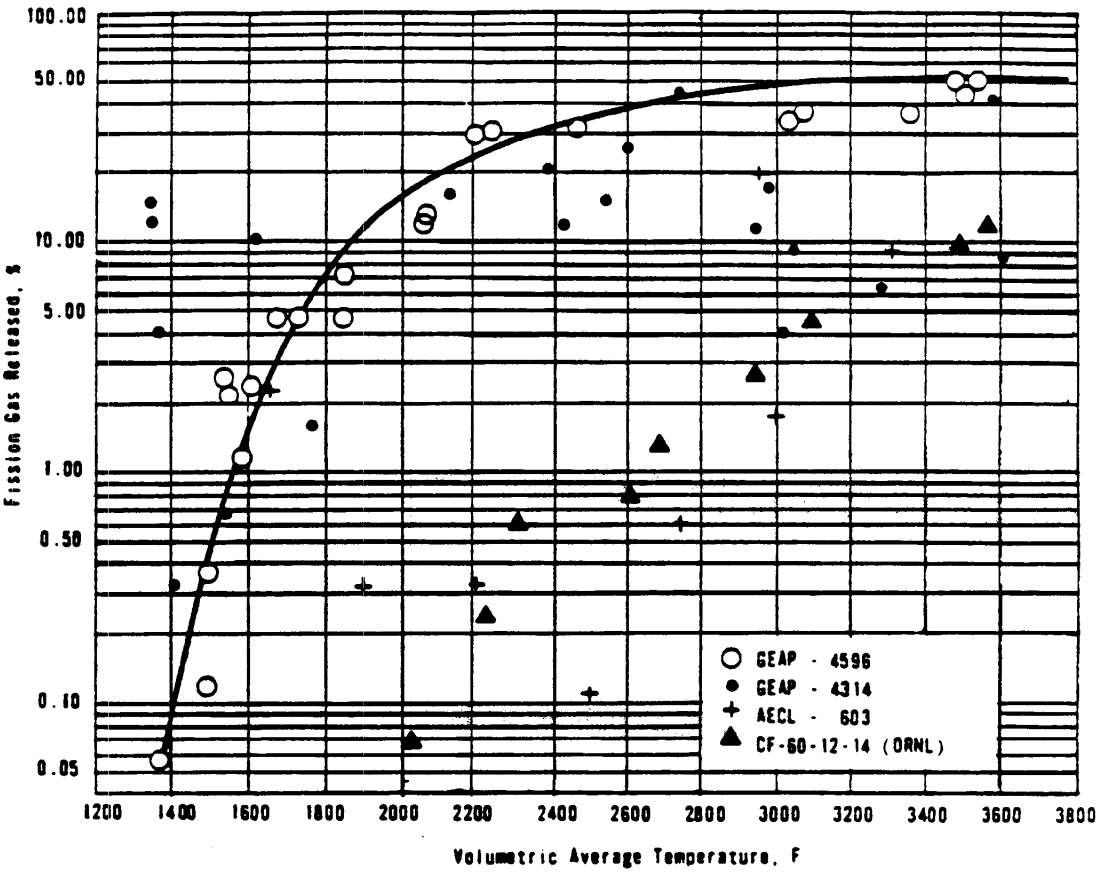

DAVIS-BESSE NUCLEAR POWER STATION
PERCENT FISSION GAS RELEASED AS A FUNCTION OF THE AVERAGE TEMPERATURE OF THE UO_2 FUEL

FIGURE 4.4-8

REVISION 0
JULY 1982

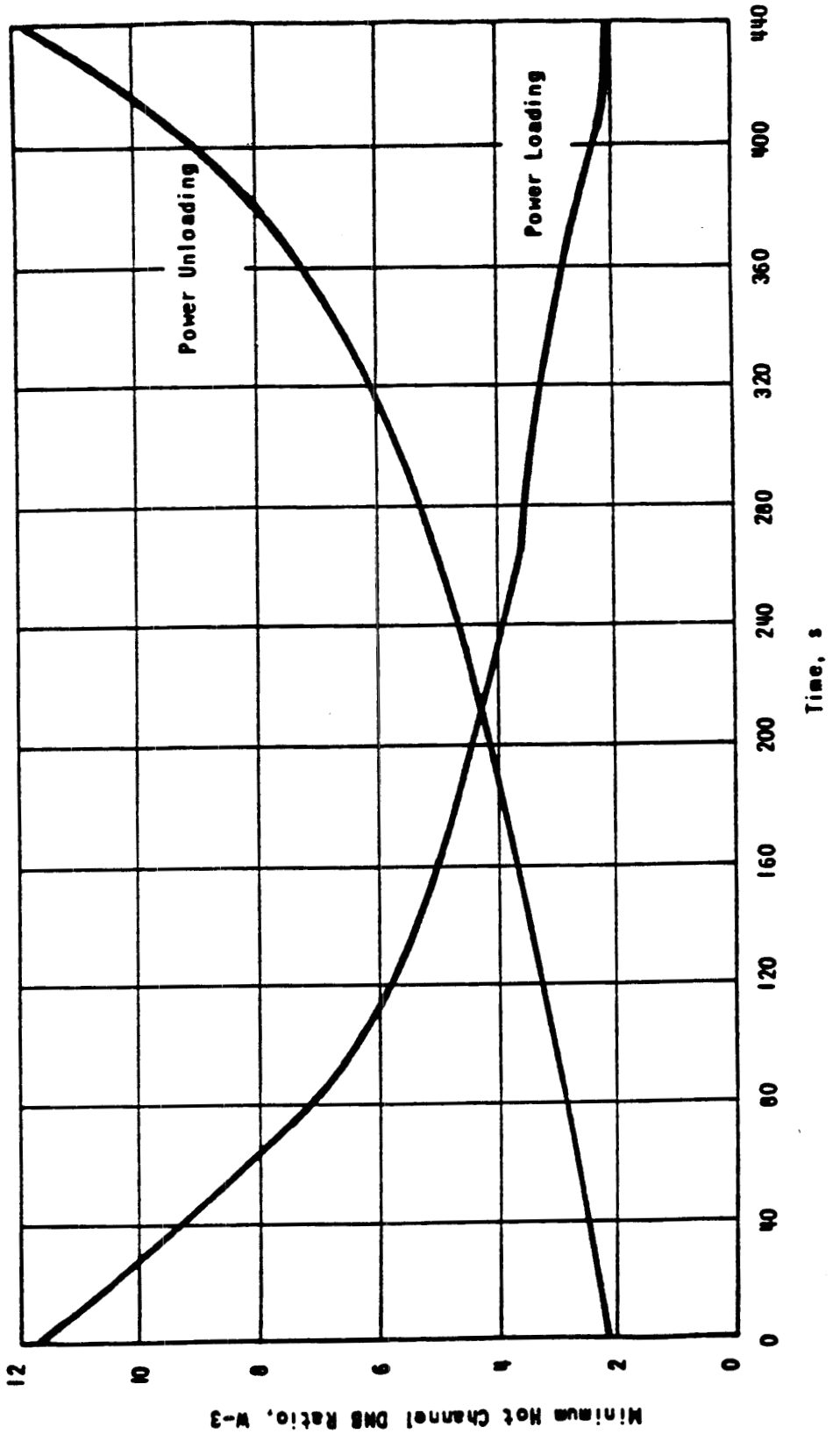

DAVIS-BESSE NUCLEAR POWER STATION
HOT CHANNEL DNBR VERSUS TIME DURING
POWER LOADING CHANGES

FIGURE 4.4-9

REVISION 0
JULY 1982

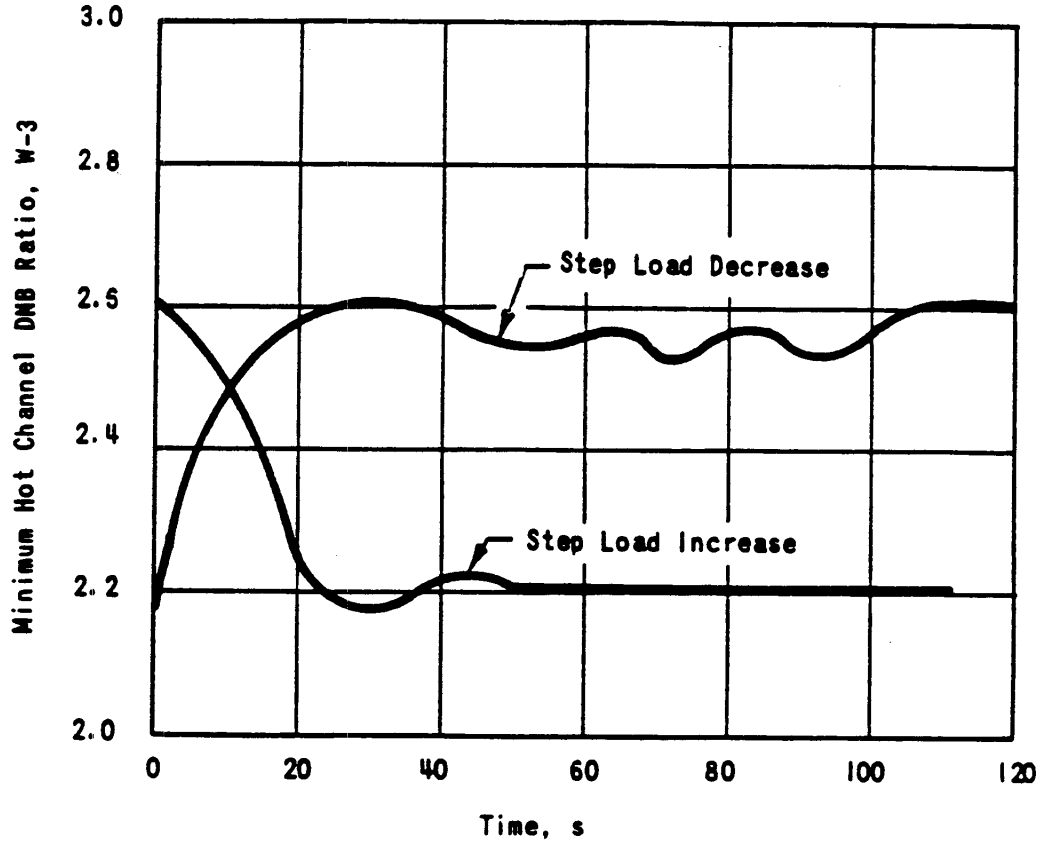

DAVIS-BESSE NUCLEAR POWER STATION
HOT CHANNEL DNBR VERSUS TIME DURING STEP LOAD CHANGES

FIGURE 4.4-10

REVISION 0
JULY 1982

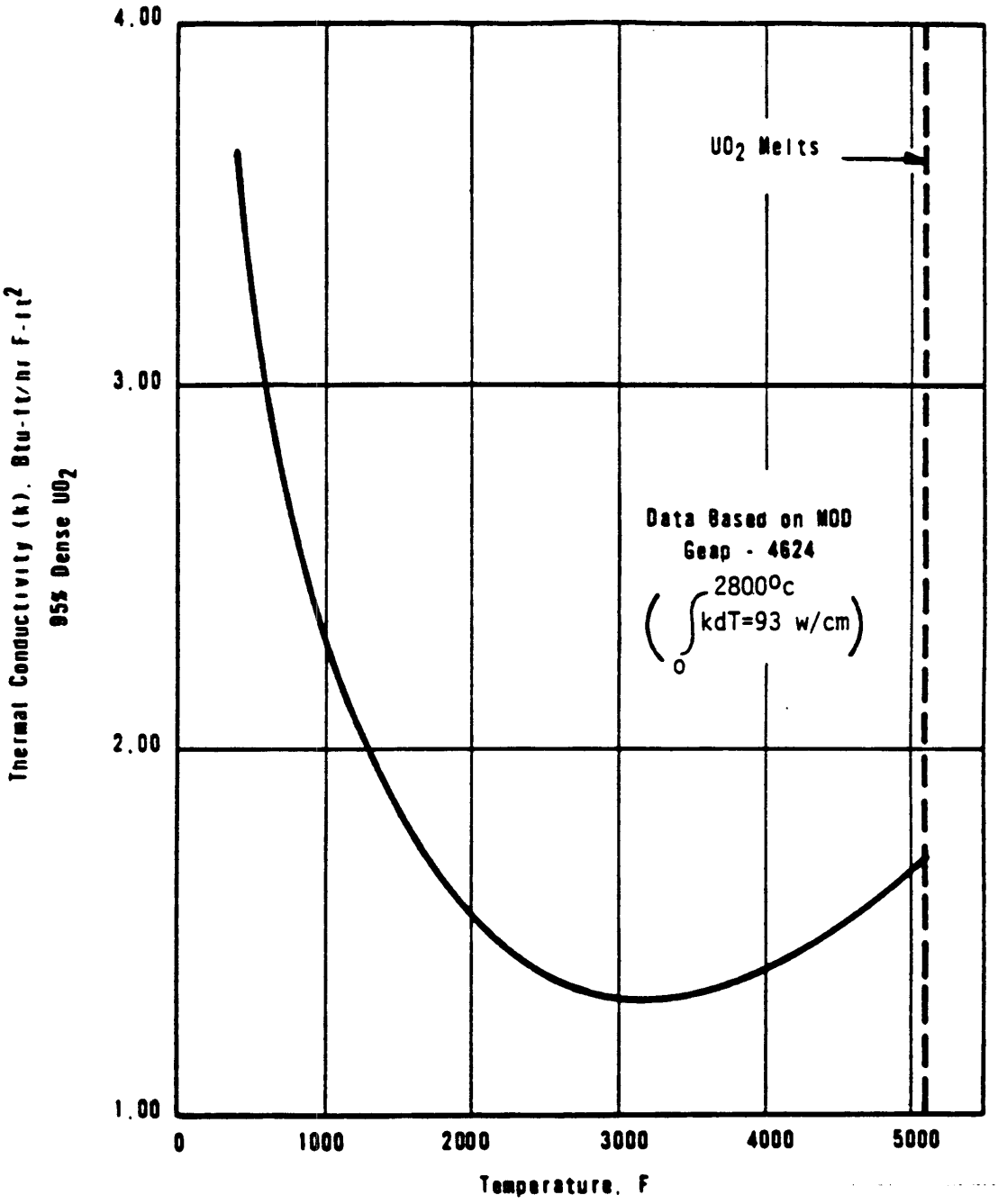

DAVIS-BESSE NUCLEAR POWER STATION
THERMAL CONDUCTIVITY OF UO_2
FIGURE 4.4-11

REVISION 0
JULY 1982

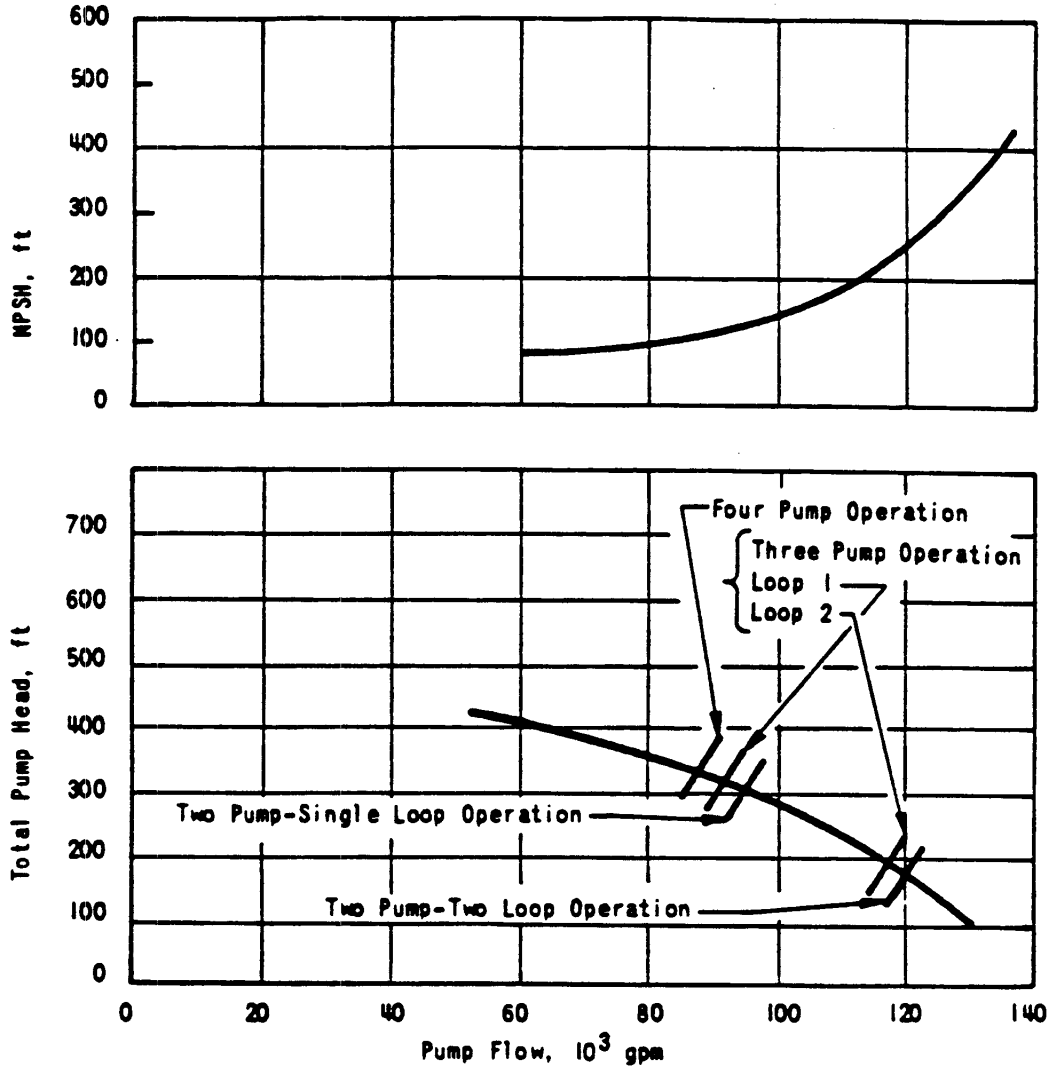

DAVIS-BESSE NUCLEAR POWER STATION
TOTAL PUMP HEAD AND
NPSH VERSUS PUMP FLOW
FIGURE 4.4-12

REVISION 0
JULY 1982

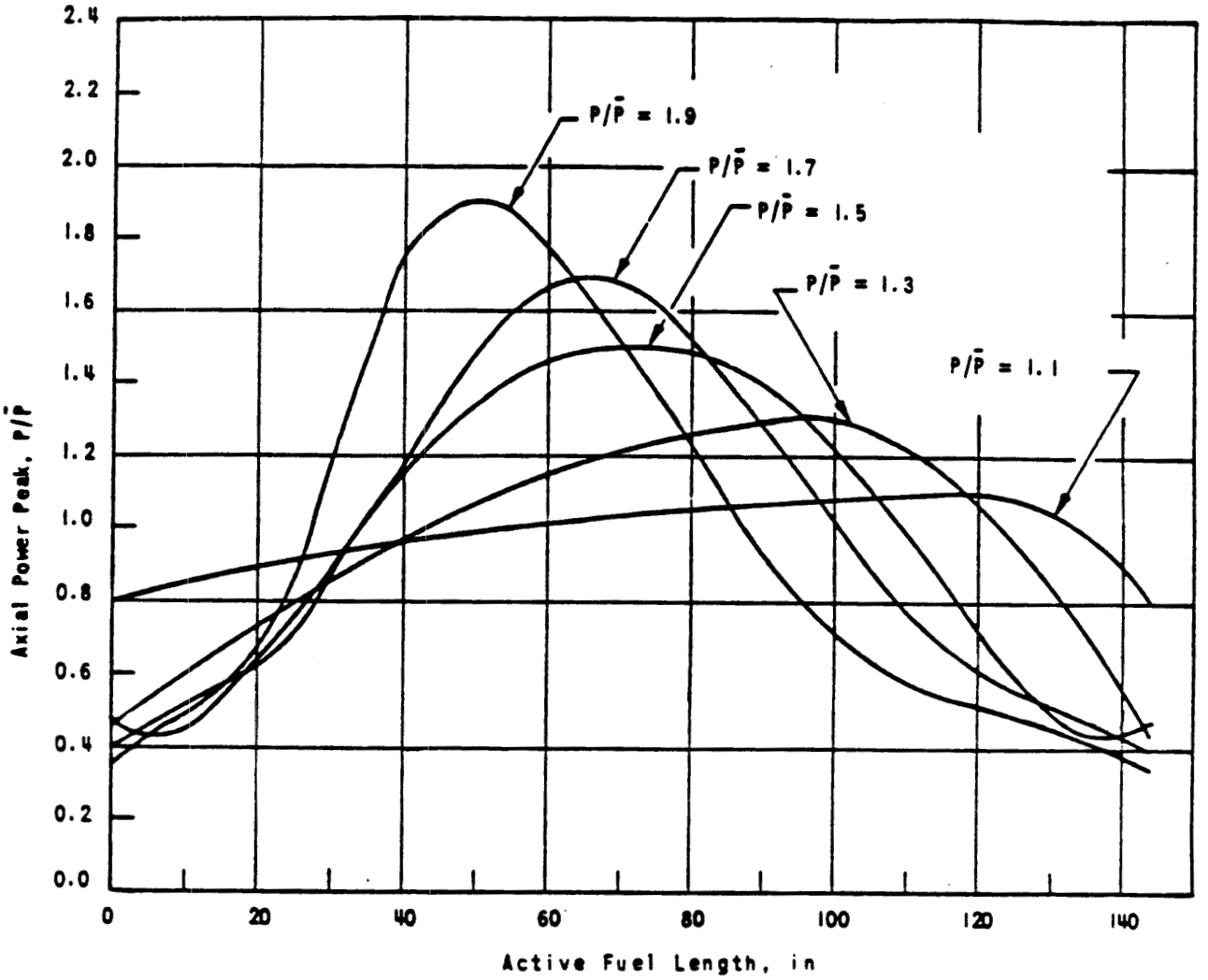

DAVIS-BESSE NUCLEAR POWER STATION
MAXIMUM ALLOWABLE AXIAL
POWER DISTRIBUTIONS FOR
MAXIMUM DESIGN RADIAL LOCAL
PEAKING FACTOR (1.71)
FIGURE 4.4-13

REVISION 0
JULY 1982

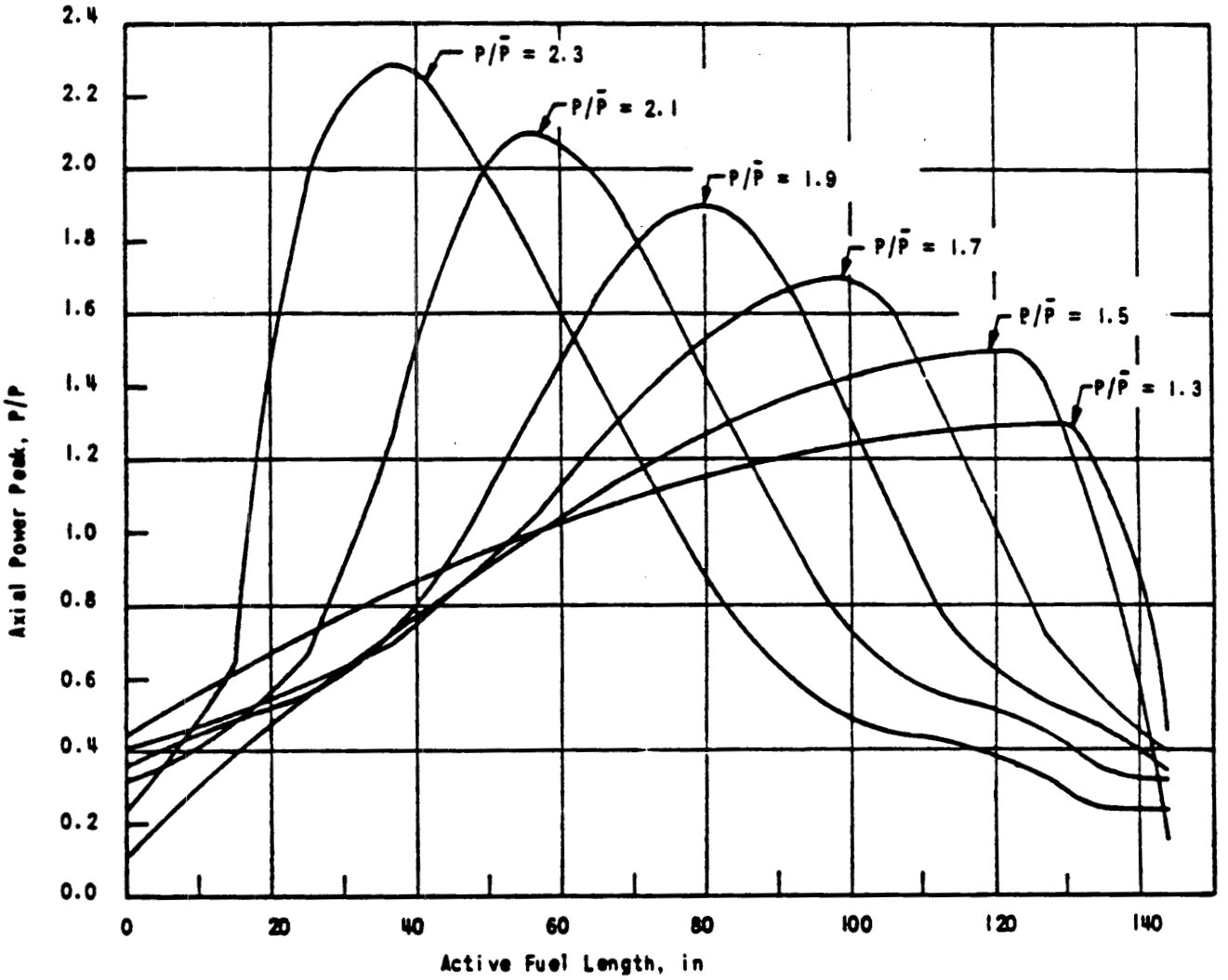

DAVIS-BESSE NUCLEAR POWER STATION
MAXIMUM ALLOWABLE AXIAL
POWER DISTRIBUTIONS FOR A
1.60 MAXIMUM RADIAL
LOCAL PEAKING FACTOR
FIGURE 4.4-14

REVISION 0
JULY 1982

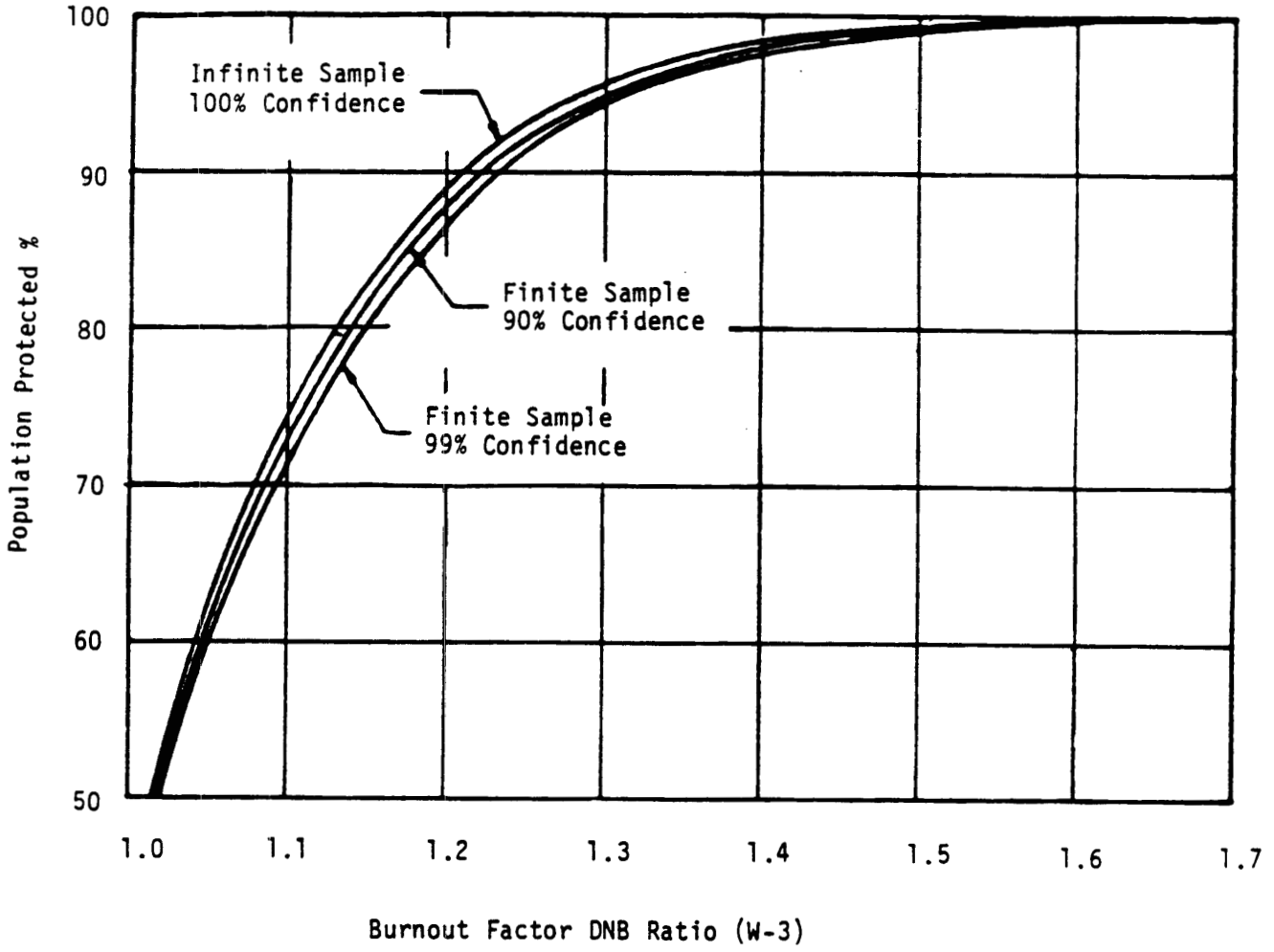

DAVIS-BESSE NUCLEAR POWER STATION
BURNOUT FACTOR (W-3)
VERSUS POPULATION FOR
VARIOUS CONFIDENCE LEVELS
FIGURE 4.4-15

REVISION 0
JULY 1982

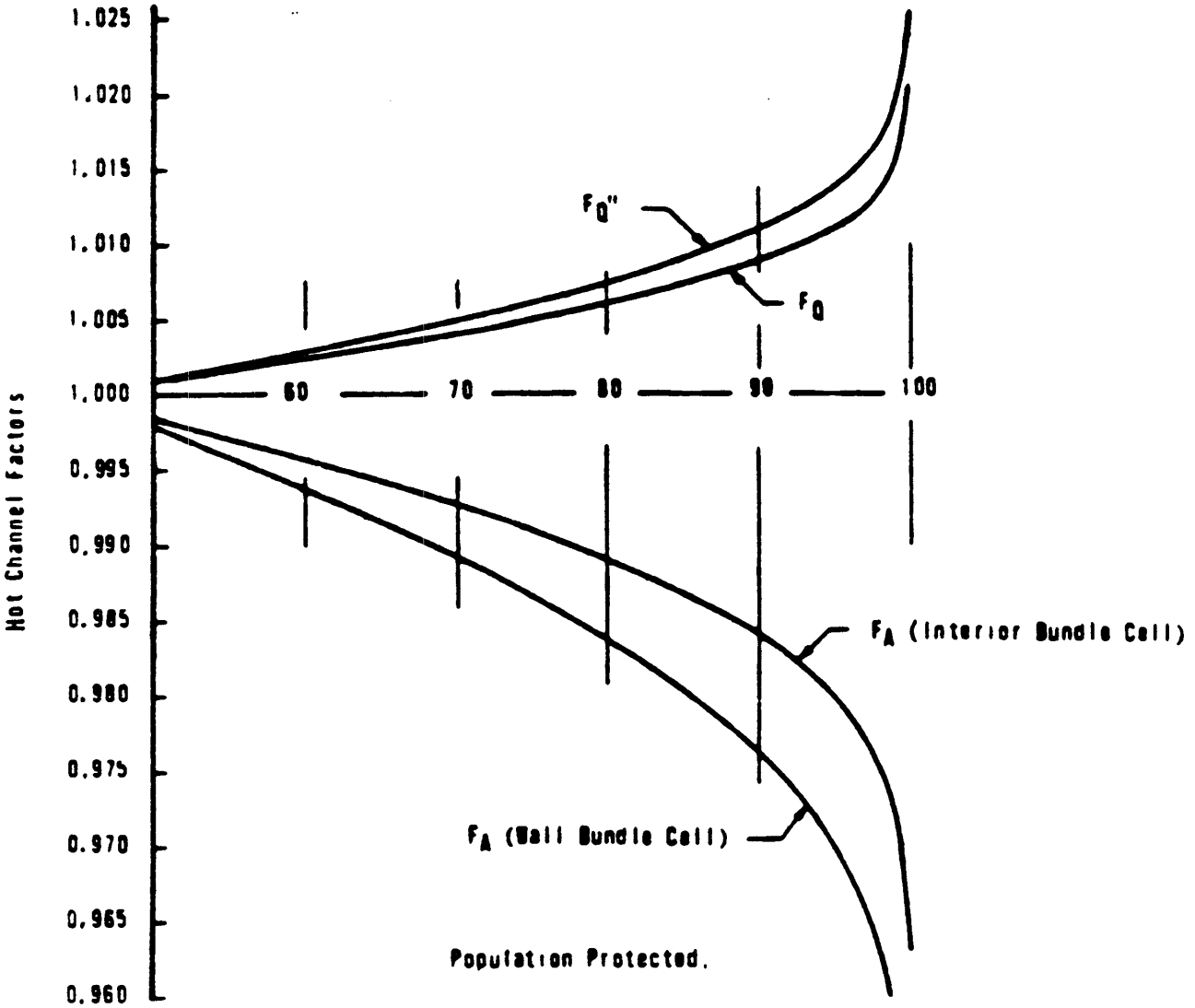

DAVIS-BESSE NUCLEAR POWER STATION
HOT CHANNEL FACTORS
VERSUS PER CENT
POPULATION PROTECTED
FIGURE 4.4-16

REVISION 0
JULY 1982

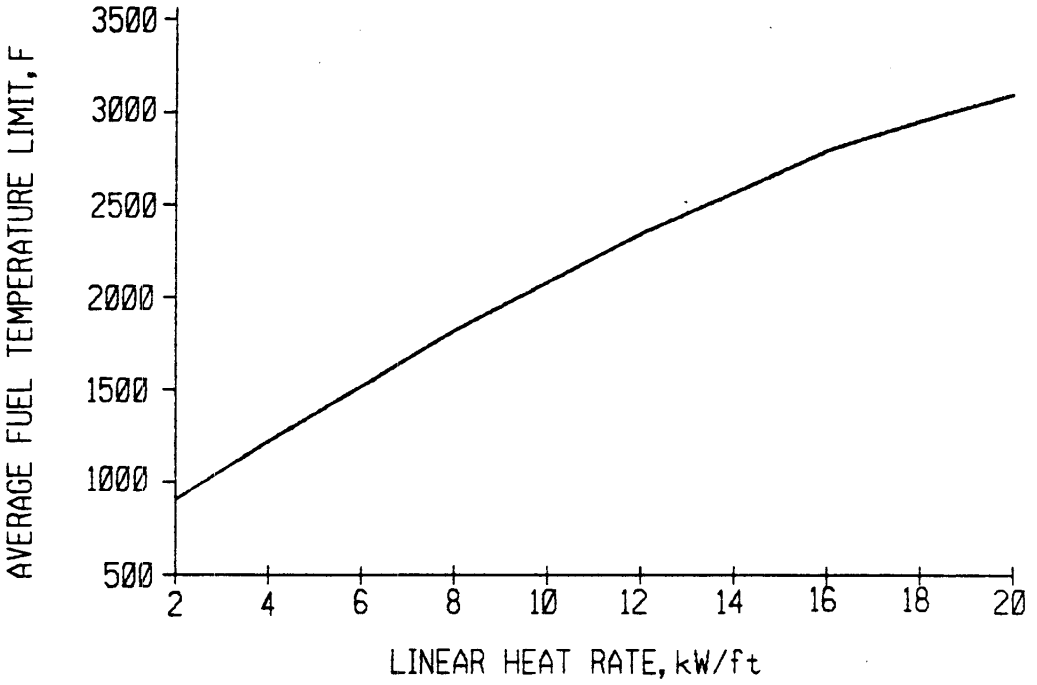

DAVIS-BESSE NUCLEAR POWER STATION
VOLUMETRIC AVERAGE FUEL TEMPERATURE LIMIT
VS LHR
FIGURE 4.4-17

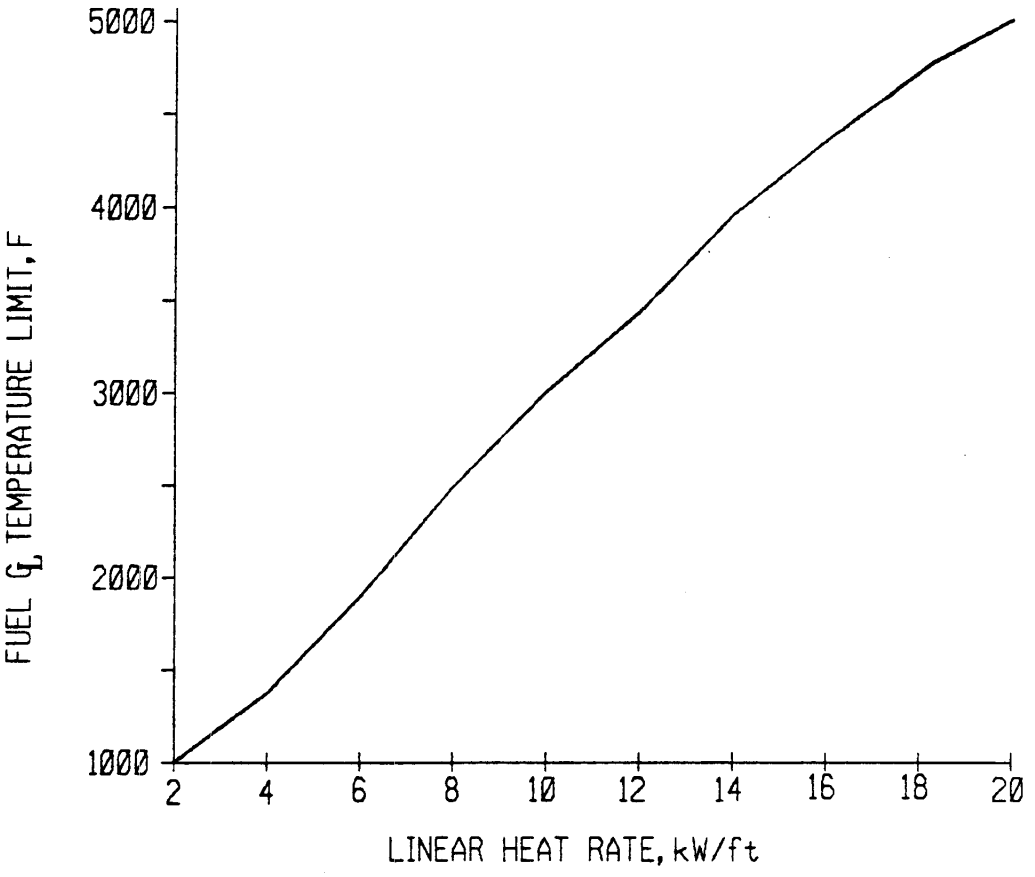

DAVIS-BESSE NUCLEAR POWER STATION
VOLUMETRIC AVERAGE FUEL TEMPERATURE LIMIT
VS LHR
FIGURE 4.4-18

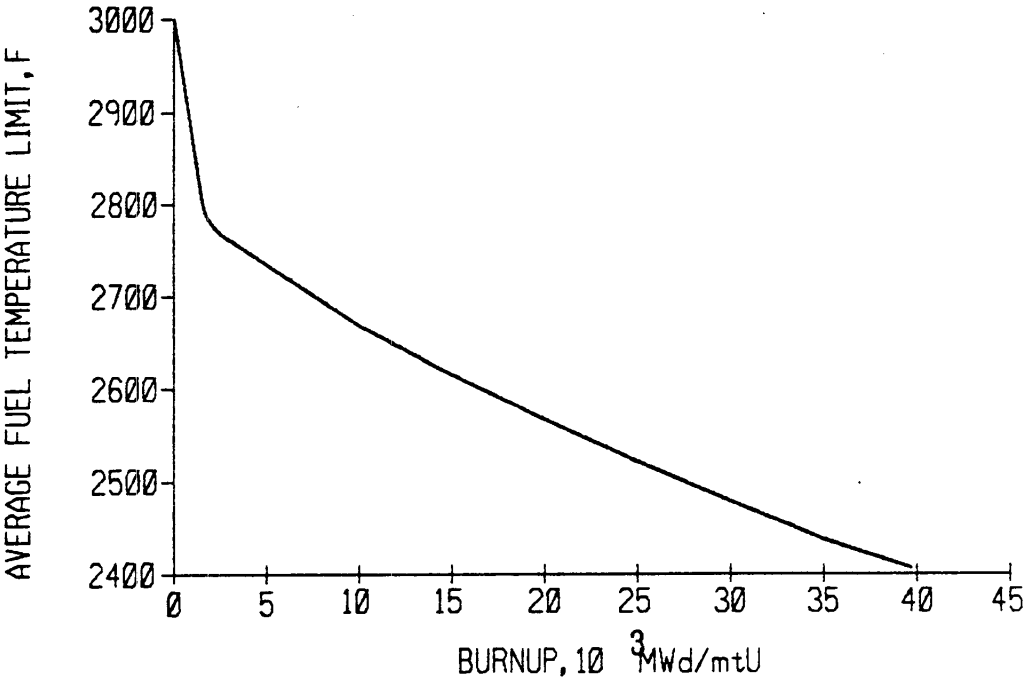

DAVIS-BESSE NUCLEAR POWER STATION
VOLUMETRIC AVERAGE FUEL TEMPERATURE LIMIT
VS BURNUP AT 18 kW/FT
FIGURE 4.4-19

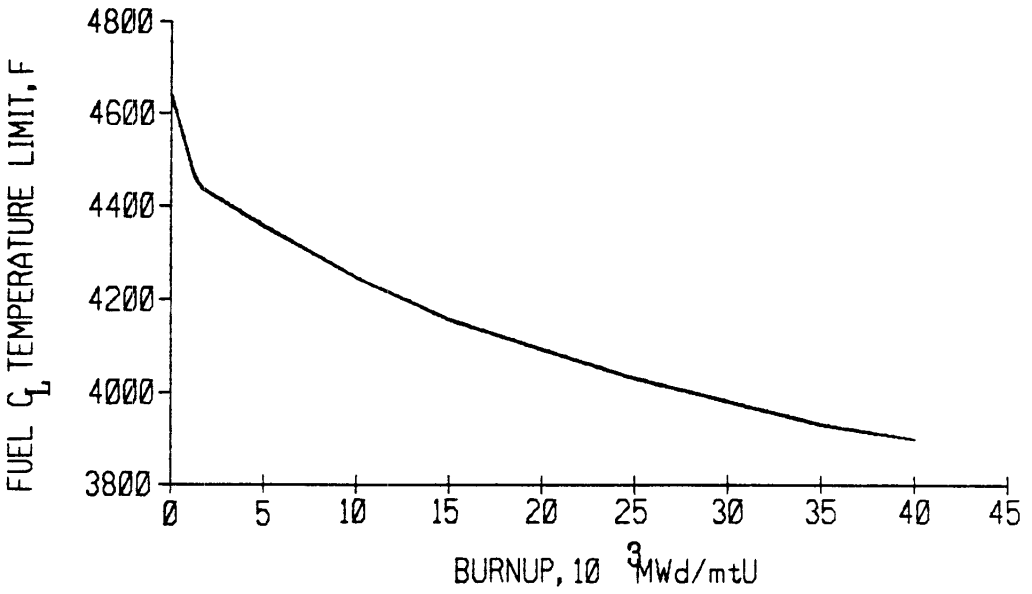

DAVIS-BESSE NUCLEAR POWER STATION
FUEL CENTERLINE TEMPERATURE LIMITS
VS BURNUP AT 18 kW/FT
FIGURE 4.4-20

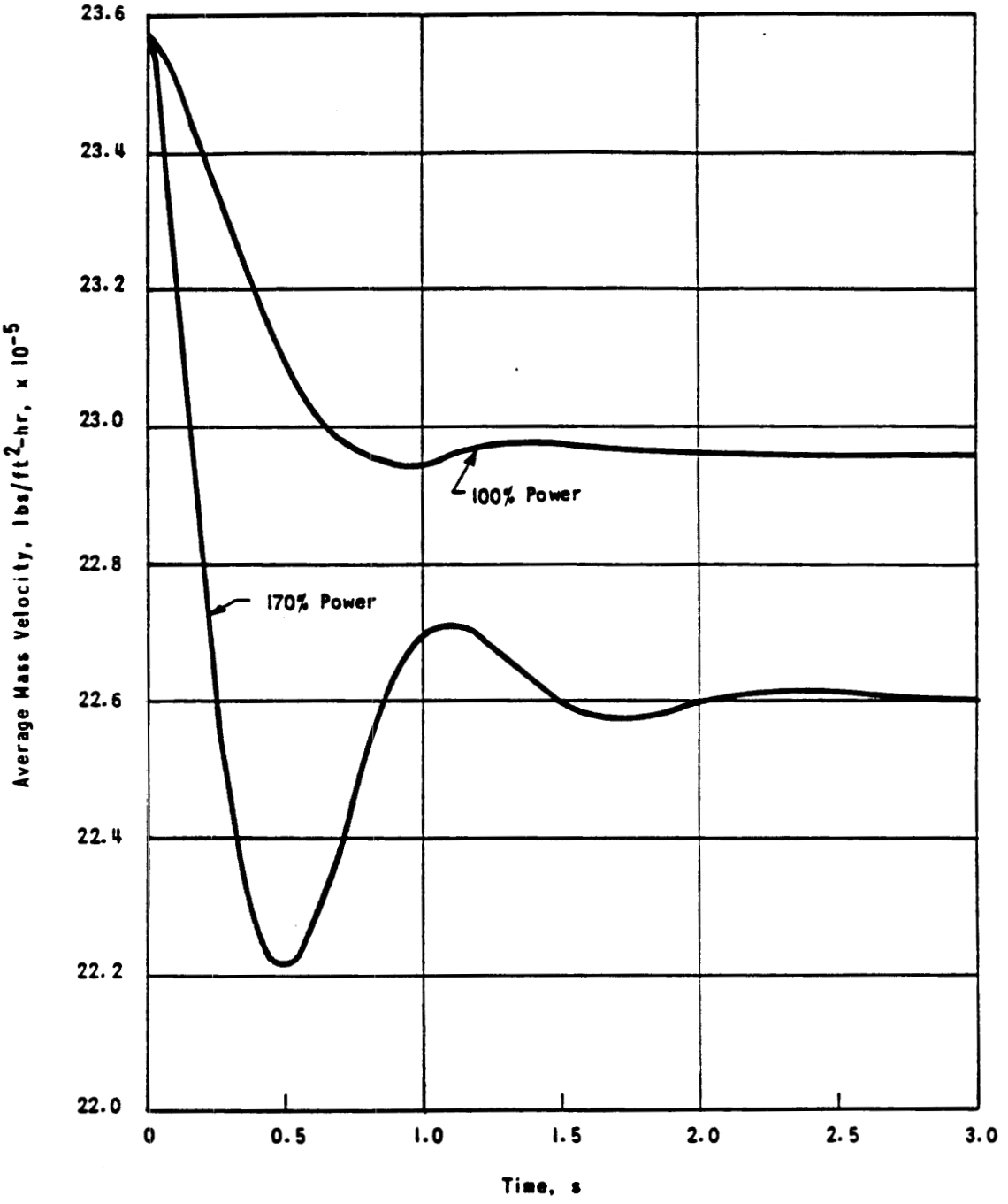

DAVIS-BESSE NUCLEAR POWER STATION
TRANSIENT MASS FLOW RATES
DUE TO POWER PERTURBATION
FIGURE 4.4-21

REVISION C
JULY 1982

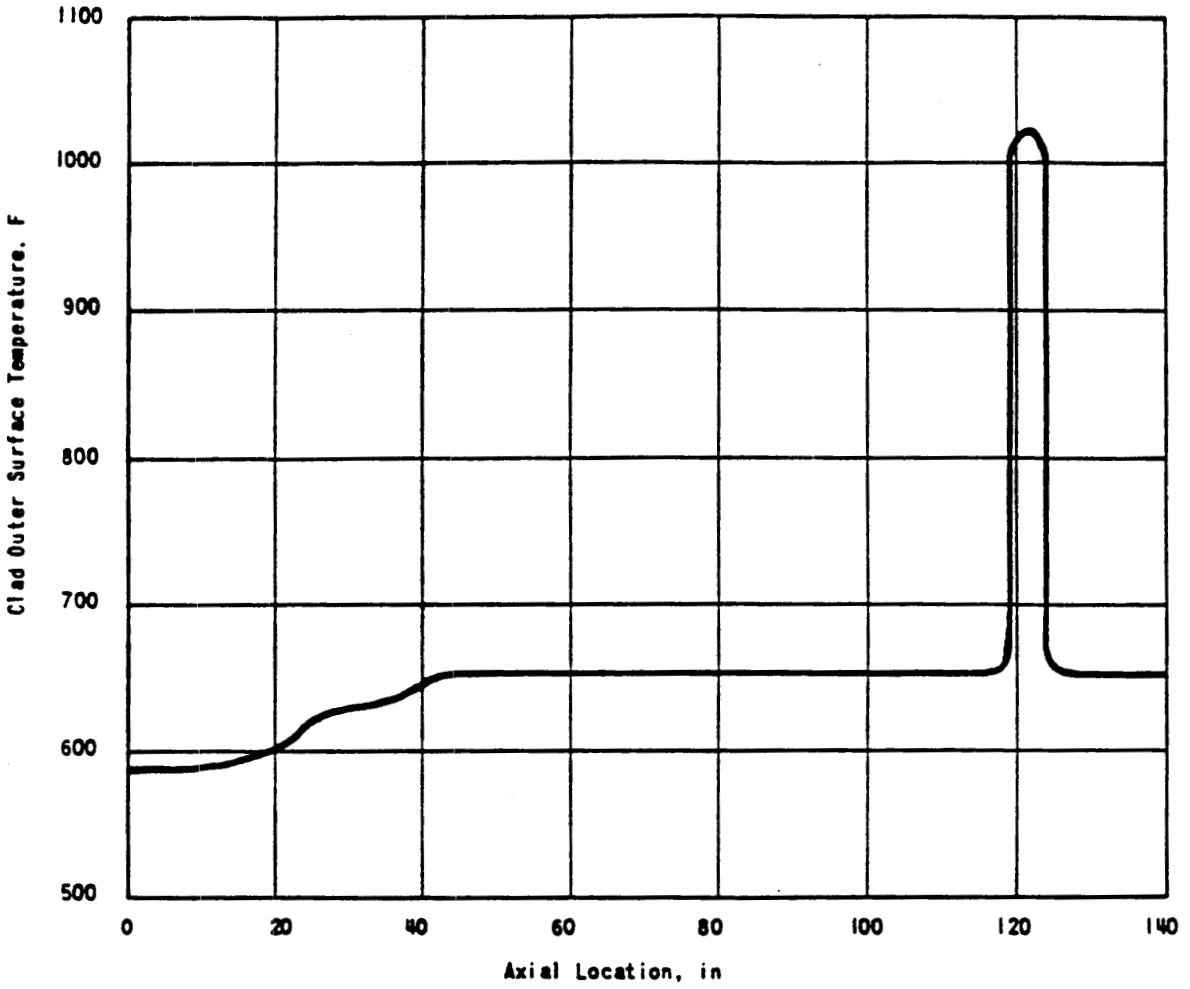

DAVIS-BESSE NUCLEAR POWER STATION
OUTSIDE CLAD SURFACE
TEMPERATURE VERSUS AXIAL
LOCATION DURING A
DEPARTURE FROM NUCLEATE BOILING

FIGURE 4.4-22

REVISION 0
JULY 1982

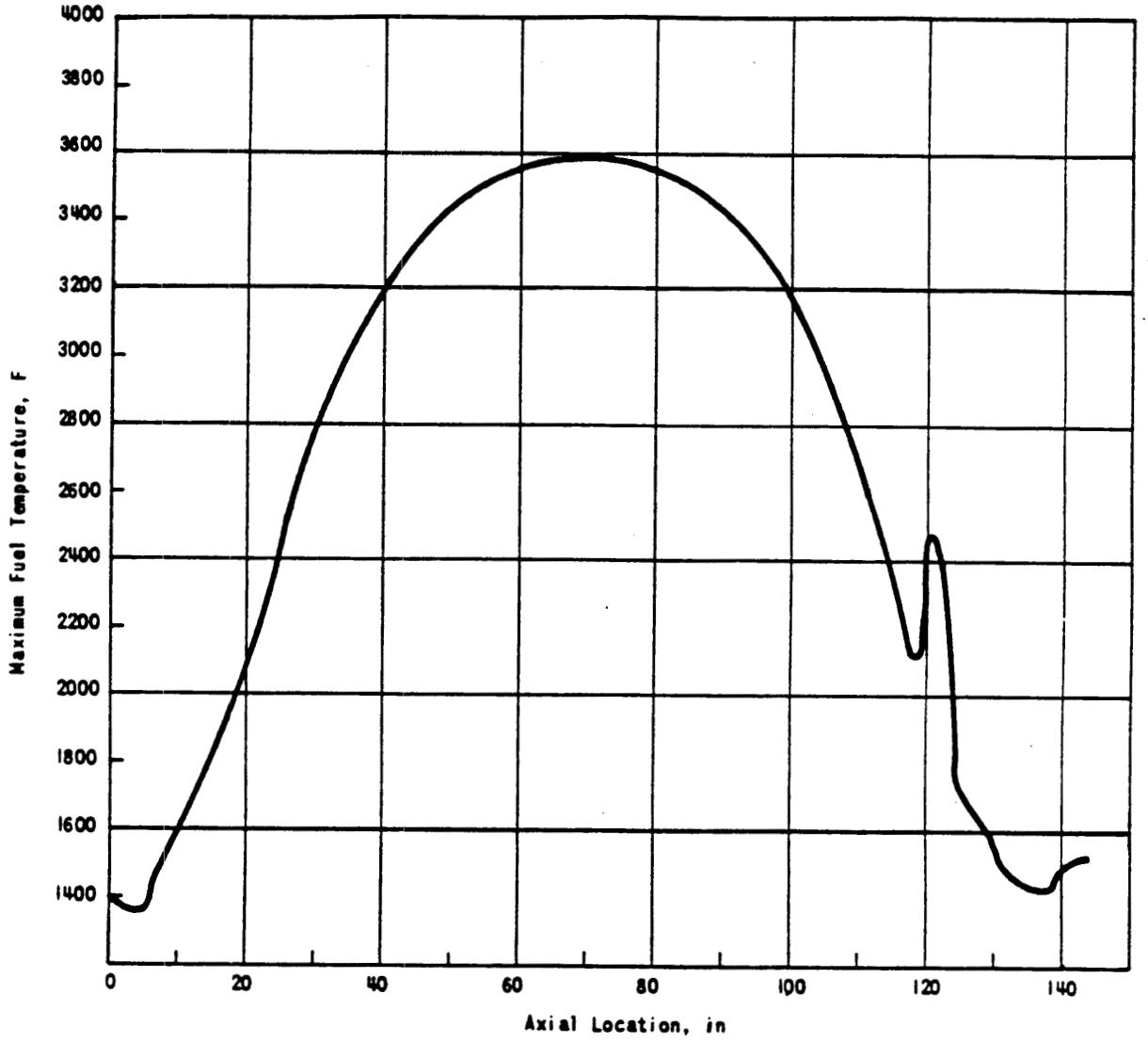

DAVIS-BESSE NUCLEAR POWER STATION
CENTERLINE TEMPERATURE VERSUS AXIAL LOCATION DURING A DEPARTURE FROM NUCLEATE BOILING

FIGURE 4.4-23

REVISION 0
JULY 1982

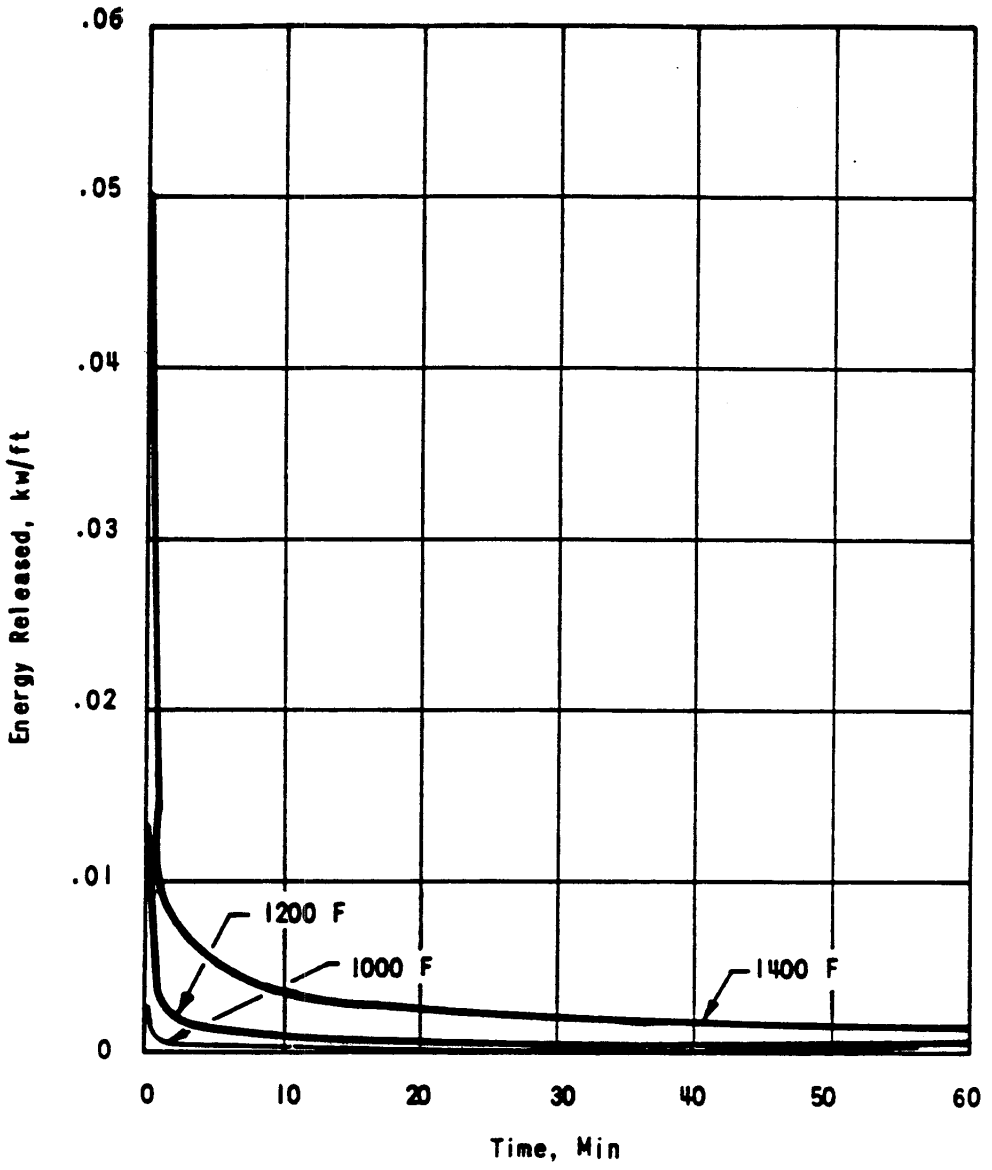

DAVIS-BESSE NUCLEAR POWER STATION
ENERGY RELEASED DURING A
DEPARTURE FROM NUCLEATE BOILING FOR A
ZIRCONIUM-WATER CHEMICAL REACTION

FIGURE 4.4-24

REVISION 0
JULY 1982

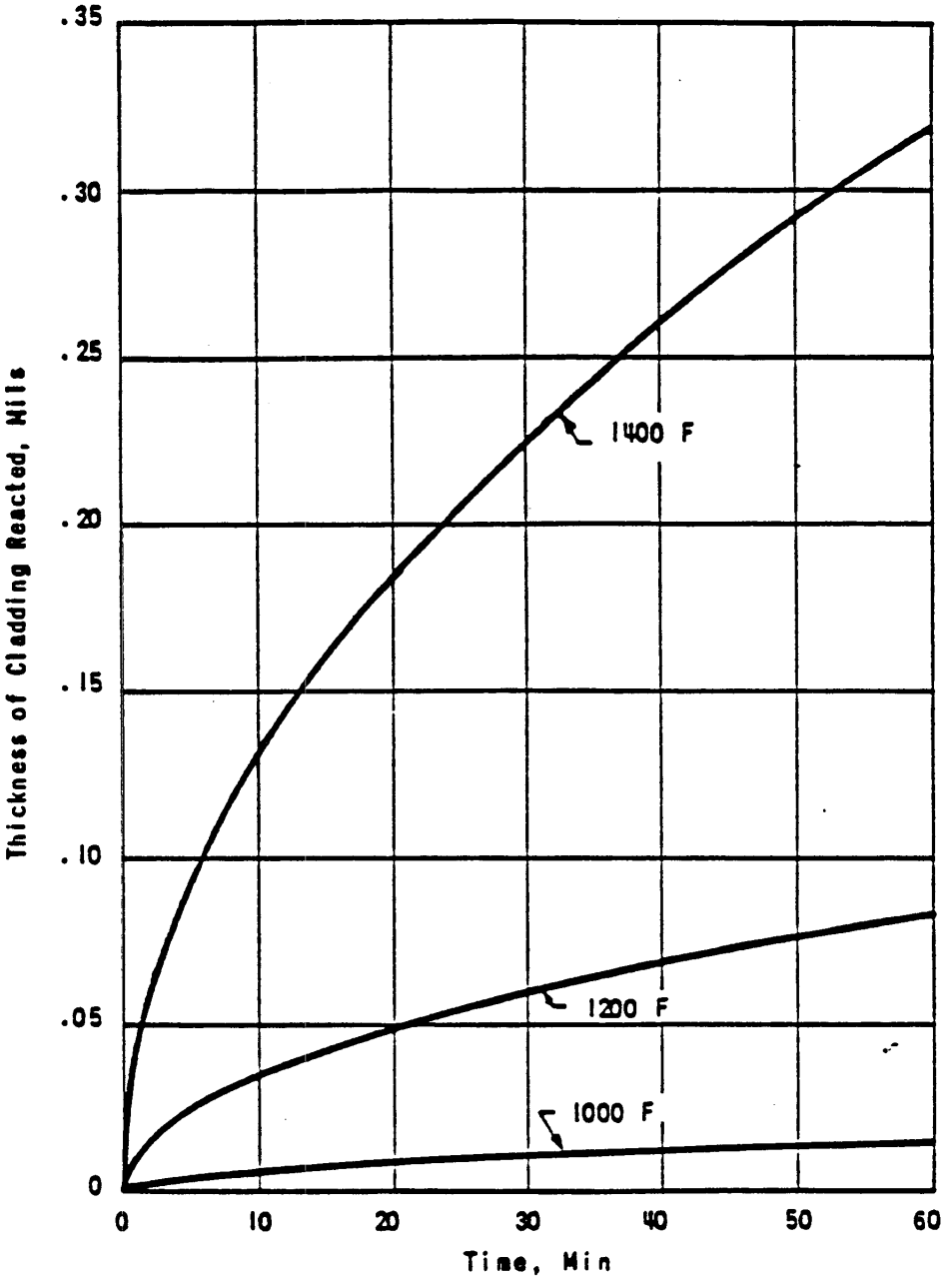

DAVIS-BESSE NUCLEAR POWER STATION
THICKNESS OF CLADDING REACTED
DURING A DEPARTURE FROM
NUCLEATE BOILING FOR A
ZIRCONIUM-WATER CHEMICAL REACTION

FIGURE 4.4-25

REVISION (
JULY 1982

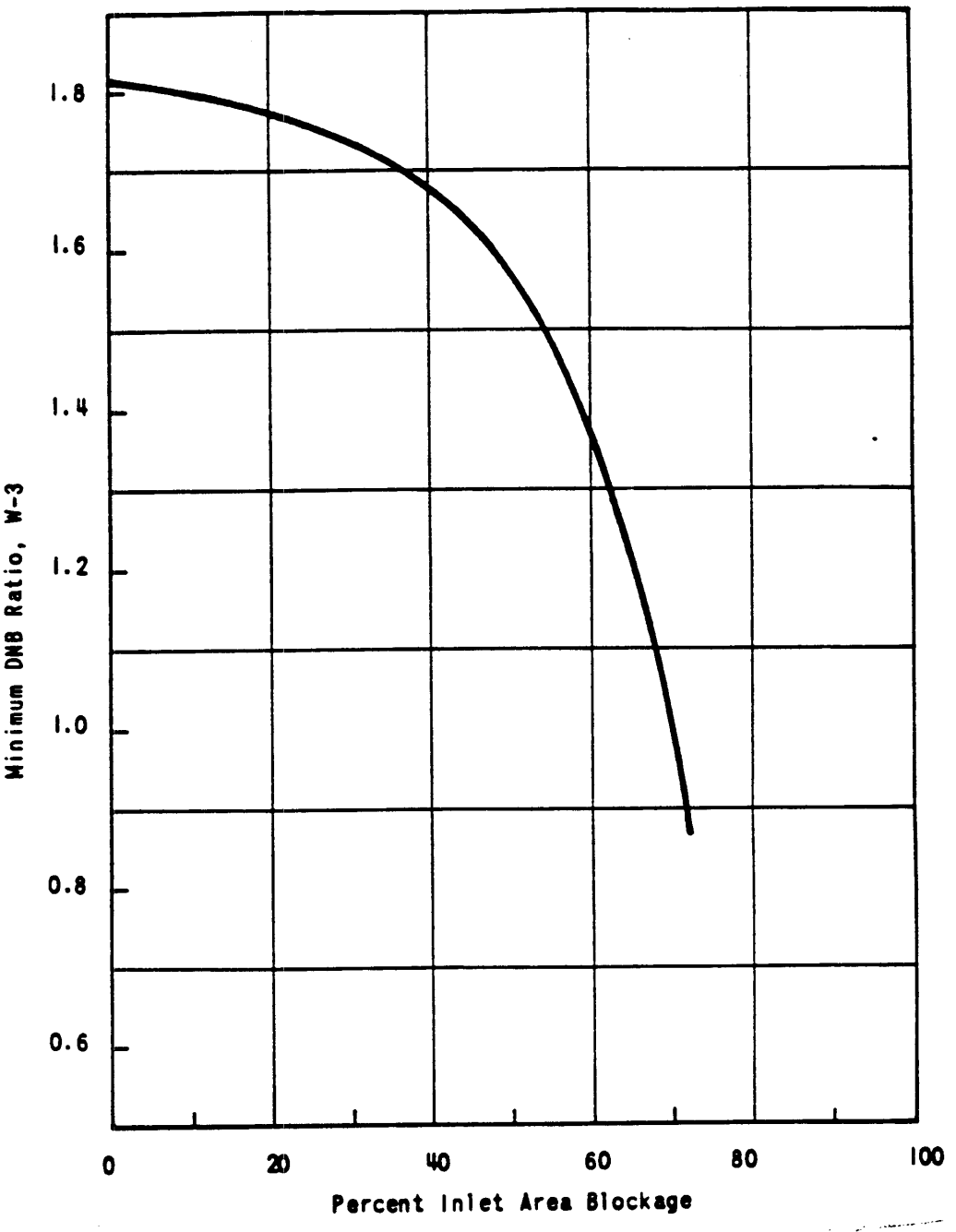

DAVIS-BESSE NUCLEAR POWER STATION
MINIMUM DNB RATIO VERSUS
PERCENT INLET AREA BLOCKAGE

FIGURE 4.4-26 REVISION 0
JULY 1982

4.5 REFERENCES

1. R. N. Duncan, Rabbit Capsule Irradiation of UO_2, CVNA -142, June 1962.

2. R. N. Duncan, CVTR Fuel Capsule Irradiations, CVNA -153, August 1962.

3. Frost, Bradbury, and Griffiths (AERE Harwell), "Irradiation Effects in Fissile Oxides and Carbides at Low and High Burnup Levels," Proceedings of IAEA Symposium on Radiation Damage in Solids and Reactor Materials, Venice, Italy, May 1962.

4. J. M. Gerhart, Post-Irradiation Examination of PuO_2–UO_2 Fast Reactor Fuel, GEAP-3833.

5. R. C. Daniel, et al., Effects of High Burnup on Zircaloy-Clad, Bulk UO_2 Plate Fuel Element Samples, WAPD-263, Westinghouse, September 1962.

6. D. B. Scott, Physical and Mechanical Properties of Zircaloy-2 and -4, WCAP-3269-41, May 1965, Figure 18.

7. R. M. Berman, et al., Properties of Zircaloy-4 Tubing, WAPD-TM-585, Westinghouse, December 1966.

8. Nuclear USA - U. S. Papers for 4th United Nations International Conference on the Peaceful Uses of Atomic Energy, Geneva, Switzerland, September 1971.

9. D. Burgreen, J. J. Byrnes and D. M. Benforado, "Vibration of Rods Induced by Water in Parallel Flow," Trans. ASME, 80 (1958), p 991.

10. D. H. Locke, "Defected Zircaloy Fuel," Nuc. Engrg. Int'l., August 1969, pp 648-652.

11. Hellstrand, Blomberg, and Horner, "The Temperature Coefficient of the Resonance Integral for Uranium Metal and Oxide," Nuc. Sci. & Engrg, 8 (1960), pp 497-506.

12. Saxton - Large Closed-Cycle Water Research and Development Work Program, July 1 - December 31, 1964, WCAP-3269-4, Westinghouse.

13. W. R. Cadwell, PDQ07 Reference Manual, WAPD-TM-678, Westinghouse, Bettis Atomic Power Laboratory, Pittsburgh, Pennsylvania, January 1967.

14. R. J. Breen, O. J. Marlowe, and C. J. Pfeifer, HARMONY: System for Nuclear Reactor Depletion Computation, WAPD-TM-478, Westinghouse, January 1965.

15. User's Manual for ANISN, a One-Dimensional Discrete Ordinates Transport Code With Anisotropic Scattering, K-1693, Union Carbide Corp. (1967).

16. Evaluated Nuclear Data File (ENDF/B), Version I, Brookhaven National Laboratory.

17. D. E. Kusner and R. A. Dannels, ETOG-1, a Fortran IV Program to Process Data From the ENDF/B File to the MUFT, GAM, and ANISN Formats, WCAP-3845-1, Westinghouse, December 1969.

18. R. G. Soltesz, R. K. Disney, and G. Collier, User's Manual for DOT-IIW Discrete Ordinates Transport Computer Code, WANL-TME-1982, Westinghouse Astronuclear Laboratory (1969).

19. M. N. Baldwin, R. H. Clark, and J. E. Rogers, Physics Verification Program, Part II – Final Report, BAW-3647-7, Babcock & Wilcox, Lynchburg, Va. (1968).

20. J. J. Sapyta, J. W. Harwell, and W. A. Wittkopf, "Pressure Vessel Fluence Calculations for Large Pressurized Water Reactors," ANS Transactions,14 (1971), p 890.

21. H. Bohl, Jr., and A. P. Hemphill, MUFT-5 – A Fast Neutron Spectrum Program for the Philco-2000 Computer, WAPD-TM-218, Westinghouse.

22. O. J. Marlowe and M. C. Suggs, WANDA-5 – A One-Dimensional Neutron Diffusion Equation Program for the Philco-2000 Computer, WAPD-TM-241, Westinghouse.

23. E. Grueling, F. Clark, and G. Goertzel, A Multigroup Approximation to the Boltzmann Equation for Critical Reactors, NDA-10-96 (1953).

24. A. Sauer, "Blackness in Cylindrical Fuel Lattices," Trans. ANS, 6, June 1963.

25. A. Sauer, "Approximate Escape Probabilities," Nuc. Sci. & Engrg., 16 (1963), pp 329-335.

26. L. Dresner, Resonance Absorption in Nuclear Reactors, Pergamon Press, New York (1960).

27. F. T. Adler, G. W. Hinmann, and L. W. Nordheim, The Quantitative Evaluation of Resonance Integrals, P/1988, Second Geneva Conference, Vol 16, (1958).

28. T. C. Engelder, et al., Measurement and Analysis of Uniform Lattices of Slightly Enriched UO_2 Moderated by D_2O-H_2O Mixtures, Babcock & Wilcox, BAW-1273, Lynchburg, Virginia, January 1962.

29. Physics Verification Program - Quarterly Technical Report No. 1, January-June 1966, BAW-3647-1, Babcock & Wilcox, Lynchburg, Virginia.

30. P. W. Davison, et al., Yankee Critical Experiments - Measurements on Lattices of Stainless Steel-Clad, Slightly Enriched Uranium Dioxide Fuel Rods in Light Water, YAEC-94, Westinghouse Atomic Power Division, Pittsburgh, Pennsylvania, April 1959.

31. V. E. Grob, et al., Multi-Region Reactor Lattice Studies - Results of Critical Experiments in Loose Lattices of UO_2 Rods in H_2O, WCAP-1412, Westinghouse Atomic Power Division, Power Division, Pittsburgh, Pennsylvania, March 1960.

32. J. R. Brown, et al., Kinetic and Buckling Measurements on Lattices of Slightly Enriched Uranium and UO_2 Rods in Light Water, WAPD-176, Westinghouse Atomic Power Division (Bettis), Pittsburgh, Pennsylvania, January 1958.

33. E. G. Taylor, Saxton Plutonium Program - Critical Experiments for the Saxton Partial Plutonium Core, WCAP-3385-54, Westinghouse Atomic Power Division, Pittsburgh, Pennsylvania, December 1965.

34. R. D. Leamer, et al., PuO_2-UO_2 Fueled Critical Experiments, WCAP-3726-1, Westinghouse Atomic Power Division, Pittsburgh, Pennsylvania, July 1967.

35. M. N. Baldwin and M. E. Stern, Physics Verification Program - Part III, Quarterly Technical Report, April-June 1969, BAW-3647-14, Babcock & Wilcox, Lynchburg, Virginia, June 1969.

36. W. R. Cadwell, P. F. Buerger, and C. J. Pfeifer, The PDQ-5 and PDQ-6 Programs for the Solution of the Two-Dimensional Neutron Diffusion-Depletion Problem, WAPD-TM-477, Westinghouse.

37. R. H. Clark and T. G. Pitts, Physics Verification Experiments, Core I, BAW-TM-455, Babcock & Wilcox, Lynchburg, Virginia.

38. R. H. Clark and T. G. Pitts, Physics Verification Experiments, Cores II and III, BAW-TM-458, Babcock & Wilcox, Lyncbburg, Virginia.

39. R. R. Hammer, Zircaloy-4, Uranium Dioxide, and Materials Formed by Their Interaction - A Literature Review With Extrapolation of Physical Properties to High Temperatures, IN-1093, Idaho Nuclear Corp., September 1967.

40. D. B. Scott, Physical and Mechanical Properties of Zircaloy-2 and -4, WCAP-3269-41, Westinghouse, Pittsburgh, Pennsylvania, May 1965.

41. High Temperature Materials Program - Progress Report No. 61, GE-NMPO, GEMP-61, General Electric Co., Cincinnati, Ohio, September 1966.

42. R. W. Bowring, Physical Model, Based on Bubble Detachment, and Calculation of Steam Voidage in the Subcooled Region of a Heated Channel, HPR-10, OECD Halden Reactor Project, December 1962.

43. N. Zuber and J. A. Findlay, “Average Volumetric Concentrations in Two-Phase Flow Systems,” Presented at ASME Winter Meeting (1964).

44. G. W. Maurer, A Method of Predicting Steady-State Boiling Vapor Fractions in Reactor Coolant Channels, WAPD-BT-19, Bettis Technical Review, Westinghouse.

45. B. W. LeTourneau and N. C. Sher, Pressure Drop Recommendations for Pressurized Water Reactor Design, WAPD-TM-326 (Revised), Westinghouse (Bettis), Pittsburgh, Pennsylvania, May 1957.

46. J. F. White, L. Sjodahl, and J. T. Bittrell, Recommended Property and Reaction Kinetics Data for Use in Evaluating a Light-Water- Cooled Reactor Loss-of-Coolant Incident Involving Zircaloy-4 or 304 SS-Clad UO_2, GEMP-482, January 1967.

47. R. M. Berman, Properties of Zircaloy-4 Tubing, WAPD-TM-585, December 1966.

48. J. A. Christensen, R. J. Allio, and A. Biancheria, Melting Point of Irradiated Uranium Dioxide, WCAP-6065, February 1965.

49. L. Baker and L. C. Just, Studies of Metal-Water Reactions at High Temperatures, "III: Experimental and Theoretical Studies of the Zirconium-Water Reaction," ANL-6548, May 1962.

50. L. A. Stephan, The Effects of Cladding Material and Heat Treatment on the Response of Waterlogged UO_2 Fuel Rods to Power Bursts, In-ITR-111, January 1970.

51. R. M. Potenze, Quarterly Technical Report - SPERT Project, IDO- 17206, September 1966.

52. J. G. Grund, Experimental Results of Potentially Destructive Reactivity Additions to an Oxide Core, IDO-17028, December 1964.

53. Fuel Rod Bowing in Babcock & Wilcox Fuel Designs, BAW-10147P-A, Rev. 1, Babcock & Wilcox, Lynchburg, Virginia, May 1983.

54. BAW-10141P-A, Rev. 1, TACO2 Fuel Pin Performance Analysis-Revision 1, June 1983.

55. BAW-10179P-A, Latest rev, per App.4-B "Safety Criteria and Methodology For Acceptable Cycle Reload Analysis", (See App.4-B).

56. BWNT Calculation 32-1239305-01 "EOC Average Temperature Reduction" 2/26/96.

57. BWFC document 51-1245290-00 "D-B Cy10 EOC T_{ave} Reduct Man.", 2/15/96.

58. BAW-10227P-A, "Evaluation of Advanced Cladding and Structural Material (M5) in PWR Reactor Fuel," February 2000.

APPENDIX 4A

FAULTED CONDITION ANALYSIS OF TOLEDO, DAVIS-BESSE 1 REACTOR INTERNALS

PREPARED BY

C.E. HARRIS
L.M. SMALEC
C.W. PRYOR
R.A. HURST

BABCOCK & WILCOX COMPANY

FEBRUARY, 1976

FOR

THE TOLEDO EDISON COMPANY

APPENDIX 4A

FAULTED CONDITION ANALYSIS OF TOLEDO EDISON, DAVIS-BESSE 1 REACTOR INTERNALS

TABLE OF CONTENTS

LIST OF TABLES

LIST OF FIGURES

4A.1.0 DAVIS-BESSE INTERNALS DESIGN DIFFERENCES

This section describes the design differences between the Davis-Besse 1 reactor internals and the Oconee-type internals described in BAW-10008, Part 1, Rev. 1. The core support structure described in BAW-10008, Part 1, Rev. 1 has eight vent assemblies while Davis-Besse 1 only has four. However, both structures have the same vent assembly opening area and the conservative assumption of no vent assemblies was made in the thermal-hydraulics LOCA analysis. The complete LOCA analysis is described in detail in the following sections.

Another significant design difference is found in the lower grid assembly. BAW-10008, Part 1, Rev. 1 describes a lower grid assembly with a support grillage constructed of welded beams which form square openings for coolant flow. The Davis-Besse 1 internals have a support plate that consists of a forging with circular flow holes. This necessitated a new core bounce analysis to account for the difference in stiffness between the forging and the welded-beam structure.

Possibly the most significant design change is in the reactor vessel support arrangement. The Davis-Besse 1 reactor vessel is supported by the inlet nozzles rather than skirt supported as is the case with the reactor vessel of BAW-10008, Part 1, Rev.1. This affects the internals because it changes the characteristics of the system dynamic analysis which results in different LOCA thrust and seismic loads from those described in BAW-10008, Part 1, Rev. 1.

4A.1.1 Introduction

The purpose of this report is to update the contents of B&W Topical Report BAW 10008, Part 1, Rev. 1 (ref. 8) to include the revised analysis performed on the Davis-Besse 1 reactor vessel internals (ref. 9). Basically, the revised analysis was performed to account for design differences between the Davis-Besse 1 internals and the Oconee-type internals, and to upgrade the state-of-the-art for conducting faulted condition analysis. The differences in the analysis are primarily centered around a better definition of LOCA forcing functions for both inlet and outlet pipe breaks. More versatile and sophisticated computer codes were used not only for the LOCA thermal-hydraulic analysis, but also for the performance of subsequent stress analyses. This report describes the revised generation of LOCA forcing functions, the application of these forces to internal structures, and the comparison of resulting stresses with limits, which can be shown to be more stringent than those of the new ASME Code, Subsection NG for core support structures. Abstracts of all new computer codes are provided at the end of the report.

4A.2.0 Development of Loadings for Davis-Besse 1 Internals

The Loss-of-Coolant-Accident (LOCA) analysis is performed by considering its effects in three parts. The accident consists of the postulated rupture of either an inlet or an outlet pipe to the reactor vessel. This results in thrust forces which dynamically load the entire nuclear steam system. The system analysis which predicts the response of all affected components, including the reactor internals, is commonly referred to as the LOCA Thrust Analysis. The pipe ruptures also induce sonic decompression waves which result in pressure differentials across the shell and plate structures which make up the reactor internals. Pressure drops across the reactor core also result from the decompression waves. The analysis to predict structural response from these pressure differentials is commonly referred to as LOCA Δp or LOCA Pressure Analysis. The analysis which predicts the response of the horizontal grid structures resulting from the pressure drops across the reactor core is referred to as the Core Bounce Analysis. This section describes the generation of LOCA loadings for these three effects for the Davis-Besse 1 internals as contrasted to that for the Oconee-type internals.

4A.2.1 Thermal-Hydraulic Pressure Analysis

Following a loss-of-coolant accident the integrity of the core and internals must be maintained to ensure safe and orderly shutdown of the reactor. This implies that gross deformation of the core and internals does not occur, that control rod insertion is not prevented, and that deformation of the internals is slight and thus does not impede coolant and safety injection flow.

The maximum values of the differential pressures acting on the reactor vessel and the internals and, hence, the maximum loadings on these components, occur during the subcooled phase of blowdown during a loss-of-coolant accident. In general, the loadings increase with increases in the break size and with the proximity of the break to the vessel.

The FLASH P computer program (see Reference 1) was developed to study the transient behavior of a Nuclear Steam System undergoing a loss-of-coolant accident. The program solves the one-dimensional mass, energy, and fluid momentum, equations, and the equation of state for water, to establish the average fluid conditions within discrete regions of space, i.e., control volumes, as functions of time. A hydraulic system is represented in the program as a series of control volumes which are in turn interconnected by flow paths to simulate the series and parallel flow channels within the system. Structural-hydraulic interactions are not considered in the program solution; that is, fixed boundaries at structures are assumed.

The FLASH P program input model of the nuclear steam supply (NSS) system primary coolant loop consists of 40 control volumes and 65 flow paths. Twenty-two (22) control volumes are utilized to represent the reactor internals region; the balance of the control volumes are used to depict the piping in the four coolant loops, the two steam generators, the pressurizer, and the containment. The input model is described in Table 4A.2-1 and in Figure 4A.2-1.

The program input includes provisions for simulating the pumps head-capacity characteristics, the core kinetics, and the heat transfer in the steam generators. While included in the model, these simulations have little effect on the maximum LOCA differential pressures, because of the system response-time characteristics.

Once control volumes have been selected to provide sufficient spatial detail to define the pressure differentials across major structural components, the fluid properties are defined. Steady-state pressure gradients around the loop are established on the basis that the average (and uniform) pressure of a control volume is located at its approximate center. Input enthalpies for control volumes are based on the local temperatures and control volume pressures.

Mass and energy conservation equations and the equation-of-state for water are applied to all control volumes. Continuous single (or two phase) equilibrium is assumed to exist within each control volume.

The internal flow paths between control volumes are represented in the program by a momentum equation having the following form:

$$\frac{(L/A)\dot{w}}{144 g_c} = (P_2 - P_1) + \frac{KW^2}{288 g_c \rho A^2} + \frac{FW^2}{\rho} + \rho \frac{(Z_2 - Z_1)}{144} \frac{g}{g_c}$$

Where,

L = Length, ft

A = Area, ft^2

.
w = flow rate change, lbm/sec^2

g_c = gravitational constant

P = pressure, psi

ρ = density, lbm/ft^3

W = flow rate, lbm/sec

Z = elevation, ft

K = unrecoverable pressure loss constant

F = recoverable pressure loss constant (area dependent only)

1 = upstream

2 = downstream

Flow path and control volumes become interrelated by the (P_2-P_1) term above. The program input values for each flow path are summarized in Table 4A.2-2.

The minor loss (form loss) and the friction loss coefficients used in the calculation of the unrecoverable pressure losses are combined into the single factor, K. The K-factor for each flow path is determined on the basis of the following considerations. Friction losses - obtained from the Moody data (Reference 6), based upon flow path surface roughness and Reynolds' number. Nozzle or orifice losses - calculated by

$$(K_{loss\ orifice}) = \left[\frac{1}{(C_D)_{orifice}} \right] 2$$

from Reference 4.

Contraction and expansion losses - calculated from Reference 5 by

$k_c = 0.4\ (1 - \sigma)$ and

$K_e = (1 - \sigma)^2$

for $RE > 10^4$, and by

$k_c = 0.5\ (1 - \sigma)$ and

$k_E = (1 - \sigma)^2$

for RE < 10^4 Sigma, σ, is the ratio of the terminal areas.

Turn losses - calculated as the sum of the dynamic heads at the beginning and end of the turn

$$(\Delta P)_{turn} = \frac{w_1^2(k)}{2g_c A_1^2 \rho_1} + \frac{w_1^2(k)}{2g_c A_1^2 \rho_2}, K = 1$$

The recoverable pressure losses in a path are due to changes in flow area, and are determined from the F-factor, which is defined as:

$$F = \frac{1}{288 g_c}\left(A_1^{-2} - A_2^{-2}\right)$$

The inertial pressure losses are determined using the L/A-factor, which is defined as:

$$L/A = \int_{O_{flowpath}}^{L} \frac{d\ell}{A}$$

In non-one-dimensional flow paths, this integral is approximated by using assumptions of effective path lengths and average flow area.

Both 0% and 100% reactor operating conditions were considered in the LOCA analysis. The system conditions are summarized below.

Power Level	100%	0%
Coolant Enthalpy, BTU, lbm	554.5/625.7	525.2
System Pressure, psi	2200	2200
System Flowrate, lbm/sec	130.9×10^6	134.82×10^6

The location and type of break, the break opening time, and the discharge correlation assumed to simulate the leakage rate out of the system, all have an effect on the system differential pressures. For design lead calculations, split breaks, as opposed to double-ended breaks, were assumed to occur at the vessel nozzle/piping interface. As modeled, the split break assumption resulted in approximately 5% greater pressure differentials on the internals, compared to the guillotine breaks.

Break areas of 14.1 ft^2 and 8.6 ft^2 were assumed for the outlet pipe and inlet pipe breaks, respectively. These areas are equivalent to twice the pipe flow area, meaning that no credit for piping stiffness or piping restraints is taken in the LOCA calculations. An instantaneous break opening time, 0.0 milliseconds, is assumed. As with the break area assumption, the instantaneous break opening assumption is ultra-conservative in terms of the magnitudes of the resultant LOCA differential pressures on the reactor internals structures. The Moody discharge flow correlation per Reference 3 was assumed, with a discharge coefficient, C, of one.

No credit was taken for the vent valves in the LOCA calculations, adding conservatism to the results. The vent valves would open in the case of a cold leg break, permitting flow from the

upper plenum region to the internals downcomer annulus which would tend to equilibrate the differential pressures across the core support cylinder.

Correlation studies using the 1968 Phillips Petroleum Company LOFT semi-scale test results per Reference 7 were made to assess the accuracy of the FLASH P program predictions. The simulation of the subcooled blowdown portion of Tests No. 711, 712, and 713 with the FLASH P model yielded predictions which were within 15% of the measurements. It should be noted that the Moody discharge model with a C_D of 0.6 was used in the correlation studies; the assumption of a C_D value of 1.0 in the LOCA calculations is therefore conservative.

For test 712, Figures 4A.2-3 through 4A.2-6 compare the measured and calculated pressure histories at four different locations within the quarter-scale vessel, shown in Figure 4A.2-2. This test 712 represents a full area break of the 4-inch I.D. discharge line. Overall, the analytical/experimental comparisons demonstrate the suitability of the FLASH P code for use in LOCA blowdown calculations.

A typical FLASH P result of the differential pressure acting across the core support shield during a LOCA is shown in Figure 4A.2-7. The maximum values of the calculated pressure differentials acting across the primary reactor internals components are collected in Table 4A.2-3. The internals components are identified in Figures 4A.2-8, 4A.2-9 and 4A.2-10, along with the fluid control volume locations used in the FLASH P simulation.

The FLASH P program has a provision for calculating the hydrodynamic force during LOCA on the fuel assemblies. The force is determined from the solution of the linear momentum equation applied to the fluid control volumes which span the length of the fuel assemblies. The force equation has the following form:

$$F = (P_T - P_B)A_B - W_{CORE} + \sum \Delta P_{UNREC} A_F$$

Where,

P_T = pressure, core top, psi

P_B = pressure, core bottom, psi

A_B = blocked area, ft^2

W_{CORE} = Dry weight of core, lbf

$\sum \Delta P_{UNREC}$ = total unrecoverable pressure drop through core, psi

A_F = Flow area, ft^2

F = Force on-the-core, lbf

In the FLASH P model, the core is represented by two control volumes and three flow paths.

A typical FLASH P result of the force on the core calculation is shown in Figure 4A.2-11, for the case of a cold leg rupture (8.6 ft^2 leak area) at a power level of 2772 megawatts.

4A.2.2 LOCA Thrust Analysis

This analysis predicts the dynamic response of the Nuclear Steam System to thrust forces applied at pipe break locations. The entire system responds to these forces and dynamic effects in the form of inertia forces are computed throughout the reactor internals.

A mathematical model is used in performing the dynamic analysis. The NSSS is idealized as a series of discrete lumped masses connected together by beams representing the appropriate structural stiffnesses. The computer code, DYNAM, is used to predict the dynamic response of the system to the LOCA thrust forcing functions. The computer code, FLASH, is used to calculate the LOCA pressure time histories at the pipe break and the thrust forcing function is calculated simply by the product of pressure and area. The LOCA thrust analysis described in BAW-10008, Part 1, Rev. 1, is similar to the Davis-Besse 1 analysis. Both analyses are performed as described above and the only difference in the models is the location of the supports, Davis-Besse being a nozzle supported reactor vessel and BAW-10008, Part 1, Rev. 1, being skirt supported. It should be noted that in both cases the model used for the LOCA thrust analysis is used for the seismic analysis. The seismic analysis for Davis-Besse 1 is different from that described in BAW-10008, Part 1, Rev. 1, to account for the different plant locations and the corresponding different base mat spectra.

4A.2.3 Core Bounce

During a hot leg LOCA the core is lifted from the lower grid, impacts the upper grid, and returns to impact the lower grid. The dynamic analysis which predicts the vertical response of the core and internals during a LOCA is referred to as the Core Bounce Analysis. The time dependent forcing function for this dynamic analysis is the pressure loading on the core from the thermal-hydraulics analysis. The method of calculating force for the Davis-Besse analysis is different from that described in BAW-10008, Part 1, Rev. 1, and has been thoroughly discussed in Article 1 of this section.

The core bounce analysis of the Davis-Besse 1 internals is quite different from that described in BAW-10008, Part 1, Rev. 1. The Davis-Besse analysis has been significantly upgraded primarily through the implementation of a more versatile and sophisticated computer code than was used in the BAW-10008, Part 1, Rev. 1, analysis. The core bounce analysis of BAW-10008, Part 1, Rev. 1 used the computer code, PNAME which calculates the response of a single-degree-of-freedom spring-mass system to a time dependent forcing function. The mathematical model of the internals that is used here is shown in Figure 4A.2-12 and is quite simplified. There is a single spring representing the stiffness of the plenum assembly and one spring representing the stiffness of the lower grid assembly. There is one mass for the plenum assembly, one mass representing the lower grid assembly, and one mass for the core to which the forcing function is applied. The Davis-Besse core bounce analysis is based on the computer code, STARS, which calculates the dynamic response of a multi-degree-of-freedom system.

The Davis-Besse model more accurately represents the dynamic behavior of the reactor internals (see Figure 4A.2-13). The plenum assembly, core, and lower grid assembly are each represented by several lumped masses rather than just one. The core mass is distributed into lumped masses representing fuel assembly “annular rings” which are connected to one another through the upper and lower grid beams. STARS accounts for each mass impacting the grids at various times as opposed to PNAME, where a single core mass limits all fuel assemblies to impacting the grids at the same time. Also the nonlinearity of the upper grid-core spring is represented in the STARS model and not in the PNAME model. The STARS code is far

superior to the PNAME code because it is much more versatile in computation of dynamic response. Abstracts of the STARS and PNAME codes are provided in a following section.

4A.3.0 LOCA Analysis of Core Support Structure

The 177FA core support structure is the primary supporting structure of the reactor vessel internals. It consists of three cylindrical shells referred to as the core support shield, core barrel, and lower grid assembly "Flange Ring". The core support shield is the upper shell which surrounds the plenum assembly and is supported by a thick flange which rests on the reactor vessel ledge. The core support shield has two reinforced cutouts for the outlet nozzles and four reinforced cutouts for the vent assemblies. The core barrel is bolted to the bottom of the core support shield and surrounds the reactor core. The lower grid assembly flanged ring is bolted to the bottom of the core barrel and supports the lower grid forging and lower lattice plate which supports the core.

While the BAW-10008, Part 1, Rev. 1, topical report emphasized the hot leg LOCA analysis of the core support structure, the Davis-Besse 1 analysis includes consideration of both hot and cold leg pipe breaks for 0% and 100% power reactor conditions. The analysis considers the effects of asymmetric pressure differentials which are created during the cold leg LOCA. LOCA thrust effects and core bounce axial loadings are also included.

The Davis-Besse 1 analysis was facilitated through the use of detailed finite element models and second generation computer codes. These models more accurately represent the core support structure and its inherent structural discontinuities. Both the BAW-10008, Part 1, Rev. 1, analysis and the Davis-Besse analysis employ axisymmetric shell elements with statically distributed loadings. In both cases, dynamic effects are accounted for either through the direct inclusion of inertial forces or through the use of appropriate dynamic load factors. However, the Toledo analysis uses the GENSH3 code (see computer abstracts in following sections) and a full Fourier expansion of the asymmetric cold leg pressure distributions.

The BAW-10008, Part 1, Rev. 1, analysis uses the computer code SOR-II for the hot leg axisymmetric analysis and the code SHELL for the hot leg asymmetric analysis. The SOR-II code is applicable only to thin shells of revolution and does not accurately represent structural discontinuities. The SHELL code determines the linear asymmetric bending behavior of arbitrarily loaded thin elastic shells of revolution. SHELL can handle changes in thickness but its results are accurate only for those areas away from structural discontinuities. The loadings that may be considered are normal, tangential, and moment surface loadings, as well as edge forces and deflections. Loadings are represented by a Fourier series expansion in the circumferential direction. SHELL was used to analyze the asymmetric hot leg pressure loading by assuming a cosine pressure distribution around the circumference.

The Davis-Besse stress analysis uses a finite element model with better structural definition. The GENSH3 code is capable of representing shells with a wide range of meridianal shapes. For better representation of the actual structure, open branches, layer constructions, and middle surface shifts are included. Each element and layer can be of varying thicknesses and have different sets of orthotropic material properties, and each element may have a unique loading condition. As with SHELL, GENSH3 represents an asymmetric load by a Fourier series expansion. Because of GENSH3's modeling techniques, it is more versatile than SOR-II and SHELL, and the resulting stress analysis should be more accurate.

The shell analysis model described in BAW-10008, Part 1, Rev. 1, is shown in Figure 4A.3-1. The Davis-Besse 1 analysis model is shown in Figure 4A.3-2. A comparison of the thermal-

hydraulic pressure loadings applied to the two models is illustrated in Figure 4A.3-3. As can readily be seen, the effects of asymmetric cold leg pressures are fully incorporated in the Davis-Besse 1 analysis. The dynamic load factors applied to these static pressure distributions are described in detail in BAW-10008, Part 1, Rev. 1, and are computed in like manner for the Toledo 1 analysis.

The core support structure is subjected to external pressures during a hot leg LOCA. The stability of the shell under external pressure was insured by performing a buckling analysis of the core support shield and core barrel and demonstrating that the critical buckling pressure was greater than the maximum dynamic external pressures acting on the structures. Stresses in the core support structure due to axial core bounce loads were calculated along with stresses due to inertia loads from the LOCA Thrust Analysis. In comparing total stresses with allowable limits, the maximum stresses from the three load sources were conservatively added without regard to their times of occurrence. For hot and cold leg LOCA, 0% power and 100% power, the conservatively calculated stress intensities (including stresses due to the Maximum Hypothetical Earthquake) are below the allowable stress limits which are discussed in Section 4A.5.0.

The stress analysis of the bolts and bolted joints of the core support structure for Davis-Besse is similar to the analysis of BAW-10008, Part 1, Rev. 1. Stresses are computed from a combination core pressure differential core vertical motion, reactions resulting from the response of the internals to LOCA thrust, seismic excitation, and dead weight. Stresses include preload, residual torsion due to initial tightening, differential thermal expansion, and mechanical loads. From a given bolt preload, axial load, moment across the joint, and assumed relative flange rotation the stresses in the bolts and flanges are calculated. Both bolt stiffness and flange stiffness are considered in the analysis. To facilitate this analysis for Davis-Besse a digital computer code, BOLT 70, was developed. This code considers the relative rotation of the flanges, compressibility of the materials, etc. The code calculates membrane bolt stresses, bending stresses, moment across the joint, shear stresses, and rotation of flanges.

4A.4.0 Comparison of Analyses of Structural Components

4A.4.1 Lower Grid Assembly

The analysis of the Lower Grid Assembly (LGA) discussed in BAW-10008, Part 1, Rev. 1 was performed through the use of the computer code SADGS. An analysis for static loads was performed by SADGS and the results of the analysis were used to determine the equivalent spring rate and mass for the simplified LOCA core bounce analysis. To obtain LGA stresses due to LOCA the maximum stresses due to the static loads were multiplied by the ratio of the dynamic deflection due to core bounce to the static deflection from the SADGS analysis. Initially the Davis-Besse core bounce analysis was carried out using the data from the above SADGS static runs. Since the Davis-Besse lower grid is a forging with circular holes as contrasted to the BAW-10008 welded beam structure, tests were conducted by the Alliance Research Center to determine the stiffness of the Davis-Besse forging. It was found that the Davis-Besse forging was stiffer than the BAW-10008, Part 1, Rev. 1, grid stiffness predicted by SADGS and the STARS core bounce model was modified accordingly. The ARC scale model tests determined a stress/inch of center deflection in critical locations of the Davis-Besse lower grid forging. The STARS core bounce analysis provided the maximum center deflection due to LOCA and the corresponding stresses in the forging were determined by simply ratioing the stress/inch results by the core bounce deflection results. The lower lattice plate was not included in the ARC tests or in the STARS core bounce analysis. The lattice plate is very thin in comparison to the lower grid forging and would have little effect on the deflection results. The

STARS deflection results are conservative since the lattice plate would supply some deflection restraint. The lower lattice plate was included in the SADGS results. Since the lower lattice plates have the same configurations, these SADGS stress results were used to analyze the Davis-Besse lattice plate. Since the lattice plate and support forging are rigidly connected by support columns the deflection of the lattice plate and support forging are assumed to be the same. Therefore, the center deflection of the lattice plate was obtained from the STARS core bounce analysis and then ratioed by the stress/deflection results of the BAW-10008, Part 1, Rev. 1, SADGS analysis.

4A.4.2 Plenum Cover

The stress analysis of the plenum cover for Davis-Besse is essentially the same as described in BAW-10008, Part 1, Rev. 1. Both LOCA and seismic conditions are considered and the LOCA core bounce loadings are the most severe. In both cases finite element computer codes are employed to calculate the equivalent stiffness and mass of the plenum cover to be used in the core bounce analysis. Also the results of these static load analyses are used to determine the faulted condition stresses by multiplying the static load stresses by the ratio of the dynamic displacement to static displacement. For the analysis discussed in BAW-10008, Part 1, Rev. 1 the computer code SADGS is used and the equivalent mass and stiffness to be used in PNAME is obtained. As mentioned previously, the Davis-Besse core bounce analysis is more refined than the “PNAME” analysis of BAW-10008, Part 1, Rev. 1. In the Davis-Besse 1 STARS analysis the plenum cover is modeled as a beam with equivalent mass and beam stiffness rather than a single mass and spring as in PNAME. To obtain the equivalent beam properties the computer code ST3DS is used to analyze the behavior of the plenum cover under static loads rather than the SADGS code. The resulting plenum cover analysis performed for Davis-Besse is more detailed than that described in BAW-10008, Part 1, Rev. 1. An abstract of the ST3DS computer code is presented in Section 4A.6.0.

4A.4.3 Thermal Shield

BAW-10008, Part 1, Rev. 1, does not address the analysis of the thermal shield, however, a detailed stress analysis has been performed on the Davis-Besse structure. A finite element analysis using GENSH3 was performed for hot and cold leg LOCA pressures distributed around the circumference and along the length of the shell. The stresses due to horizontal loads from LOCA thrust and seismic dynamic system analyses were combined with the stresses due to LOCA pressure. The resulting maximum stresses are demonstrated to be below the allowable limits discussed in Section 4A.5.0.

4A.5.0 Comparison of Allowable Stress Limits

The allowable stress limits have been established for stress intensities. The Davis-Besse stress analysis calculates stress intensities in the usual manner. From a given state of stress, the three principal stresses are determined and the three stress differences are calculated. The absolute value of the largest stress difference is defined as the stress intensity. For evaluation of faulted conditions, only primary stresses are considered. The allowable limits for faulted conditions have been established according to the ASME Boiler and Pressure Vessel Code, Section III, Nuclear Vessels, 1968 edition. The limits used in the Davis-Besse analysis are the same as presented in BAW-10008, Part 1, Rev. 1; however, these limits differ somewhat from the limits of Subsection NG and Appendix F for the evaluation of faulted conditions. These limits are presented below for comparison.

Toledo and BAW-10008 Part 1, Rev 1 Limits: $Pm \leq 2/3\ Su$
$Pm + Pb \leq 2/3\ Su$

Subsection NG and Appendix F: $Pm \leq$ the lesser of $2.4\ Sm$ or $0.7\ Su$
$Pm + Pb \leq$ the lesser of $3.6\ Sm$ or $1.05\ Su$

Where Pm = primary membrane stress intensity
Pb = primary bending stress intensity
Su = ulitmate stress for unirradiated material at operating temperature
Sm = Material design stress intensity

The Davis-Besse allowable limit on primary membrane stress is compatible with the values specified by Subsection NG and Appendix F. The allowable limit for primary membrane plus bending is conservatively taken to be the same as for primary membrane alone. Therefore, the allowable stress limits for Faulted Conditions used in the Davis-Besse analysis are conservative when compared to the allowables of Subsection NG and Appendix F.

4A.6.0 Abstract of Computer Codes Used in Stress Analysis

DYNAM:

The DYNAM digital computer code calculates the dynamic response of a lumped-mass model as a function of time for a specified force-time input using a normal mode expansion solution. The dynamic model is input to the code as mass matrix, natural frequencies, and mode shapes, calculated using one of the other dynamics codes (such as SHOCK). The model assumptions are necessarily consistent with those for the code calculating these input quantities. No damping is included in the solution.

The applied external force is input in a force vs. time digitized form. The response of the model is calculated assuming that the force is linear over a given increment of time. The response in each mode is evaluated for time steps within the linear force increment and then summed over all modes to give the total response of each mass. The code calculates the displacements, velocities, accelerations, and effective static forces at each time step. The time-varying effective static forces are then used to determine the shear and bending moments at points of interest in the model.

PNAME:

The PNAME digital computer code calculates the response of a single-degree-of-freedom spring and mass dynamic model for a specified forcing function. The assumed spring may be nonlinear to represent plastic behavior or a gap (a zero stiffness spring). The displacement, velocity, and acceleration of the mass are calculated as a function of time using the linear acceleration method.

STARS:

The STARS digital computer code calculates the dynamic response of a discrete-mass, planar model idealized by an assemblage of one-dimensional finite elements, i.e., elastic beam members with shear and bending stiffness and nonlinear spring elements, which may be gapped. The code monitors and accumulates the permanent deformations in the nonlinear springs and accounts for impacting. Seven types of spring elements are provided in the STARS code element library, in addition to the elastic beam elements. STARS is flexible with respect to

geometry, since the structural system is synthesized from compatibility requirements defined by the user.

The dynamic equations of motion of the discrete-mass system are formed and the coupled response is obtained in steps corresponding to specific instants of time. At a given time the motions are held fixed, so that the internal forces can be calculated. Based on the response motion and internal forces at earlier times, the responses at the time in question are predicted. With the predicted values of motion, the internal forces are recalculated. Using these forces, a new response motion can then be determined. Therefore, at each time step, the relationship between the response motion and the internal forces is satisfied. This process is continued step-by-step throughout the time interval of interest. The numerical method used for this step-by-step solution involves two types of integration formulas. The fourth-order Adams-Bashforth "2/3" predictor-corrector method, which is a stable solution method, is used for a majority of the solution. However, this method is not self-starting, and the fourth-order Runge-Kutta method is used to start the solution process.

In addition to the step-by-step solution of the nonlinear equations of motion, the STARS code provides for the solution of the natural frequencies and mode shapes of the elastic system. The frequencies and modes are obtained by solving the eigenvalue problem using the sweeping technique. This technique uses a power method (i.e., an iterative method) and the orthogonality relationships among the normal modes.

Reference Material:

Babcock & Wilcox User's Guide for the STARS code, December 10, 1969.

SOR-II:

SOR-II is a FORTRAN program that solves for the forces, deflections, stresses, and strains in thin shells of revolution. The shells may be general surfaces of revolution with variable thicknesses and elastic moduli. This includes the more familiar forms: the circular flat plate, cone, cylinder, sphere, ellipse, and tori with circular or elliptical cross sections, for which a simplified input is used. The axisymmetric loadings considered include arbitrary distributions of normal, tangential, and moment surface loadings, as well as edge forces and deflections. The effects of temperature variations in the meridianal and thickness directions, as well as centrifugal loading due to rotation about the axis, and vibration are included.

The program will solve and join together up to 30 shells. The additional effects of misalignment, line loads, and elastic supports at the shell intersections are considered.

SOR-II numerically integrates the shell equations using a generalized Adams-Moulton method. The integration proceeds along the shell with automatic adjustment of interval size for maximum speed within the limitations of the preset error bounds. The method used permits solution of problems in which the shell includes the axis of revolution. It also allows step changes in loadings and some shell properties.

Reference Material:

J.A. Mirabel and D.G. Dight, SOR-II, A Program to Perform Stress Analysis of Shells of Revolution, KAPL 2292, September 15, 1963.

SHELL:

SHELL is a computer program that determines the linear asymmetric bending behavior of arbitrarily loaded thin elastic shells of revolution. The loadings that may be considered are normal, tangential, and moment surface loadings, as well as edge forces and deflections. Loadings are represented by a Fourier series expansion in the circumferential direction.

A finite difference method of solution of the shell equations is used. A maximum of 500 equal increments along the shell's meridian is allowed.

In the analysis, the shell material is assumed to be isotopic, and Poisson's ratio and the modulus of elasticity are constant in the circumferential direction. The stiffnesses and the Fourier coefficients for the surface loads and temperature distribution may have smooth variations in the meridianal direction.

Reference Material:

H.G. Schaeffer, Computer Program for Finite-Difference Solutions of Shells of Revolution Under Asymmetric Loads, NASA TW D-3926, May 1967.

GENSH3:

The GENSH3 digital computer code is used to determine stresses and deflections in shells of revolution. While the theory is valid for arbitrary shells, the code is designed to handle thin shells of revolution only. It is assumed that nonsymmetric loadings can be expanded in even harmonies of the circumferential coordinate. The differential equations of equilibrium are solved by the numerical integration technique of Runge-Kutta. The code is designed to evaluate the responses of shells of revolution subjected to static and periodic mechanical loadings and/or thermal loadings. All loadings must be symmetrical with respect to a plane containing the axis of rotation.

The mathematical model employed in the code is capable of representing shells with a wide range of meridianal shapes. For better representation of the actual structure, open branches, layer constructions, and middle surface shift are included. Each element and layer can be of varying thickness and have different set of orthotropic material properties. Each element may have different pressure, thermal, and ring loadings included.

The code has incorporated within 16 sets of natural boundary conditions. They include forces, displacement, and mixed conditions. A number of special boundary conditons of non-diagonal type can also be represented. The special boundary conditions become useful if the structure is attached to some elastic foundation or another structural element exhibiting certain stiffness properties.

The input to the code consists of data describing the geometry of the structure, the material properties, and the loadings. The output includes stress resultants, stress couples, displacements, and stresses along the shell contour. It will also give the circumferential variation of all quantities resulting from superposition of several harmonic numbers. Plotted results of all output quantities can be obtained.

BOLT 70:

BOLT 70 is a digital computer code written by J.W. Mitchem of NSE Stress Analysis Group. The code calculates bolt stresses in a flanged section. The relative rotation of the flanges, compressibility of the materials, etc., are taken into account in the analysis. The code calculated membrane stresses, bending stresses, moment acting across joint, shear stresses, rotation of flanges and several other quantities. The code was used to calculate bolt stresses in the core support structure bolts.

SADGS:

SADGS is a digital computer code to determine the stresses and deflections in flat grid structures connected by short columns. The plate-like grid structures are assumed to be composed of interconnected, simply-supported beams and to have quadrant symmetry. The beams are further assumed to have a uniform rectangular cross section except at the ends, where a straight taper may be included.

The solution is essentially based on an interaction or discontinuity analysis. The conjugate beam method solves for deflection and slope of free beams. Next, the condition of equal displacement at beam intersections generates a system of simultaneous equations. These equations are solved for the balancing forces. The balancing forces, initial thermal effects, and transverse loads are superimposed to obtain a total stress analysis.

ST3DS:

The ST3DS code is designed to compute the reactions and stresses in complex piping systems. The method used is based on the analysis of moderately large three-dimensional structures composed of either piping or non-piping elements. The non-piping elements can be straight and/or curved bars. The mass of the structure is concentrated at a few rationally selected points that coincide with the centers of mass as near as possible. The flexibility matrix of the system is obtained by applying unit forces and moments at each mass joint in the directions corresponding to the degrees of freedom chosen. The flexibility matrix is stored and used to calculate the desired results when the actual loadings are applied. The output consists of joint coordinates, cross-sectional properties of the various sections, boundary conditions, flexibility matrix, loads, and stresses. Frequencies and mode shapes can also be obtained as output.

4A.7.0 References

1. WAPD-TM-666, “FLASH 2: A Fortran II Program for the Digital Simulation of a Multinode Reactor Plant During Loss-of-Coolant”, April 1967.

2. “Prediction of Forces on Pressurized Water Reactor Vessel Internals Following a Loss-of-Coolant Accident”, by H. Watzinger, P. Gruber, F. Winkler, for presentation at the CREST meeting, Munich, October, 1972.

3. F.J. Moody, “Maximum Flow Rate of a Single Component Two-Phase Mixture:, ASME Paper 64 HT-35 (1964).

4. Kent’s Mechanical Engineer’s Handbook, 12th Edition, Page 5-09.

5. B&W Calculational Standard, 2A3N Manual, Nuclear Engineering Calculations.

6. L.F. Moody, “Friction Factors for Pipe Flow”, ASME Paper, Vol. 66, 1944.

7. “Quarterly Technical Report - LOFT Program Office, April 1 - June 30, 1969. IDO-17303, dated March 1970. Also, Phillips Petroleum Co. Letter to Babcock & Wilcox, April 9, 1968.

8. BAW-10008 Part 1, Rev. 1, “Reactor Internals STress and Deflection Due to Loss-of-Coolant Accident and Maximum Hypothetical Earthquake.” (June 1970).

9. C.H. Riddel, “Internals Design Stress Report”, Toledo Edison Company, Contract Number 620-0014, February 1971.

TABLE 4A.2-1

Description of Flash P Model Used for Reactor Vessel Pressure Drop Analysis for Davis-Besse

Node Number	Identification & (Volume, FT^3)
1	*Downcomer, Upper Level - (119.68 FT^3)
2	*Downcomer, Upper Level - (119.68)
3	*Downcomer, Lower Level - (131.21)
4	*Downcomer, Lower Level - (131.21)
5	*Bottom of Reactor Vessel - (356.15)
6	*Region Just Below Core - (301.38)
7	*Lower Half of Core - (349.18)
8	*Upper Half of Core - (364.50)
9	*Region Just Above Core - (783.30)
10	*Top of Reactor Vessel - (508.00)
11	*Exit Nozzle, Hot Leg - (51.42)
12	*Exit Nozzle, Hot Leg - (51.42)
13	*Region Between Plenum Assembly and Core Shield Support - (92.45)
14	*Region Between Plenum Assembly and Core Shield Support - (92.45)
15	Hot Leg (89.6 ft) - (633.72)
16	Hot Leg (89.6 ft) - (633.72)
17	Reactor Building
18	Hot Leg (6.0 ft) - (42.17)
19	Steam Generator, Upper Half - (1015.18)
20	Steam Generator, Upper Half - (1015.18)
21	Cold Leg (20.7 ft) - (186.59)
22	Cold Leg (20.7 ft) - (186.59)
23	Cold Leg (20.7 ft) - (186.59)
24	Cold Leg (20.7 ft) - (186.59)
25	Pressurizer - (1664.62) (818.73 Liquid, 845.89 Steam)
26	*Inlet Nozzle - (84.56)
27	*Inlet Nozzle - (84.56)
28	*Inlet Nozzle - (84.56)
29	*Inlet Nozzle - (84.56)
30	*Downcomer, Between Core Barrel and Thermal Shield - (22.55)
31	*Downcomer, Between Core Barrel and Thermal Shield - (22.55)
32	*Core Bypass, Lower Level - (94.88)
33	*Core Bypass, Upper Level - (99.37)
34	Hot Leg (6.0 ft) - (42.12)
35	Cold Leg (6.0 ft) - (25.66)
36	Cold Leg (6.0 ft) - (25.66)
37	Steam Generator, Lower Half - (1015.18)
38	Steam Generator, Lower Half - (1015.18)
39	Cold Leg (6.0 ft) - (25.66)
40	Cold Leg (6.0 ft) - (25.66)

*Total Reactor Vessel Volume = 4029.62 FT^3

TABLE 4A.2-2

Flow Path Input for FLASH P Internals Model

Path Description	Flow Path #	K-Factor[2] #	A-Area[1] ft^2	F-Factor[2] $\frac{lbf\ sec^2}{lbm\ in^2\ ft^3}$	L/A ft^{-1}	Flow lbm/sec
Inlet/Downcomer	29,31,39,44	0.0591	10.140	-1.0466-6	0.7910	9306.4
Downcomer/Downcomer	38,32	0.0404	17.563	0.0	0.4033	18613.0
Downcomer/Bottom of Vessel	59,22	3.7790	25.855	3.0585-7	0.3410	18613.0
Bottom of Vessel/Just Below Core	5	3.396	46.882	-1.6160-8	0.0999	37226.0
Just Below Core/Lower Half Core	1	2.818	49.193	-1.7460-8	0.0839	36728.0
Lower Half Core/Upper Half Core	2	5.522	49.193	0.0	0.1220	36728.0
Upper Half Core/Just Above Core	3	2.701	49.193	-1.1200-8	0.0872	36728.0
Just Above Core/ Top of Vessel	6	0.4546	11.712	1.1624-6	0.9187	7965.4
Just Above Core/Plenum Assy. CSS	9,10	9.406	0.5824	0.0	0.9650	299.0
Just Above Core/Plenum Assy. CSS	13,14	3.620	18.97	-8.5040-7	0.5631	11745.0
Top of Vessel/Plenum Assy. CSS	7,8	0.6015	2.8438	-1.2053-5	1.6849	3984.6
Plenum Assy.CSS/ Exit Noz	15,16	1.366	12.128	-7.545-7	0.1900	16099.0
Just Below Core/Core Bypass	21	60.590	3.471	0.0	0.9600	598.1
Core Bypass/Core Bypass	19	107.010	3.471	0.0	1.9200	598.1
Core Bypass/Just Above Core	20	56.078	3.471	0.0	0.9600	598.1
Inlet Noz/Downcomer Barrel-Shld	33,34,41,44	10.137	2.5432	0.0	4.5464	24.9
Downcomer Barrel-shld/Just Below Core	23,24	507.110	0.5436	0.0	11.4200	49.8
Downcomer Side-side/Downcomer Upper Level	36	0.158	11.8060	0.0	1.7851	0.0
Downcomer Side-side/Downcomer Lower Level	36	0.158	11.8060	0.0	1.7851	0.0
Inlet Noz 28/Inlet Noz 26	28	0.7739	3.091	0.0	2.529	0.0
Inlet Noz 26/Inlet Noz 27	37	0.02612	4.849	0.0	1.612	0.0
Plenum Assy CSS/Plenum Assy CSS	56	0.1406	11.973	-4.7148-6	0.7544	0.0
Downcomer Barrel-shld/Downcomer Barrel-shld	25	1.5276	2.6406	0.0	3.616	0.0

[1] The unrecoverable resistance term in the FLASH P Computer Code is K/A^2

[2] The F-factor is defined $$F = \frac{1}{2g_c}\left(\frac{1}{A^2_2} - \frac{1}{A^2_1}\right)$$

$$\Delta Prec = \frac{FW^2}{\rho}$$

TABLE 4A.2-3

Maximum Differential Pressure Values

Component	100% Power Outlet Break	0% Power Outlet Break	100% Power Inlet Break	0% Power Inlet Break
Core Support Shield (29-13)	345 psi	515 psi	-540 psi	-760 psi
Core Barrel (31-33)	225 psi	365 psi	-410 psi	-585 psi
Thermal Shield (3-31)	-120 psi	-235 psi	225 psi	300 psi
Plenum Assembly (9-10)	80 psi	145 psi	140 psi	240 psi
Downcomer (1-8)	160 psi	255 psi	-320 psi	-445 psi
Flow Distributor (5-6)	40 psi	70 psi	-60 psi	-90 psi
Across Core (6-9)	125 psi	175 psi	-150 psi	-210 psi
Force-on-Core	0.67×10^4 lbf	1.03×10^4 lbf	-1.05×10^4 lbf	-1.46×10^4 lbf

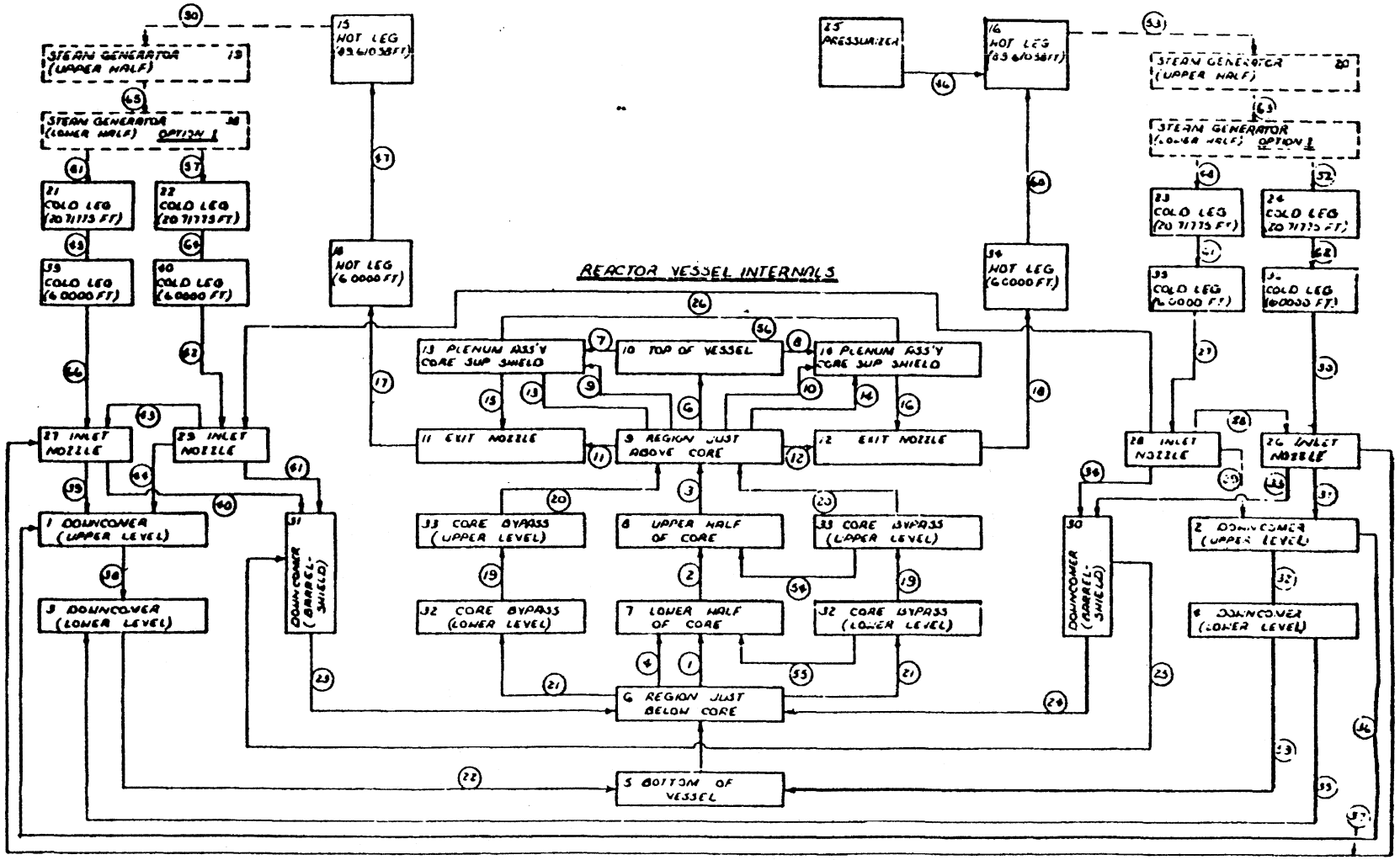

FIGURE 4A.2-1 REVISION 0 JULY 1982

FLASH P MODEL USED FOR REACTOR VESSEL INTERNAL PRESSURE DROP ANALYSIS - DAVIS BESSE
17-CONTAINMENT NODE

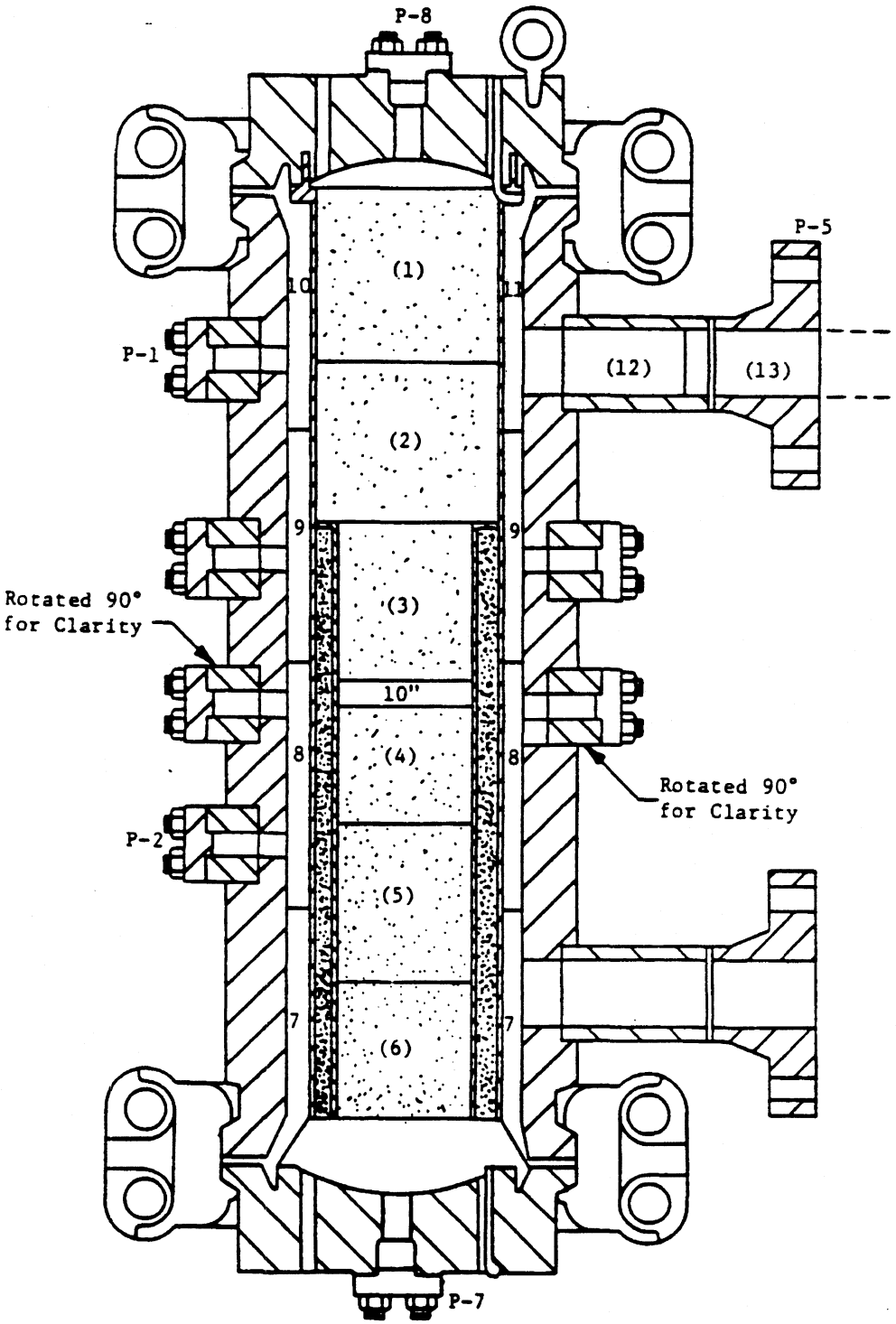

Quarter Scale Vessel
(PWR Core)

DAVIS-BESSE NUCLEAR POWER STATION
TEST No. 712
FIGURE 4A.2-2

REVISION 0
JULY 1982

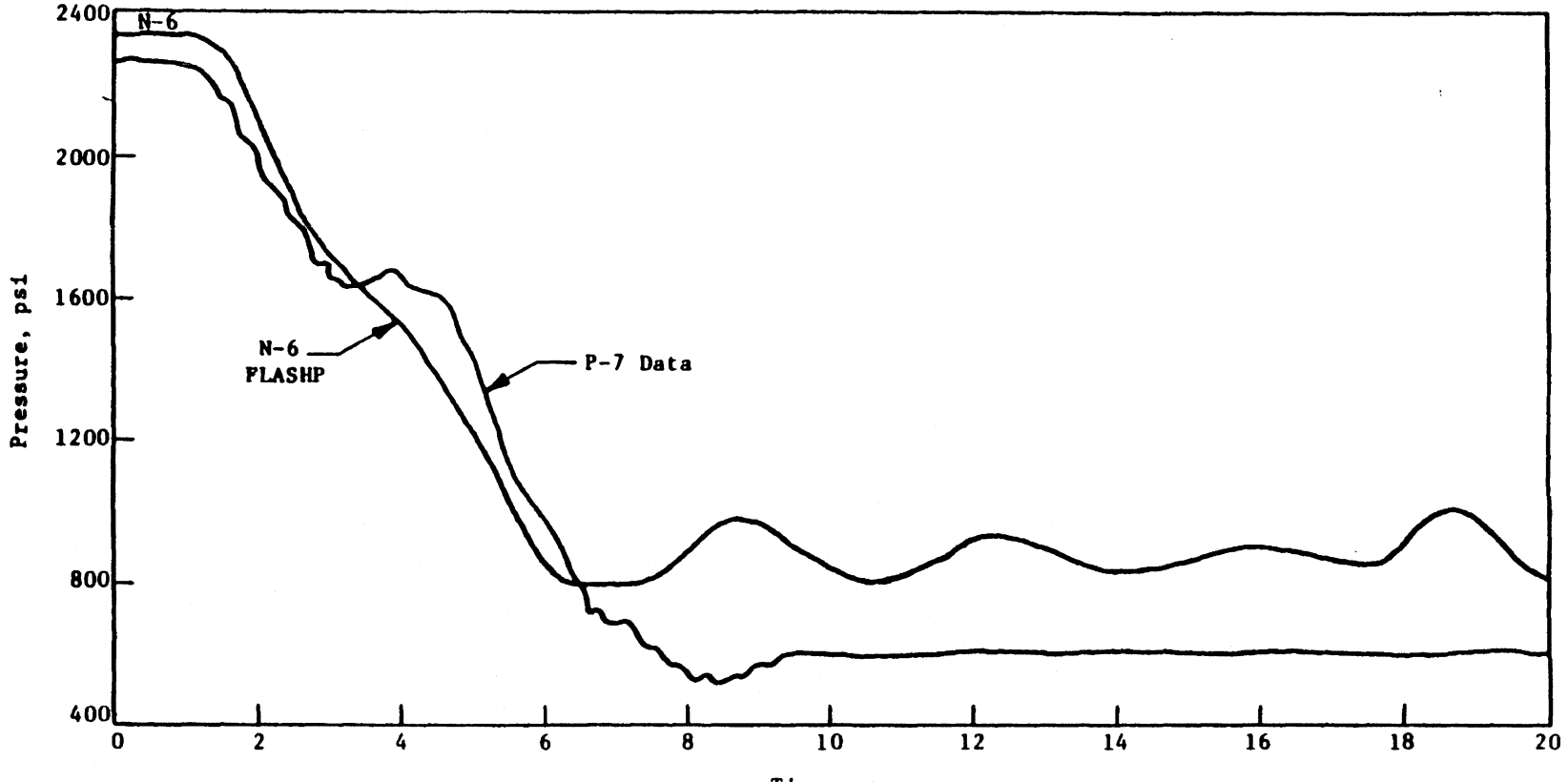

DAVIS-BESSE NUCLEAR POWER STATION
TEST No. 712, BOTTOM OF VESSEL
FIGURE 4A.2-3

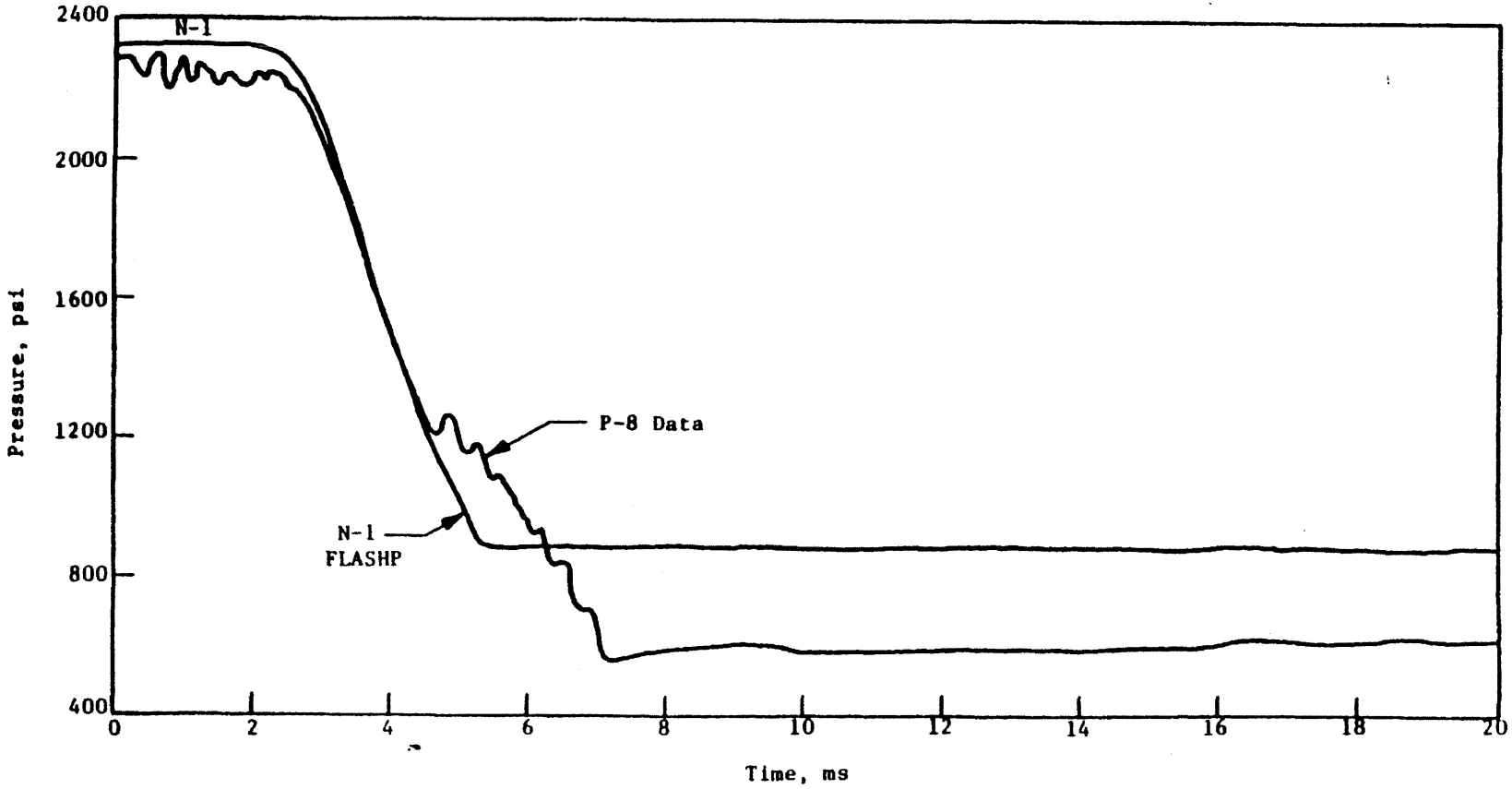

DAVIS-BESSE NUCLEAR POWER STATION
TEST No. 712, TOP OF VESSEL
FIGURE 4A.2-4

REVISION 0
JULY 1982

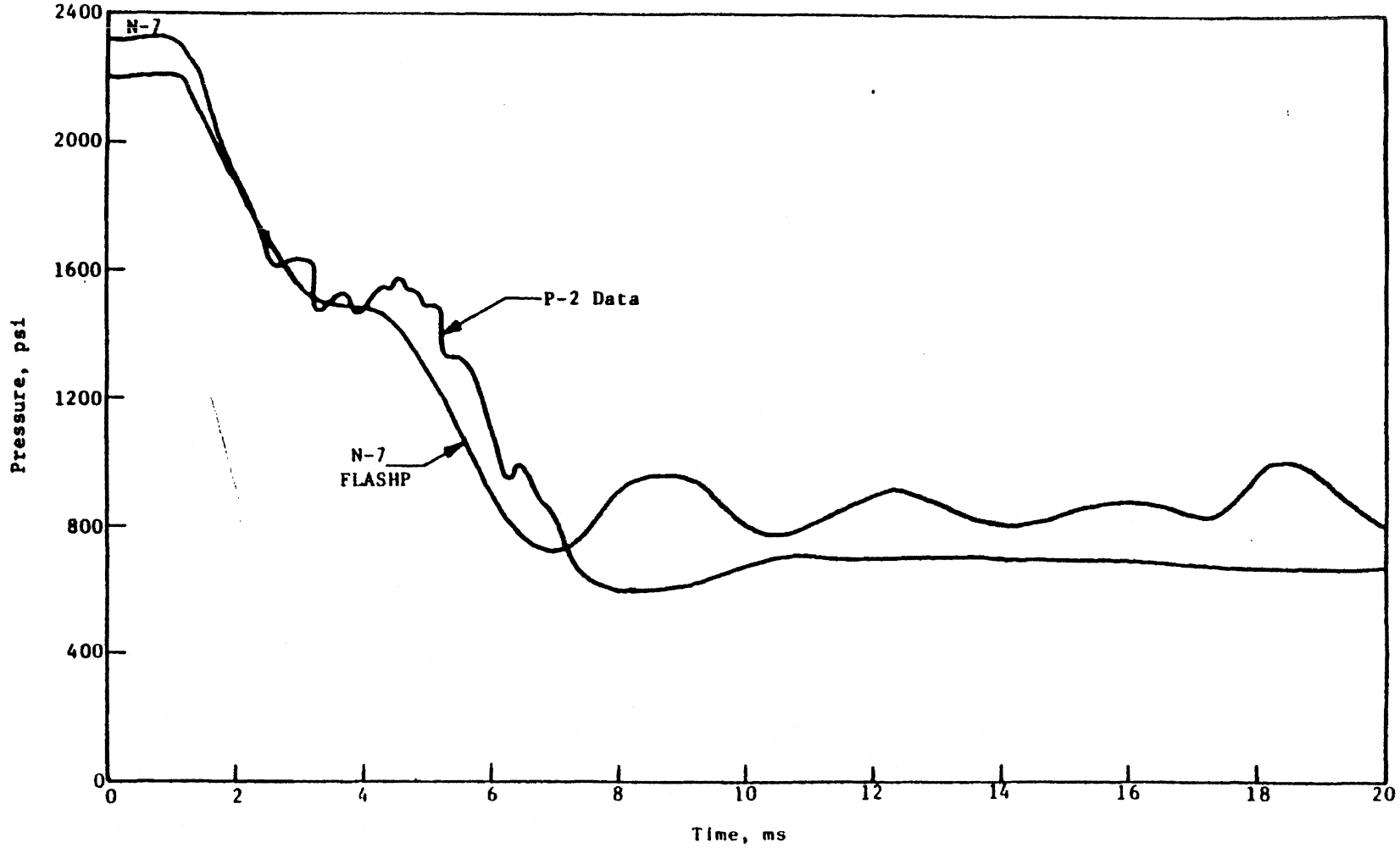

DAVIS-BESSE NUCLEAR POWER STATION
TEST No. 712, BOTTOM OF ANNULUS
FIGURE 4A.2-5

REVISION 0

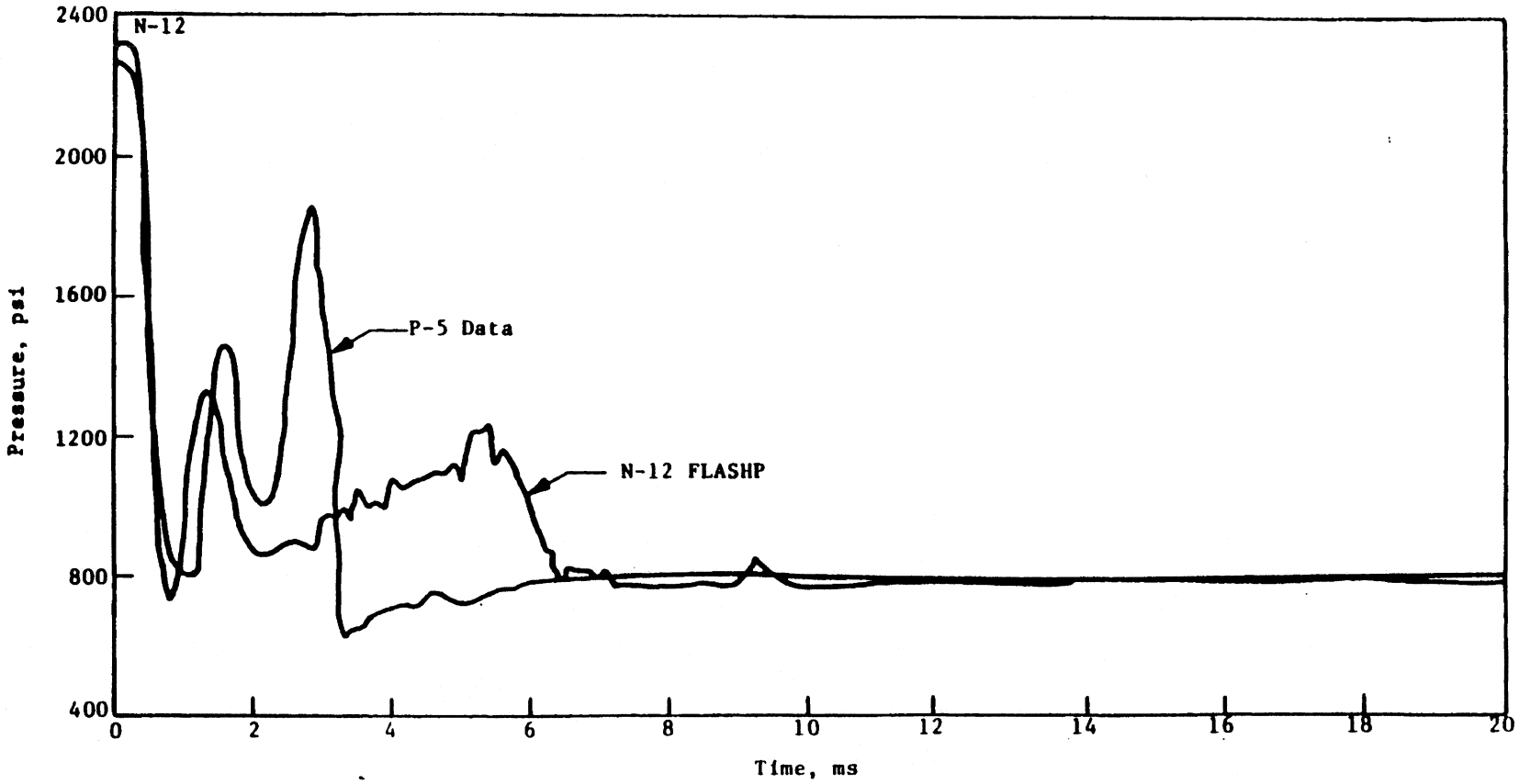

DAVIS-BESSE NUCLEAR POWER STATION
TEST No. 712, BREAK NOZZLE
FIGURE 4A.2-6

REVISION 0
JULY 1982

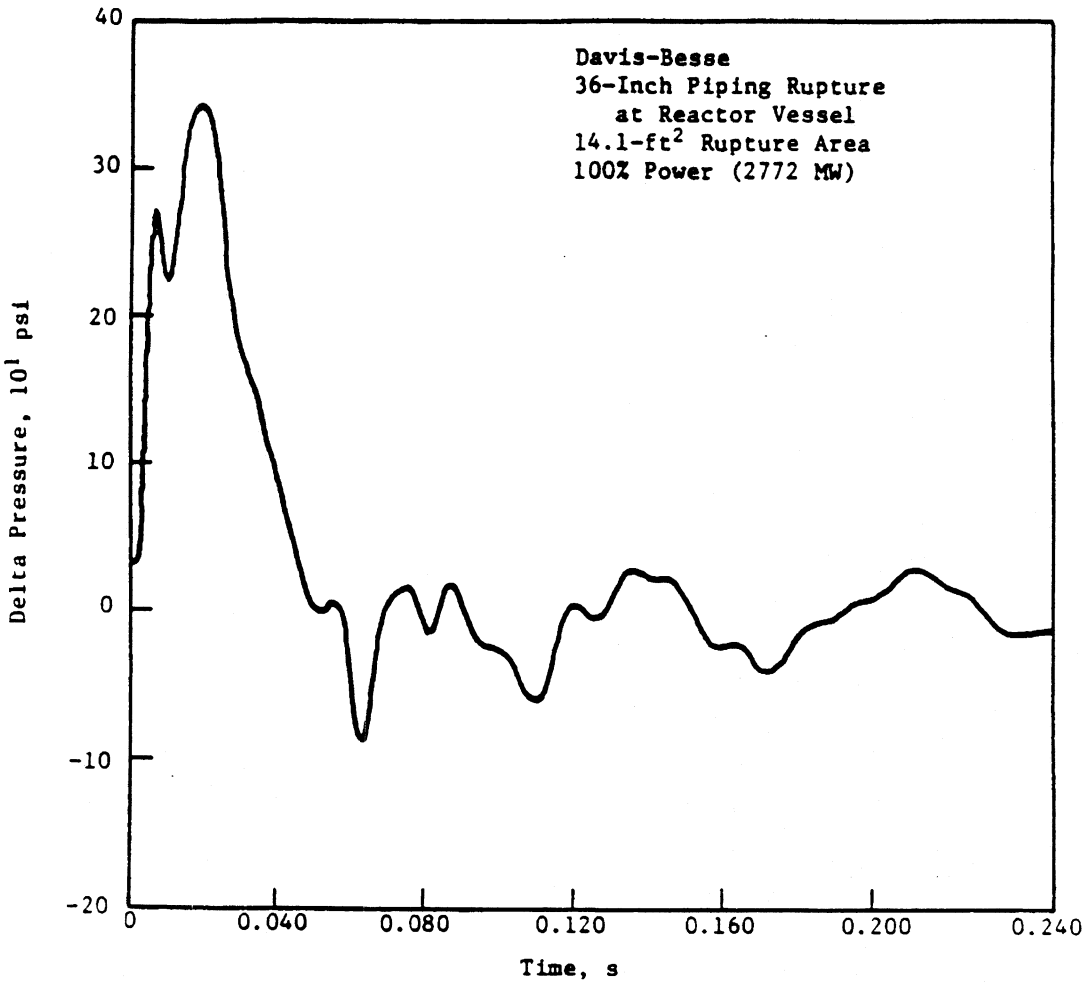

PRESSURE GRADIENT TIME HISTORY FOR CORE SUPPORT SHIELD

FIGURE 4A.2-7

REVISION 0
JULY 1982

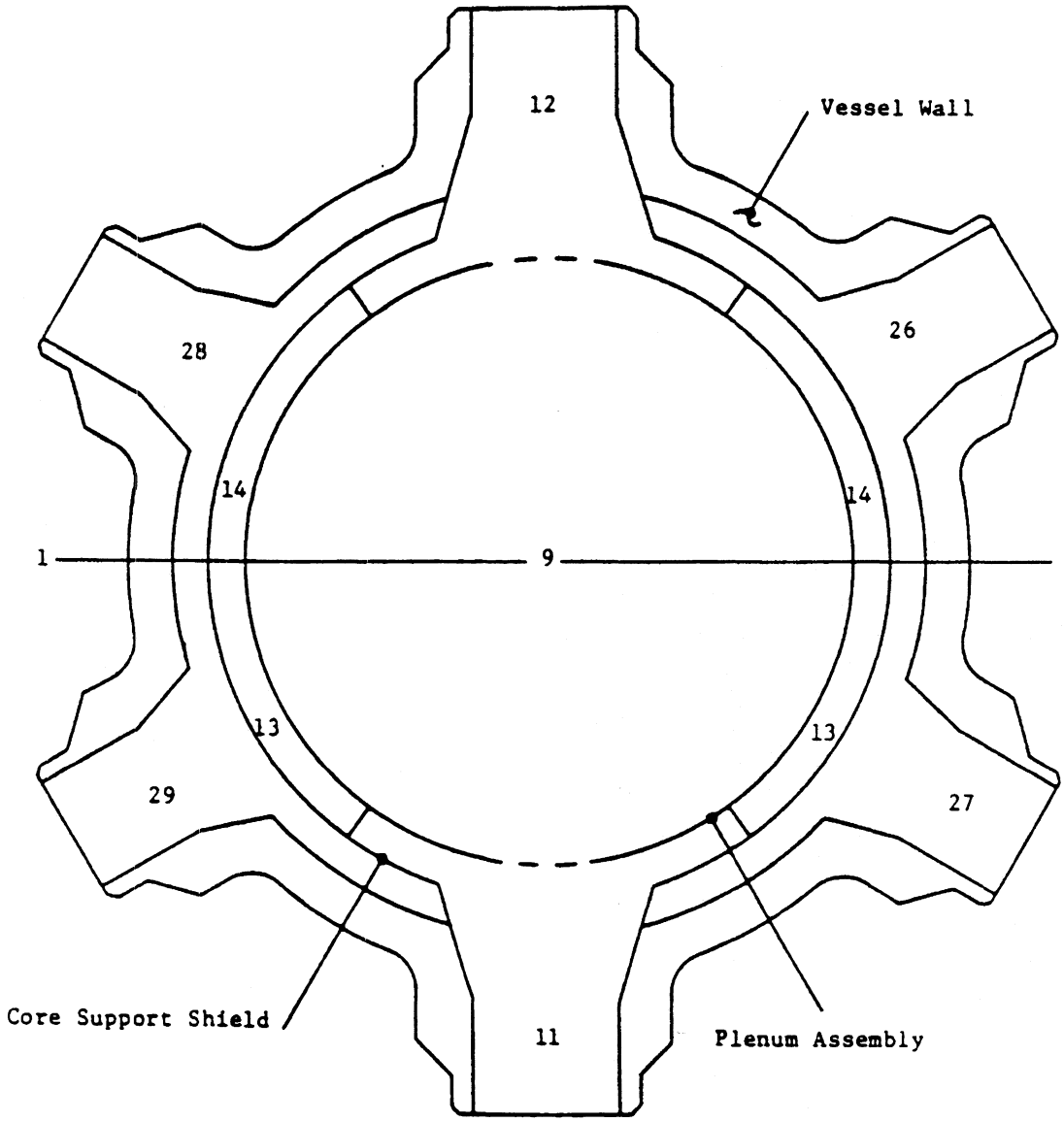

DAVIS-BESSE NUCLEAR POWER STATION
NOZZLE CONTROL VOLUME ARRANGEMENT
FIGURE 4A.2-8

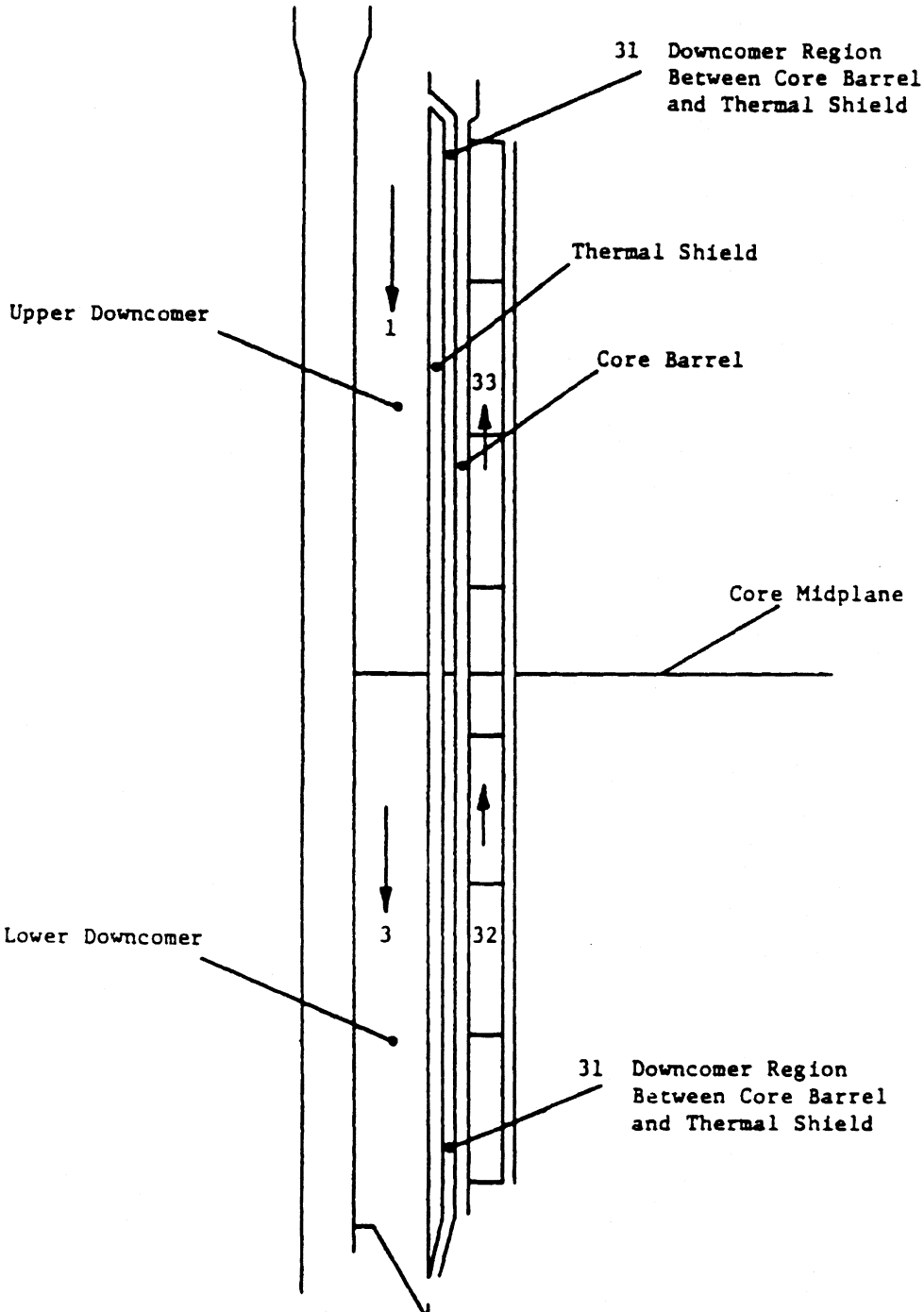

REACTOR VESSEL CONTROL VOLUME ARRANGEMENT
(BLOWDOWN SIDE)

FIGURE 4A.2-9

REVISION 0
JULY 1982

Reactor Vessel Node Arrangement
(Side Opposite Blowdown)

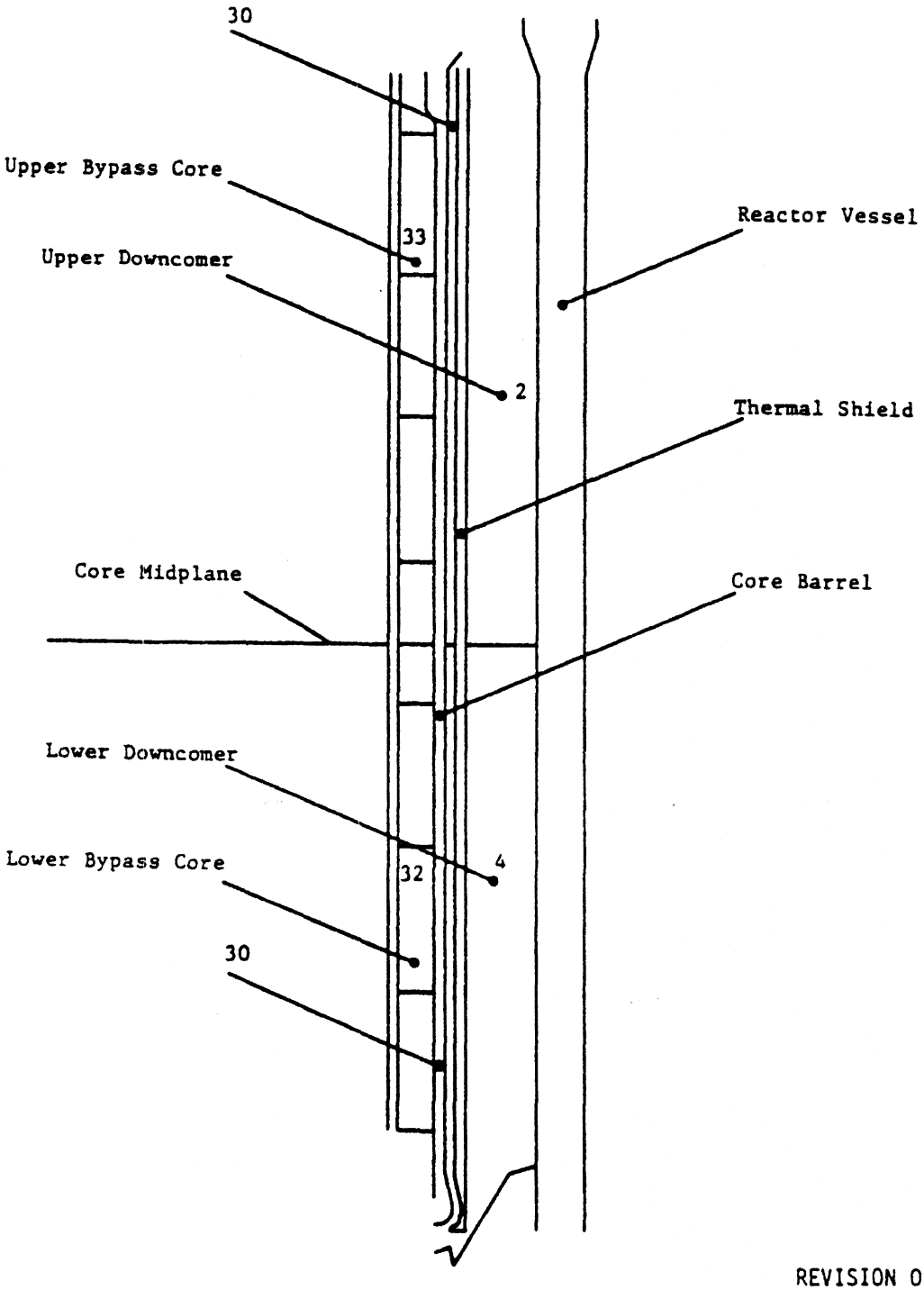

FIGURE 4A.2-10

REVISION 0
JULY 1982

FORCE ON CORE DURING LOCA

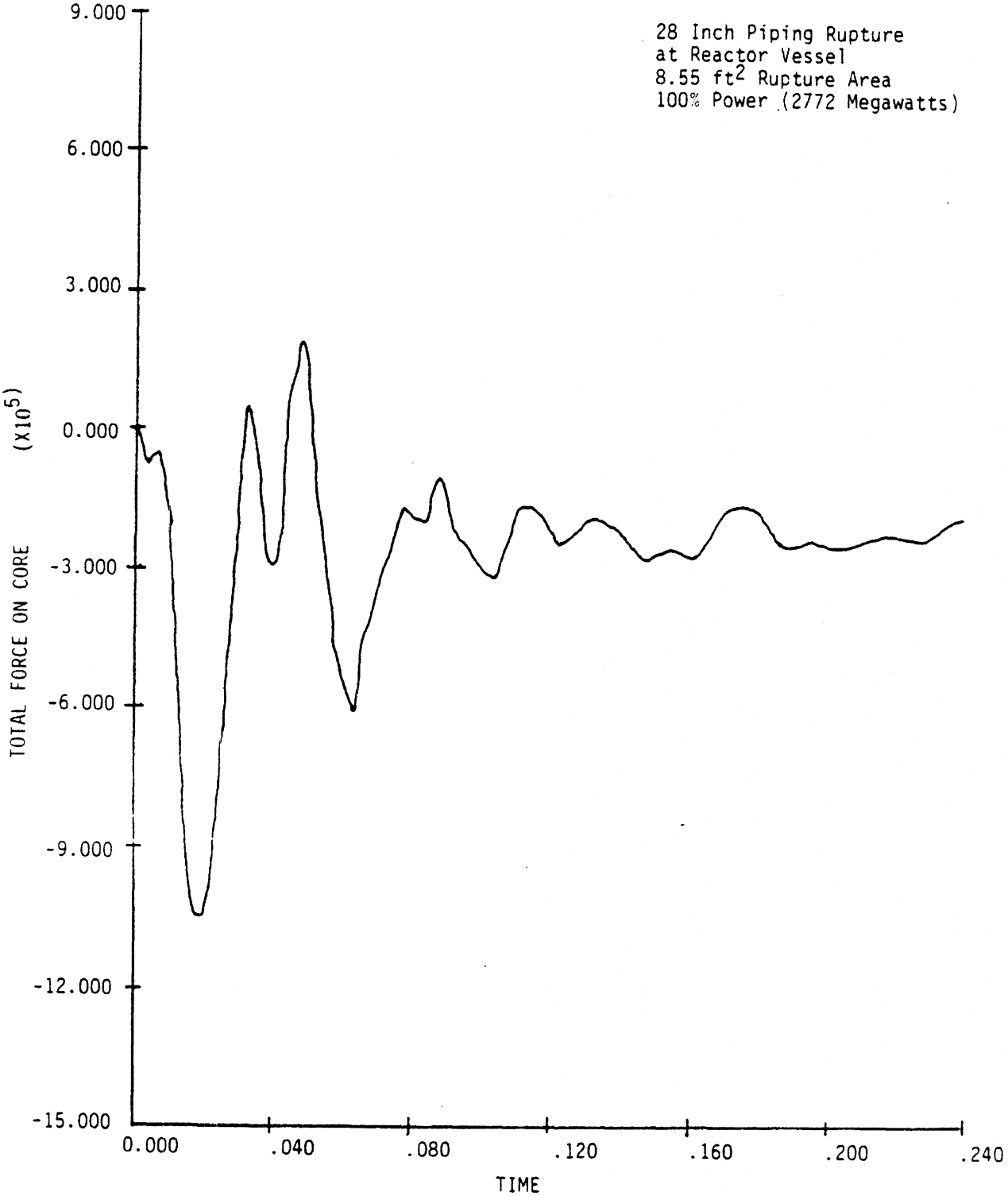

FIGURE 4A.2-11

REVISION 0
JULY 1982

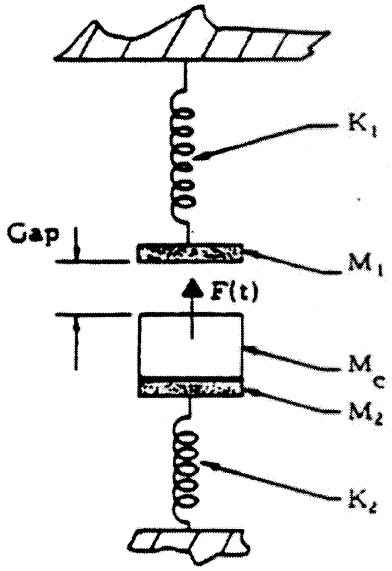

K_1 = spring rate of upper grid - plenum cover assembly.

M_1 = mass of upper grid - plenum cover assembly.

K_2 = spring rate of lower grid assembly.

M_2 = mass of lower grid assembly.

M_c = core mass.

$F(t)$ = LOCA force acting on core = $\Delta P \times$ area + F_{shear}.

DAVIS-BESSE NUCLEAR POWER STATION
CORE BOUNCE MODEL FOR PNAME ANALYSIS OF BAW 10008

FIGURE 4A.2-12

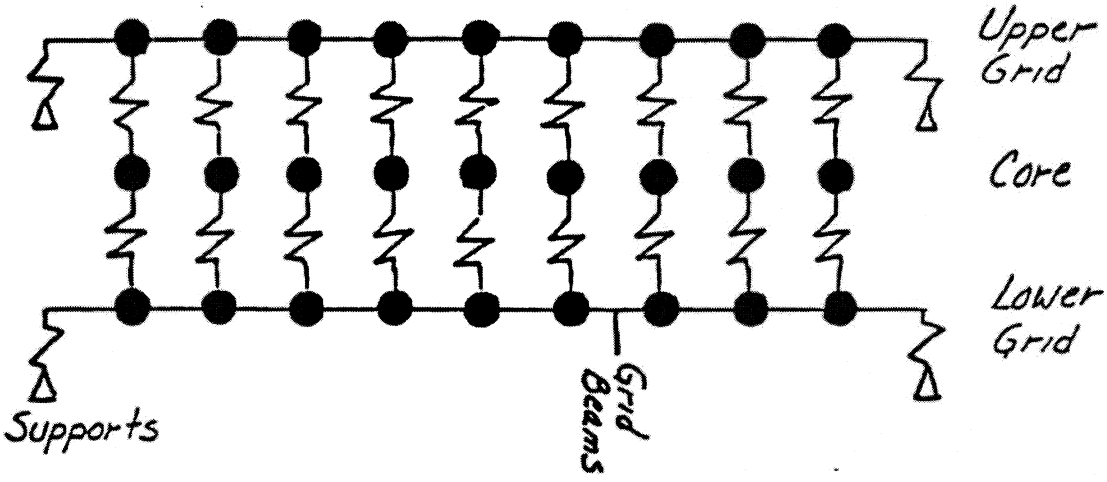

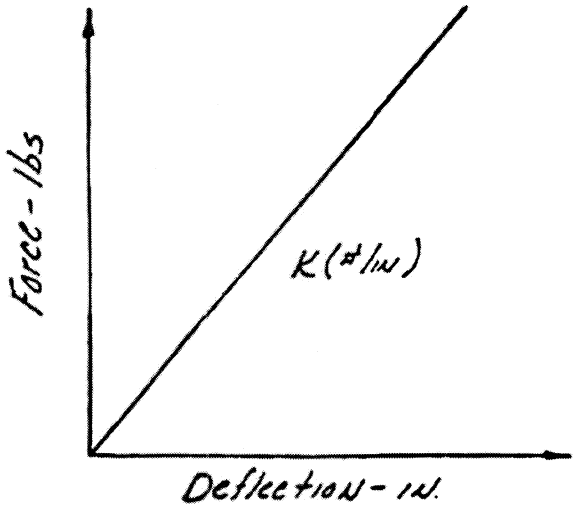

Lower Grid - Core Spring

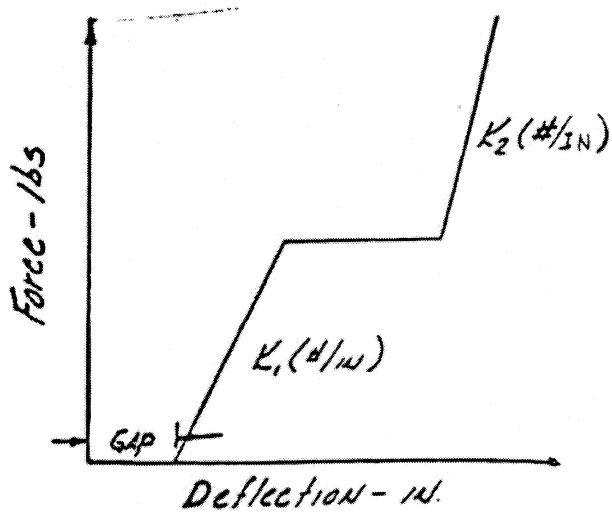

Upper Grid - Core Spring

DAVIS-BESSE NUCLEAR POWER STATION
CORE BOUNCE MODEL FOR STARS ANALYSIS
FOR DAVIS-BESSE 1
FIGURE 4A.2-13

REVISION 0
JULY 1982

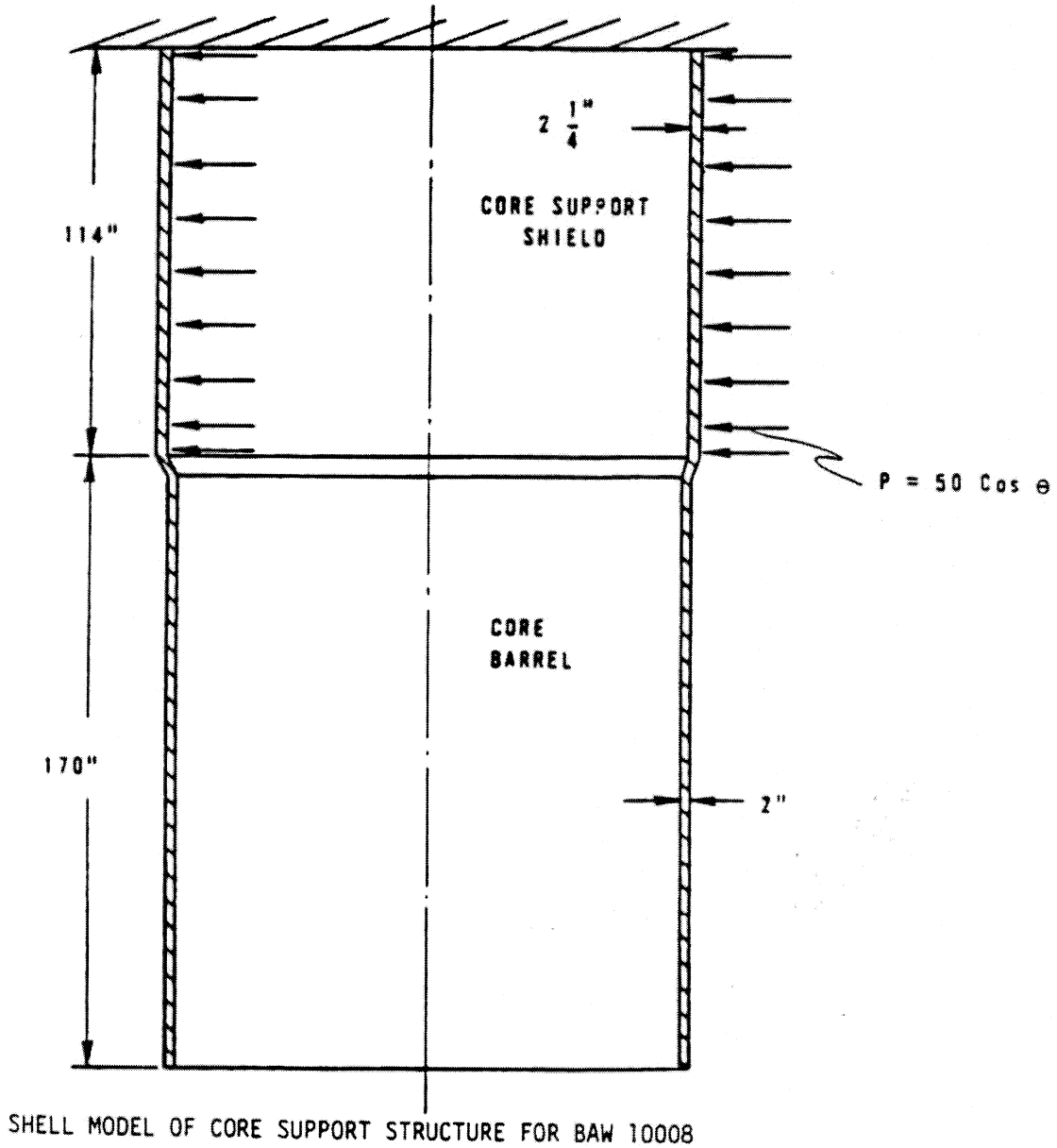

SHELL MODEL OF CORE SUPPORT STRUCTURE FOR BAW 10008

FIGURE 4A.3-1

REVISION 0
JULY 1982

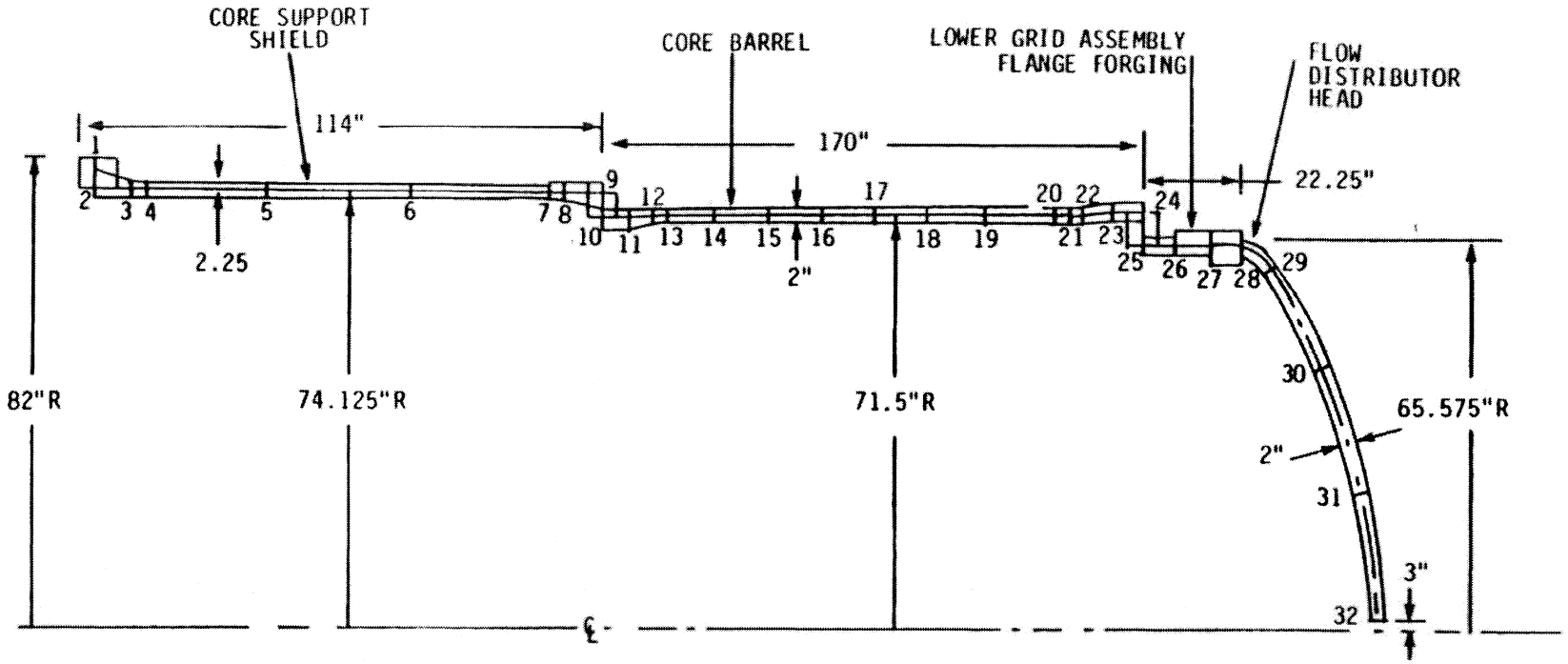

DAVIS-BESSE NUCLEAR POWER STATION
GENSH3 MODEL OF CORE SUPPORT
STRUCTURE FOR DAVIS-BESSE 1
FIGURE 4A.3-2

REVISION 0
JULY 1982

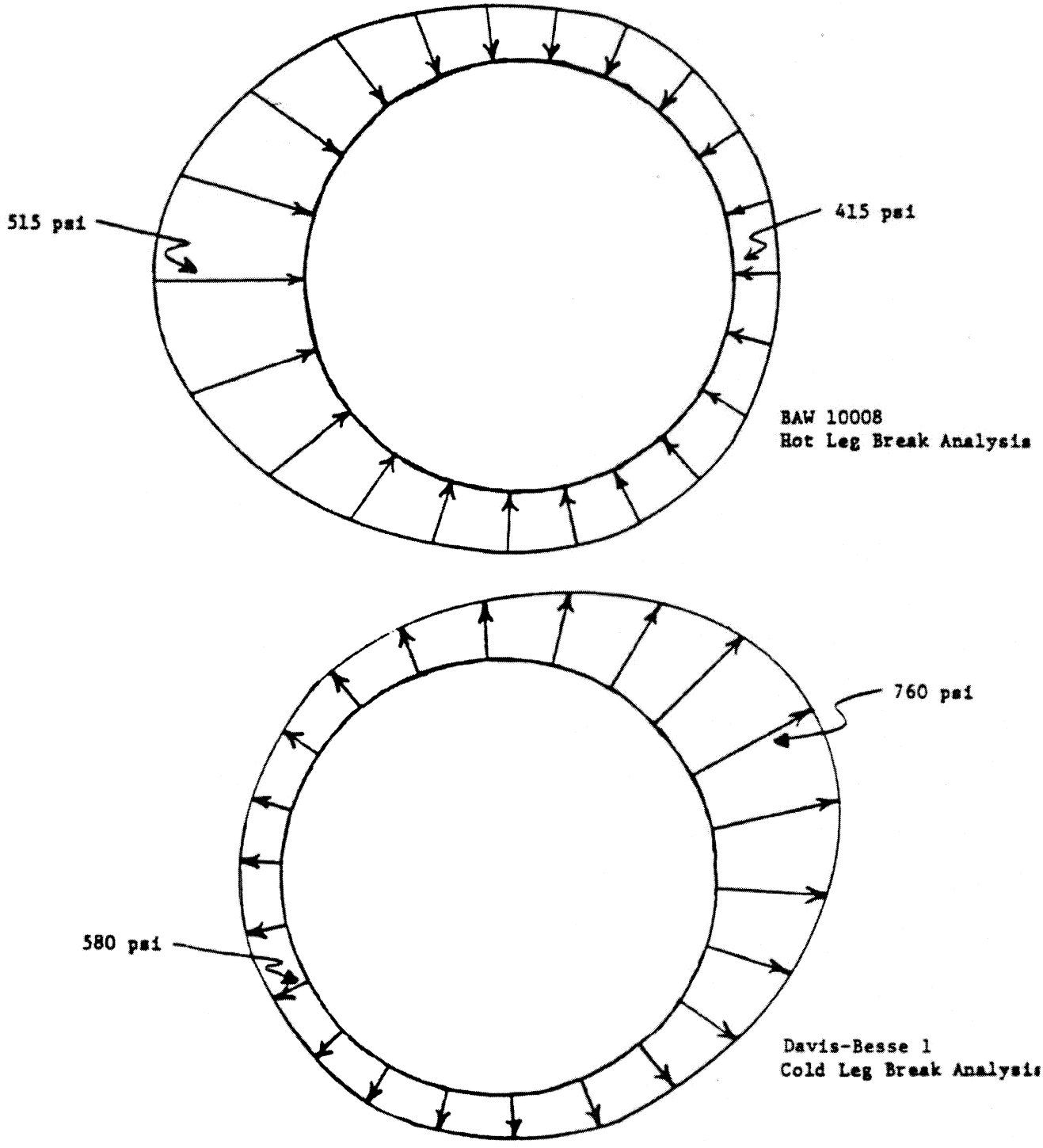

DAVIS BESSE NUCLEAR POWER STATION
COMPARISON OF LOCA PRESSURE ON CORE SUPPORT STRUCTURE FOR BAW 10008 AND DAVIS BESSE 1
FIGURE 4A.3-3

REVISION 0
JULY 1982

ANP-3257, Rev. 0
March 2014
Doc. ID 103-3257-000

DAVIS-BESSE NUCLEAR POWER STATION
UNIT 1, CYCLE 19 – RELOAD REPORT

AREVA NP Inc.
P.O. Box 10935
Lynchburg, Virginia 24506-0935

CONTENTS

LIST OF TABLES

LIST OF FIGURES

1.0 INTRODUCTION AND SUMMARY

The analyses described in this report justify cycle 19 operation of the Davis-Besse Nuclear Power Station Unit 1 at a rated thermal power (RTP) of 2817 MWt. All analytical techniques and design bases utilized in the analyses summarized in this report have been approved by the Nuclear Regulatory Commission (NRC) for the intended application. These methodologies, described in BAW-10179P-A, Rev. 8, "Safety Criteria and Methodology for Acceptable Cycle Reload Analyses," (Reference 1) and subsequently approved documents, represent no departure from methods of evaluation approved for Davis-Besse application.

The current RTP for Davis-Besse Unit 1 is 2817 MWt, following a measurement uncertainty recovery (MUR) power uprate from an RTP of 2772 MWt in cycle 16. All cycle 18 and cycle 19 EFPDs in this report are based on an RTP of 2817 MWt. Cycle 19 reactor and fuel parameters related to full power capability are summarized in this report and compared to those for cycle 18. The radiological dose consequences, system responses for non loss-of-coolant accident (LOCA) analyses, 10 CFR 50.46 LOCA analyses, and departure from nucleate boiling (DNB) analyses of Davis-Besse Updated Safety Analysis Report (USAR, Reference 2) Chapter 15 accidents have been reviewed for cycle 19 operation. In all cases, the initial conditions of the transients in cycle 19 are bounded by the initial conditions of previous analyses or by the Mark-B-HTP first-of-a-kind analyses.

The original Once-Through Steam Generators (OTSGs) were replaced in RFO18. The impact of the new Replacement Once-Through Steam Generators (ROTSGs) has been evaluated, and the analyses and results presented in the subsequent sections of this reload report, including the COLR figures and tables for cycle 19, include impact of the ROTSGs.

The cycle 19 design incorporates an end-of-cycle (EOC) hot full power (HFP) extension maneuver that reduces the moderator average temperature (T_{avg}) by a maximum of 12°F (analyzed, including uncertainty). The effects of the EOC T_{avg} reduction on the reactor coolant system (RCS) structural, RCS operation, core mechanical (fuel), radiological dose consequences, nuclear (design-peaking), and thermal-hydraulic parameters, as well as any potential effects and/or consequences on LOCA and non-LOCA safety analyses, were evaluated and found to be acceptable. The analyses also verified that the operational maneuver at EOC is bounded by the safety analyses assumptions and will be accommodated by the core protective and operating limits. The EOC T_{avg} reduction has been analyzed for the ROTSGs and is acceptable for use in extending hot full power operation.

Cycle 19 includes a full core of the Mark-B-HTP fuel assemblies. The Mark-B-HTP fuel assembly includes the following design features: the FUELGUARD™ lower end fitting, the M5® HTP intermediate spacer grids, a six-leaf holddown spring that optimizes the holddown load in order to reduce the anticipated magnitude of fuel assembly bow and twist, and the MONOBLOC™ instrument tube, which is a single-piece instrument tube with a variable inner diameter for incore instrumentation guidance.

Four fuel assemblies being shuffled from the cycle 18 core to the cycle 19 core contain a total of six (6) stainless steel rods (SSRs). All four fuel assemblies had fuel baffle rod wear observed during the fuel inspection during RFO18. Information about these four fuel assemblies and the SSRs in them is shown in the table below.

Assembly ID	Cycle 19 Batch ID	Cycle 18 Core Location	Cycle 19 Core Location	Observed Damage	# SSRs / Rod Locations[1]
UDDA54	20D	M14	F13	Baffle rod wear	2 / S15 & R15
UDDA55	20D	P11	O06	Baffle rod wear	1 / A1
UDDA59	20D	B11	C06	Baffle rod wear	1 / S1
UDDA57	20D	B05	C10	Baffle rod wear	2 / S15 & S14

[1] Rod locations are consistent with manufacturing coordinates

The effects of the SSRs on nuclear, thermal-hydraulic, mechanical, thermal design, LOCA and non-LOCA safety, and maneuvering analyses have been evaluated using NRC approved methodologies and the guidelines prescribed in Reference 15. All design criteria are met.

The Technical Specifications have been reviewed and verified for cycle 19. The Core Operating Limits Report (COLR) figures and tables referenced by the Technical Specifications are provided in Section 8.0.

2.0 OPERATING HISTORY

The reference cycle for the nuclear and thermal-hydraulic analyses of Davis-Besse Unit 1 is cycle 18 (Reference 3), which achieved criticality on June 11, 2012. Full power was reached on June 15, 2012.

During cycle 18 operation, no operating anomalies have occurred that would adversely affect fuel performance during cycle 19. Cycle 19 has a licensed length of 700 effective full power days (EFPD) at 2817 MWt based on cycle 18 operation of 578 +15/-15 EFPD at 2817 MWt. The cycle 19 design includes an APSR pull, end-of-cycle (EOC) T_{avg} reduction, control rod group (CRG) 7 withdrawal to 97%WD, and power coastdown.

3.0 GENERAL DESCRIPTION

The cycle 19 core consists of 177 fuel assemblies (FAs), each of which is a 15x15 array normally containing 208 fuel rods, 16 control rod guide tubes, and one incore instrument guide tube. The fuel consists of dished-end cylindrical pellets of uranium dioxide. The batch 20 and batch 21 fuel include a chamfer on the fuel pellet. All of the assemblies are clad in M5® cladding. In batch 21, 1488 rods contain UO_2/Gd_2O_3 pellets in the central 123.20 inches of the fuel stack. All batch 21 fuel assemblies include 32 radially zone-loaded fuel rods containing reduced ^{235}U enrichments. Implementation of radially zone-loaded enrichments within the fuel assembly results in a reduction in the radial peak pin power relative to an assembly with a uniform enrichment loading. The nominal fuel loadings for all fuel assemblies in cycle 19 are listed in Table 3-1. The undensified nominal active fuel lengths, theoretical densities, fuel and fuel rod dimensions, and other related fuel parameters are provided in Table 4-1.

Figure 3-1 is the core loading diagram for Davis-Besse Unit 1, cycle 19. Batch 21 fuel contains gadolinia (Gd_2O_3) and axial blankets. The initial enrichments in wt% ^{235}U and gadolinia concentration in wt% Gd_2O_3 of all of the cycle 19 batches are listed in Table 3-1. All batch 21 fuel rods except those bearing gadolinia have an upper and lower 6.05 inch blanket of 3.90 wt% ^{235}U pellets, which is higher than in previous batches. Those fuel rods that contain gadolinia as a burnable absorber in a matrix of urania (UO_2), i.e. “Gd rods,” have an upper and lower 9.90 inch blanket of 2.50 wt% ^{235}U pellets.

Four batch 18A3 assemblies, 1 batch 18A4 assembly, 8 batch 18B assemblies, 20 batch 18C2 assemblies, 12 batch 19A assemblies, and 36 batch 19C assemblies will be discharged at the end of cycle 18. The remaining batch 19C assemblies (designated batch 19C2), along with the batch 19B, 19D, 20A, 20B, 20C and 20D fuel assemblies will be shuffled to their cycle 19 locations. The number of SSRs in cycle 19 is six (6) rods, all of which are in a total of four (4) batch 20D assemblies; two assemblies have two SSRs each and two assemblies have one SSR each as noted in Figure 3-1. One batch 18A5 assembly is a reinsert from cycle 16 and will be located in the center location, H08. All of the batch 19B, 19C2 and 19D assemblies are on the periphery for cycle 19.

The 80 Mark-B-HTP assemblies in the feed batch consist of 16 batch 21A, 24 batch 21B, 28 batch 21C, 4 batch 21D and 8 batch 21E assemblies. The feed batch will be loaded in a symmetric checkerboard and ring pattern throughout the core. The cycle 19 shuffle scheme is a low leakage core loading. The cycle 19 design minimizes the number of same-quadrant shuffles into control rod positions to reduce the potential for incomplete rod insertion and excessive control rod assembly drag. The reduction in same-quadrant shuffles results in several cross-core shuffles despite past practices to avoid such shuffles. Nevertheless, the design maintains the number of cross-core shuffles as low as practical to reduce the potential for quadrant power tilt amplification. Figure 3-2 is a quarter core map showing each assembly’s burnup at the beginning of cycle 19 and its initial base enrichment.

Cycle 19 will be operated in a feed-and-bleed mode. Fifty-three full length Ag-In-Cd control rod

assemblies, 1488 Gd rods in the feed batch, and soluble boron are used to control the core reactivity. In addition to the full-length control rods, eight partial length Inconel-600 axial power shaping rods (gray APSRs) are provided for additional control of the axial power distribution. The core locations and the rod group designations of the 61 control rods in cycles 18 and 19 are the same. Figure 3-3 shows the distribution of the Gd rods in the fresh fuel. The number for Gd rods per fuel assembly and initial Gd_2O_3 concentrations are also shown in Figure 3-3.

Table 3-1 Fuel Assembly Composition Data for Davis-Besse, Cycle 19

Fuel Batch Number	Number of FAs	Base Enrichment(1) (wt% ^{235}U)	Zone-Loaded Enrichment(1,2) (wt% ^{235}U)	Gadolinia Rods(1) No. x wt% Gd_2O_3	Carrier Enrichment(1) (wt% ^{235}U)	Nominal Loading KgU
18A5	1	4.59	----	12 x 4.0 8 x 8.0	3.67 2.75	486.83
19B	4	4.81	----	12 x 4.0	3.85	488.54
19C2	8	4.81	----	12 x 4.0 8 x 8.0	3.85 2.89	486.83
19D	16	4.81	----	8 x 4.0	3.85	488.97
20A	32	3.88	3.58	12 x 4.0 8 x 8.0	2.86 2.14	485.42
20B	16	4.52	4.22	12 x 4.0	3.37	487.13
20C	4	4.52	4.22	4 x 4.0 12 x 6.0	3.37 2.95	486.06
20D	16	4.87	4.57	12 x 4.0	3.65	487.13
21A	16	4.30	4.00	12 x 4.0 8 x 8.0	3.20 2.40	485.42
21B	24	4.70	4.40	12 x6.0 8 x 8.0	3.08 2.64	484.79
21C	28	4.95	4.65	16 x 4.0	3.72	486.70
21D	4	4.95	4.65	20 x 4.0	3.72	486.27
21E	8	4.95	4.65	12 x 4.0 8 x 8.0	3.72 2.79	485.42

(1) Batch 18, 19 and 20 Uranium fuel rods have 6.050 inch top and bottom blankets of 2.50 wt% ^{235}U. Batch 21 Uranium fuel rods have 6.050 inch top and bottom blankets of 3.90 wt% ^{235}U. Batch 18, 19, 20 and 21 gadolinia (Gd_2O_3) rods have 9.90 inch top and bottom blankets of 2.50 wt% ^{235}U.

(2)Zone-loaded enrichment refers to the enrichment of the three rods in each assembly corner, four rods around the instrument tube and four rods near the control rod guide tubes in each quadrant of the fuel assembly.

Figure 3-1 Davis-Besse Cycle 19 Core Loading Diagram

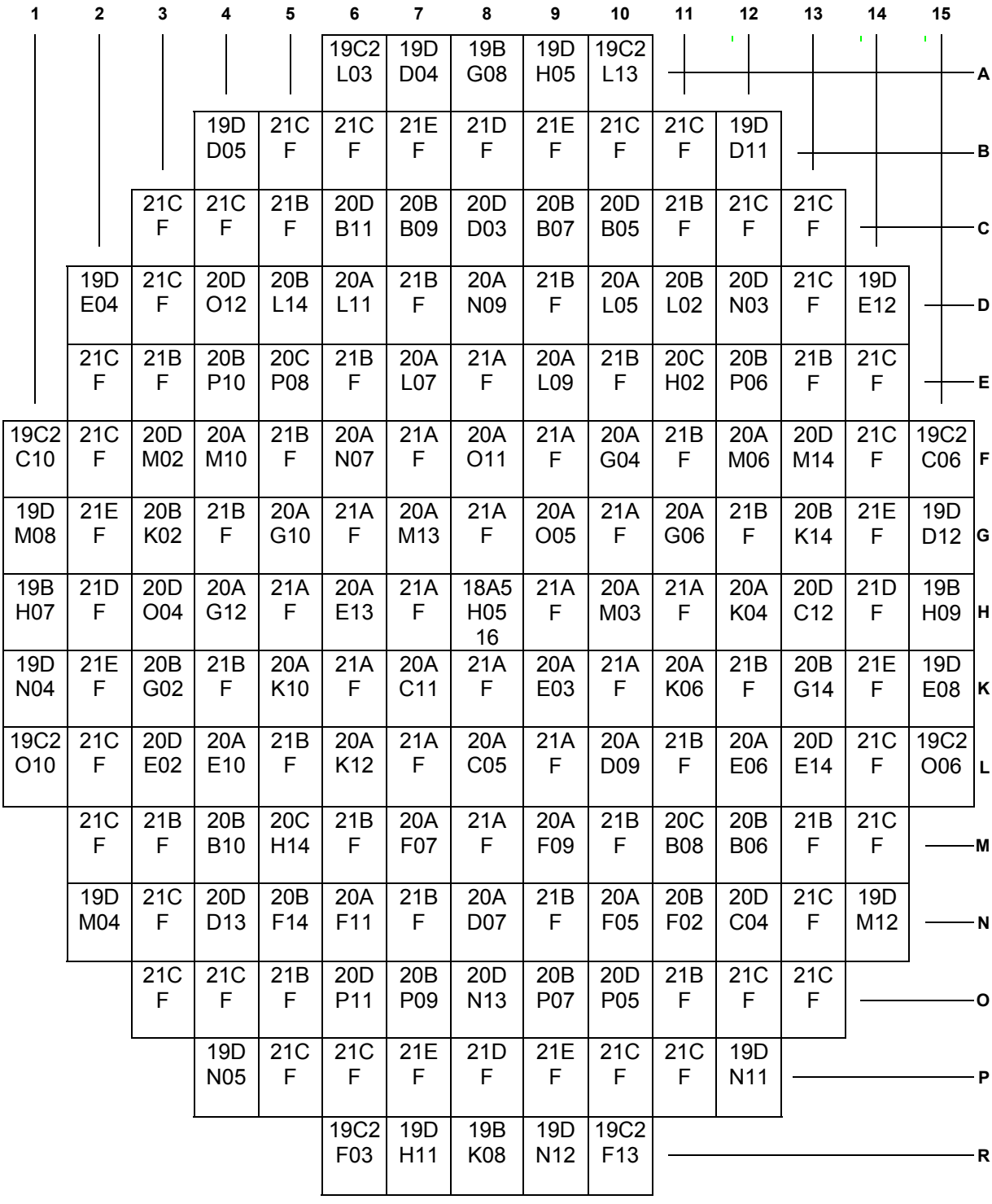

Key

xxxx yyy zz

Batch ID
Previous Cycle Location
Reinsert Cycle Number

Notes:
--"F" denotes fresh fuel assembly.
--FAs in locations C10 and F13 each have two SSRs;
--FAs in locations C06 and O06 each have one SSR.

Figure 3-2 Davis-Besse Cycle 19 Enrichment and BOC Burnup Distribution

	8	9	10	11	12	13	14	15
H	4.59 30,118	4.30 0	3.88 22,448	4.30 0	3.88 22,988	4.87 20,841	4.95 0	4.81 43,836
K	4.30 0	3.88 22,494	4.30 0	3.88 23,306	4.70 0	4.52 22,569	4.95 0	4.81 43,570
L	3.88 22,448	4.30 0	3.88 22,937	4.70 0	3.88 23,697	4.87 18,306	4.95 0	4.81 44,296
M	4.30 0	3.88 23,161	4.70 0	4.52 22,075	4.52 21,492	4.70 0	4.95 0	
N	3.88 22,988	4.70 0	3.88 23,659	4.52 21,387	4.87 20,733	4.95 0	4.81 42,134	
O	4.87 20,841	4.52 22,533	4.87 18,270	4.70 0	4.95 0	4.95 0		
P	4.95 0	4.95 0	4.95 0	4.95 0	4.81 42,136			
R	4.81 43,836	4.81 42,958	4.81 44,269					

Key

x.xx xx,xxx

Initial Base Enrichment of Central Region (not weighted for Gd_2O_3 rods or zone-loaded rods)
Burnup, MWd/mtU off 578 EFPD (nominal) cycle 18

Figure 3-3 Davis-Besse Cycle 19 Gadolinia Concentrations in Fresh Assemblies

	8	9	10	11	12	13	14	15
H		12x4.0 8x8.0		12x4.0 8x8.0			20x4.0	
K	12x4.0 8x8.0		12x4.0 8x8.0		12x6.0 8x8.0		12x4.0 8x8.0	
L		12x4.0 8x8.0		12x6.0 8x8.0			16x4.0	
M	12x4.0 8x8.0		12x6.0 8x8.0			12x6.0 8x8.0	16x4.0	
N		12x6.0 8x8.0				16x4.0		
O				12x6.0 8x8.0	16x4.0	16x4.0		
P	20x4.0	12x4.0 8x8.0	16x4.0	16x4.0				
R								

Key

NxZ.Z	Number of Gd Rods @ wt% Gd_2O_3

4.0 FUEL SYSTEM DESIGN

The Mark-B-HTP design includes M5® fuel rod cladding and guide tubes, the M5® HTP grid design that provides improved mechanical performance and has increased resistance to flow induced fuel rod fretting failures relative to earlier Mark-B designs, and the FUELGUARD™ debris resistant lower end fitting which increases the debris resistance of the Mark-B-HTP fuel assembly. The Mark-B-HTP fuel assembly design also features a six-leaf holddown spring which reduces susceptibility to fuel assembly bow, the MONOBLOC™ instrument tube, fuel rod bar coding, and lead-in corners on the upper and lower end fittings. The batch 21 fuel will make use of Upset Shape Welded fuel rods similar to batch 20. Design details of the Mark-B-HTP fuel assembly are provided in Reference 19. The batch 21 Mark-B-HTP fuel assembly design does not include any significantly different design features than used for batch 20.

4.1 Fuel Assembly Mechanical Design

Table 4-1 lists the types of fuel assemblies and pertinent fuel parameters for Davis-Besse cycle 19. Batches 18, 19, 20 and 21 incorporate the Mark-B-HTP fuel assembly design as described above.

Mark-B-HTP fuel assemblies contain gadolinia (Gd_2O_3) fuel rods in select locations of the 15x15 fuel rod array. The Gd_2O_3 rods are designed similar to the uranium (UO_2) fuel rods and are pressurized and upset shape welded. One difference between the rod types for batch 21 compared to the other batches in cycle 19 is that the Gd_2O_3 rods contain axial blanket pellets with 2.50 wt% ^{235}U enrichment, while the UO_2 rods contain axial blanket pellets with 3.90 wt% ^{235}U enrichment. The other batches in cycle 19 use 2.5 wt% ^{235}U enrichment in both the Gd_2O_3 and UO_2 rods.

Eight gray axial power shaping rod assemblies (APSRAs) and 53 silver-indium-cadmium (Ag-In-Cd) control rod assemblies (CRAs) will be used in cycle 19. All of the CRAs are of the extended life design (ELCRA). No BPRAs will be used in cycle 19.

4.2 Fuel Rod Design

The fuel rod design and mechanical evaluation are discussed in this section.

The Replacement Once-Through Steam Generators (ROTSGs) in cycle 19 have no impact on the results of the fuel rod thermal and mechanical analyses. The 12°F Tavg reduction fuel rod thermal-mechanical performance assessment remains valid for the ROTSGs. The plant and fuel parameters used in the analyses of record models and the power histories are not impacted by the ROTSGs.

All fuel assemblies in cycle 19 have B-HTP fuel rods which use M5® cladding. The fresh fuel design (batch 21) is the same as batch 20 except for the axial blanket enrichments noted above. Fuel rods in all cycle 19 batches have a 143.00 inch fuel stack.

The effects of six (6) SSRs have been analyzed and the cladding collapse, stress, strain, fatigue and oxide thickness have been determined to remain within their design limits.

4.2.1 Cladding Collapse

The computer code COPERNIC (Reference 18) is used to provide conservative values of cladding temperature and pin pressure to the computer code CROV (Reference 5), which determines whether or not cladding collapse is predicted during the cycle.

The fuel rod power histories were shown to be enveloped by the power history used in a previous B-HTP fuel rod creep collapse analysis. The fuel rod cladding creep collapse analysis for the B-HTP fuel rods determined that these rods have creep collapse lifetimes that exceed 65 GWd/mtU. The analysis applies to both the UO_2 and Gd_2O_3 rods. All cycle 19 resident fuel rods are resistant to creep collapse and will not reach a burnup of 65 GWd/mtU during cycle 19.

4.2.2 Cladding Stress

The stress parameters for the fuel rod designs are enveloped by conservative generic fuel rod stress analyses. For design evaluation, certain stress intensity limits for all Condition I and II events must be met. Limits are based on ASME criteria. Stress intensities are calculated in accordance with the ASME Code (Section III, Division I), which includes both normal and shear stress effects. These stress intensities are compared to S_m. The definition of S_m for M5® differs from that for Zircaloy-4 cladding, as described in the following discussion.

The methodology that governs the stress analysis of the cycle 19 resident M5® fuel rods is described in AREVA NP's advanced cladding topical report (Reference 6). The major differences in the stress analysis methodology for M5® cladding are described below:

S_m for the M5® cladding material is equal to two-thirds of the minimum yield strength in the hoop direction as a function of operating temperature. Note that the S_m for Zircaloy-4 is defined as equal to two-thirds of the minimum specified unirradiated yield strength of the material at the operating temperature (650 °F).

The stress intensity limit for primary general membrane stress intensity (P_m) is S_m in tension, and 1.5 S_m in compression. Note that the Zircaloy-4 primary general membrane stress intensities (P_m) shall not exceed S_m.

The remainder of the methodology is similar to the methodology for the Zircaloy-4 cladding material and is outlined as follows:

Local primary membrane stress intensities (P_l) shall not exceed 1.5 S_m. These include the contact stresses from the spacer grid stop and the fuel rod.

Primary membrane + bending stress intensities ($P_l + P_b$) shall not exceed 1.5 S_m.

Primary membrane + bending + secondary stress intensities ($P_l + P_b + Q$) shall not exceed 3.0 S_m.

where

P_m = General primary membrane stress intensity

P_l = Local primary membrane stress intensity

P_b = Primary bending stress intensity

Q = Secondary stress intensity

Stress intensity calculations combine stresses so that the resulting stress intensity is maximized.

The B-HTP fuel rod stress analysis report minimum margins for Normal Operation and Faulted conditions of 2% and 9%, respectively. The margins for the corresponding Gd_2O_3 fuel rods are the same as those for the UO_2 rods due to the similarity of the designs.

The following sources of conservatism were used in the stress analyses to ensure that all Condition I and II operating parameters were enveloped:

1. Low post-densification internal pressure, or as-built pre-pressure;
2. High system pressure;
3. High thermal gradient across the cladding;
4. Minimum specified cladding thickness.

4.2.3 Cladding Strain

The fuel design criteria of Reference 7 specify a limit of 1.0% transient circumferential strain on the cladding. Cladding transient strain linear heat rate (LHR) limits were generated for each of the fuel rod types in cycle 19 (B-HTP UO_2 and B-HTP Gd_2O_3). Operation within these LHR limits ensures that the fuel rod cladding will not exceed the 1.0% transient strain limit. Table 4-2 lists limits for the B-HTP UO_2 rods of batches to be operated in the cycle 19 core, and Table 4-3 lists limits for the B-HTP Gd_2O_3 rods.

4.2.4 Cladding Fatigue

Per Reference 7, the predicted total fatigue utilization factor must be less than or equal to 0.90 for the life of each fuel rod. The table below shows the maximum incore time for each batch at EOC 19 and the time limit resulting from the fatigue analysis. Results in the table show that all the fuel rods satisfy the cladding fatigue criterion for cycle 19.

Rod Design (Batch)	Maximum Incore Time	Fatigue Limit	Fatigue Factor at Limit
B-HTP (Batch 18)	< 10.0 years	10 years	0.218
B-HTP (Batch 19)	< 10.0 years	10 years	0.218
B-HTP (Batch 20)	< 10.0 years	10 years	0.218
B-HTP (Batch 21)	< 10.0 years	10 years	0.218

4.2.5 Cladding Oxide

Cladding waterside oxide thickness for AREVA NP fuel is limited to 100 microns. The approved fuel performance code COPERNIC (Reference 18) was used to qualify cladding corrosion. The COPERNIC model generates oxide predictions at each input time step and at each input axial node. Per the licensed methodology, the high burnup fuel rod for each batch in cycle 19 was evaluated for oxide using cycle 19 power histories to the maximum pin burnup for each batch. Acceptable oxide predictions were obtained for each batch.

4.3 Thermal Design

All fuel assemblies in the cycle 19 core are thermally similar. The fresh batch 21 fuel assemblies are of the Mark-B-HTP design. The axial blanket pellet ^{235}U enrichment in the UO_2 rods will be increased to 3.9 weight percent while the axial blanket pellet enrichment of the gadolinia fuel rods remains the same at 2.5 weight percent. The batch 21 Mark-B-HTP fuel rod has the same design as batch 20. Fuel performance for the Mark-B-HTP fuel was evaluated with COPERNIC (Reference 18); however, the LOCA initialization analysis continues to use the TACO3 (Reference 4) and GDTACO (Reference 8) fuel rod analysis codes. See Section 7.3 for discussion of the use of the TACO3 and GDTACO fuel rod analysis codes for LOCA initialization analysis. The impact of increased axial blanket pellet enrichment in the UO_2 rods has been evaluated in the fuel rod thermal analyses. Nominal undensified input parameters used in the analyses are presented in Table 4-1. Densification effects were accounted for in the COPERNIC code densification models.

The presence of six (6) SSRs in the cycle 19 core was considered in the thermal evaluation by analyzing the increase in local peaking and burnup. The nominal LHR for each batch is shown at rated thermal power of 2817 MWt. Cycle 19 core protection limits were based on LHR to centerline fuel melt (CFM) limits determined by the COPERNIC code. Table 4-4 lists the Linear Heat Rate to Melt (LHRTM) limits for the B-HTP UO_2 rods of all batches to be operated in the cycle 19 core, and Table 4-5 lists LHRTM limits for the B-HTP Gd_2O_3 rods for those same batches.

The maximum fuel rod burnup at EOC 19 for each batch is provided in Table 4-1. The fuel rod internal pressures were evaluated with COPERNIC for the highest burnup of each fuel batch, adjusted to account for cycle 18 shutdown flexibility. The predicted internal pressures for all cycle 19 fuel rods were evaluated with the approved fuel rod gas pressure criterion methodology described in Reference 9.

4.4 Spacer Grid Deformation

The structural integrity of the fuel assembly spacer grids under faulted conditions was evaluated based on leak-before-break (LBB) methodology described in Reference 10 and the latest NRC approved fuel assembly (FA) faulted methodology as described in Reference 11. LBB and FA faulted methodologies are consistent with AREVA NP LOCA evaluations for B&W-designed raised and lowered loop plants, which includes Davis-Besse. Application of the LBB and FA faulted methodologies confirmed that the requirement to maintain a coolable geometry is satisfied for all faulted loading cases and for all fuel assemblies in the core.

4.5 Material Compatibility

The compatibility of all possible fuel-cladding-coolant-assembly material interactions for all cycle 19 fuel assemblies was demonstrated to be acceptable (the fuel cladding material M5® is approved in the advanced cladding topical report per Reference 6).

4.6 Operating Experience

AREVA NP operating experience with the Mark-B 15x15 assembly has verified the adequacy of its design. Mark-B fuel assemblies have operated successfully in over 100 fuel cycles at multiple nuclear power plant facilities. Axial blanket as well as Gd_2O_3 fuel has operated successfully in multiple cycles at various operating B&W units.

M5® cladding material has been implemented on a batch basis in multiple B&W and Westinghouse units. The FUELGUARD™ debris resistant lower end fitting has operated at multiple Westinghouse and CE units and is currently being used in B&W units. All the operating B&W plants have implemented the MONOBLOC™ instrument tube.

Cycle 19 is the fifth usage of fuel assemblies with HTP™ spacers at Davis-Besse. HTP™ spacers have been successfully implemented in over 15,464 fuel assemblies (arrays ranging from 14x14 to 18x18) at over 47 nuclear power plant facilities world-wide. Many of these fuel assemblies utilized the HTP™ spacer and the FUELGUARD™ debris filtering lower end fitting. The HTP™ grid provides improved mechanical performance and has increased resistance to flow induced fuel rod fretting failures relative to earlier Mark-B designs. The fifth batch implementation of the HTP™ design at Davis-Besse will continue to maintain the improved mechanical performance of the fuel, while also maintaining resistance to grid-to-rod fretting failures, and decreasing the likelihood of the occurrence of loose fuel rods.

Table 4-1 Fuel Design Parameters Davis-Besse, Cycle 19

Batch	18A5	19B	19C2	19D
Fuel assembly type	Mark-B-HTP	Mark-B-HTP	Mark-B-HTP	Mark-B-HTP
Number of assemblies	1	4	8	16
Fuel cladding material	M5®	M5®	M5®	M5®
Fuel rod outside diameter, in.	0.430	0.430	0.430	0.430
Fuel rod inside diameter, in.	0.380	0.380	0.380	0.380
Undensified active fuel length, in.				
UO_2 rods	143.0	143.0	143.0	143.0
Gd_2O_3 rods	143.0	143.0	143.0	143.0
Pellet outside diameter, in.	0.3735	0.3735	0.3735	0.3735
Fuel pellet initial density, %TD mean	96.0	96.0	96.0	96.0
Average burnup BOC, MWd/mtU[(a)]	30,118	43,836	44,282	42,700
Cladding collapse burnup, MWd/mtU[(b)]	> 65,000	> 65,000	> 65,000	> 65,000
Maximum pin burnup, MWd/mtU[(a)]	56,105	57,491	56,929	57,003
Initial fuel enrichment, wt% ^{235}U				
UO_2 rods	4.59	4.81	4.81	4.81
Gd_2O_3 rods	3.67 & 2.75	3.85	3.85 & 2.89	3.85
Nominal LHR at 2817 MWt, kW/ft[(c)]	6.25	6.25	6.25	6.25
Minimum LHR to melt, kW/ft				
UO_2 rods	19.80	19.80	19.80	19.80
4 wt% Gd_2O_3 rods	19.47	19.47	19.47	19.47
6 wt% Gd_2O_3 rods	---	---	---	---
8 wt% Gd_2O_3 rods	19.01	---	19.01	---
Fuel rod pitch, in.	0.568	0.568	0.568	0.568
Fuel assembly pitch, in.	8.587	8.587	8.587	8.587
Fuel assembly overall length, in.	165. 895[(f)]	165.835	165.835	165.835
Guide tube material	M5®	M5®	M5®	M5®
Guide tube outside diameter / wall thickness, in.	0.530 / 0.016	0.530 / 0.016	0.530 / 0.016	0.530 / 0.016
Instrument tube material	M5®	M5®	M5®	M5®
Instrument tube outside diameter, in.	0.493	0.493	0.493	0.493
Instrument tube inside diameter (upper / lower region), in.	0.352 / 0.400	0.352 / 0.400	0.352 / 0.400	0.352 / 0.400
End fitting material	Stainless Steel	Stainless Steel	Stainless Steel	Stainless Steel
Spacer grid strip material (intermediate / bottom end grid)	M5® / Inconel-718	M5® / Inconel-718	M5® / Inconel-718	M5® / Inconel-718
Spacer strip thickness (external / internal), in.	0.026/0.028 (HTP)[(d)] 0.025/0.025 (HMP)[(e)]	0.026/0.028 (HTP)[(d)] 0.025/0.025 (HMP)[(e)]	0.026/0.028 (HTP)[(d)] 0.025/0.025 (HMP)[(e)]	0.026/0.028 (HTP)[(d)] 0.025/0.025 (HMP)[(e)]
Dummy fuel material	N/A	N/A	N/A	N/A
Dummy fuel outside diameter, in.	N/A	N/A	N/A	N/A

[(a)] Does not include allowances for SSRs or cycle 18 shutdown flexibility
[(b)] Calculated using method from Reference 5
[(c)] LHR calculations include a 0.973 energy deposition factor
[(d)]HTP = intermediate spacer grid
[(e)]HMP = bottom end grid
[(f)]Initial length prior to UEF replacement

Table 4-1 (continued)

Batch	20A	20B	20C	20D
Fuel assembly type	Mark-B-HTP	Mark-B-HTP	Mark-B-HTP	Mark-B-HTP
Number of assemblies	32	16	4	16
Fuel cladding material	M5®	M5®	M5®	M5®
Fuel rod outside diameter, in.	0.430	0.430	0.430	0.430
Fuel rod inside diameter, in.	0.380	0.380	0.380	0.380
Undensified active fuel length, in.				
UO_2 rods	143.0	143.0	143.0	143.0
Gd_2O_3 rods	143.0	143.0	143.0	143.0
Pellet outside diameter, in.	0.3735	0.3735	0.3735	0.3735
Fuel pellet initial density, %TD mean	96.0	96.0	96.0	96.0
Average burnup BOC, MWd/mtU[(a)]	23,086	21,995	22,075	19,538
Cladding collapse burnup, MWd/mtU[(b)]	> 65,000	> 65,000	> 65,000	> 65,000
Maximum pin burnup, MWd/mtU[(a)]	48,483	50,485	49,205	50,130
Initial fuel enrichment, wt% ^{235}U				
UO_2 rods	3.88 (3.58 ZL[(f)])	4.52 (4.22 ZL[(f)])	4.52 (4.22 ZL[(f)])	4.87 (4.57 ZL[(f)])
Gd_2O_3 rods	2.86 & 2.14	3.37	3.37 & 2.95	3.65
Nominal LHR at 2817 MWt, kW/ft[(c)]	6.25	6.25	6.25	6.25
Minimum LHR to melt, kW/ft				
UO_2 rods	19.80	19.80	19.80	19.80
4 wt% Gd_2O_3 rods	19.47	19.47	19.47	19.47
6 wt% Gd_2O_3 rods	---	---	19.14	---
8 wt% Gd_2O_3 rods	19.01	---	---	---
Fuel rod pitch, in.	0.568	0.568	0.568	0.568
Fuel assembly pitch, in.	8.587	8.587	8.587	8.587
Fuel assembly overall length, in.	165.835	165.835	165.835	165.835
Guide tube material	M5®	M5®	M5®	M5®
Guide tube outside diameter / wall thickness, in.	0.530 / 0.016	0.530 / 0.016	0.530 / 0.016	0.530 / 0.016
Instrument tube material	M5®	M5®	M5®	M5®
Instrument tube outside diameter, in.	0.493	0.493	0.493	0.493
Instrument tube inside diameter (upper / lower region), in.	0.352 / 0.400	0.352 / 0.400	0.352 / 0.400	0.352 / 0.400
End fitting material	Stainless Steel	Stainless Steel	Stainless Steel	Stainless Steel
Spacer grid strip material (intermediate / bottom end grid)	M5® / Inconel-718	M5® / Inconel-718	M5® / Inconel-718	M5® / Inconel-718
Spacer strip thickness (external / internal), in.	0.026/0.028 (HTP)[(d)] 0.025/0.025 (HMP)[(e)]	0.026/0.028 (HTP)[(d)] 0.025/0.025 (HMP)[(e)]	0.026/0.028 (HTP)[(d)] 0.025/0.025 (HMP)[(e)]	0.026/0.028 (HTP)[(d)] 0.025/0.025 (HMP)[(e)]
Dummy fuel material	N/A	N/A	N/A	Stainless Steel
Dummy fuel outside diameter, in.	N/A	N/A	N/A	0.430

[(a)] Does not include allowances for SSRs or cycle 18 shutdown flexibility
[(b)] Calculated using method from Reference 5
[(c)] LHR calculations include a 0.973 energy deposition factor
[(d)]HTP = intermediate spacer grid
[(e)]HMP = bottom end grid
[(f)]ZL = zone-loaded fuel rods

Table 4-1 (continued)

Batch	21A	21B	21C	21D	21E
Fuel assembly type	Mark-B-HTP	Mark-B-HTP	Mark-B-HTP	Mark-B-HTP	Mark-B-HTP
Number of assemblies	16	24	28	4	8
Fuel cladding material	M5®	M5®	M5®	M5®	M5®
Fuel rod outside diameter, in.	0.430	0.430	0.430	0.430	0.430
Fuel rod inside diameter, in.	0.380	0.380	0.380	0.380	0.380
Undensified active fuel length, in.					
UO_2 rods	143.0	143.0	143.0	143.0	143.0
Gd_2O_3 rods	143.0	143.0	143.0	143.0	143.0
Pellet outside diameter, in.	0.3735	0.3735	0.3735	0.3735	0.3735
Fuel pellet initial density, %TD mean	96.0	96.0	96.0	96.0	96.0
Average burnup BOC, MWd/mtU[(a)]	0	0	0	0	0
Cladding collapse burnup, MWd/mtU[(b)]	> 65,000	> 65,000	> 65,000	> 65,000	> 65,000
Maximum pin burnup, MWd/mtU[(a)]	30,214	31,050	31,642	31,684	31,362
Initial fuel enrichment, wt% ^{235}U					
UO_2 rods	4.30 (4.00 ZL[(f)])	4.70 (4.40 ZL[(f)])	4.95 (4.65 ZL[(f)])	4.95 (4.65 ZL[(f)])	4.95 (4.65 ZL[(f)])
Gd_2O_3 rods	3.20 & 2.40	3.08 & 2.64	3.72	3.72	3.72 & 2.79
Nominal LHR at 2817 MWt, kW/ft[(c)]	6.25	6.25	6.25	6.25	6.25
Minimum LHR to melt, kW/ft					
UO_2 rods	19.80	19.80	19.80	19.80	19.80
4 wt% Gd_2O_3 rods	19.47	---	19.47	19.47	19.47
6 wt% Gd_2O_3 rods	---	19.14	---	---	---
8 wt% Gd_2O_3 rods	19.01	19.01	---	---	19.01
Fuel rod pitch, in.	0.568	0.568	0.568	0.568	0.568
Fuel assembly pitch, in.	8.587	8.587	8.587	8.587	8.587
Fuel assembly overall length, in.	165.835	165.835	165.835	165.835	165.835
Guide tube material	M5®	M5®	M5®	M5®	M5®
Guide tube outside diameter / wall thickness, in.	0.530 / 0.016	0.530 / 0.016	0.530 / 0.016	0.530 / 0.016	0.530 / 0.016
Instrument tube material	M5®	M5®	M5®	M5®	M5®
Instrument tube outside diameter, in.	0.493	0.493	0.493	0.493	0.493
Instrument tube inside diameter (upper / lower region), in.	0.352 / 0.400	0.352 / 0.400	0.352 / 0.400	0.352 / 0.400	0.352 / 0.400
End fitting material	Stainless Steel	Stainless Steel	Stainless Steel	Stainless Steel	Stainless Steel
Spacer grid strip material (intermediate / bottom end grid)	M5® / Inconel-718	M5® / Inconel-718	M5® / Inconel-718	M5® / Inconel-718	M5® / Inconel-718
Spacer strip thickness (external / internal), in.	0.026/0.028 (HTP)[(d)] 0.025/0.025 (HMP)[(e)]	0.026/0.028 (HTP)[(d)] 0.025/0.025 (HMP)[(e)]	0.026/0.028 (HTP)[(d)] 0.025/0.025 (HMP)[(e)]	0.026/0.028 (HTP)[(d)] 0.025/0.025 (HMP)[(e)]	0.026/0.028 (HTP)[(d)] 0.025/0.025 (HMP)[(e)]
Dummy fuel material	N/A	N/A	N/A	N/A	N/A
Dummy fuel outside diameter, in.	N/A	N/A	N/A	N/A	N/A

[(a)] Does not include allowances for SSRs or cycle 18 shutdown flexibility
[(b)] Calculated using method from Reference 5
[(c)] LHR calculations include a 0.973 energy deposition factor
[(d)]HTP = intermediate spacer grid
[(e)]HMP = bottom end grid
[(f)]ZL = zone-loaded fuel rods

Table 4-2 B-HTP UO_2 Rod Transient Strain Limits Davis-Besse, Cycle 19

Burnup (MWd/mtU)	LHR at 1.0% Strain (kW/ft)
20,000	24.47
30,000	23.70
40,000	22.01
50,000	20.23
60,000	18.05
62,000	17.37

Table 4-3 B-HTP Gd_2O_3 Rod Transient Strain Limits Davis-Besse, Cycle 19

Burnup (MWd/mtU)	LHR at 1.0% Strain (kW/ft)		
	4 wt% Gd_2O_3	6 wt% Gd_2O_3	8 wt% Gd_2O_3
20,000	21.18	20.40	20.19
30,000	20.60	19.27	19.07
40,000	19.40	18.52	18.21
50,000	17.54	16.40	16.23
55,000	16.26	15.60	15.43

Table 4-4 B-HTP UO_2 Rod Linear Heat Rate to Melt (LHRTM) Limits Davis-Besse, Cycle 19

Burnup (MWd/mtU)	LHR to Melt (kW/ft)
50	25.11
1,000	25.35
5,000	25.36
10,000	24.99
20,000	24.10
30,000	23.13
40,000	22.18
50,000	21.13
60,000	19.97
62,000	19.80

Table 4-5 B-HTP Gd_2O_3 Rod Linear Heat Rate to Melt (LHRTM) Limits Davis-Besse, Cycle 19

Burnup (MWd/mtU)	LHR to Melt (kW/ft)		
	4 wt% Gd_2O_3	6 wt% Gd_2O_3	8 wt% Gd_2O_3
50	22.55	21.79	21.29
1,000	24.21	23.57	23.02
5,000	23.20	24.15	25.63
10,000	22.25	22.41	22.13
20,000	21.74	21.39	21.24
30,000	21.24	20.97	20.86
40,000	20.58	20.31	20.22
50,000	19.76	19.48	19.39
55,000	19.47	19.14	19.01

5.0 NUCLEAR DESIGN

5.1 Physics Characteristics

Table 5-1 compares the core physics parameters for the cycle 18 and 19 designs. The values for cycles 18 and 19 were generated with the NRC approved NEMO code (Reference 12). Differences in core physics parameters are to be expected between the cycles due to changes in fuel enrichments, burnable poison concentrations, and loading patterns, which create changes in flux and burnup distributions. Figure 5-1 illustrates a representative relative power distribution for BOC 19 at full power with equilibrium xenon, group 7 inserted to nominal HFP position and gray APSRs partially inserted.

All analyses of the nuclear physics parameters were performed with NRC approved methodologies. The physics characteristics of the cycle 19 design were evaluated with respect to the applicable design criteria for the accident and transient analysis as described in Section 7. The rod position limits presented in Section 8 considered the shutdown margin requirements and the calculated ejected rod worths and their adherence to design criteria at all times in life and at all power levels. The ejected rod worths in Table 5-1 are the maximum calculated values. The adequacy of the shutdown margin with cycle 19 rod worths is shown in Table 5-2. The following conservatisms were applied to the shutdown calculations:

1. 6% uncertainty on net rod worth (Reference 13).
2. Off-nominal flux distribution (e.g. xenon transient allowance).

The off-nominal flux distribution allowance was taken into account to ensure that the effects of operational maneuvering transients were included in the shutdown analysis. Calculations for cycle 19 have verified that the poison material depletion allowance is adequately bounded by the off-nominal flux distribution allowance.

The rod index (RI) of 260 is used for the illustrative purposes of Table 5-2, and the actual rod insertion limits are set during the maneuvering analysis. Power dependent rod worth curves and additional conservatism are utilized during shutdown margin determination in the maneuvering analysis.

5.2 Changes in Nuclear Design

Cycle 19 has a larger feed batch, different fuel loading pattern, and a longer cycle length compared to cycle 18. In addition, increased axial blanket enrichments are used for UO_2 rods in the batch 21 fuel. These changes were incorporated into the physics model. The impact of the six (6) SSRs was evaluated and determined to have less than minimal impact on core reactivity, stuck rod worth, or ejected rod worth. Reference 12 illustrates the calculational accuracy obtainable with NEMO for gadolinia cores.

No significant operational or procedural changes exist with regard to axial or radial power shape, xenon, or tilt control. The stability and control of the core with APSRs withdrawn was analyzed. The operating limits (COLR changes) for the reload cycle are provided in Section 8.

Table 5-1 Davis-Besse, Cycle 19 Physics Parameters[a]

	Cycle 18[b]	Cycle 19[c]
Cycle length, EFPD	600	700
Cycle burnup, MWd/mtU	19,611	22,907
Average core burnup - 700 EFPD[b], MWd/mtU	38,432	38,382
Initial core loading, mtU	86.2	86.1
Critical boron[d] - 0 EFPD, ppm		
HZP	1,859	1,911
HFP	1,602	1,657
Critical boron[d] - 700 EFPD[b], ppm		
HZP	218	163
HFP	5[e]	5[e]
Control rod worths - HFP, 4 EFPD, %Δk/k		
Group 6	0.93	0.86
Group 7	0.97	0.97
Group 8	0.13	0.11
Control rod worths - HFP, 700 EFPD[b], %Δk/k		
Group 7	0.96	0.94
Max ejected rod worth - HZP, %Δk/k		
4 EFPD, Groups 5-8 inserted (N12)[j]	0.24	0.54
700 EFPD[b], Groups 5-7 inserted (N12)	0.60	0.67
Max stuck rod worth - HZP, %Δk/k		
4 EFPD (N12)	0.76	0.86
700 EFPD[b], (M13)	1.01	1.04
Power deficit[f] - HZP to HFP, %Δk/k		
4 EFPD	-1.83	-1.81
700 EFPD[b]	-2.99	-3.01
Doppler coeff[f] [g] - HFP, 10^{-3} %Δk/k/°F		
0 EFPD[h]	-1.60	-1.51
700 EFPD[b], 0 ppm	-1.71	-1.74
Moderator coeff[f] - HFP, 10^{-2} %Δk/k/°F		
0 EFPD[h]	-0.84	-0.75
700 EFPD[b], 0 ppm[i]	-3.49	-3.50
Temperature coeff[f] - HZP (532 to 510 °F), 10^{-2} %Δk/k/°F		
700 EFPD[b], Groups 1-7 Inserted, M13 out, 0 ppm	-2.80	-2.89

Table 5-1 (continued)

	Cycle 18[b]	Cycle 19[c]
Boron worth[f] - HFP, ppm/%Δk/k		
0 EFPD	162	164
700 EFPD[b]	127	126
Xenon worth[f] - HFP, %Δk/k		
4 EFPD	2.47	2.43
700 EFPD[b]	2.70	2.69
Effective delayed neutron fraction[f] - HFP		
4 EFPD	0.00634	0.00648
700 EFPD[b]	0.00532	0.00531

(a) Calculations at 0 EFPD are done with No Xenon. All other calculations are at 100%FP Eq Xe where Eq Xe is calculated for Groups 1-6 at 100%WD, Group 7 at 90%WD and Group 8 at nominal HFP position.

(b) Cycle 18 values and conditions are from Reference 3. EOC values are calculated at 600 EFPD for cycle 18.

(c) Based on a cycle 17 length of 599 EFPD and a cycle 18 length of 578 EFPD.

(d) Control rod group 8 is inserted for calculation at 0 EFPD and withdrawn for calculation at 700 EFPD.

(e) Power coastdown to 600 EFPD at 5 ppm for cycle 18 and to 700 EFPD at 5 ppm for cycle 19. All HFP EOC calculations are modeled with 0 ppm boron.

(f) All calculations done with control rod groups 1-7 at 100%WD and control rod group 8 at nominal HFP position, unless otherwise noted.

(g) Doppler temperature coefficient calculated using a distributed fuel temperature.

(h) Cycle 19 values are calculated at 1768 ppm (includes allowances for reactivity anomaly and shutdown window flexibility); cycle 18 values were calculated at 1713 ppm. For the purposes of comparison to cycle 19 in this table, the standard flexibility window of +/-15 EFPD is used for the cycle 18 data.

(i) These values are calculated with the control rods at a rod index of 260% WD.

(j) Cycle 18 value based on maximum ejected rod worth location L10.

Table 5-2 Shutdown Margin Calculation for Davis-Besse, Cycle 19

	BOC, %Δk/k	EOC, %Δk/k	
	4 EFPD	610 EFPD	700 EFPD*
Available Rod Worth			
Total rod worth, HZP	6.275	6.660	6.780
Maximum stuck rod worth, HZP	-0.857	-0.997	-1.041
Net Worth	5.418	5.663	5.739
Less 6% Uncertainty	-0.325	-0.340	-0.344
Total available worth	5.093	5.323	5.395
Required Rod Worth			
Power deficit, HFP to HZP	1.812	2.892	3.008
Off-nominal flux distribution allowance	0.350	0.250	0.250
Max allowable inserted rod worth at RI = 260% WD	0.366	0.481	0.505
Total required worth	2.528	3.623	3.763
Shutdown Margin			
Total available minus total required	2.565	1.700	1.632

Note: Required shutdown margin is 1.000%Δk/k.

* Group 8 out

Figure 5-1 Davis-Besse Cycle 19 Relative Power Distribution at BOC (4 EFPD), Full Power, Equilibrium Xenon, Group 7 at 90 %WD, Group 8 at 30 %WD

	8	9	10	11	12	13	14	15
H	0.935	1.068	0.981	1.142	7 1.055	1.263	1.114	0.372
K	1.068	0.965	1.116	1.028	1.257	1.206	1.089	0.362
L	0.981	1.115	1.035	1.260	8 1.059	1.296	1.098	0.294
M	1.142	1.030	1.257	1.228	1.237	1.221	0.868	
N	7 1.055	1.265	8 1.061	1.238	7 1.238	1.114	0.387	
O	1.263	1.223	1.305	1.226	1.116	0.695		
P	1.114	1.101	1.107	0.872	0.388			
R	0.372	0.368	0.297					

x x.xxx	Inserted Rod Group Number Relative Power Density

6.0 THERMAL-HYDRAULIC DESIGN

The cycle 19 core is composed entirely of Mark-B-HTP fuel assemblies, as shown in Table 4-1. The Mark-B-HTP design contains a slightly higher hydraulic resistance for the lower end fitting and intermediate spacer grids than the previous Mark-B fuel designs. A core analysis at a thermal power of 2820 MWt consisting of a full core of Mark-B-HTP fuel assemblies was analyzed for cycle 19. The approved analysis methodology described in Reference 1, the statistical core design (SCD) methodology described in Reference 14, and the BHTP CHF correlation described in Reference 20, were utilized in this analysis.

The effects of adding six SSRs to four once-burned batch 20D assemblies (two SSRs in each of two assemblies and one SSR in each of two assemblies) were considered in the thermal-hydraulic analyses for cycle 19. The effects of the SSRs were evaluated in accordance with Reference 15.

Two design modifications that were initially implemented for the batch 17 fuel were evaluated with respect to their impact on thermal-hydraulic performance: the FUELGUARD^{TM} lower end fitting and the HTP intermediate spacer grids. The combination of these two modifications results in a higher fuel assembly pressure drop. The hold down capability of the six-leaf hold down spring was evaluated using the approved statistical hold down (SHD) analysis methods described in Reference 22. The replacement UEFs and the 0.060-inch fuel assembly length reduction were addressed in the hold down analysis. The analysis establishes a 4th reactor coolant pump startup temperature limit to assure that a positive holddown force will be maintained when the 4th pump is energized. Positive fuel assembly hold down is required during Condition I and Condition II operation.

The DNB-based thermal-hydraulic analyses for cycle 19 are applicable for urania (UO_2) and gadolinia (Gd_2O_3) fuel rods. The applicability of the DNBR results to the assemblies containing axial blanket fuel rods was further verified in the evaluation of power distribution check cases where the DNB peaking margin for the cycle-specific axial flux shapes was confirmed.

Table 6-1 provides a summary comparison of the DNB analysis parameters for cycles 18 and 19. The cycle 18 and 19 values are based on a DNB analysis for a rated thermal power of 2820 MWt and a full core of Mark-B-HTP fuel assemblies.

The thermal-hydraulic design-based analyses were performed with NRC approved methodologies and where applicable, show that all design criteria are met.

Table 6-1 Limiting Thermal-Hydraulic Design Conditions, Davis-Besse Cycles 18 and 19

	Cycle 18	Cycle 19
Design power level, MWt	2820[a]	2820[a]
Nominal core exit pressure, psia	2200	2200
Minimum core exit pressure, psia	2135	2135
Minimum RCS flow, gpm	380,000	380,000
Core bypass flow, %	6.24[b]	6.24[b]
DNBR modeling	SCD	SCD
Reference design power peaking factor (radial x local)	1.800	1.800
Reference design axial power peaking factor flux shape	1.65 chopped cosine	1.65 chopped cosine
Hot channel factors		
Enthalpy rise	1.0[c]	1.0[c]
Heat flux	N/A[d]	N/A[d]
Flow Area	1.0[e]	1.0[e]
Active fuel length, in.	143.00[h]	143.00[h]
Avg. heat flux at 100% power, 10^5 Btu/hr-ft^2 (2820 MWt)[a]	1.90[f]	1.90[f]
Max. heat flux at 100% power, 10^5 Btu/hr-ft^2 (2820 MWt)[a]	5.62[f]	5.62[f]
CHF Correlation	BHTP	BHTP
CHF Correlation DNB limit	1.65 TDL[g]	1.65 TDL[g]
Minimum DNBR		
@ 100.37% power (2820 MWt)[a]	1.92	1.92
@ 110.37% power (2820 MWt)[a]	1.75	1.75

[a] Analysis was performed at a conservative thermal power of 2820 MWt. The MUR Uprate Rated Thermal Power is 2817 MWt. The 2820 MWt analysis bounds operation below 2820 MWt.
[b] Used in the analysis.
[c] 1.015 enthalpy rise hot channel factor was used in the derivation of the Statistical Design Limit (SDL).
[d] The heat flux hot channel factor is no longer applicable in DNB calculations as allowed by Reference 1.
[e] 1.015 radial hot channel factor to account for flow area variability was used in the derivation of the SDL.
[f] These heat flux values are calculated with a stack height of 143.00 inches. A stack height of 142.75 inches was used in the DNB analysis and is conservative for cycle 19.
[g] Thermal Design Limit
[h] The reference analyses are based on a nominal active fuel length of 142.75 inches. The stack height in cycle 18 was 143.00 inches and continues to be 143.00 inches in cycle 19.

7.0 ACCIDENT AND TRANSIENT ANALYSIS

7.1 General Safety Analysis

Each Updated Safety Analysis Report (USAR) accident analysis has been examined with respect to changes in the cycle 19 parameters to determine the effects of the cycle 19 reload and to ensure that thermal performance during hypothetical transients is not degraded.

The radiological dose consequences of the USAR Chapter 15 accidents have been evaluated using conservative radionuclide source terms that bound the cycle specific source terms for Davis-Besse cycle 19. None of the accident doses are adversely impacted by the cycle 19 design and all accident doses remain below the respective acceptance criteria values as documented in the USAR. The cycle 19 doses also remain below the NUREG-0800 (Reference 16) acceptance criteria.

The current Davis-Besse fuel handling accident (FHA) analyses of record remain bounding for the Davis-Besse cycle 19 fuel parameters for both the offsite doses and the control room doses, and are not affected by the installation of the ROTSGs during Refueling Outage 18.

7.2 Non-LOCA Evaluation

A comparison of the key kinetics parameters from the USAR and cycle 19 is provided in Table 7-1.

The end-of-cycle (EOC) moderator temperature coefficient listed in Table 7-1 for cycle 19 is the 3-D, hot full power (HFP) temperature coefficient. An evaluation was performed to verify the acceptability of the cycle 19 moderator temperature coefficients for all USAR system response analyses excluding steam line breaks. The results of the evaluation were acceptable for all USAR system response analyses, excluding steam line breaks.

The steam line break accident was evaluated based on the total reactivity change from 532°F to a minimum temperature of 510°F. The temperature coefficient used in safety analysis of the steam line break is -3.10×10^{-2} %Δk/k/°F. This value is based on the combined effects of moderator density, boron worth, control rod worth degradation and Doppler reactivity, over the temperature range from 532°F to 510°F. The combined EOC temperature coefficient for cycle 19 is shown in Table 7-1 as -2.89×10^{-2} %Δk/k/°F. Since the system response analysis value for the EOC temperature coefficient is more negative than the cycle 19 value, the steam line break analysis remains bounding for cycle 19.

The continued validity of the non-LOCA (loss-of-coolant accident) USAR system response analyses was assessed for cycle 19 operation. It was determined that the non-LOCA USAR system response analyses remain valid for Davis-Besse cycle 19.

The continued validity of the non-LOCA USAR system response analyses was assessed for a maneuver near EOC 19 that involves the complete withdrawal of the axial power shaping rods (APSRs) and an actual reduction in the average reactor coolant temperature (T_{avg}) of as much as 12°F including 1.5°F

uncertainty (10.5°F indicated). It was determined that the non-LOCA USAR system response analyses remain valid.

It is concluded by the examination of cycle 19 core thermal, thermal-hydraulic, and kinetics properties of the system response analyses, with respect to acceptable previous cycle values, that the cycle 19 core reload will not adversely affect the ability to safely operate the Davis-Besse plant during cycle 19. The previously accepted system response analysis basis for Davis-Besse consists of the analyses presented in the USAR. The system response analysis basis was developed using kinetics parameter values that were shown to bound the corresponding cycle 19 parameter values. Consequently, it is concluded that the existing analysis basis is bounding for cycle 19.

The replacement of the OTSGs with ROTSGs has been taken into account for the non-LOCA accident and transient analysis for cycle 19.

Inspections during refueling determined that some of the FAs scheduled for reinsertion had wear, and the damaged fuel rods were replaced with SSRs. Those have been taken into account for the non-LOCA accident and transient analysis for cycle 19.

7.3 LOCA Evaluation

Loss-of-coolant accident (LOCA) analyses for the B&W 177-FA raised-loop nuclear steam system (NSS) have been performed to calculate allowable LOCA linear heat rate (LHR) limits that are applicable to the Mark-B-HTP fuel. The LOCA LHR limits are analyzed at a power level that includes the power level uncertainty. Therefore, the LOCA LHR limits are applicable to a cycle 19 rated thermal power of 100.37 percent of 2817 MWt with the ultrasonic flow measurement system in operation.

The NRC-approved RELAP5/MOD2-B&W Emergency Core Cooling System (ECCS) Evaluation Model techniques and assumptions, as described in BAW-10192P-A (Reference 17), as amended by the NRC-approved M5® advanced cladding topical report (Reference 6), were used in the full-core and mixed-core Mark-B-HTP LOCA analyses. These assemblies were analyzed at 3025 MWt including uncertainty in the current LOCA analyses of record (AOR).

The analysis of record (AOR) large break LOCA (LBLOCA) and small break LOCA (SBLOCA) analyses incorporated the BHTP critical heat flux (CHF) correlation into the computer codes based on the guidance in the Evaluation Model. This change was necessary to be consistent with the Evaluation Model and was reportable as required by 10 CFR 50.46. The changes associated with the implementation of the BHTP CHF correlation into the RELAP5/MOD2-B&W computer code have been approved in revision 6 of the RELAP5 topical report, BAW-10164P-A (Reference 23).

Cycle 19 is the first cycle that will operate with the newly installed ROTSGs. The applicability of the current full-core Mark-B-HTP LOCA AOR considering the ROTSGs was evaluated. The evaluation of the applicability of the LOCA analyses showed that the current analyses based on the OTSGs with 20% steam generator tube plugging bound the Davis-Besse plant configuration following the steam generator

replacement with the ROTSGs up to 5% symmetric steam generator tube plugging.

The cycle 19 core design includes a full core of Mark-B-HTP fuel assemblies. The full-core Mark-B-HTP LOCA analyses were performed for the Mark-B-HTP fuel with the RELAP5/MOD2-B&W ECCS Evaluation Model that is applicable to the batches 18, 19, 20, and 21 Mark-B-HTP fuel. Chamfered pellets in the Mark-B-HTP fuel were introduced in cycle 18, batch 20, and will also be used in batch 21 for cycle 19. In cycle 19, batch 21, the axial blanket pellet enrichment in the UO_2 fuel rods will be increased from 2.5 wt% to 3.9 wt% UO_2 enrichment. The change in UO_2 axial blanket enrichment has been analyzed and found to result in no change to the existing LHR limits.

The LHR limits for batches 18, 19, 20 and 21 fuel rods containing gadolinia (Gd_2O_3), which are determined based on fuel rod performance data from the GDTACO (Reference 8) fuel rod performance code, were determined for use in the subsequent power distribution analysis. The LHR limits for the Gd_2O_3 fuel are based on percentages of the urania (UO_2) LHR limits to account for the reduction in thermal conductivity in the fuel rod. The reduced Gd_2O_3 fuel LHR limits are between 96 percent and 85 percent of the UO_2 LHR limits for Gd_2O_3 concentrations between 2 and 8 wt%.

The TACO3 and GDTACO codes do not explicitly model degradation in fuel thermal conductivity versus burnup that the newer state-of-the-art codes employ. An evaluation was performed to confirm the appropriateness and adequacy of the TACO3 and GDTACO codes for use in LOCA fuel initializations. The evaluation identified that conservatisms used in the methods of analysis, along with burnup dependent fuel temperature uncertainties that are applied to the inputs prior to their use in the LOCA analyses, adequately produce a fuel temperature that considers the effects of degraded thermal conductivity with burnup.

Two additional adjustments were made to ensure the LOCA fuel initializations were consistent with the evaluations: 1) beginning with cycle 17, a linear heat rate limit reduction of 0.5 kW/ft for end-of-life (EOL) conditions to ensure the fuel temperatures used in the LOCA analyses were bounded, and 2) beginning with cycle 18, moving the rod average burnup at middle-of-life (MOL) from 40 GWd/mtU to 34 GWd/mtU to ensure the fuel temperature uncertainty used in the analyses was consistent with the hot spot burnup of approximately 40 GWd/mtU. These adjustments provide a prudent level of margin to accommodate a future transition to the latest state-of-the-art fuel performance codes and methods for LOCA analyses. The LHR limits presented in Table 7-2 include these changes.

Table 7-2 shows the maximum allowable LOCA LHR limits for the Mark-B-HTP fuel in the Davis-Besse Unit 1 cycle 19 core as functions of burnup. Sensitivity studies showed that certain power levels below the analyzed 3025 MWt uprated power produced more severe results (i.e. increased PCT, hydrogen generation, and peak local oxidation). Therefore, a reduction of up to 0.2 kW/ft to the Mark-B-HTP LHR limits is necessary for certain power levels to ensure that the LHRs determined at 3025 MWt remain limiting. For the Mark-B-HTP assemblies, the power level penalty is applied to the LHR limits reported in Table 7-2 prior to use in the maneuvering analyses.

All LOCA linear heat rate limits are reported on a nuclear source basis that represents all useable energy produced by the fuel rod, some of which is deposited in the moderator and surrounding fuel rods. The thermal source LHR is related to the nuclear source LHR by the steady-state energy deposition factor (EDF_{ss}). The EDF_{ss} is defined as $LHR_{Thermal}$ / $LHR_{Nuclear}$ and varies from 0.973 for fresh fuel to greater than 1.0 for low power, high burnup fuel. The appropriate EDFs have been considered in the LOCA analyses supporting the LOCA LHR limits provided in Table 7-2.

LBLOCA analyses for the Davis-Besse plant do not currently support a moderator temperature coefficient (MTC) of $+0.9 \times 10^{-2}$ $\%\Delta k/k/^{o}F$ for core power levels at or below 95 percent full power. LOCA analyses were performed at various partial power levels to define a maximum permissible (most positive) MTC versus power level. The predicted MTC curve for cycle 19 was compared to the resulting allowable MTC curve (shown in Section 8) to confirm that the cycle design is sufficiently bounded.

An analysis was performed using the RELAP5/MOD2-B&W ECCS Evaluation Model to assess the conditions under which the EOC moderator average temperature (T_{avg}) reduction maneuver could be performed. The results of the analysis showed that a maximum T_{avg} reduction of up to 12°F is considered, consisting of an indicated 10.5°F T_{avg} reduction with a 1.5°F uncertainty, and a MTC more negative than -10 pcm/°F provides LOCA results that are bounded by the nominal T_{avg} LOCA results. The planned T_{avg} reduction for Davis-Besse cycle 19 is verified as no greater than 12°F, for an EOC MTC more negative than -10 pcm/°F.

The effect of the inclusion of six (6) SSRs on the maximum predicted pin peaks and LOCA LHR limits for all batches was evaluated according to Reference 15. It was confirmed that no changes to the LOCA LHR limits or additional evaluations were required as a result of inclusion of these SSRs in cycle 19.

The bounding allowable LOCA LHR limits that are applicable to the Mark-B-HTP fuel type are reported in Table 7-2. The analyses consider the required criteria and acceptable features for evaluation model set forth in Appendix K of 10 CFR 50 to show compliance to the five 10 CFR 50.46 criteria. These LHR limits are based on the cycle 19 evaluation that verified that the previous analyses are still applicable and valid, and do not adversely affect the ability of the Davis-Besse plant to operate safely under postulated LOCA conditions during cycle 19.

Table 7-1 Comparison of Key Parameters for Accident Analysis Davis-Besse, Cycle 19

Parameter	Analysis of Record (AOR) Value	Cycle 19 Value	AOR Value is Bounding if AOR Value is:
BOC[a] Doppler coefficient, 10^{-3} %Δk/k/°F	-1.34	-1.51	Less Negative
EOC[a,i] Doppler coefficient, 10^{-3} %Δk/k/°F	-1.45	-1.60	Less Negative
EOC Doppler coefficient, 10^{-3} %Δk/k/°F	-1.77[b]	-1.74[e]	More Negative
BOC HFP moderator coefficient, 10^{-2} %Δk/k/°F	+0.0	-0.75	Less Negative/ More Positive
BOC HZP moderator coefficient, 10^{-2} %Δk/k/°F	+0.9	-0.01	Less Negative/ More Positive
EOC HFP moderator coefficient, 10^{-2} %Δk/k/°F	-4.0	-3.50	More Negative
EOC temperature coefficient (532 to 510°F), 10^{-2} %Δk/k/°F	-3.10[e]	-2.89	More Negative
BOC all rod group worth (HZP), %Δk/k	13.9	6.83[j]	Larger[f]
Boron reactivity worth (HFP), ppm/%Δk/k	100	166[k]	Note [g]
Maximum ejected rod worth (HFP), %Δk/k	0.65	< 0.65[c]	Larger
Maximum dropped rod worth (HFP), %Δk/k	0.65[h]	< 0.20	Larger
Initial boron concentration (HFP), ppm	1407	1768[d]	Note [g]

[a] BOC denotes beginning-of-cycle; EOC denotes end-of-cycle.

[b] -1.77×10^{-3} %Δk/k/°F was used for steam line failure analysis (also see Note e).

[c] Cycle-specific rod position limits ensure that the maximum HFP ejected rod worth plus 15% uncertainty remains less than 0.65 %Δk/k.

[d] Includes allowances for ^{10}B atom variations and reactivity anomalies. The BOC HFP critical boron from Table 5-1 is augmented by 111 ppm to account for boron anomaly based on ZPPT acceptance criterion and HFP review criterion (50ppmB for both), B10 receipt tolerance (25 ppmB) and previous cycle shutdown flexibility (36 ppmB).

[e] The EOC Doppler coefficient value used in the steam line break analysis is more negative than, and therefore is bounding for, the cycle 19 Doppler coefficient. However, the steam line break is evaluated based on the EOC temperature coefficient, which considers the combined effects of the temperature decrease on the MTC, Doppler coefficient, control rod worth, boron concentration and moderator density. The analysis value for the EOC temperature coefficient is more negative than, and therefore bounding for, the cycle 19 temperature coefficient.

[f] For the analysis to remain bounding, the cycle-specific value must be ≤ 13.9 %Δk/k.

[g] For the analysis of the Moderator Dilution Accident at Power to remain bounding, the ratios of critical boron concentration to boron reactivity worth, for the safety analysis and for the cycle, must be such that the reactivity insertion rate calculated for the analysis is larger than that calculated for the cycle.

[h] Davis-Besse specific dropped rod accident analyses performed subsequent to the issuance of the Davis-Besse USAR determined that the acceptance criteria for this event are met for dropped rod worths of ≤ 0.28 %Δk/k, which also bounds the cycle 19 value, accounting for a 15% rod worth uncertainty.

[i] Two cycle-specific EOC Doppler coefficients are provided: a maximum value (-1.60×10^{-3} %Δk/k/°F for CRG 7 at 60%WD) and a minimum value (-1.74×10^{-3} %Δk/k/°F for CRG 1-8 at 100%WD).

[j] This value includes a 9% increase for control rod worth uncertainty.

[k] The BOC HFP boron worth from Table 5-1 is augmented by 2.5 ppmB/%Δk/k for B10 receipt tolerance.

Table 7-2 Bounding Values for Allowable LOCA Peak Linear Heat Rates Davis-Besse, Cycle 19

Mark-B-HTP Fuel Type as Analyzed at 3025 MWt [1, 2]
Allowable UO_2 LHR for Specified Burnup, kW/ft

Core Elevation, ft	0 MWd/mtU	34,000 MWd/mtU	62,000 MWd/mtU
0.0	17.8	17.4	13.3
2.506	17.8	17.4	13.3
4.264	17.7	17.3	13.3
6.021	17.0	17.0	13.3
7.779	17.2	16.9	13.3
9.536	16.4	16.5	13.3
12.0	15.6	15.7	12.6

Mark-B-HTP Fuel Type as Analyzed at 3025 MWt [1, 2, 3]
Allowable 4 Weight Percent Gadolinia LHR for Specified Burnup, kW/ft

Core Elevation, ft	0 MWd/mtU	34,000 MWd/mtU	62,000 MWd/mtU
0.0	16.0	15.9	12.0
2.506	16.0	15.9	12.0
4.264	15.9	15.7	12.0
6.021	15.3	15.4	12.0
7.779	15.5	15.4	12.0
9.536	14.8	15.0	12.0
12.0	14.0	14.3	11.4

Mark-B-HTP Fuel Type as Analyzed at 3025 MWt [1, 2, 3]
Allowable 6 Weight Percent Gadolinia LHR for Specified Burnup, kW/ft

Core Elevation, ft	0 MWd/mtU	34,000 MWd/mtU	62,000 MWd/mtU
0.0	15.5	15.6	11.6
2.506	15.5	15.6	11.6
4.264	15.4	15.6	11.6
6.021	14.7	15.3	11.6
7.779	15.0	15.2	11.6
9.536	14.3	14.9	11.6
12.0	13.5	14.2	11.0

Table 7-2 (continued)

Mark-B-HTP Fuel Type as Analyzed at 3025 MWt [1, 2, 3]

Allowable 8 Weight Percent Gadolinia LHR for Specified Burnup, kW/ft

Core Elevation, ft	0 MWd/mtU	34,000 MWd/mtU	62,000 MWd/mtU
0.0	15.1	15.1	11.2
2.506	15.1	15.1	11.2
4.264	15.0	15.1	11.2
6.021	14.4	14.7	11.2
7.779	14.6	14.7	11.2
9.536	13.9	14.4	11.2
12.0	13.2	13.7	10.6

[1] Linear interpolation between burnup points and elevations is permitted to calculate the allowable LHR.

[2] These LHR limits must be reduced by up to 0.2 kW/ft for power levels less than 3025 MWt.

[3] The LHR limits for the Gd_2O_3 fuel are based on percentages of the UO_2 LHR limits to account for the reduction in fuel thermal conductivity.

8.0 PROPOSED CORE OPERATING LIMITS REPORT

The Core Operating Limits Report (COLR) has been revised for cycle 19 operation to accommodate the influence of the cycle 19 core design, which includes the effects of six (6) SSRs in four (4) fuel assemblies, on power peaking, reactivity, and control rod worth. Revisions to the cycle-specific parameters were made in accordance with the requirements of NRC Generic Letter 88-16 and Technical Specification 5.6.3. The core protective and operating limits were determined from a cycle 19-specific power distribution analysis using NRC approved methodology provided in the references of Technical Specification 5.6.3.

A cycle 19-specific analysis was conducted to generate the axial power imbalance protective limits, corresponding power/imbalance/flow trip allowable values, and the Limiting Conditions for Operation (LCO) (rod insertion, axial power imbalance, and quadrant power tilt), based on the NRC-approved methodology described in Reference 1. The regulating group position operating limits, axial power imbalance operating limits, quadrant power tilt operating limits, and APSR position operating limits are provided in the COLR. The rated thermal power level for the cycle 19 design is 2817 MWt. The analysis incorporates departure from nucleate boiling (DNB) maximum allowable peaking limits based on the allowable increase in design (radial x local) peaking provided by the statistical core design (SCD) methodology described in Reference 14. The effects of control rod group 7 and gray APSR repositioning were included explicitly in the analysis. The analysis also determined that the cycle 19 core operating limits provide protection for the overpower condition that could occur during an overcooling transient because of nuclear instrumentation errors. The cycle 19 analysis also determined that the core safety limits are not violated in the event of a dropped or misaligned control rod assembly initiated from within the limits of normal operation.

The analysis verified that the end-of-cycle (EOC) hot full power maneuver is bounded by the safety analysis assumptions, and is accommodated in the core Reactor Protection System (RPS) protective limits and trip allowable values. The maneuver consists of an APSR withdrawal designed to occur at 600 $\pm$ 10 EFPD and a T_{avg} reduction of up to 12°F (analyzed) to extend HFP operation. The EOC T_{avg} reduction has been analyzed for the ROTSGs and is acceptable for use in extending hot full power operation. The xenon stability index after APSR withdrawal was determined to be -0.012793 h^{-1}, which demonstrates the axial stability of the core during operation with the APSRs fully withdrawn.

The maximum allowable loss-of-coolant accident (LOCA) linear heat rate (LHR) limits used in the analysis are based on the Emergency Core Cooling System (ECCS) analysis described in Section 7.3. The large break LOCA (LBLOCA) and small break LOCA (SBLOCA) analyses were based on the approved methods listed in Reference 1 and any changes reported via 50.46 requirements.

As part of determining the core protective and operating limits, an evaluation of margin to the LOCA limits for the individual gadolinia fuel rods was performed. The gadolinia rods were determined to be non-

limiting for LOCA during the entire cycle 19. This evaluation is not required for DNB, transient cladding strain (TCS) or centerline fuel melt (CFM) due to the implementation of the COPERNIC fuel performance code.

Table 8-1 provides the shutdown margin requirements for cycle 19, and Table 8-2 provides the moderator temperature coefficient limits for cycle 19. Table 8-3 provides the Absolute Position Indication (API) and Relative Position Indication (RPI) Agreement Limit for cycle 19, and Table 8-4 provides the power-dependent quadrant power tilt operating limits for cycle 19. Table 8-5 provides the burnup- and elevation-dependent LOCA linear heat rate limits for input to the Fixed Incore Detector Monitoring System (FIDMS). The linear heat rate limits in Table 8-5 are reduced by 0.2 kW/ft compared to those provided in Section 7.3 (Table 7-2). The reduction is reflected in the maneuvering analysis and was made in order to account for the power level dependence of the LOCA kW/ft limits calculated for cycle 19 operation. The linear heat rate limits provided in Table 8-5 are the basis of the F_Q power peaking surveillance limits required by Technical Specification 3.2.5.1.

Table 8-7 and Figure 8-9 provide the cycle 19 $F^N_{\Delta H}$ maximum allowable radial peaking limits (MARPs) to be used in the calculation of the $F^N_{\Delta H}$ factors specified in Table 8-6 for the resident Mark-B-HTP fuel assemblies. They are the basis of the $F^N_{\Delta H}$ power peaking surveillance limits required by Technical Specification 3.2.5.1. The values specified in Tables 8-6 and 8-7 and Figure 8-9 are used by the FIDMS. The family of curves in Figure 8-9 preserves the initial condition DNBR limit in the form of equivalent allowable initial condition peaking for the Mark-B-HTP fuel assemblies. The curves are based on the MARPs provided in Table 8-7. Allowable $F^N_{\Delta H}$ values can be determined based on particular axial peaks at a given axial elevation for either three or four reactor coolant pump operation. The $F^N_{\Delta H}$ relationship defined in Table 8-6 ensures acceptable departure from nucleate boiling ratio (DNBR) performance using SCD methodology in the event of the limiting Condition I and II transient.

The measurement system-independent rod position and axial power imbalance limits determined by the cycle 19 analysis were error adjusted to generate operating limits for power operation. Figures 8-1 and 8-10 are the cycle 19-specific core protective limits and RPS imbalance trip allowable values, respectively. Limiting nuclear instrumentation scaled difference amplifier gains of 2.0 and 5.0 were used as appropriate, to establish these values. Figures 8-2 through 8-5 and Figures 8-7 and 8-8 are revisions to the LCO rod position and axial power imbalance operating limits, respectively, contained in the COLR and have been adjusted for instrument error. Figure 8-6 provides the APSR position operating limits for cycle 19. The axial power imbalance operating limits provided in Figures 8-7 and 8-8 are based on Initial Condition DNB (IC-DNB) allowable peaking limits, the LOCA linear heat rates at maximum allowable power conditions, and the impact of the PSC 7-78 overcooling transient and PSC 15-74 dropped rod/misaligned rod transient. The rod insertion and axial power imbalance operating limits, required by Technical Specification 3.2.1.1, 3.2.1.2, 3.2.2.1 and 3.2.3.1, preserve the F_Q and $F^N_{\Delta H}$ limits for cycle 19.

Volume requirements for the boric acid addition system (BAAS) required by Technical Requirements

Manual 8.1.1, 8.1.2, and Figure 8.1.1-1 were verified to be acceptable for cycle 19. In addition, the minimum boron concentration requirements and boric acid volume storage for the borated water storage tank (BWST) given in Technical Specification 3.5.4 and Technical Requirements Manual 8.1.2 were verified to be acceptable for achieving cold shutdown during cycle 19 operation.

Table 8-8 provides the subcriticality requirement for the minimum refueling boron concentration, and Figure 8-11 provides the control rod core locations and group assignments for cycle 19.

Davis-Besse Unit 1 cycle 19 will be operated in accordance with the safety analysis and applicable power calorimetric measurement uncertainty analysis. The core may be operated at a nominal core power of up to 2817 MWt when the ultrasonic flow measurement system is in operation. The Davis-Besse Unit 1 Technical Requirements Manual (TRM) and procedures specify the appropriate actions to be taken when the ultrasonic flow measurement system is not available. The procedural guidance contains instructions on the power level reductions that are required under circumstances when the ultrasonic flow measurement system is not available or not in service.

Based on the analyses and operating limit revisions described in this report, the Final Acceptance Criteria ECCS limits will not be exceeded, nor will the thermal design criteria be violated provided the plant operates within the constraints specified in the COLR.

Figure 8-1

Figure AXIAL POWER IMBALANCE Protective Limits
2817 MWt RTP, Davis-Besse 1, Cycle 19

This Figure is referred to by
Technical Specification 2.1.1.1

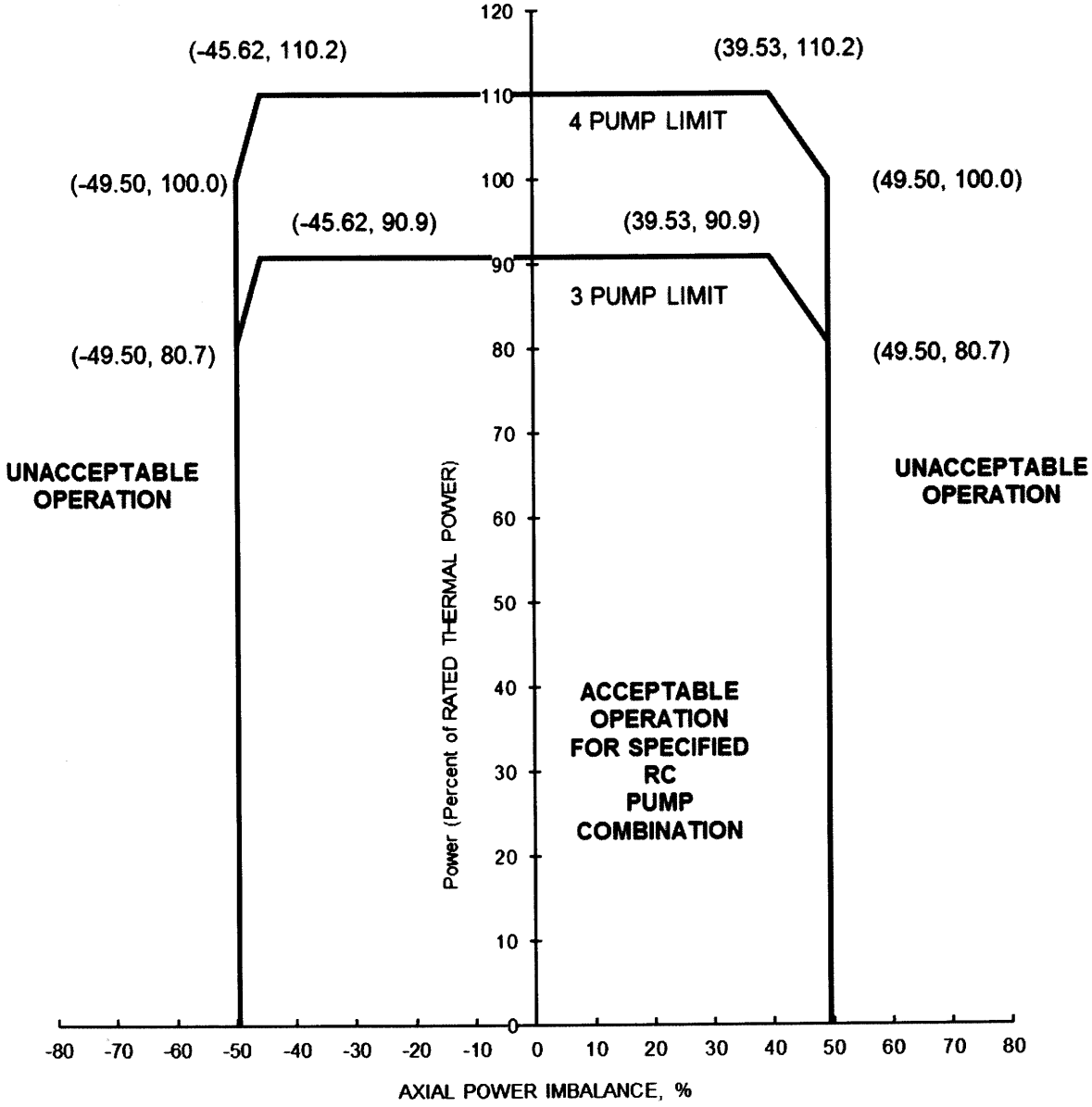

Pumps Operating	Reactor Coolant Flow, gpm	Required Measured Flow to Ensure Compliance, gpm
4	380,000	389,500
3	283,860	290,957

Table 8-1

Table Shutdown Margin Requirements for Davis-Besse, Cycle 19

Verify SHUTDOWN MARGIN per the table below.

APPLICABILITY	REQUIRED SHUTDOWN MARGIN	TECHNICAL SPECIFICATION LCO REFERENCE
MODE 1*	≥ 1 %Δk/k	3.1.4, 3.1.5
MODE 2*	≥ 1 %Δk/k	3.1.4, 3.1.5, 3.3.9
MODE 3	≥ 1 %Δk/k	3.1.1, 3.3.9
MODE 4	≥ 1 %Δk/k	3.1.1, 3.3.9
MODE 5	≥ 1 %Δk/k	3.1.1, 3.3.9
MODE 1 PHYSICS TESTS Exceptions**	≥ 1 %Δk/k	3.1.8
MODE 2 PHYSICS TESTS Exceptions	≥ 1 %Δk/k	3.1.9

* The required Shutdown Margin capability of 1%Δk/k in MODE 1 and MODE 2 is preserved by the Regulating Rod Insertion Limits specified in Figures 8-2 through 8-5 as required by Technical Specification 3.2.1.

** Entry into Mode 1 Physics Tests Exceptions is not supported by existing analyses. For example, Regulating Rod Shutdown Margin Insertion Limits assumptions may not be met and as such requires actual shutdown margin to be ≥ 1 %Δk/k via alternate verification or calculation.

Table 8-2

Table Moderator Temperature Coefficient Limit Davis-Besse, Cycle 19

These limits are referred to by Technical Specification 3.1.3

1. Lower Limit:

   MTC at HFP ≥ -3.54×10^{-4} Δk/k/°F

2. The following Upper Limits may not be exceeded without prior NRC approval:

   MTC $< 0.9 \times 10^{-4}$ Δk/k/°F when Thermal Power <95% RTP

   MTC $< 0.0 \times 10^{-4}$ Δk/k/°F when Thermal Power ≥95% RTP

3. The following Upper Limits may not be exceeded for operation in Modes 1 and 2:

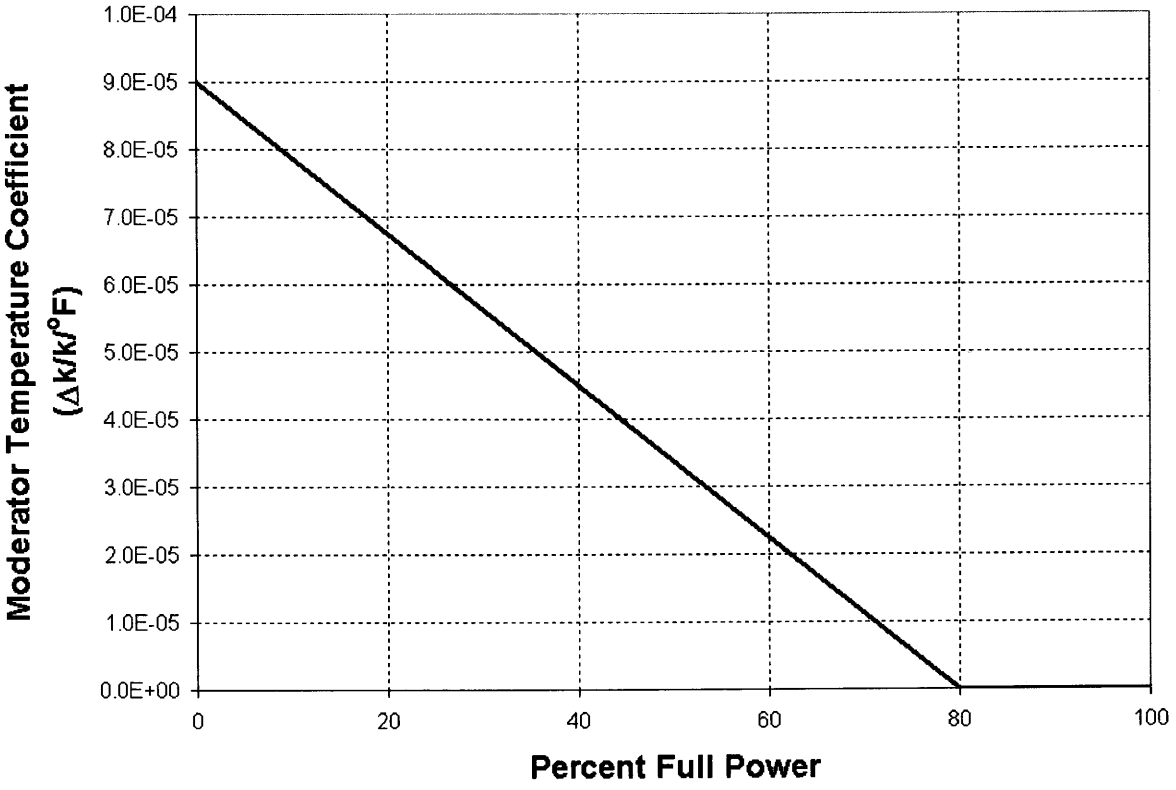

Table 8-3

Table Absolute Position Indicator (API) / Relative Position Indicator (RPI) Agreement Limit for Davis-Besse, Cycle 19

This limit is referred to by Technical Specification 3.1.7

The absolute position indicator channels and the relative position indicator channels agree within 3.46%.

Figure 8-2

Figure Regulating Group Position Operating Limits
0 to 300 ±10 EFPD, Four RC Pumps--2817 MWt RTP
Davis-Besse 1, Cycle 19

This Figure is referred to by Technical Specifications 3.2.1

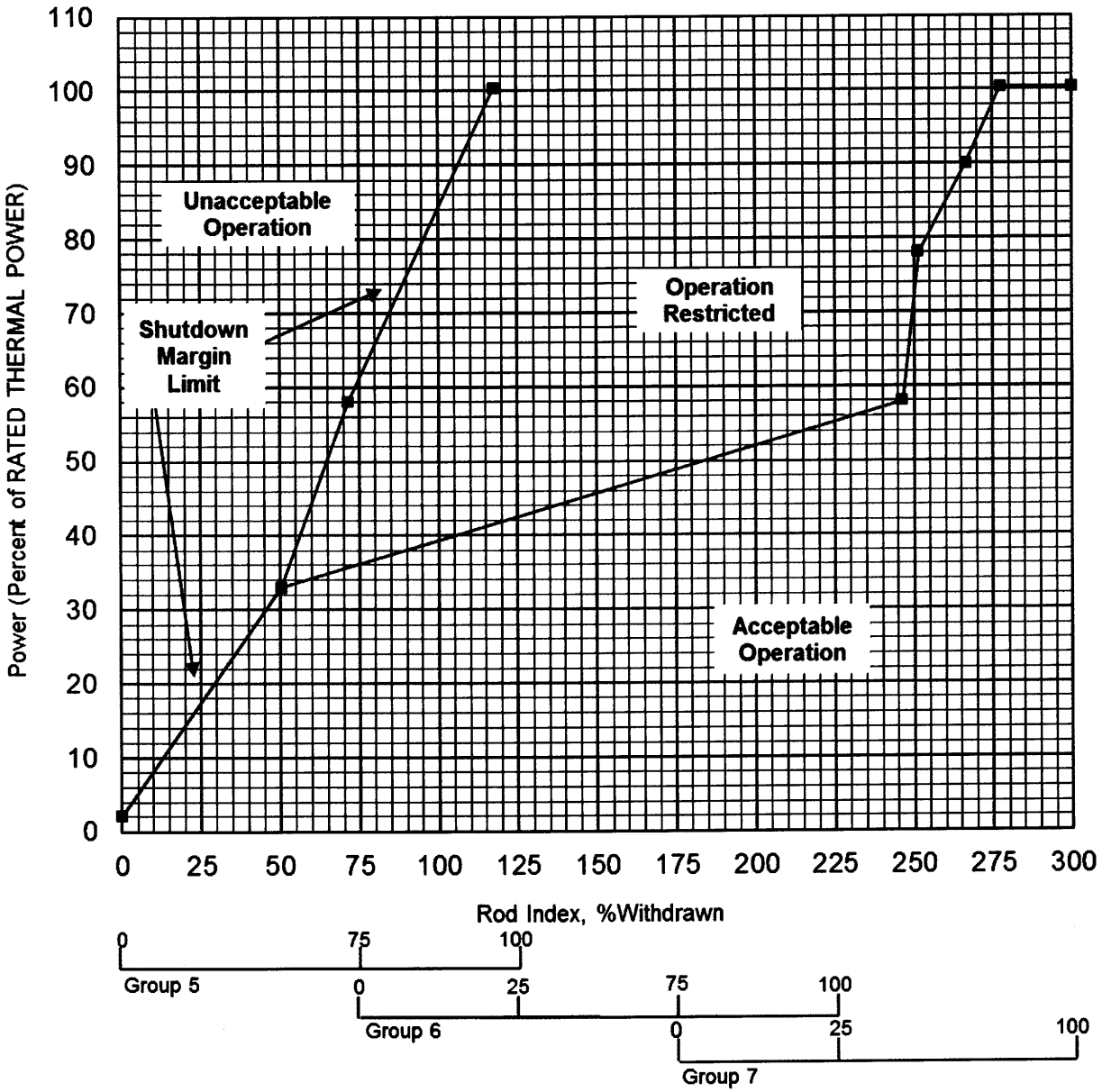

Note 1: A Rod Group overlap of 25 +/- 5% between sequential withdrawn groups 5 and 6, and 6 and 7, shall be maintained.
Note 2: Instrument error is accounted for in these Operating Limits.
Note 3: Maximum plotted power level is 100.37 %RTP.

Figure 8-3

Figure Regulating Group Position Operating Limits
After 300 ±10 EFPD, Four RC Pumps--2817 MWt RTP
Davis-Besse 1, Cycle 19

This Figure is referred to by Technical Specifications 3.2.1

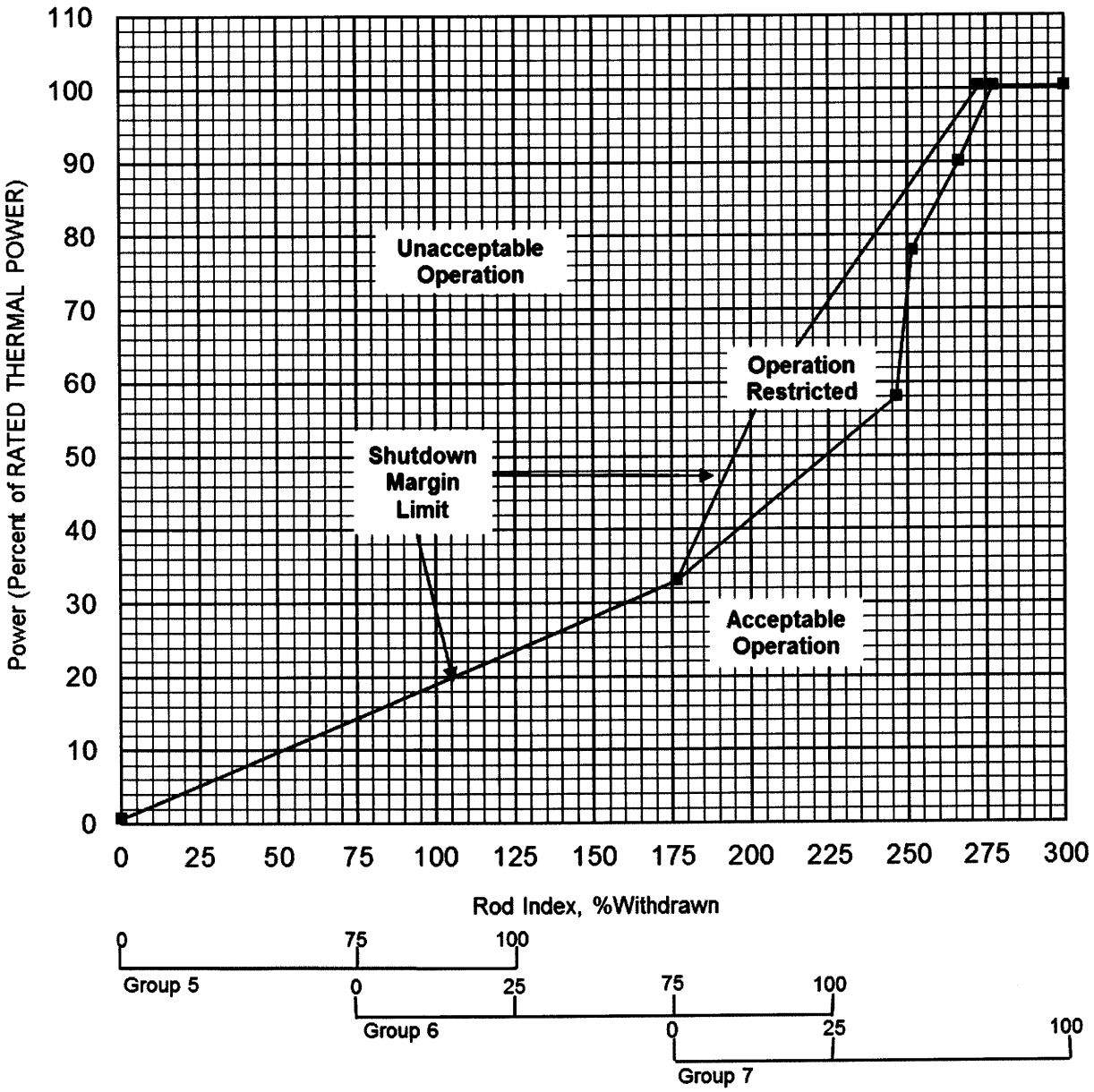

Note 1: A Rod Group overlap of 25 ±5% between sequential withdrawn groups 5 and 6, and 6 and 7, shall be maintained.
Note 2: Instrument error is accounted for in these Operating Limits.
Note 3: Maximum plotted power level is 100.37 %RTP.

Figure 8-4

Figure Regulating Group Position Operating Limits
0 to 300 ±10 EFPD, Three RC Pumps--2817 MWt RTP
Davis-Besse 1, Cycle 19

This Figure is referred to by Technical Specifications 3.2.1

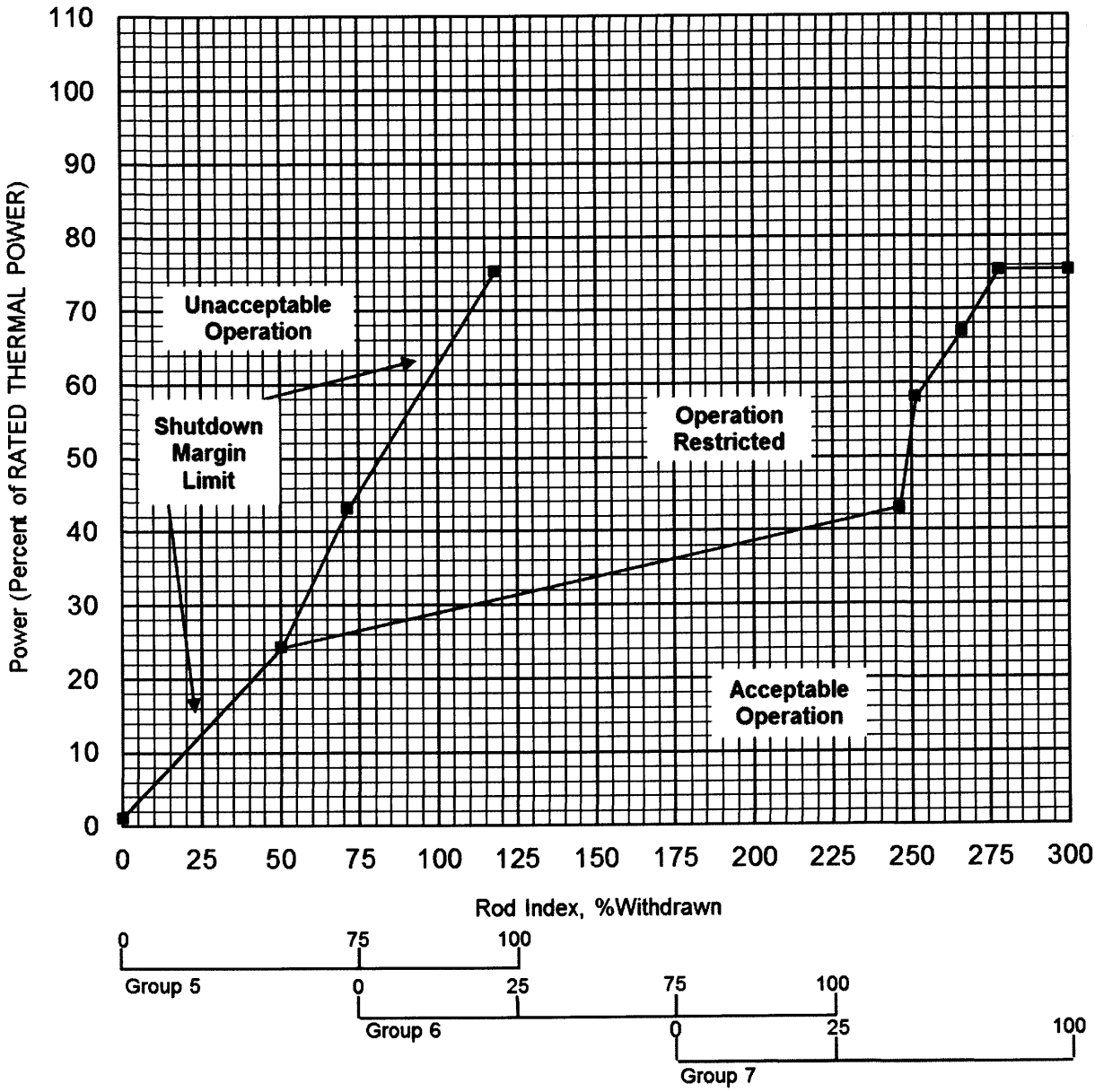

Note 1: A Rod Group overlap of 25 +/- 5% between sequential withdrawn groups 5 and 6, and 6 and 7, shall be maintained.
Note 2: Instrument error is accounted for in these Operating Limits.
Note 3: Maximum plotted power level is 75.37 %RTP.

Figure 8-5

Figure Regulating Group Position Operating Limits
After 300 ±10 EFPD, Three RC Pumps--2817 MWt RTP
Davis-Besse 1, Cycle 19

This Figure is referred to by Technical Specifications 3.2.1

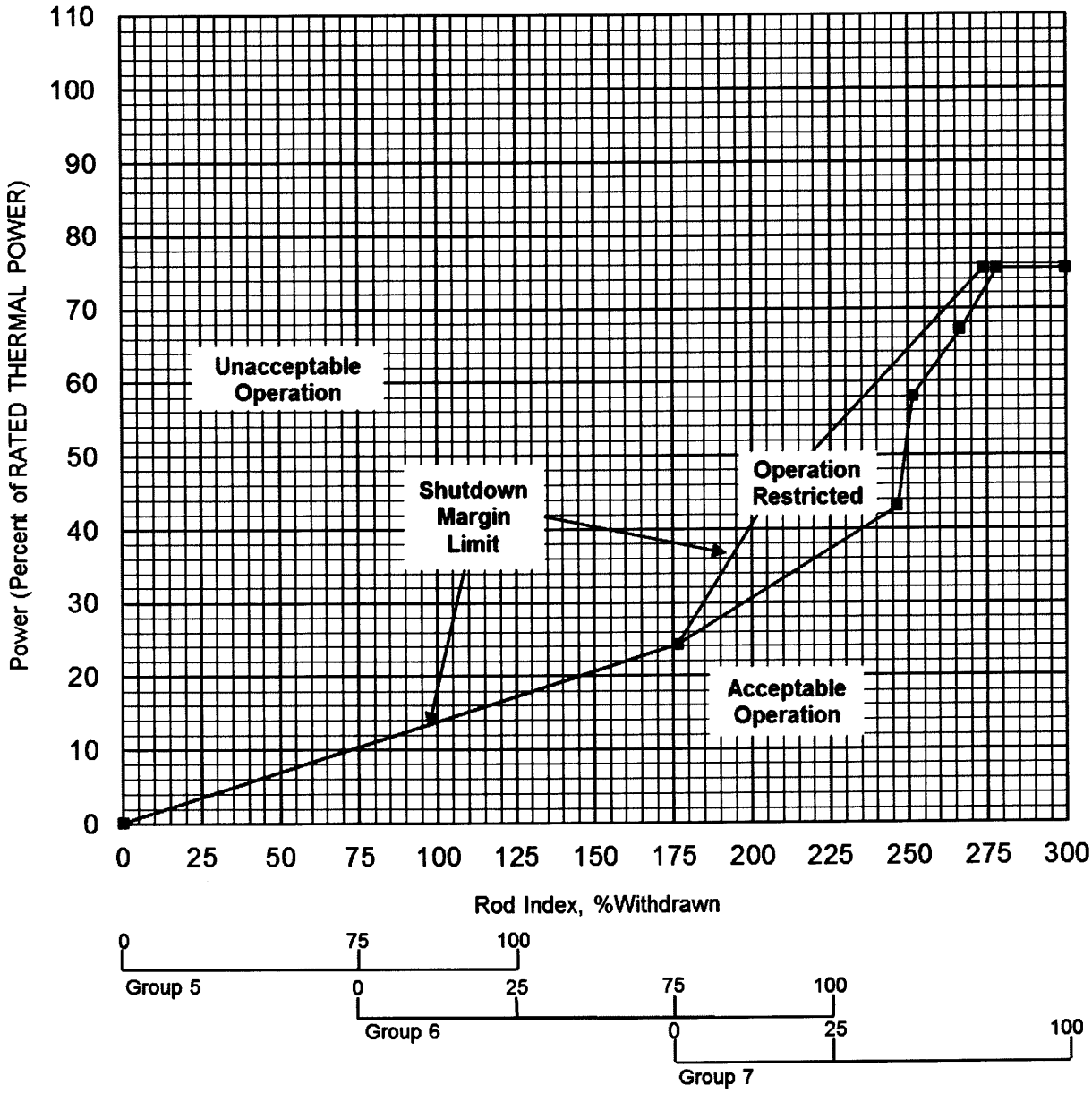

Note 1: A Rod Group overlap of 25 ±5% between sequential withdrawn groups 5 and 6, and 6 and 7, shall be maintained.
Note 2: Instrument error is accounted for in these Operating Limits.
Note 3: Maximum plotted power level is 75.37 %RTP.

Figure 8-6

Figure APSR Position Operating Limits—2817 MWt RTP Davis-Besse, Cycle 19

This Figure is referred to by Technical Specification 3.2.2

Before APSR Pull: 0 EFPD to 600 ± 10 EFPD,
Three or Four RC pumps operation*

Lower Limit: 0 %WD

Upper Limit: 100 %WD

After APSR Pull: 600 ± 10 EFPD to End-of-Cycle
Three or Four RC pumps operation*

Insertion Prohibited (maintain ≥ 99%WD)**

*** Power restricted to 75.37 %RTP for 3-pump operation**

****Reinsertion is allowed only during the end of cycle shutdown when the reactor power is equal to, or less than, 30%RTP**

Figure 8-7

Figure AXIAL POWER IMBALANCE Operating Limits
0 EFPD to EOC, Four RC Pumps--2817 MWt RTP
Davis-Besse 1, Cycle 19

This Figure is referred to by
Technical Specification 3.2.3

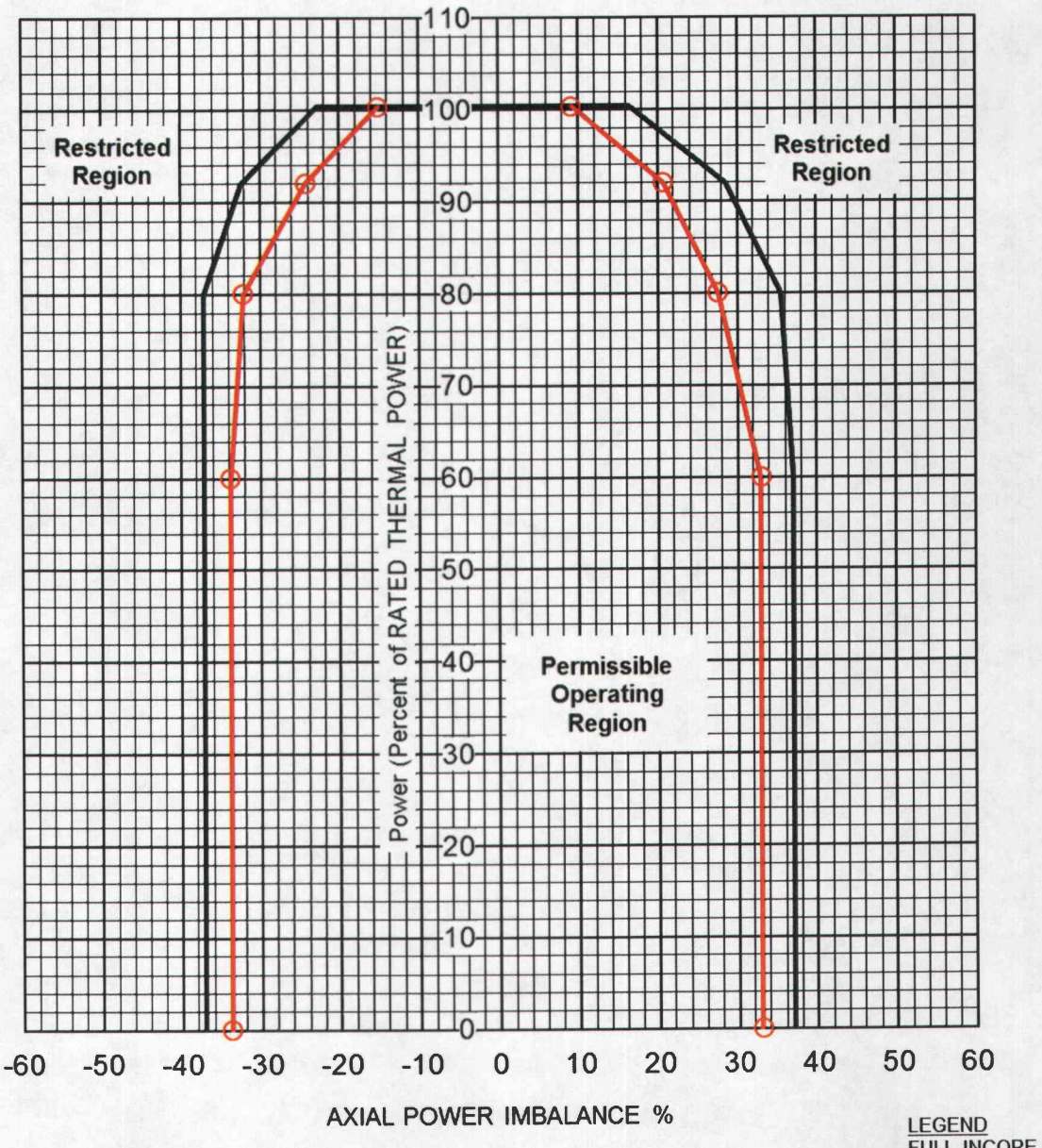

Note 1: Instrument error is accounted for in these Operating Limits.
Note 2: The Excore Imbalance Operating Limits are available for use when the Full Incore system is non-functional.
Note 3: Maximum plotted power level is 100.37 %RTP.

Figure 8-8

Figure AXIAL POWER IMBALANCE Operating Limits
0 EFPD to EOC, Three RC Pumps–2817 MWt RTP
Davis-Besse 1, Cycle 19

This Figure is referred to by
Technical Specification 3.2.3

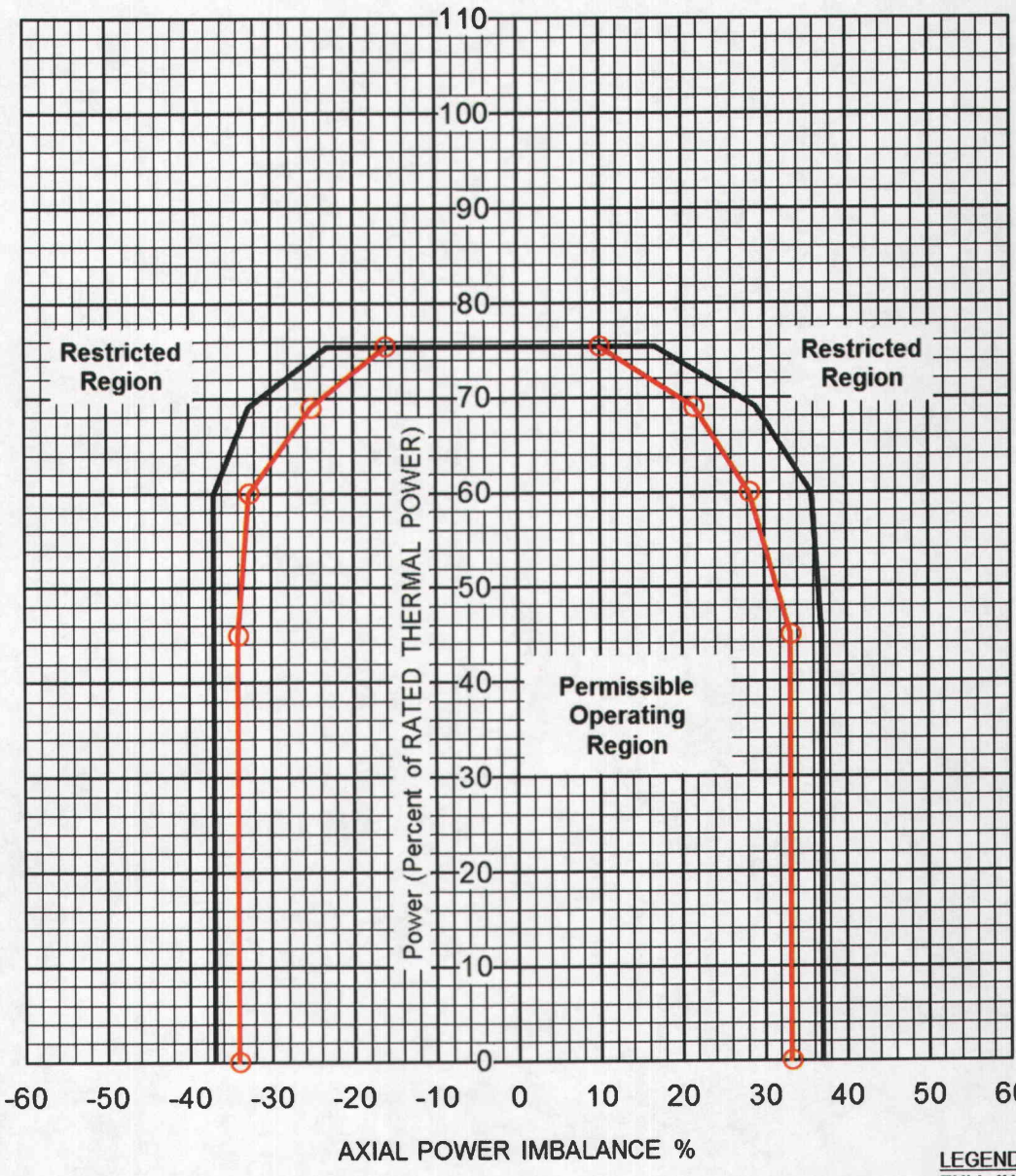

Note 1: Instrument error is accounted for in these Operating Limits.
Note 2: The Excore Imbalance Operating Limits are available for use when the Full Incore system is non-functional.
Note 3: Maximum plotted power level is 75.37 %RTP.

Table 8-4

Table QUADRANT POWER TILT Operating Limits—2817 MWt RTP, Davis-Besse, Cycle 19

This Table is referred to by Technical Specification 3.2.4

QUADRANT POWER TILT as measured by:	From 0 EFPD to EOC-19			
	Steady-state Limit for THERMAL POWER ≤ 60% (%)	Steady-state Limit for THERMAL POWER > 60% (%)	Transient Limit (%)	Maximum Limit (%)
Symmetric Incore Detector System	7.90	3.90	10.03	20.00

Table 8-5

Table Power Peaking Factors - F_Q Davis-Besse, Cycle 19

This Table is referred to by Technical Specification 3.2.5

The measured F_Q shall be increased by 1.4% to account for manufacturing tolerances and further increased by 7.5% to account for measurement uncertainty before comparing to the limits.

Heat Flux Hot Channel Factor F_Q

F_Q shall be limited by the following relationships:

$F_Q \leq LHR^{allow}$ (Bu) / [LHR^{avg} * P] (for P ≤ 1.0)

LHR^{allow} (Bu) = See the following tables

LHR^{avg} = 6.4209 kW/ft at 2817 MWt for Batches 18, 19, 20 and 21 Mark-B-HTP fuel

P = ratio of THERMAL POWER / RATED THERMAL POWER (current fraction of power)

Bu = fuel burnup (MWd/mtU)

UO_2 Fuel (Mark-B-HTP) – All Batches LHR^{ALLOW} kW/ft[(a)]

Core Elevation (ft)	0 MWd/mtU	34,000 MWd/mtU	62,000 MWd/mtU
0	17.6	17.2	13.1
2.506	17.6	17.2	13.1
4.264	17.5	17.1	13.1
6.021	16.8	16.8	13.1
7.779	17.0	16.7	13.1
9.536	16.2	16.3	13.1
12.000	15.4	15.5	12.4

(a) Linear interpolation for allowable LHR between specified burnup points is valid for these tables.

Table 8-5 (continued)

4 wt% Gad Fuel (Mark-B-HTP) – All Batches except 21B LHR^{ALLOW} kW/ft[(a)]

Core Elevation (ft)	0 MWd/mtU	34,000 MWd/mtU	62,000 MWd/mtU
0	15.8	15.7	11.8
2.506	15.8	15.7	11.8
4.264	15.7	15.5	11.8
6.021	15.1	15.2	11.8
7.779	15.3	15.2	11.8
9.536	14.6	14.8	11.8
12.000	13.8	14.1	11.2

6 wt% Gad Fuel (Mark-B-HTP) – Batch 20C and 21B LHR^{ALLOW} kW/ft[(a)]

Core Elevation (ft)	0 MWd/mtU	34,000 MWd/mtU	62,000 MWd/mtU
0	15.3	15.4	11.4
2.506	15.3	15.4	11.4
4.264	15.2	15.4	11.4
6.021	14.5	15.1	11.4
7.779	14.8	15.0	11.4
9.536	14.1	14.7	11.4
12.000	13.3	14.0	10.8

8 wt% Gad Fuel (Mark-B-HTP) – Batches 18A5, 19C2, 20A, 21A, 21B and 21E LHR^{ALLOW} kW/ft[(a)]

Core Elevation (ft)	0 MWd/mtU	34,000 MWd/mtU	62,000 MWd/mtU
0	14.9	14.9	11.0
2.506	14.9	14.9	11.0
4.264	14.8	14.9	11.0
6.021	14.2	14.5	11.0
7.779	14.4	14.5	11.0
9.536	13.7	14.2	11.0
12.000	13.0	13.5	10.4

[(a)] Linear interpolation for allowable LHR between specified burnup points is valid for these tables.

Table 8-6

Table Power Peaking Factors - $F^N_{\Delta H}$ Davis-Besse, Cycle 19

This Table is referred
to by Technical Specification 3.2.5

Enthalpy Rise Hot Channel Factors - $F^N_{\Delta H}$

$F^N_{\Delta H} \leq MARP\ [1 + (1/RH)\ (1 - P/P_m)]$ (see note below)

MARP = Maximum Allowable Radial Peak, see MARP Figures and data Tables

P = THERMAL POWER / RATED THERMAL POWER and $P \leq 1.0$

P_m = 1.0 for 4-RCP operation

P_m = 0.75 for 3-RCP operation

1/RH = 0.3

Note: The measured $F^N_{\Delta H}$ shall be increased by 5.0% to account for measurement uncertainty prior to comparing to the limits.

Figure 8-9

Figure Maximum Allowable Radial Peak for $F^N_{\Delta H}$ Davis-Besse, Cycle 19

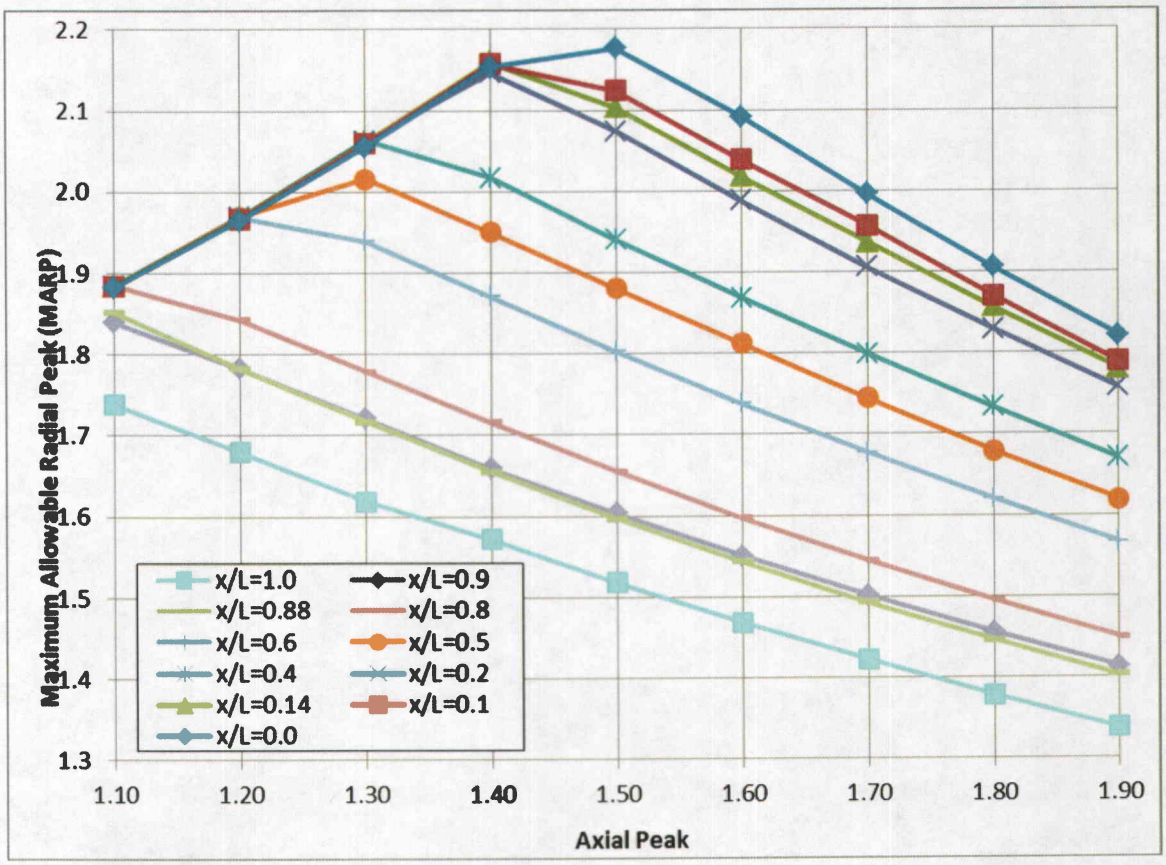

Linear interpolation is acceptable.

Table 8-7

Table Maximum Allowable Radial Peak for $F^N_{\Delta H}$ Davis-Besse, Cycle 19

Axial Peak	x/L	Axial Height (inches)	MARP Limit	Axial Peak	x/L	Axial Height (inches)	MARP Limit
	0.0	0.00	1.88299		0.0	0.00	2.09189
	0.1	14.30	1.88398		0.1	14.30	2.03919
	0.14	20.02	1.88428		0.14	20.02	2.01827
	0.2	28.60	1.88461		0.2	28.60	1.98801
	0.4	57.20	1.88490		0.4	57.20	1.86840
1.1	0.5	71.50	1.88439	1.6	0.5	71.50	1.81257
	0.6	85.80	1.88451		0.6	85.80	1.73794
	0.8	114.40	1.88421		0.8	114.40	1.59754
	0.88	125.84	1.85239		0.88	125.84	1.54331
	0.9	128.70	1.83969		0.9	128.70	1.55084
	1.0	143.00	1.73842		1.0	143.00	1.46874
	0.0	0.00	1.96511		0.0	0.00	1.99604
	0.1	14.30	1.96705		0.1	14.30	1.95702
	0.14	20.02	1.96804		0.14	20.02	1.93661
	0.2	28.60	1.96825		0.2	28.60	1.90615
	0.4	57.20	1.96936		0.4	57.20	1.79933
1.2	0.5	71.50	1.96984	1.7	0.5	71.50	1.74468
	0.6	85.80	1.96919		0.6	85.80	1.67736
	0.8	114.40	1.84278		0.8	114.40	1.54415
	0.88	125.84	1.78287		0.88	125.84	1.49299
	0.9	128.70	1.78220		0.9	128.70	1.50138
	1.0	143.00	1.67994		1.0	143.00	1.42245
	0.0	0.00	2.05580		0.0	0.00	1.90606
	0.1	14.30	2.05912		0.1	14.30	1.87049
	0.14	20.02	2.06036		0.14	20.02	1.85710
	0.2	28.60	2.06155		0.2	28.60	1.82954
	0.4	57.20	2.06343		0.4	57.20	1.73365
1.3	0.5	71.50	2.01583	1.8	0.5	71.50	1.67902
	0.6	85.80	1.93900		0.6	85.80	1.62023
	0.8	114.40	1.77864		0.8	114.40	1.49550
	0.88	125.84	1.71670		0.88	125.84	1.44607
	0.9	128.70	1.72105		0.9	128.70	1.45590
	1.0	143.00	1.61890		1.0	143.00	1.37861
	0.0	0.00	2.15314		0.0	0.00	1.82131
	0.1	14.30	2.15758		0.1	14.30	1.78903
	0.14	20.02	2.15910		0.14	20.02	1.78024
	0.2	28.60	2.14648		0.2	28.60	1.75713
	0.4	57.20	2.01712		0.4	57.20	1.67040
1.4	0.5	71.50	1.95015	1.9	0.5	71.50	1.61847
	0.6	85.80	1.87083		0.6	85.80	1.56653
	0.8	114.40	1.71630		0.8	114.40	1.44958
	0.88	125.84	1.65545		0.88	125.84	1.40281
	0.9	128.70	1.65903		0.9	128.70	1.41322
	1.0	143.00	1.57207		1.0	143.00	1.33783
	0.0	0.00	2.17667				
	0.1	14.30	2.12413				
	0.14	20.02	2.10403				
	0.2	28.60	2.07451				
	0.4	57.20	1.94104				
1.5	0.5	71.50	1.88067				
	0.6	85.80	1.80330				
	0.8	114.40	1.65555				
	0.88	125.84	1.59706				
	0.9	128.70	1.60415				
	1.0	143.00	1.51859				

Figure 8-10

Figure Flux-ΔFlux-Flow
(or Power/Imbalance/Flow)
Allowable Values--2817 MWt RTP,
Davis-Besse 1, Cycle 19

This Figure is referred to by Technical Specification 3.3.1

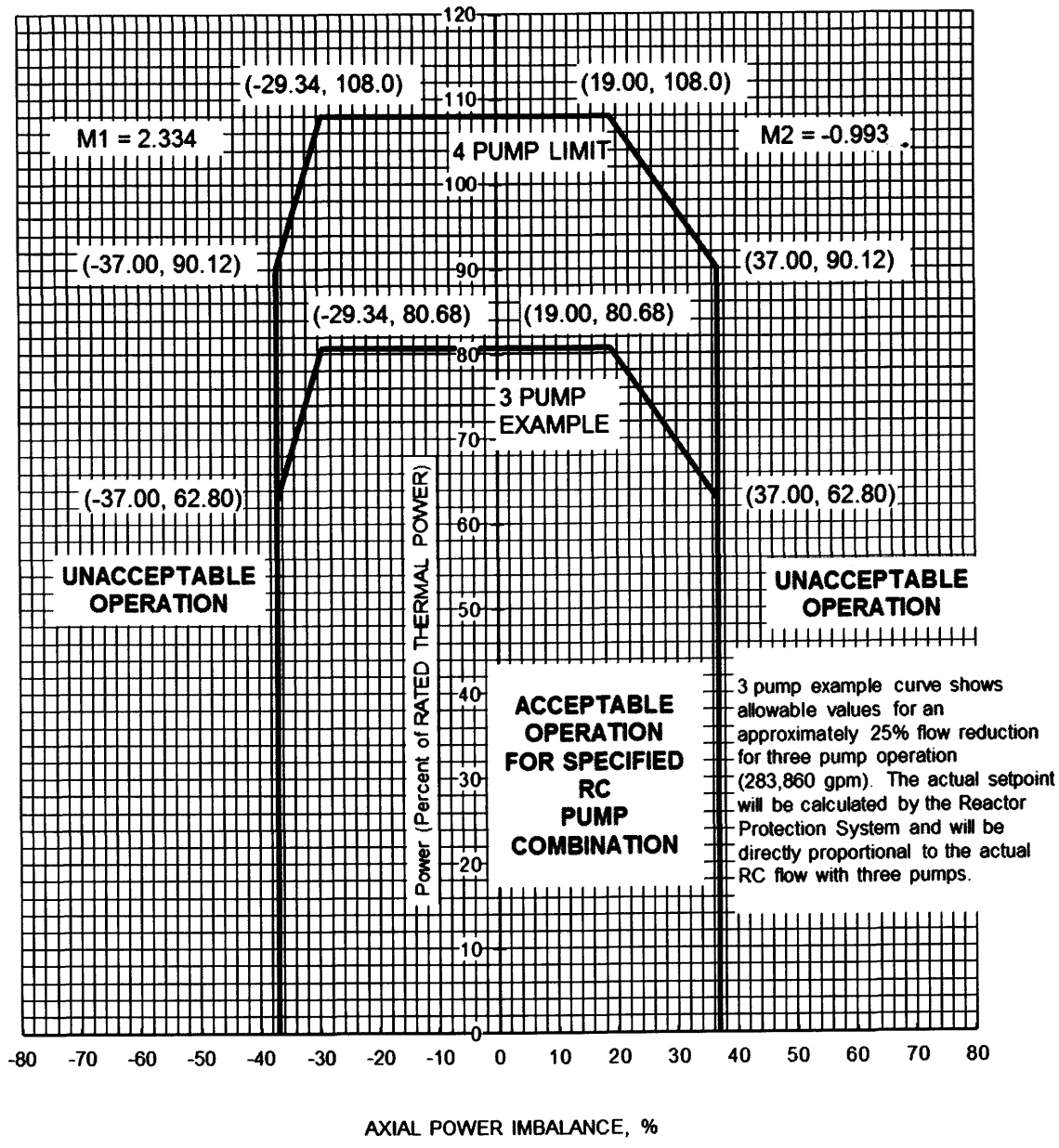

Table 8-8

Table Refueling Boron Concentration Limit for Davis-Besse, Cycle 19

This limit is referred to by Technical Specification 3.9.1

The minimum required boron concentration for Mode 6 shall be sufficient to ensure a K_{eff} of 0.95 or less, plus an additional 1% $\Delta k/k$ conservatism allowance for uncertainties.

Figure 8-11

Figure Control Rod Core Locations and Group Assignments
Davis-Besse, Cycle 19

This Figure is referred to by the
Technical Requirements Manual 8.1.3

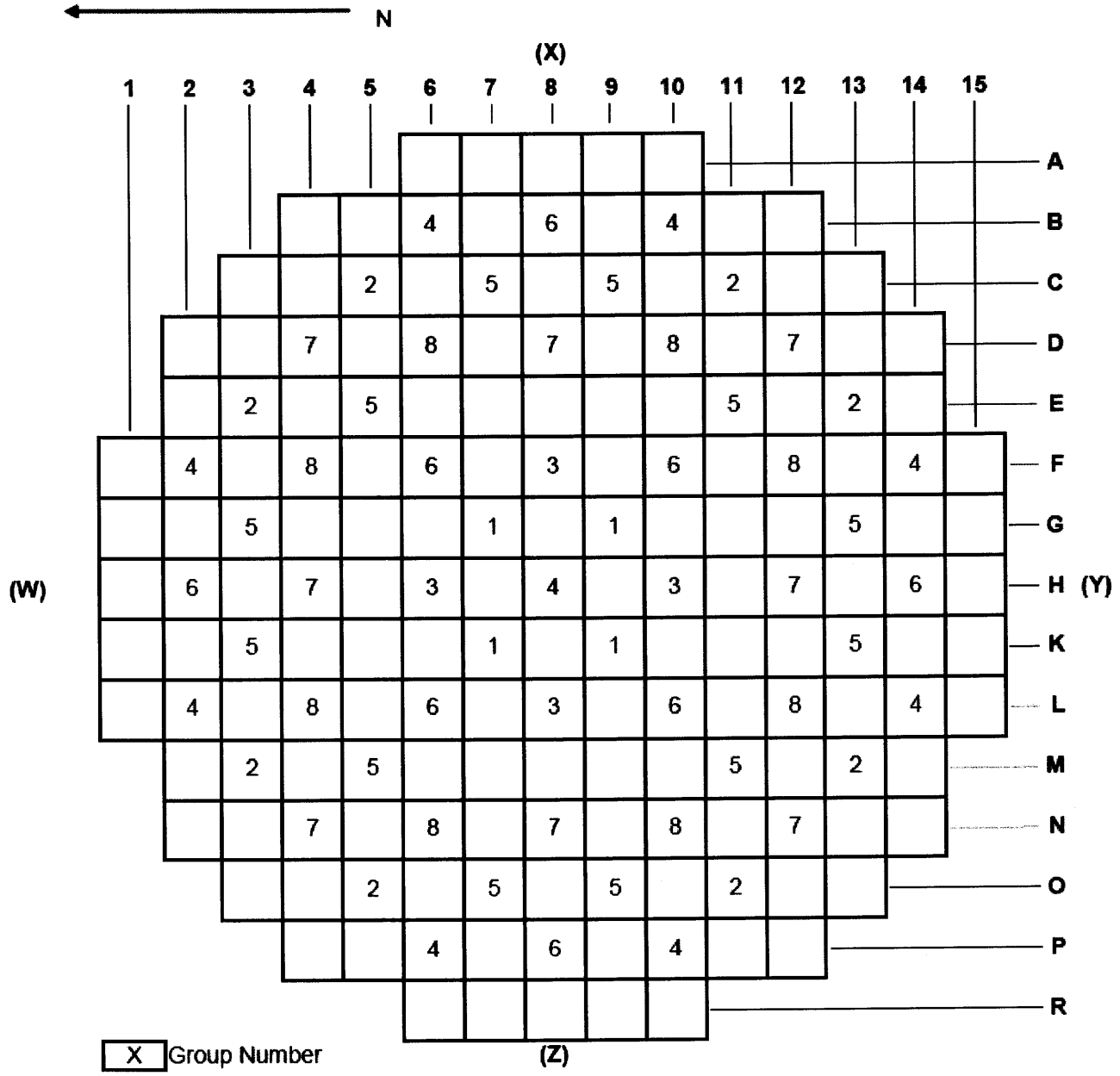

Group	No. of Rods	Function
1	4	Safety
2	8	Safety
3	4	Safety
4	9	Safety
5	12	Control
6	8	Control
7	8	Control
8	8	APSRs
Total	61	

9.0 STARTUP PROGRAM - PHYSICS TESTING

The planned startup test program associated with core performance is outlined below. These tests verify that core performance is within the assumptions of the safety analysis and provide information for continued safe operation of the unit. Reference 21 provides the guidance for the testing.

9.1 Precritical Tests

9.1.1 Control Rod Trip Test

Precritical control rod drop times are recorded for all control rods at hot full-flow conditions before zero power physics testing begins. Acceptance criteria state that the rod drop time from fully withdrawn to 75% inserted shall be less than or equal to 1.58 seconds at the conditions above.

It should be noted that safety analysis calculations are based on a rod drop from fully withdrawn to two-thirds inserted. Since the most accurate position indication is obtained from the zone reference switch at the 75% inserted position, this position is used instead of the two-thirds inserted position for data gathering.

9.1.2 RC Flow

Reactor coolant flow with four reactor coolant pumps running will be measured at hot standby conditions. The measured flow shall be within allowable limits.

9.2 Zero Power Physics Tests

9.2.1 Critical Boron Concentration

Once initial criticality is achieved, equilibrium boron is obtained and the critical boron concentration determined. The critical boron concentration is calculated by correcting for any inserted rod worth and/or control rod withdrawal required to obtain an all rods out equilibrium boron. The acceptance criterion placed on critical boron concentration is that the actual boron concentration shall be within $\pm$ 50 ppm boron of the predicted value. An additional review criterion of $\pm$ 45 ppm is applied if any predicted control rod group (CRG) worth is used to correct the measured critical boron concentration to appropriate conditions corresponding to the predicted value.

9.2.2 Temperature Reactivity Coefficient

The isothermal hot zero power (HZP) temperature coefficient is measured at approximately the all-rods-out configuration. During changes in temperature, reactivity feedback may be compensated by control rod movement. The change in reactivity is then calculated by the summation of reactivity associated with the temperature change. The acceptance criterion for the temperature coefficient is that the measured value shall not differ from the predicted value by more than $\pm$ 0.2 x 10^{-2} $\%\Delta k/k/^{\circ}F$.

The moderator temperature coefficient (MTC) of reactivity is calculated in conjunction with the

temperature coefficient measurement. After the temperature coefficient has been measured, a predicted value of fuel Doppler coefficient of reactivity is subtracted to obtain the MTC. This value shall be less than + 0.9 x 10^{-2} %Δk/k/°F. The MTC is also extrapolated to full power conditions, and is then compared to the appropriate hot full power (HFP) limit.

9.2.3 Control Rod Group/Boron Reactivity Worth

Individual CRG reactivity worths (CRG 6 and 7) are measured at HZP conditions using the boron/rod swap method. CRG 5 is required to be tested if the CRG 6 and 7 measured worth acceptance criteria are not met, or if new control rods are placed in CRG 5. If a control rod has previously been operated in any location, it is not required to be measured when shuffled to a CRG 5 location. In all cases, CRG 5 worth may be measured when deemed prudent by plant personnel.

This technique consists of deborating the reactor coolant system and compensating for the reactivity changes from this deboration by inserting individual CRGs 7 and 6 (and 5 if measured) in incremental steps. The reactivity changes that occur during these measurements are calculated based on reactimeter data, and incremental rod worths are obtained from the measured reactivity worth versus the change in rod group position. The incremental rod worths of each of the controlling groups are then summed to obtain integral rod group worths. Note that the integral rod group worth for group 7 may not include the entire group worth. The initial critical conditions obtained may result in a partial measurement of group 7 worth; however, the measured value will always be matched with an appropriate predicted value. The acceptance criteria for the control rod group worths are as follows:

1. Individual group 6 & 7 (and 5 if measured) worth:

$$\left|\frac{\text{predicted value - measured value}}{\text{predicted value}}\right| \times 100\% \text{ shall be} \leq 15\%$$

2. Sum of groups 6 and 7 (and 5 if measured) worth:

$$\frac{\text{predicted value - measured value}}{\text{predicted value}} \times 100\% \text{ shall be} \leq 6\% \text{ and} \geq -9\%$$

The predicted rod worths are taken from the Automated Testing and Operations Manual (ATOM).

9.3 Power Escalation Tests

9.3.1 Core Symmetry Test

The purpose of this test is to evaluate the symmetry of the core at low power during the initial power escalation following a refueling. Symmetry evaluation is based on incore quadrant power tilts during escalation to the intermediate power level. The absolute values of the quadrant power tilts should be less than the Core Operating Limits Report (COLR) limit.

9.3.2 Core Power Distribution Verification at Intermediate Power Level (IPL) and ~100% FP

Core power distribution tests are performed at the intermediate power level (IPL) and approximately 100% full power (FP). Equilibrium xenon is established prior to the ~100% FP test. The test at the IPL (40–80 %FP) is essentially a check of the power distribution in the core to identify any abnormalities before escalating to the ~100% FP plateau. Peaking factor criteria are applied to the IPL core power distribution results to determine if additional tests or analyses are required prior to ~100% FP operation.

The following acceptance criteria are placed on the IPL and ~100% FP tests:

1. The maximum F_Q values shall not exceed the limits specified in the COLR.
2. The maximum $F^N_{\Delta H}$ value shall not exceed the limits specified in the COLR.
3. The measured radial (assembly) peaks for each 1/8 core fresh fuel location and any limiting burned fuel location shall be within the following limits:

$$\frac{\text{predicted value - measured value}}{\text{predicted value}} \times 100\% \text{ more positive than } -3.8\%$$

4. The measured total (segment) peaks for each 1/8 core fresh fuel location and any limiting burned fuel location shall be within the following limits:

$$\frac{\text{predicted value - measured value}}{\text{predicted value}} \times 100\% \text{ more positive than } -4.8\%$$

The following review criteria also apply to the core power distribution results at the IPL and at ~100% FP.

5. The 1/8 core RMS of the differences between predicted and measured radial (assembly) peaking factors should be less than 0.05.
6. For all 1/8 core locations, the (absolute) difference between predicted and measured radial (assembly) peaking factors should be less than 0.10.

Items 1 and 2 ensure that the initial condition limits are maintained at the IPL and ~100% FP.

Items 3 and 4 are established to determine if measured and predicted power distributions are within allowable tolerances assumed in the reload analysis.

Items 5 and 6 are review criteria, established to determine if measured and predicted power distributions are consistent.

9.3.3 Incore vs. Excore Detector Imbalance Correlation Verification

Imbalances, set up in the core by control rod positioning, are read simultaneously on the incore detectors and excore power range detectors. The excore detector offset versus incore detector offset slope shall be greater than 0.96 for the six-point method and 0.98 for the three-point method, and the y-intercept (excore offset) shall be between -2.5% and 2.5%. If either of these criteria is not met, gain amplifiers on

the excore detector signal processing equipment are adjusted to provide the required slope and/or intercept. The maximum power level for the Power Imbalance Detector Correlation (PIDC) test for +/-100% offset is 71% RTP for 4 pump operation and 61% RTP for 3 pump operation.

9.3.4 Hot Full Power All Rods Out Critical Boron Concentration

The HFP all rods out critical boron concentration (AROCBC) is determined at ~100% FP by first recording the reactor coolant system boron concentration during equilibrium, steady state conditions. Corrections to the measured reactor coolant system boron concentration are made for CRG insertion and power deficit (if not at 100% FP) using predicted data for CRG worth, power Doppler coefficient, and differential boron worth. The review criterion placed on the HFP AROCBC is that the measured AROCBC should be within $\pm$ 50 ppm boron of the predicted value. In addition, the predicted AROCBC at HFP is compared to the measured value at HFP AROCBC to obtain the HFP delta. This HFP delta is then compared to the difference between the predicted and measured HZP AROCBC values (HZP delta). The acceptance criterion stipulates that the HFP delta shall be within $\pm$ 75 ppm boron of the HZP delta.

9.4 Procedure for Use if Acceptance/Review Criteria Not Met

If an acceptance criterion ("shall" as opposed to "should") for any test is not met, an evaluation is performed before continued testing at a higher power plateau is allowed. This evaluation is performed by site test personnel with participation by AREVA technical personnel as required. Further specific actions depend on evaluation results. These actions can include repeating the tests with more detailed test prerequisites and/or steps, added tests to search for anomalies, or design personnel performing detailed analyses of potential safety problems because of parameter deviation. Power is not escalated until evaluation shows that plant safety will not be compromised by such escalation.

If a review criterion ("should" as opposed to "shall") for any test is not met, an evaluation is recommended before continued testing at a higher power plateau. This evaluation is similar to that performed to address failure of an acceptance criterion.

10.0 REFERENCES

1. Safety Criteria and Methodology for Acceptable Cycle Reload Analyses, BAW-10179P-A, Rev. 8, Framatome ANP, Lynchburg, Virginia, dated May 2010.

2. Davis-Besse Nuclear Power Station No. 1, Updated Safety Analysis Report, Docket No. 50-346.

3. Davis-Besse Nuclear Power Station Unit 1, Cycle 18 – Reload Report, ANP-3094, Rev. 0, AREVA NP Inc., Lynchburg, Virginia, dated May 2012.

4. TACO3: Fuel Pin Thermal Analysis Computer Code, BAW-10162P-A, B&W Fuel Company, Lynchburg, Virginia, dated October 1989.

5. Program to Determine In-Reactor Performance of BWFC Fuel Cladding Creep Collapse, BAW-10084P-A, Rev. 3, B&W Fuel Company, Lynchburg, Virginia, dated July 1995.

6. Evaluation of Advanced Cladding and Structural Material (M5®) in PWR Reactor Fuel, BAW-10227P-A, Rev. 1, Framatome Cogema Fuels, Lynchburg, Virginia, dated June 2003.

7. Extended Burnup Evaluation, BAW-10186P-A, Rev. 2, Framatome Cogema Fuels, Lynchburg, Virginia, dated June 2003.

8. GDTACO – Urania-Gadolinia Fuel Pin Thermal Analysis Code, BAW-10184P-A, B&W Fuel Company, Lynchburg, Virginia, dated February 1995.

9. Fuel Rod Gas Pressure Criterion (FRGPC), BAW-10183P-A, B&W Fuel Company, Lynchburg, Virginia, dated July 1995.

10. Framatome Mark-B Fuel Assembly Spacer Grid Deformation in B&W Designed 177 Fuel Assembly Plants, BAW-2292P, Framatome Technologies Group, Lynchburg, Virginia, dated February 1997 (SER dated August 20, 1997).

11. Mark-C Fuel Assembly LOCA-Seismic Analyses, BAW-10133P-A, Rev. 1, Addendum 1 and Addendum 2, Framatome Cogema Fuels, Lynchburg, Virginia, dated October 2000.

12. NEMO – Nodal Expansion Method Optimized, BAW-10180-A, Rev. 1, B&W Fuel Company, Lynchburg, Virginia, dated March 1993.

13. Letter, Robert Jones (NRC) to J. H. Taylor (FTI), Subject: Acceptance of Revised Measurement Uncertainty for Control Rod Worth Calculations, dated January 26, 1996.

14. Statistical Core Design for B&W-Designed 177-FA Plants, BAW-10187P-A, B&W Fuel Company, Lynchburg, Virginia, dated March 1994.

15. Evaluation of Replacement Rods in BWFC Fuel Assemblies, BAW-2149-A, B&W Fuel Company, Lynchburg, Virginia, dated September 1993.

16. NUREG-0800, Standard Review Plan for the Review of Safety Analysis Reports for Nuclear Power Plants, LWR Ed., USNRC.

17. BWNT LOCA – BWNT Loss-of-Coolant Accident Evaluation Model for Once-Through Steam Generator Plants, BAW-10192P-A, Framatome Technologies Inc., Lynchburg, Virginia, dated June 1998.

18. COPERNIC Fuel Rod Design Computer Code, BAW-10231P-A, Revision 1, Framatome ANP, Lynchburg, Virginia, dated January 2004.

19. Mark-B-HTP Fuel Assembly Design Report Davis-Besse Unit 1, ANP-2505(P), Revision 0, Framatome ANP, Lynchburg, Virginia, dated January 2006.

20. BHTP DNB Correlation Applied with LYNXT, BAW-10241(P)(A), Revision 1, Framatome ANP, Inc., Lynchburg, Virginia, dated July 2005.

21. ZPPT Modifications for B&W Designed Reactors, BAW-10242(NP)-A, Revision 0, Framatome ANP, Lynchburg, Virginia, dated November 2003.

22. Statistical Fuel Assembly Hold Down Methodology, BAW-10243P-A, Framatome ANP, Inc., Lynchburg, Virginia, dated September 2005.

23. RELAP5/MOD2-B&W- An Advanced Computer Program for Light Water Reactor LOCA and Non-LOCA Transient Analysis, BAW-10164P-A, Revision 6, AREVA NP Inc., Lynchburg, Virginia, dated June 2007.